



ISSN 2686-7575 (Online)

ТОНКИЕ ХИМИЧЕСКИЕ ТЕХНОЛОГИИ

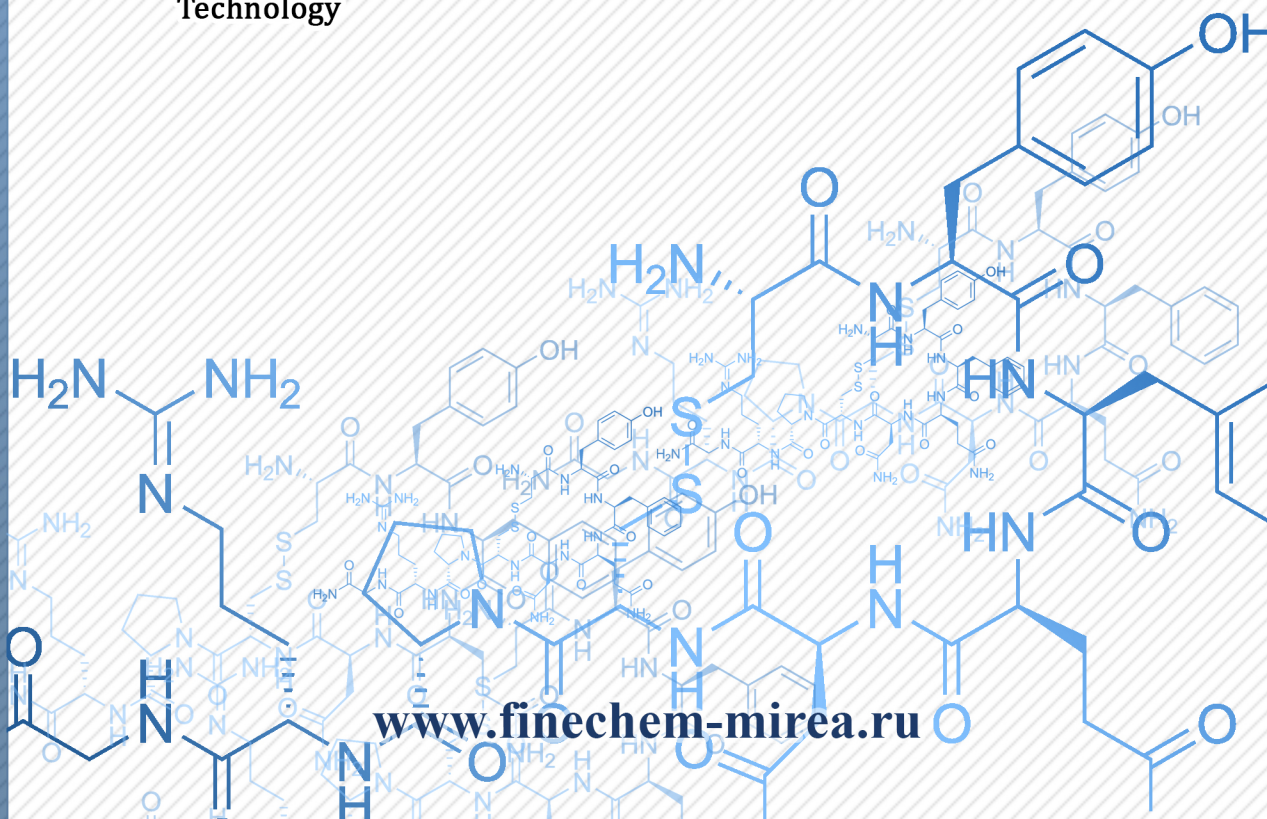
Fine Chemical Technologies

- | Theoretical Basis of Chemical Technology
- | Chemistry and Technology of Organic Substances
- | Chemistry and Technology of Medicinal Compounds and Biologically Active Substances
- | Biochemistry and Biotechnology
- | Synthesis and Processing of Polymers and Polymeric Composites
- | Chemistry and Technology of Inorganic Materials
- | Analytical Methods in Chemistry and Chemical Technology
- | Mathematical Methods and Information Systems in Chemical Technology

20(4)

2025

www.finechem-mirea.ru





ТОНКИЕ ХИМИЧЕСКИЕ ТЕХНОЛОГИИ

Fine Chemical Technologies

- | Theoretical Basis of Chemical Technology
- | Chemistry and Technology of Organic Substances
- | Chemistry and Technology of Medicinal Compounds and Biologically Active Substances
- | Biochemistry and Biotechnology
- | Synthesis and Processing of Polymers and Polymeric Composites
- | Chemistry and Technology of Inorganic Materials
- | Analytical Methods in Chemistry and Chemical Technology
- | Mathematical Methods and Information Systems in Chemical Technology

Tonkie Khimicheskie Tekhnologii =
Fine Chemical Technologies.
Vol. 20, No. 4, 2025

Тонкие химические технологии =
Fine Chemical Technologies.
Том 20, № 4, 2025

<https://doi.org/10.32362/2410-6593-2025-20-4>

www.finechem-mirea.ru

**Tonkie Khimicheskie Tekhnologii =
Fine Chemical Technologies
2025, Vol. 20, No. 4**

The peer-reviewed scientific and technical journal Fine Chemical Technologies highlights the modern achievements of fundamental and applied research in the field of fine chemical technologies, including the theoretical basis of chemical technology, chemistry and technology of medicinal compounds and biologically active substances, organic substances and inorganic materials, biochemistry and biotechnology, synthesis and processing of polymers and polymeric composites, analytical and mathematical methods and information systems in chemistry and chemical technology.

Founder and Publisher

Federal State Budget
Educational Institution of Higher Education
“MIREA – Russian Technological University”
78, Vernadskogo pr., Moscow, 119454, Russian Federation.
Publication frequency: bimonthly.
The journal was founded in 2006. The name was Vestnik MITHT until 2015 (ISSN 1819-1487).

The journal is included into the List of peer-reviewed science press of the State Commission for Academic Degrees and Titles of the Russian Federation.

The journal is indexed: SCOPUS, DOAJ, Chemical Abstracts, Science Index, RSCI, Ulrich's International Periodicals Directory

Editor-in-Chief:

Andrey V. Timoshenko – Dr. Sci. (Eng.), Cand. Sci. (Chem.), Professor, MIREA – Russian Technological University, Moscow, Russian Federation. Scopus Author ID 56576076700, ResearcherID Y-8709-2018, <https://orcid.org/0000-0002-6511-7440>, timoshenko@mirea.ru

Deputy Editor-in-Chief:

Valery V. Fomichev – Dr. Sci. (Chem.), Professor, MIREA – Russian Technological University, Moscow, Russian Federation. Scopus Author ID 57196028937, <http://orcid.org/0000-0003-4840-0655>, fomichev@mirea.ru

Editorial staff:

Managing Editor	Cand. Sci. (Eng.) Galina D. Seredina
Editor	Sofya M. Mazina
Executive Editor	Elizaveta I. Kuricheva
Science editors	Dr. Sci. (Chem.), Prof. Tatyana M. Buslaeva Dr. Sci. (Chem.), Prof. Anatolii A. Ischenko Dr. Sci. (Eng.), Prof. Anatolii V. Markov Dr. Sci. (Chem.), Prof. Vladimir A. Tverskoy
Desktop publishing	Sergey V. Trofimov

86, Vernadskogo pr., Moscow, 119571, Russian Federation.
Phone: +7 (499) 600-80-80 (#31288)
E-mail: seredina@mirea.ru

The registration number ПИ № ФС 77-74580 was issued in December 14, 2018 by the Federal Service for Supervision of Communications, Information Technology, and Mass Media of Russia

The subscription index of *Pressa Rossii*: **36924**

Publication date 29.08.2025

The Editorial Board's viewpoint may not coincide with the viewpoint of the authors of the articles published in the journal.

**Тонкие химические технологии =
Fine Chemical Technologies
2025, том 20, № 4**

Научно-технический рецензируемый журнал «Тонкие химические технологии» освещает современные достижения фундаментальных и прикладных исследований в области тонких химических технологий, включая теоретические основы химической технологии, химию и технологию лекарственных препаратов и биологически активных соединений, органических веществ и неорганических материалов, биохимию и биотехнологию, синтез и переработку полимеров и композитов на их основе, аналитические и математические методы и информационные системы в химии и химической технологии.

Учредитель и издатель

федеральное государственное бюджетное образовательное учреждение высшего образования «МИРЭА – Российский технологический университет» 119454, РФ, Москва, пр-т Вернадского, д. 78.
Периодичность: один раз в два месяца.
Журнал основан в 2006 году. До 2015 года издавался под названием «Вестник МИТХТ» (ISSN 1819-1487).

Журнал входит в Перечень ведущих рецензируемых научных журналов ВАК РФ.

Индексируется: SCOPUS, DOAJ, Chemical Abstracts, РИНЦ (Science Index), RSCI, Ulrich's International Periodicals Directory

Главный редактор:

Тимошенко Андрей Всеволодович – д.т.н., к.х.н., профессор, МИРЭА – Российский технологический университет, Москва, Российская Федерация. Scopus Author ID 56576076700, ResearcherID Y-8709-2018, <https://orcid.org/0000-0002-6511-7440>, timoshenko@mirea.ru

Заместитель главного редактора:

Фомичёв Валерий Вячеславович – д.х.н., профессор, МИРЭА – Российский технологический университет, Москва, Российская Федерация. Scopus Author ID 57196028937, <http://orcid.org/0000-0003-4840-0655>, fomichev@mirea.ru

Редакция:

Зав. редакцией	к.т.н. Г.Д. Середина
Редактор	С.М. Мазина
Выпускающий редактор	Е.И. Куричева
Научные редакторы	д.х.н., проф. Т.М. Буслаева д.х.н., проф. А.А. Ищенко д.т.н., проф. А.В. Марков д.х.н., проф. В.А. Тверской
Компьютерная верстка	С.В. Трофимов

РФ, 119571, Москва, пр. Вернадского, 86, оф. Р-108.
Тел.: +7 (499) 600-80-80 (#31288)
E-mail: seredina@mirea.ru

Регистрационный номер и дата принятия решения о регистрации СМИ: ПИ № ФС 77-74580 от 14.12.2018 г. СМИ зарегистрировано Федеральной службой по надзору в сфере связи, информационных технологий и массовых коммуникаций (Роскомнадзор)

Индекс по Объединенному каталогу «Пресса России»: **36924**

Дата опубликования 29.08.2025 г.

Мнение редакции может не совпадать с мнением авторов публикуемых в журнале статей.

EDITORIAL BOARD

Andrey V. Blokhin – Dr. Sci. (Chem.), Professor, Belarusian State University, Minsk, Belarus. Scopus Author ID 7101971167, ResearcherID AAF-8122-2019, <https://orcid.org/0000-0003-4778-5872>, blokhin@bsu.by.

Sergey P. Verevkin – Dr. Sci. (Eng.), Professor, University of Rostock, Rostock, Germany. Scopus Author ID 7006607848, ResearcherID G-3243-2011, <https://orcid.org/0000-0002-0957-5594>, Sergey.verevkin@uni-rostock.de.

Konstantin Yu. Zhizhin – Corresponding Member of the Russian Academy of Sciences (RAS), Dr. Sci. (Chem.), Professor, N.S. Kurnakov Institute of General and Inorganic Chemistry of the RAS, Moscow, Russian Federation. Scopus Author ID 6701495620, ResearcherID C-5681-2013, <http://orcid.org/0000-0002-4475-124X>, kyuzhizhin@igic.ras.ru.

Igor V. Ivanov – Dr. Sci. (Chem.), Professor, MIREA – Russian Technological University, Moscow, Russian Federation. Scopus Author ID 34770109800, ResearcherID I-5606-2016, <http://orcid.org/0000-0003-0543-2067>, ivanov_i@mirea.ru.

Carlos A. Cardona – PhD (Eng.), Professor, National University of Columbia, Manizales, Colombia. Scopus Author ID 7004278560, <http://orcid.org/0000-0002-0237-2313>, ccardonaal@unal.edu.co.

Elvira T. Krut'ko – Dr. Sci. (Eng.), Professor, Belarusian State Technological University, Minsk, Belarus. Scopus Author ID 6602297257, ela_krutko@mail.ru.

Anatolii I. Miroshnikov – Academician at the RAS, Dr. Sci. (Chem.), Professor, M.M. Shemyakin and Yu.A. Ovchinnikov Institute of Bioorganic Chemistry of the RAS, Member of the Presidium of the RAS, Chairman of the Presidium of the RAS Pushchino Research Center, Moscow, Russian Federation. Scopus Author ID 7006592304, ResearcherID G-5017-2017, aiv@ibch.ru.

Aziz M. Muzafarov – Academician at the RAS, Dr. Sci. (Chem.), Professor, A.N. Nesmeyanov Institute of Organoelement Compounds of the RAS, Moscow, Russian Federation. Scopus Author ID 7004472780, ResearcherID G-1644-2011, <https://orcid.org/0000-0002-3050-3253>, aziz@ineos.ac.ru.

РЕДАКЦИОННАЯ КОЛЛЕГИЯ

Блохин Андрей Викторович – д.х.н., профессор Белорусского государственного университета, Минск, Беларусь. Scopus Author ID 7101971167, ResearcherID AAF-8122-2019, <https://orcid.org/0000-0003-4778-5872>, blokhin@bsu.by.

Верёвкин Сергей Петрович – д.т.н., профессор Университета г. Росток, Росток, Германия. Scopus Author ID 7006607848, ResearcherID G-3243-2011, <https://orcid.org/0000-0002-0957-5594>, Sergey.verevkin@uni-rostock.de.

Жижин Константин Юрьевич – член-корр. Российской академии наук (РАН), д.х.н., профессор, Институт общей и неорганической химии им. Н.С. Курнакова РАН, Москва, Российская Федерация. Scopus Author ID 6701495620, ResearcherID C-5681-2013, <http://orcid.org/0000-0002-4475-124X>, kyuzhizhin@igic.ras.ru.

Иванов Игорь Владимирович – д.х.н., профессор, МИРЭА – Российский технологический университет, Москва, Российская Федерация. Scopus Author ID 34770109800, ResearcherID I-5606-2016, <http://orcid.org/0000-0003-0543-2067>, ivanov_i@mirea.ru.

Кардона Карлос Ариэль – PhD, профессор Национального университета Колумбии, Манизалес, Колумбия. Scopus Author ID 7004278560, <http://orcid.org/0000-0002-0237-2313>, ccardonaal@unal.edu.co.

Крутько Эльвира Тихоновна – д.т.н., профессор Белорусского государственного технологического университета, Минск, Беларусь. Scopus Author ID 6602297257, ela_krutko@mail.ru.

Мирошников Анатолий Иванович – академик РАН, д.х.н., профессор, Институт биоорганической химии им. академиков М.М. Шемякина и Ю.А. Овчинникова РАН, член Президиума РАН, председатель Президиума Пущинского научного центра РАН, Москва, Российская Федерация. Scopus Author ID 7006592304, ResearcherID G-5017-2017, aiv@ibch.ru.

Музафаров Азиз Мансурович – академик РАН, д.х.н., профессор, Институт элементоорганических соединений им. А.Н. Несмеянова РАН, Москва, Российская Федерация. Scopus Author ID 7004472780, ResearcherID G-1644-2011, <https://orcid.org/0000-0002-3050-3253>, aziz@ineos.ac.ru.

Ivan A. Novakov – Academician at the RAS, Dr. Sci. (Chem.), Professor, President of the Volgograd State Technical University, Volgograd, Russian Federation.
Scopus Author ID 7003436556, ResearcherID I-4668-2015,
<http://orcid.org/0000-0002-0980-6591>,
president@vstu.ru.

Alexander N. Ozerin – Corresponding Member of the RAS, Dr. Sci. (Chem.), Professor, Enikolopov Institute of Synthetic Polymeric Materials of the RAS, Moscow, Russian Federation.
Scopus Author ID 7006188944, ResearcherID J-1866-2018,
<https://orcid.org/0000-0001-7505-6090>,
ozerin@ispm.ru.

Tapani A. Pakkanen – PhD, Professor, Department of Chemistry, University of Eastern Finland, Joensuu, Finland.
Scopus Author ID 7102310323,
tapani.pakkanen@uef.fi.

Armando J.L. Pombeiro – Academician at the Academy of Sciences of Lisbon, PhD, Professor, President of the Center for Structural Chemistry of the Higher Technical Institute of the University of Lisbon, Lisbon, Portugal.
Scopus Author ID 7006067269, ResearcherID I-5945-2012,
<https://orcid.org/0000-0001-8323-888X>,
pombeiro@ist.utl.pt.

Dmitrii V. Pyshnyi – Corresponding Member of the RAS, Dr. Sci. (Chem.), Professor, Institute of Chemical Biology and Fundamental Medicine, Siberian Branch of the RAS, Novosibirsk, Russian Federation.
Scopus Author ID 7006677629, ResearcherID F-4729-2013,
<https://orcid.org/0000-0002-2587-3719>,
pyshnyi@niboch.nsc.ru.

Alexander S. Sigov – Academician at the RAS, Dr. Sci. (Phys. and Math.), Professor, President of MIREA – Russian Technological University, Moscow, Russian Federation.
Scopus Author ID 35557510600, ResearcherID L-4103-2017,
sigov@mirea.ru.

Alexander M. Toikka – Dr. Sci. (Chem.), Professor, Institute of Chemistry, Saint Petersburg State University, St. Petersburg, Russian Federation.
Scopus Author ID 6603464176, ResearcherID A-5698-2010,
<http://orcid.org/0000-0002-1863-5528>,
a.toikka@spbu.ru.

Andrzej W. Trochimczuk – Dr. Sci. (Chem.), Professor, Faculty of Chemistry, Wrocław University of Science and Technology, Wrocław, Poland.
Scopus Author ID 7003604847,
andrzej.trochimczuk@pwr.edu.pl.

Aslan Yu. Tsivadze – Academician at the RAS, Dr. Sci. (Chem.), Professor, A.N. Frumkin Institute of Physical Chemistry and Electrochemistry of the RAS, Moscow, Russian Federation.
Scopus Author ID 7004245066, ResearcherID G-7422-2014,
tsiv@phych.ac.ru.

Новаков Иван Александрович – академик РАН, д.х.н., профессор, президент Волгоградского государственного технического университета, Волгоград, Российская Федерация.
Scopus Author ID 7003436556, ResearcherID I-4668-2015,
<http://orcid.org/0000-0002-0980-6591>,
president@vstu.ru.

Озерин Александр Никифорович – член-корр. РАН, д.х.н., профессор, Институт синтетических полимерных материалов им. Н.С. Ениколопова РАН, Москва, Российская Федерация.
Scopus Author ID 7006188944, ResearcherID J-1866-2018,
<https://orcid.org/0000-0001-7505-6090>,
ozerin@ispm.ru.

Пакканен Тапани – PhD, профессор, Департамент химии, Университет Восточной Финляндии, Йоенсуу, Финляндия.
Scopus Author ID 7102310323,
tapani.pakkanen@uef.fi.

Помбейро Армандо – академик Академии наук Лиссабона, PhD, профессор, президент Центра структурной химии Высшего технического института Университета Лиссабона, Португалия.
Scopus Author ID 7006067269, ResearcherID I-5945-2012,
<https://orcid.org/0000-0001-8323-888X>,
pombeiro@ist.utl.pt.

Пышный Дмитрий Владимирович – член-корр. РАН, д.х.н., профессор, Институт химической биологии и фундаментальной медицины Сибирского отделения РАН, Новосибирск, Российская Федерация.
Scopus Author ID 7006677629, ResearcherID F-4729-2013,
<https://orcid.org/0000-0002-2587-3719>,
pyshnyi@niboch.nsc.ru.

Сигов Александр Сергеевич – академик РАН, д.ф.-м.н., профессор, президент МИРЭА – Российского технологического университета, Москва, Российская Федерация.
Scopus Author ID 35557510600, ResearcherID L-4103-2017,
sigov@mirea.ru.

Тойкка Александр Матвеевич – д.х.н., профессор, Институт химии, Санкт-Петербургский государственный университет, Санкт-Петербург, Российская Федерация.
Scopus Author ID 6603464176, ResearcherID A-5698-2010,
<http://orcid.org/0000-0002-1863-5528>,
a.toikka@spbu.ru.

Трохимчук Анджей – д.х.н., профессор, Химический факультет Вроцлавского политехнического университета, Вроцлав, Польша.
Scopus Author ID 7003604847,
andrzej.trochimczuk@pwr.edu.pl.

Цивадзе Аслан Юсупович – академик РАН, д.х.н., профессор, Институт физической химии и электрохимии им. А.Н. Фрумкина РАН, Москва, Российская Федерация.
Scopus Author ID 7004245066, ResearcherID G-7422-2014,
tsiv@phych.ac.ru.

Contents

CHEMISTRY AND TECHNOLOGY OF MEDICINAL COMPOUNDS AND BIOLOGICALLY ACTIVE SUBSTANCES

- 297** *Herman D. Moshkov, Andrey M. Normov, Elizaveta A. Shnyak, Alexey V. Panov*
Development of technology for producing submicron emulsion of propofol
using a high-pressure homogenizer

SYNTHESIS AND PROCESSING OF POLYMERS AND POLYMERIC COMPOSITES

- 310** *Shahad M. Hussain, Ahmed Ahmed, Mohammed Kadhom, Dina S. Ahmed,
Shams S. Hameed, Omar G. Mousa, Ahmed A. Ahmed, Muna Bufaroosha, Rahimi Yusop,
Emad Yousif*
Aging effects on polystyrene thin films containing high aromatic moiety compounds
under UV irradiation

CHEMISTRY AND TECHNOLOGY OF INORGANIC MATERIALS

- 324** *Nailya S. Akhmadullina, Aleksey V. Ishchenko*
Aluminum oxynitrides doped with rare-earth and transition metal ions
- 344** *Alena R. Zyкова, Andrey I. Kovalev, Darya P. Sherstyuk, Vladimir E. Zhivulin,
Sergey V. Taskaev, Denis A. Vinnik*
Cr-substituted M-type hexaferrite solid solutions with high level of substitution

ANALYTICAL METHODS IN CHEMISTRY AND CHEMICAL TECHNOLOGY

- 357** *Yaroslava N. Golubeva, Alexander V. Krylov, Tatyana A. Chebotareva*
Interaction of poly(diallyldimethylammonium chloride) with inorganic acids
- 372** *Timofey V. Kryukov, Mariana A. Feofanova, Viktor M. Nikol'skii, Alexandra I. Ivanova,
Ivan A. Kaplunov*
Rare-earth element complexes with complexones, heparin, and antibiotics in biosystems
for use as electrode-active materials in membrane ion-selective electrodes
- 382** *Pavel V. Postnikov, Alexander D. Askretkov, Andrey V. Polosin, Yuliya A. Efimova,
Elena S. Mochalova*
Semiquantitative determination of meldonium and emoxypine in human urine
by HPLC–MS/MS after receiving a single therapeutic dose of Brainmax[®]
and milk from cows receiving a preventive course of Emidonol[®]

СОДЕРЖАНИЕ

- 297** | **ХИМИЯ И ТЕХНОЛОГИЯ ЛЕКАРСТВЕННЫХ ПРЕПАРАТОВ И БИОЛОГИЧЕСКИ АКТИВНЫХ СОЕДИНЕНИЙ**
Г.Д. Мошков, А.М. Нормов, Е.А. Шняк, А.В. Панов
Разработка технологии получения субмикронной эмульсии пропופола с помощью гомогенизатора высокого давления
- 310** | **СИНТЕЗ И ПЕРЕРАБОТКА ПОЛИМЕРОВ И КОМПОЗИТОВ НА ИХ ОСНОВЕ**
Shahad M. Hussain, Ahmed Ahmed, Mohammed Kadhom, Dina S. Ahmed, Shams S. Hameed, Omar G. Mousa, Ahmed A. Ahmed, Muna Bufaroosha, Rahimi Yusop, Emad Yousif
Aging effects on polystyrene thin films containing high aromatic moiety compounds under UV irradiation
- 324** | **ХИМИЯ И ТЕХНОЛОГИЯ НЕОРГАНИЧЕСКИХ МАТЕРИАЛОВ**
Н.С. Ахмадуллина, А.В. Ищенко
Оксинитриды алюминия, легированные ионами редкоземельных и переходных металлов
- 344** | *Alena R. Zykova, Andrey I. Kovalev, Darya P. Sherstyuk, Vladimir E. Zhivulin, Sergey V. Taskaev, Denis A. Vinnik*
Cr-substituted M-type hexaferrite solid solutions with high level of substitution
- 357** | **АНАЛИТИЧЕСКИЕ МЕТОДЫ В ХИМИИ И ХИМИЧЕСКОЙ ТЕХНОЛОГИИ**
Я.Н. Голубева, А.В. Крылов, Т.А. Чеботарева
Взаимодействие полидиметилдиаллиламмоний хлорида с неорганическими кислотами
- 372** | *Т.В. Крюков, М.А. Феофанова, В.М. Никольский, А.И. Иванова, И.А. Каплунов*
Комплексы редкоземельных элементов в биосистемах с комплексонами, гепарином, антибиотиками для применения в качестве электродактивного вещества мембранных ионселективных электродов
- 382** | *П.В. Постников, А.Д. Аскретков, А.В. Полосин, Ю.А. Ефимова, Е.С. Мочалова*
Полуколичественное определение мельдония и эмоксипина в моче методом ВЭЖХ–МС/МС после приема однократной терапевтической дозы препарата Брейнмакс® и молока коров, получавших профилактический курс Эмидонола®

Chemistry and technology of medicinal compounds
and biologically active substances

Химия и технология лекарственных препаратов
и биологически активных соединений

UDC 615.456.3

<https://doi.org/10.32362/2410-6593-2025-20-4-297-309>

EDN ZFDCMS



RESEARCH ARTICLE

Development of technology for producing submicron emulsion of propofol using a high-pressure homogenizer

Herman D. Moshkov¹, Andrey M. Normov^{1,2,✉}, Elizaveta A. Shnyak^{1,2}, Alexey V. Panov^{1,2}

¹ MIREA – Russian Technological University (M.V. Lomonosov Institute of Fine Chemical Technologies), Moscow, 119454 Russia

² Institute of Pharmaceutical Technologies, Moscow, 121353 Russia

✉ Corresponding author, e-mail: a.m.normov@ipt.ru.com

Abstract

Objectives. Currently, propofol emulsions are widely used in clinical practice due to their rapid action, low toxicity, and ease of administration, including control of anesthetic depth and rapid recovery of the patient following anesthesia. The market offers drugs from both foreign and domestic manufacturers containing imported pharmaceutical substances. The study set out to develop a technology for obtaining a fat emulsion of propofol for parenteral purposes using a high-pressure homogenizer based on pharmaceutical propofol obtained by alkylation and subsequent decarboxylation of 4-hydroxybenzoic acid, as well as to study the physicochemical properties of the obtained submicron emulsions.

Methods. A submicron propofol emulsion was prepared using a high-pressure homogenizer. pH was determined using a pH meter equipped with a combined glass electrode. Particle size and zeta potential of the submicron emulsion were determined on a laser particle analyzer using the dynamic and electrophoretic light-scattering methods, respectively. Quantitative propofol content in the resulting emulsion was determined using high-performance liquid chromatography.

Results. Optimal technological parameters of the high-pressure homogenization process were selected. The method of adding the oil phase directly into the high-pressure homogenizer is shown to entail lower time and energy costs as compared to the homogenization method involving a preliminary stage of obtaining a pre-emulsion. The physicochemical characteristics of the obtained submicron emulsions were subsequently determined to correspond to the characteristics required for the original drug Propofol-Lipuro®.

Conclusions. The proposed technology for obtaining a submicron propofol emulsion for parenteral use is based on dispersion of the aqueous and oil phases using a high-pressure homogenizer. As a result of the study, it was found that adding the oil phase directly into the high-pressure homogenizer at 20 MPa, including further dispersion at 60 MPa for 8 cycles, is optimal for obtaining a submicron propofol emulsion with the required characteristics.

Keywords

propofol, Propofol-Lipuro®, pre-emulsion, submicron emulsion, high-pressure homogenizer

Submitted: 04.02.2025

Revised: 24.03.2025

Accepted: 10.06.2025

For citation

Moshkov H.D., Normov A.M., Shnyak E.A., Panov A.V. Development of technology for producing submicron emulsion of propofol using a high-pressure homogenizer. *Tonk. Khim. Tekhnol. = Fine Chem. Technol.* 2025;20(4):297–309. <https://doi.org/10.32362/2410-6593-2025-20-4-297-309>

НАУЧНАЯ СТАТЬЯ

Разработка технологии получения субмикронной эмульсии пропофола с помощью гомогенизатора высокого давления

Г.Д. Мошков¹, А.М. Нормов^{1,2,✉}, Е.А. Шняк^{1,2}, А.В. Панов^{1,2}

¹ МИПЭА – Российский технологический университет (Институт тонких химических технологий им. М.В. Ломоносова), Москва, 119454 Россия

² Институт фармацевтических технологий, Москва, 121353 Россия

✉ Автор для переписки, e-mail: a.m.normov@ipt.ru.com

Аннотация

Цели. В настоящее время в клинической практике активно используются эмульсии пропофола, обладающие быстрым действием, низкой токсичностью, легкостью введения, контролем глубины анестезии и быстрым восстановлением пациента после наркоза. На рынке представлены лекарственные препараты как иностранных, так и российских производителей, содержащие импортные фармацевтические субстанции. Целью данной работы являлась разработка технологии получения жировой эмульсии пропофола для парентерального применения с помощью гомогенизатора высокого давления на основе фармацевтической субстанции пропофола, полученной по методу алкилирования и последующего декарбоксилирования 4-гидроксibenзойной кислоты, а также изучение физико-химических свойств полученных субмикронных эмульсий.

Методы. Субмикронную эмульсию пропофола получали с помощью гомогенизатора высокого давления. Значения pH определяли с использованием pH-метра, оснащенного комбинированным стеклянным электродом. Определение размера частиц и дзета-потенциала субмикронной эмульсии проводили на лазерном анализаторе частиц методом динамического светорассеивания и методом электрофоретического светорассеивания соответственно. Количественное содержания пропофола в полученной эмульсии определяли с помощью высоко эффективной жидкостной хроматографии.

Результаты. Подобраны оптимальные технологические параметры процесса гомогенизации высокого давления. Установлено, что методика введения масляной фазы напрямую в гомогенизатор высокого давления осуществляется с меньшими временными и энергетическими затратами по сравнению с методикой гомогенизации с предварительной стадией получения предэмульсии. Определено, что физико-химические характеристики полученных субмикронных эмульсий соответствуют характеристикам, предъявляемых оригинальному препарату Пропофол-Липуро®.

Выводы. Предложена технология получения субмикронной эмульсии пропофола для парентерального применения, основанная на диспергировании водной и масляной фазы с помощью гомогенизатора высокого давления. В результате проведенного исследования было установлено, что введение масляной фазы напрямую в гомогенизатор высокого давления при 20 МПа, а также дальнейшее проведение процесса диспергирования при 60 МПа в течение 8 циклов является оптимальным для получения субмикронной эмульсии пропофола с требуемыми характеристиками.

Ключевые слова

пропофол, Пропофол-Липуро®, предэмульсия, субмикронная эмульсия, гомогенизатор высокого давления

Поступила: 04.02.2025

Доработана: 24.03.2025

Принята в печать: 10.06.2025

Для цитирования

Мошков Г.Д., Нормов А.М., Шняк Е.А., Панов А.В. Разработка технологии получения субмикронной эмульсии пропофола с помощью гомогенизатора высокого давления. *Тонкие химические технологии*. 2025;20(4):297–309. <https://doi.org/10.32362/2410-6593-2025-20-4-297-309>

INTRODUCTION

Propofol (2,6-diisopropylphenol) is a potent intravenous anesthetic widely used for administration and maintenance of anesthesia and for sedation in intensive care units [1–3].

2,6-Diisopropylphenol is an oily liquid at room temperature. The $\log P$ value for the 2,6-diisopropylphenol molecule, reflecting its hydrophobic properties, is 4.0; the distribution coefficient between octanol and water is 6761. These indices indicate the near complete insolubility of the molecule in aqueous solutions; consequently, it is necessary to use different carriers to administer propofol in the human body [4].

Among the significant pharmacological effects of Propofol are its ability to reduce cerebral blood flow, cerebral metabolic rate, and intracranial pressure. In addition, it acts as an antioxidant to remove free radicals and reduce lipid peroxidation, as well as activating gamma-aminobutyric acid (GABA) receptors [2, 3].

Clinical trials of a drug product in the form of an emulsion containing propofol were first conducted in 1977. However, due to the occurrence of anaphylactic reactions to polyethoxylated castor oil (Cremophor EL[®]), which was used as a solvent for the pharmaceutical substance, the product was withdrawn from the market. Nevertheless, research into the development of a drug based on 2,6-diisopropylphenol continued. In 1983 in Europe and later in 1986 in the United States, an oil-in-water emulsion was demonstrated to offer an anesthetic effect similar to that of a drug containing polyethoxylated castor oil, but without any anaphylactic reactions [5]. In 1989, Diprivan[®], comprising a propofol-containing phospholipid emulsion for the intravenous induction and maintenance of general anesthesia in adult patients was brought to market in the United States. This drug product was the initial model for this type of medication [6].

Currently, there are various types of propofol-based emulsion drugs on the market, including Propofol-Lipuro[®] (Germany), Propofol-Egen[®] (Russia), Propofol-Binergy[®] (Russia), Propofol[®] (Korea), Propofol Fresenius[®] (Austria), Diprivan[®] (Italy). These drugs are produced in the form of 1–2% lipid emulsions for parenteral use^{1,2}, which include soybean oil (5–10%), medium-chain triglycerides (0–5%), glycerol (2.25–2.5%), egg lecithin (1.2%). The surfactants used

in these products are either 0.03% sodium oleate or the combination of 0.04–0.08% oleic acid and 0.005–0.011% sodium hydroxide [6–8].

In Russia, the production of drugs containing propofol as an active ingredient is based on the use of imported pharmaceutical substances. In the present study, we used a pharmaceutical substance of propofol obtained by the method of alkylation and subsequent decarboxylation of 4-hydroxybenzoic acid³. The structure of the obtained propofol substance was confirmed by ¹H nuclear magnetic resonance (NMR) spectroscopy [9].

The obtained submicron emulsions should meet the requirements in accordance with GPA.1.4.1.0007 of the 15th edition of the State Pharmacopoeia of the Russian Federation (SP RF XV)⁴: the average particle size should be less than 500 nm in accordance with GPA.1.4.2.0028 of the SP RF XV, while the zeta potential should be more than ± 30 mV [10, 11].

The importance of maintaining a constant emulsion particle size is due to the necessity of ensuring the stability of the final dosage form [12]. Oils in the form of emulsions are better absorbed in the body because the absorption of oils into the gastrointestinal tract occurs only in the presence of surfactants [13]. However, particles larger than 300 nm may increase the risk of fat embolism. The stability of the emulsion is determined by the zeta potential. A decrease in the modulus of the electric charge value at the interface between the electric double layer and the dispersion medium can increase the rate of aggregation and coalescence [14].

Submicron emulsions can be produced using both high-energy and low-energy methods. High-energy methods generally involve the use of mechanical devices that generate high disruptive forces. Conversely, low-energy methods rely on changes in internal parameters that affect the hydrophilic-lipophilic balance of the systems. Although low-energy approaches are generally more effective and do not cause disruption or damage to encapsulated molecules, they have certain limitations related to the components used. In such cases, high concentrations of synthetic surfactants are required to achieve stable emulsions, which limits the scope of their application. In the context of obtaining emulsions for parenteral use, high-energy methods are favored, where mechanical dispersion is performed using high-pressure homogenizers, high-speed agitation, and

¹ Products. Binergia.ru. 2024. URL: <https://binergia.ru/en/catalog/products.php>. Accessed November 01, 2024.

² Propofol-Egen[®]. ArmBio.bio. 2017. URL: https://armbio.bio/catalog/medications_contracts/non-inhalation_general_anesthetic_contract/propofol_egen. Accessed November 01, 2024.

³ CN 106565424 A. Preparation method for high-purity propofol. Date of publication: 04.19.2017. URL: <https://patentimages.storage.googleapis.com/36/be/e3/540d7228956dba/CN106565424A.pdf>. Accessed September 12, 2024.

⁴ The State Pharmacopoeia of the Russian Federation. 15th Ed. Moscow: 2023. URL: <https://pharmacopoeia.regmed.ru/pharmacopoeia/izdanie-15/>. Accessed December 12, 2024.

ultrasonic generators. The external load applied to the system (ultrasonic waves and pressure rise) breaks down droplets to the nanoscale to form stable thermokinetic stable emulsions [15–16].

Therefore, the present study sets out to develop a technology for obtaining a submicron emulsion of propofol for parenteral use using a high-pressure homogenizer, as well as to investigate the physicochemical properties of the obtained submicron emulsions.

MATERIALS AND METHODS

The following substances were used in the study: propofol substance obtained by alkylation and subsequent decarboxylation of 4-hydroxybenzoic acid (*Acros Organics*, Belgium); LIPOID Purified Soybean Oil (*LIPOID*, Germany); egg yolk phospholipid LIPOID E80 (*LIPOID*, Germany); LIPOID Sodium Oleate B (*LIPOID*, Germany); medium-chain triglyceride Lipoid MCT (*LIPOID*, Germany); glycerin (*ChemMed*, Russia); water for injection (SP RF XV, PA.2.2.0019).

The percentage of components (Table 1) in the submicron emulsion was chosen based on the original Propofol-Lipuro® 1% formulation⁵.

In order to confirm the structure of the pharmaceutical substance propofol (Fig. 1) obtained by alkylation and subsequent decarboxylation of 4-hydroxybenzoic acid, ¹H NMR spectroscopy was used. Figure 2 summarizes the results of the analysis.

The ¹H NMR spectra of propofol measured in dimethyl sulfoxide DMSO-*d*₆ and deuterated chloroform CDCl₃ are consistent with the structure of 2,6-diisopropylphenol in accordance with literature data [9]. In the spectra of purified propofol samples, the signals of external impurities are absent.

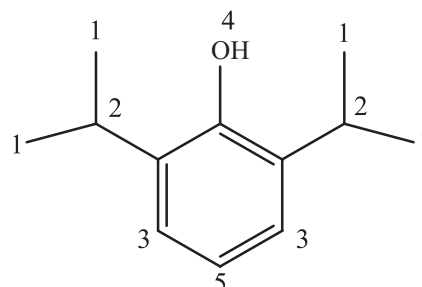


Fig. 1. Structure of the pharmaceutical substance propofol

¹H NMR (DMSO-*d*₆, 400 MHz): δ 8.01 (s, 1H, H4), 6.98–6.97 (m, 2H, H3), 6.81–6.77 (m, 1H, H5), 3.33 (hept., *J* = 6.9 Hz, 2H, H2) 1.16 (d, *J* = 6.9 Hz, 12H, H1).

¹H NMR (CDCl₃, 400 MHz): δ 7.19–7.17 (m, 2H, H3), 7.05–7.01 (m, 1H, H5), 4.98 (br., 1H, H4), 3.28 (hept., *J* = 6.9 Hz, 2H, H2) 1.39 (d, *J* = 6.9 Hz, 12H, H1).

Preparation of the submicron emulsion consists of the preparation of aqueous and oil phases followed by their homogenization. In order to prepare the aqueous phase, we mixed exact weights of glycerol and sodium oleate with water for injection in beaker 1. Next the obtained

Table 1. Composition of the original drug Propofol-Lipuro®

Component	Quantitative content, wt %/wt
Oil phase	
Medium chain triglyceride	5
Soybean oil	5
Lecithin	1.2
Propofol	1
Water phase	
Glycerol	2.5
Sodium oleate	0.03
Water for injection (PA.2.2.0019.15)	Up to 100%

⁵ Propofol-Lipuro® 10 mg/mL (1%). Bbraun.ru. B. Braun Melsungen AG; 2024. URL: <https://www.bbraun.ru/ru/products/b/propofol-lipuro10mgml1.html>. Accessed December 05, 2024.

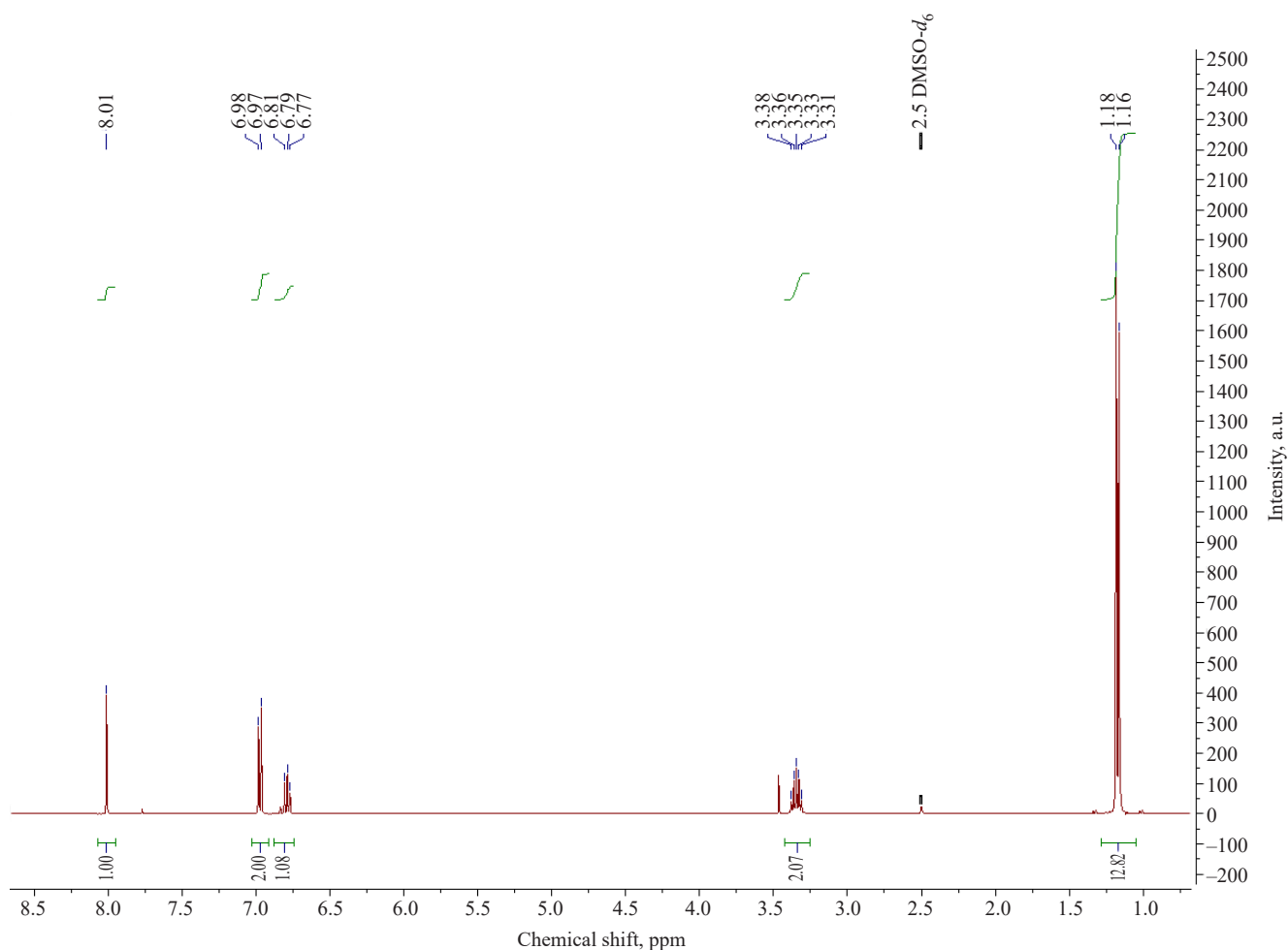


Fig. 2. ^1H NMR spectra of the pharmaceutical substance propofol obtained by alkylation and subsequent decarboxylation of 4-hydroxybenzoic acid

mixture was placed on a water bath at a temperature of 55–65°C and stirred using a ULABUS-2200D paddle top-driven stirrer (ULAB, Russia) until complete dissolution of the components.

Preparation of the oil phase was carried out as follows: accurate weights of medium-chain triglyceride and lecithin were measured into beaker 2, then the beaker was placed on a water bath at a temperature of 55–65°C and stirred with a paddle top-driven stirrer for 45 min. Exact weights of soybean oil and propofol were added to beaker 3 and stirred thoroughly for 3 min at the speed of rotation of the top-drive stirrer (500 rpm). After that, the contents of beaker 3 were added to beaker 2, and the resulting mixture was stirred for 5 min.

In this study, the submicron emulsion of propofol was obtained by high-pressure homogenization using two methods.

Method 1. Based on experimental studies [17–19], emulsion production was carried out with a preliminary stage of pre-emulsion preparation. The

oil phase was added to the aqueous phase in portions with constant stirring using dispersing devices (ULABUS-2200D top-drive stirrer (ULAB, Russia), T25 BASIC ULTRA-TURRAX® disperser (IKA, Germany) and GL-P 500/30000 laboratory homogenizer (Wiggins, China)) for 5 min until a visually homogeneous system was obtained.

Then dispersion of pre-emulsion was carried out using a Donor-3 high-pressure homogenizer (Donor, Russia). Homogenization was carried out at pressures of 40, 60, 80, 100 MPa to obtain a product with the required degree of particle size.

Method 2. The aqueous phase was added into the Donor-3 high-pressure homogenizer. A syringe dispenser (Hunan Beyond Medical Technology Co., China) was used to feed the oil phase into the aqueous phase at a pressure of 20 MPa. After the oil phase was completely added, the homogenization pressure was increased to 40, 60, 80, 100 MPa. Dispersion was carried out until a product with the desired particle size was obtained.

Homogenization in both cases was carried out under constant temperature control of the unit at 6°C. The temperature in the homogenization chamber was measured throughout the experiment using a GEMLUX GL-DT-11 thermometer (GEMLUX, China).

The pH was measured according to the pharmacopoeia article GPA 1.2.3.0004 “Ionometry” SP RF XV using pH-150MI pH meter (portable, with tripod) (*Izmeritel'naya tekhnika*, Russia) equipped with an ESC-10603/7 combined glass electrode (*Izmeritel'naya tekhnika*, Russia).

Determination of particle size and zeta potential of the submicron emulsion was carried out at the RTU MIREA Collective Use Center using a DelsaNano C laser particle analyzer (Beckman Coulter, USA).

The quantitative content of propofol in the final product was determined by the previously developed methodology using high-performance liquid chromatography on a Stayer system (*Aquilon*, Russia). A Luna column (*Phenomenex*, USA), 250 × 4.6 mm, filled with C18(2) sorbent with a particle size of 5 µm and a pore size of 10 nm was used. The mobile phase A was 0.276% solution of sodium phosphate monohydrate in purified water, pH of the solution was adjusted to 3.0 with 85% phosphoric acid, mobile phase B was acetonitrile.

The concentration of propofol (C_{propofol}) in the product (in g/L) was determined according to the following formula:

$$C_{\text{propofol}} = \frac{A_{\text{PRL}} \times W_{\text{ST}}}{A_{\text{ST}} \times 10},$$

where A_{PRL} is the area of propofol peak on the chromatogram of the test solution; A_{ST} is the area of propofol peak on the chromatogram of the standard solution; W_{ST} is the weight of propofol standard, g.

RESULTS AND DISCUSSION

The main criterion for selection of technological parameters of the submicron emulsion is compliance of the obtained product quality with the emulsion quality of the original drug Propofol-Lipuro® in terms of the following parameters: average particle size, particle size distribution by volume and number, zeta potential.

The original drug product is characterized by a narrow unimodal distribution of particle size by volume and number (Fig. 3). The average particle size in the emulsion of the original drug Propofol-Lipuro® was 186.2 ± 15.0 nm. The zeta potential value was 35 mV.

The first stage of the study consisted in studying the influence of the type of dispersing on the quality of the obtained propofol macroemulsion; the results are presented in Table 2.

As seen from the results, the propofol macroemulsion obtained when using the GL-P 500/30000 laboratory homogenizer is characterized by a smaller average particle size and the greatest stability, which is optimal for the high-pressure homogenization process further down the line.

Next, we selected the modes of high-pressure homogenization with a preliminary stage of pre-emulsion production according to Method 1. Table 3 shows the homogenization parameters, including the average particle sizes and distributions for the obtained emulsions.

According to the results of the experiments shown in Table 3, the following conclusions can be drawn. The lipid emulsions obtained in experiments 1–6, 9, 15, and 16 have a bimodal particle volume distribution, while those obtained in experiments 7, 8, 10–13, 14, 17 are characterized by a narrow unimodal distribution; however, the average particle size does not correspond to the average particle size of the original drug. The emulsions obtained

Table 2. Characteristics of propofol macroemulsion

Dispersing device type	Rotation speed of the dispersing device, rpm	Average particle size, nm	Description of macroemulsion
Overhead stirrer	2200	5350 ± 800	After 5 min of completion of the dispersion process, the formation of oil droplets on the surface of the macroemulsion was observed
Dispersant	25000	5520 ± 500	After 5 min of completion of the dispersion process, the formation of oil droplets on the surface of the macroemulsion was observed
Laboratory homogenizer	30000	2140 ± 500	No oil droplets were observed on the surface of the macroemulsion. The resulting macroemulsion was stable for 1 h

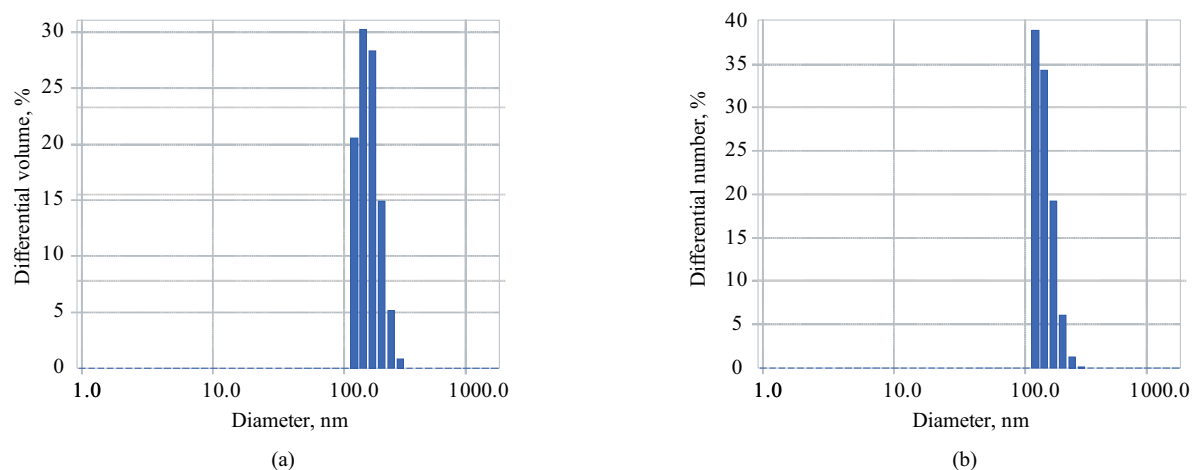


Fig. 3. Differential distribution of volume (a) and numerical (b) fraction of particles by size for a submicron emulsion of the original drug Propofol-Lipuro®

Table 3. Homogenization parameters and characteristics of the resulting emulsion according to method 1

No.	Temperature inside the unit, °C	Number of cycles at 40 MPa, pcs.	Number of cycles at 60 MPa, pcs.	Number of cycles at 80 MPa, pcs.	Number of cycles at 100 MPa, pcs.	Average particle size, nm	Particle distribution
1	24	2	—	—	—	655.8 ± 29.9	Bimodal
2	24	4	—	—	—	423.3 ± 23.0	Bimodal
3	23	6	—	—	—	334.9 ± 25.1	Bimodal
4	24	8	—	—	—	320.7 ± 17.9	Bimodal
5	23	10	—	—	—	276.4 ± 12.4	Bimodal
6	24	—	2	—	—	578.7 ± 15.8	Bimodal
7	24	—	4	—	—	439.3 ± 14.5	Unimodal
8	25	—	6	—	—	370.6 ± 21.6	Unimodal
9	25	—	8	—	—	307.5 ± 29.4	Bimodal
10	25	—	10	—	—	271.1 ± 11.2	Unimodal
11	25	—	—	2	—	264.7 ± 18.9	Unimodal
12	27	—	—	4	—	223.1 ± 23.1	Unimodal
13	27	—	—	6	—	215.1 ± 21.7	Unimodal
14	35	—	—	8	—	203.8 ± 15.4	Unimodal
15	34	—	—	10	—	198.8 ± 24.5	Bimodal
16	29	—	—	—	2	243.4 ± 12.3	Bimodal

Table 3. Continued

No.	Temperature inside the unit, °C	Number of cycles at 40 MPa, pcs.	Number of cycles at 60 MPa, pcs.	Number of cycles at 80 MPa, pcs.	Number of cycles at 100 MPa, pcs.	Average particle size, nm	Particle distribution
17	37	–	–	–	4	203.3 ± 16.8	Unimodal
18	42	–	–	–	6	191.9 ± 9.4	Unimodal
19	41	–	–	–	8	180.1 ± 11.2	Unimodal
20	42	–	–	–	10	174.0 ± 12.5	Unimodal

in experiments 18–20 have a unimodal particle distribution with the desired average particle size corresponding to the target range of values. At the same time, it was found that increasing the pressure and the number of homogenization cycles directly decreases the particle size of the final emulsion.

At the next stage of the study, we selected the modes of high-pressure homogenization in accordance with Method 2. The oil phase injection in all experiments was carried out at a pressure of 40 MPa. Table 4 shows the homogenization parameters, distribution and average particle sizes for the obtained emulsions.

According to the results of the experiments shown in Table 4, the following conclusions can be drawn. The lipid emulsions obtained in experiments 21–23, 26, 30, 33 have a bimodal distribution of particles by volume, while those obtained in experiments 24, 25, 27, 31, 34–40 are characterized by a narrow unimodal distribution; here, the average particle size does not

correspond to the average particle size of the original drug. The emulsions obtained in experiments 28, 29, 32 show a unimodal distribution of particles with the desired average particle size, which corresponds to the target range of values of the original drug Propofol-Lipuro®.

Thus, both developed methods can be used to obtain a product having characteristics similar to those of the original Propofol-Lipuro® product. Nevertheless, Method 2 is preferred due to the reduced time of obtaining the final product. Moreover, the lower homogenization pressure used to achieve the required parameters (average particle size and particle size distribution by volume and number) results in a longer service life of the working parts of the device. It should be noted that heating of the internal chamber of the unit and the product at homogenization pressures over 80 MPa can lead to oxidation of components included in the emulsion.

Table 4. Homogenization parameters and characteristics of the resulting emulsion according to method 2

No.	Temperature inside the unit, °C	Number of cycles at 40 MPa, pcs.	Number of cycles at 60 MPa, pcs.	Number of cycles at 80 MPa, pcs.	Number of cycles at 100 MPa, pcs.	Average particle size, nm	Particle distribution
21	24	2	–	–	–	464.6 ± 25.2	Bimodal
22	24	4	–	–	–	371.7 ± 22.4	Bimodal
23	24	6	–	–	–	278.0 ± 23.4	Bimodal
24	24	8	–	–	–	267.1 ± 17.5	Unimodal
25	23	10	–	–	–	244.9 ± 18.1	Unimodal
26	25	–	2	–	–	249.2 ± 26.9	Bimodal

Table 4. Continued

No.	Temperature inside the unit, °C	Number of cycles at 40 MPa, pcs.	Number of cycles at 60 MPa, pcs.	Number of cycles at 80 MPa, pcs.	Number of cycles at 100 MPa, pcs.	Average particle size, nm	Particle distribution
27	24	—	4	—	—	225.3 ± 17.1	Unimodal
28	25	—	6	—	—	202.8 ± 15.8	Unimodal
29	26	—	8	—	—	185.9 ± 12.1	Unimodal
30	25	—	10	—	—	179.2 ± 24.5	Bimodal
31	25	—	—	2	—	210.6 ± 16.4	Unimodal
32	28	—	—	4	—	195.8 ± 11.9	Unimodal
33	29	—	—	6	—	181.3 ± 21.8	Bimodal
34	33	—	—	8	—	175.1 ± 11.4	Unimodal
35	33	—	—	10	—	172.0 ± 15.6	Unimodal
36	30	—	—	—	2	180.9 ± 14.4	Unimodal
37	37	—	—	—	4	160.8 ± 13.1	Unimodal
38	42	—	—	—	6	141.4 ± 10.6	Unimodal
39	44	—	—	—	8	144.5 ± 10.1	Unimodal
40	43	—	—	—	10	139.1 ± 11.8	Unimodal

The result obtained in experiment No. 29 was chosen as the most optimal. The obtained product is characterized by a narrow unimodal distribution of particle size by volume and number (Fig. 4); the average particle size in the submicron emulsion is 185.9 ± 12.1 nm.

Five series of propofol emulsion were then prepared in accordance with the conditions of experiment No. 29, for which the following parameters were determined: pH, quantitative propofol content, and zeta potential. The obtained results are presented in Table 5.

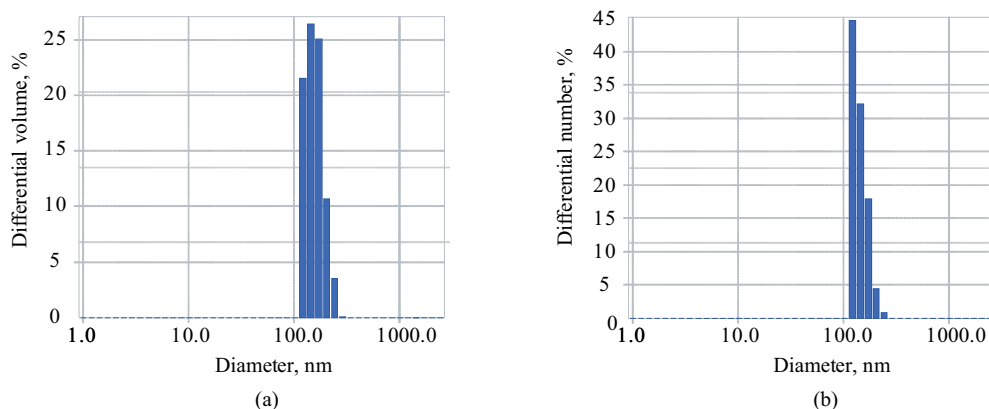


Fig. 4. Differential distribution of volume (a) and numerical (b) fraction of particles by size for a submicron emulsion obtained in experiment No. 29

Table 5. Results of determination of pH, quantitative content of propofol, and zeta potential in the obtained submicron emulsions

Series No. (number/date of manufacture)	Quantitative content, g/L	pH	Zeta potential, mV	Average particle size, nm	Particle distribution
01/15.05.2023	9.97	7.6	35.0	185.5 ± 1.31	Unimodal
02/16.05.2023	9.75	7.4	35.3	186.1 ± 1.42	Unimodal
03/17.05.2023	9.78	7.7	34.5	185.9 ± 1.26	Unimodal
04/20.05.2023	9.99	7.6	34.6	186.2 ± 1.50	Unimodal
05/21.05.2023	9.85	7.6	35.1	184.7 ± 1.38	Unimodal
Average	9.87 ± 0.13	7.60 ± 0.09	34.90 ± 0.42	185.68 ± 0.76	—

Analysis of the results confirms the possibility of obtain reproducible results by high-pressure homogenization.

The quality parameters (pH, quantitative propofol content and particle size) for 5 series of propofol emulsions correspond to the values required for this dosage form. The zeta potential value is 34.9 mV.

CONCLUSIONS

As a result of the conducted studies, a technology for obtaining a submicron emulsion of propofol for parenteral use using a high-pressure homogenizer was developed. The homogenization process carried out at a pressure of 60 MPa for 8 cycles is optimal for obtaining an emulsion with the required characteristics. A distinctive feature of this technology is the addition of the oil phase directly

into the high-pressure homogenizer directly during the dispersion process.

The physicochemical characteristics of the obtained submicron propofol emulsion correspond to the original Propofol-Lipuro[®] product. The average value of propofol quantitative content in the 5 obtained series was 9.87 ± 0.13 g/L at a pH of 7.60 ± 0.09 . The zeta potential is 34.90 ± 0.42 mV and the average particle size is 185.68 ± 0.76 nm. Particle distribution is unimodal for all obtained emulsions.

Authors' contribution

All the authors actively participated in the discussion, analysis, and design of the experiment, processing the obtained results, writing the text of the article and discussing it.

The authors declare no conflict of interest.

REFERENCES

1. Sahinovic M.M., Struys M.M.R.F., Absalom A.R. Clinical Pharmacokinetics and Pharmacodynamics of Propofol. *Clin. Pharmacokinet.* 2018;57:1539–1558. <https://doi.org/10.1007/s40262-018-0672-3>
2. Kotani Y., Nakajima Y., Hasegawa T., *et al.* Propofol Exerts Greater Neuroprotection with Disodium Edetate than without It. *J. Cereb. Blood Flow Metab.* 2008;28(2):354–366. <https://doi.org/10.1038/sj.jcbfm.9600532>
3. Kotani Y., Shimazawa M., Yoshimura S., Iwama T., Hara H. The experimental and clinical pharmacology of propofol, an anesthetic agent with neuroprotective properties. *CNS Neurosci. Ther.* 2008;14(2):95–106. <https://doi.org/10.1111/j.1527-3458.2008.00043.x>
4. Walsh C.T. Propofol: Milk of Amnesia. *Cell.* 2018;175(1):10–13. <https://doi.org/10.1016/j.cell.2018.08.031>
5. Baker M.T., Naguib M., *et al.* Propofol: The challenges of formulation. *Anesthesiology.* 2005;103(4):860–876. <https://doi.org/10.1097/00005542-200510000-00026>
6. Thompson K., Goodale D. The Recent Development of Propofol (DIPRIVAN®). *Intensive Care Med.* 2000;26(3):400–404. <https://doi.org/10.1007/PL00003783>
7. Kam E., Abdul-Latif M.S., McCluskey A. Comparison of Propofol-Lipuro with propofol mixed with lidocaine 10 mg on propofol injection pain. *Anaesthesia.* 2004;59(12):1167–1169. <https://doi.org/10.1111/j.1365-2044.2004.03964.x>
8. Sorokina Ye.Yu. Propofol in modern multicomponent general anesthesia. *Meditcina neotlozhnykh sostoyanii = Emergency Medicine.* 2014;3(58):69–75 (in Russ.).
9. Pramanik C., Kotharkar S.A., Patil P., Gotrane D., More Y.W., Borhade A.S., Chaugule B., Khaladkar T.P., Neelakandan K., Chaudhari A., Kulkarni M.G., Tripathy N.K., Gurjar M.K. Commercial Manufacturing of Propofol: Simplifying the Isolation Process and Control on Related Substances. *Org. Process Res. Dev.* 2014;18(1):152–156. <https://doi.org/10.1021/op400300t>
10. Onugwu A.L., Nwagwu C.S., Onugwu O.S., Echezona A.C., *et al.* Nanotechnology based drug delivery systems for the treatment of anterior segment eye diseases. *J. Control. Release.* 2023;354:465–488. <https://doi.org/10.1016/j.jconrel.2023.01.018>
11. Honary S., Zahir F. Effect of Zeta Potential on the Properties of Nano-Drug Delivery Systems – A Review (Part 1). *Tropical J. Pharmaceutical Res.* 2013;12(2):19. <https://doi.org/10.4314/tjpr.v12i2.19>
12. Gunar O.V., Dorenskaya A.V. Determination of the size of fat droplets in emulsions for parenteral use. *Farmatsiya = Pharmacy.* 2022;71(5):11–17 (in Russ.). <https://doi.org/10.29296/25419218-2022-05-02>
13. Alekseev K.V., Kedik S.A. *Farmatsevticheskaya tekhnologiya (Pharmaceutical Technology)*. Moscow: IFT; 2025. 592 p. (in Russ.).
14. Alison G.F. Top ten considerations in the development of parenteral emulsions. *Pharm. Sci. Technol. Today.* 1999;2(4):134–143. [https://doi.org/10.1016/S1461-5347\(99\)00141-8](https://doi.org/10.1016/S1461-5347(99)00141-8)
15. Kumar M., Bishnoi R.S., Shukla A.K., Jain C.P. Techniques for Formulation of Nanoemulsion Drug Delivery System: A Review. *Prev. Nutr. Food Sci.* 2019;24(3):225–234. <https://doi.org/10.3746/pnf.2019.24.3.225>
16. Çinar K. A Review on Nanoemulsion: preparation method and method stability. *Tarkya University J. Eng. Sci.* 2017;18(1):73–87.
17. Prasetyo B., Shamsuddin A., Azmi N. Preparation and Physical Stability Evaluation of Palm Oil-Based Nanoemulsion as a Drug Delivery System for Propofol. *Jurnal Sains Kesihatan Malaysia (Malaysian J. Health Sci.)*. 2018;16(02):5–13. <https://doi.org/10.17576/JSKM-2018-1602-02>

СПИСОК ЛИТЕРАТУРЫ

1. Sahinovic M.M., Struys M.M.R.F., Absalom A.R. Clinical Pharmacokinetics and Pharmacodynamics of Propofol. *Clin. Pharmacokinet.* 2018;57:1539–1558. <https://doi.org/10.1007/s40262-018-0672-3>
2. Kotani Y., Nakajima Y., Hasegawa T., *et al.* Propofol Exerts Greater Neuroprotection with Disodium Edetate than without It. *J. Cereb. Blood Flow Metab.* 2008;28(2):354–366. <https://doi.org/10.1038/sj.jcbfm.9600532>
3. Kotani Y., Shimazawa M., Yoshimura S., Iwama T., Hara H. The experimental and clinical pharmacology of propofol, an anesthetic agent with neuroprotective properties. *CNS Neurosci. Ther.* 2008;14(2):95–106. <https://doi.org/10.1111/j.1527-3458.2008.00043.x>
4. Walsh C.T. Propofol: Milk of Amnesia. *Cell.* 2018;175(1):10–13. <https://doi.org/10.1016/j.cell.2018.08.031>
5. Baker M.T., Naguib M., *et al.* Propofol: The challenges of formulation. *Anesthesiology.* 2005;103(4):860–876. <https://doi.org/10.1097/00005542-200510000-00026>
6. Thompson K., Goodale D. The Recent Development of Propofol (DIPRIVAN®). *Intensive Care Med.* 2000;26(3):400–404. <https://doi.org/10.1007/PL00003783>
7. Kam E., Abdul-Latif M.S., McCluskey A. Comparison of Propofol-Lipuro with propofol mixed with lidocaine 10 mg on propofol injection pain. *Anaesthesia.* 2004;59(12):1167–1169. <https://doi.org/10.1111/j.1365-2044.2004.03964.x>
8. Сорокина Е.Ю. Пропофол в современной поликомпонентной общей анестезии. *Медицина неотложных состояний.* 2014;3(58):69–75.
9. Pramanik C., Kotharkar S.A., Patil P., Gotrane D., More Y.W., Borhade A.S., Chaugule B., Khaladkar T.P., Neelakandan K., Chaudhari A., Kulkarni M.G., Tripathy N.K., Gurjar M.K. Commercial Manufacturing of Propofol: Simplifying the Isolation Process and Control on Related Substances. *Org. Process Res. Dev.* 2014;18(1):152–156. <https://doi.org/10.1021/op400300t>
10. Onugwu A.L., Nwagwu C.S., Onugwu O.S., Echezona A.C., *et al.* Nanotechnology based drug delivery systems for the treatment of anterior segment eye diseases. *J. Control. Release.* 2023;354:465–488. <https://doi.org/10.1016/j.jconrel.2023.01.018>
11. Honary S., Zahir F. Effect of Zeta Potential on the Properties of Nano-Drug Delivery Systems – A Review (Part 1). *Tropical J. Pharmaceutical Res.* 2013;12(2):19. <https://doi.org/10.4314/tjpr.v12i2.19>
12. Гунар О.В., Доренская А.В. Определение размеров жировых капель в эмульсиях для парентерального применения. *Фармация.* 2022;71(5):11–17. <https://doi.org/10.29296/25419218-2022-05-02>
13. Алексеев К.В., Кедик С.А. *Фармацевтическая технология*. М.: АО ИФТ; 2025. 592 с.
14. Alison G.F. Top ten considerations in the development of parenteral emulsions. *Pharm. Sci. Technol. Today.* 1999;2(4):134–143. [https://doi.org/10.1016/S1461-5347\(99\)00141-8](https://doi.org/10.1016/S1461-5347(99)00141-8)
15. Kumar M., Bishnoi R.S., Shukla A.K., Jain C.P. Techniques for Formulation of Nanoemulsion Drug Delivery System: A Review. *Prev. Nutr. Food Sci.* 2019;24(3):225–234. <https://doi.org/10.3746/pnf.2019.24.3.225>
16. Çinar K. A Review on Nanoemulsion: preparation method and method stability. *Tarkya University J. Eng. Sci.* 2017;18(1):73–87.
17. Prasetyo B., Shamsuddin A., Azmi N. Preparation and Physical Stability Evaluation of Palm Oil-Based Nanoemulsion as a Drug Delivery System for Propofol. *Jurnal Sains Kesihatan Malaysia (Malaysian J. Health Sci.)*. 2018;16(02):5–13. <https://doi.org/10.17576/JSKM-2018-1602-02>

18. Rooimans T., Damen M., Markesteyn C.M.A., Schuurmans C.C.L., de Zoete N.H.C., van Hasselt P.M., Hennink W.E., van Nostrum C.F., Hermes M., Besseling R., Vromans H. Development of a compounded propofol nanoemulsion using multiple non-invasive process analytical technologies. *Int. J. Pharm.* 2023;640:122960. <https://doi.org/10.1016/j.ijpharm.2023.122960>
19. Prasetyo B., Azmi N., Shamsuddin A. *In vivo* characterization of less painful propofol nanoemulsion using palm oil for intravenous drug delivery. *Int. J. Appl. Pharm.* 2019;11(4): 98–102. <https://doi.org/10.22159/ijap.2019v11i4.33039>
18. Rooimans T., Damen M., Markesteyn C.M.A., Schuurmans C.C.L., de Zoete N.H.C., van Hasselt P.M., Hennink W.E., van Nostrum C.F., Hermes M., Besseling R., Vromans H. Development of a compounded propofol nanoemulsion using multiple non-invasive process analytical technologies. *Int. J. Pharm.* 2023;640:122960. <https://doi.org/10.1016/j.ijpharm.2023.122960>
19. Prasetyo B., Azmi N., Shamsuddin A. *In vivo* characterization of less painful propofol nanoemulsion using palm oil for intravenous drug delivery. *Int. J. Appl. Pharm.* 2019;11(4): 98–102. <https://doi.org/10.22159/ijap.2019v11i4.33039>

About the Authors

Herman D. Moshkov, Postgraduate Student, Department of Biotechnology and Industrial Pharmacy, M.V. Lomonosov Institute of Fine Chemical Technologies, MIREA – Russian Technological University (78, Vernadskogo pr., Moscow, 119454, Russia). E-mail: hdmannihalation@gmail.com. <https://orcid.org/0009-0009-0598-6992>

Andrey M. Normov, Laboratory Assistant, Department of Biotechnology and Industrial Pharmacy, M.V. Lomonosov Institute of Fine Chemical Technologies, MIREA – Russian Technological University (78, Vernadskogo pr., Moscow, 119454, Russia); Technologist of the Production Department, Institute of Pharmaceutical Technologies (of. 1, 21, Skolkovskoe sh., Moscow, 121353, Russia). E-mail: a.m.normov@ipt.ru.com. <https://orcid.org/0009-0004-7720-6530>

Elizaveta A. Shnyak, Can. Sci. (Pharm.), Associate Professor, Department of Biotechnology and Industrial Pharmacy, M.V. Lomonosov Institute of Fine Chemical Technologies, MIREA – Russian Technological University (78, Vernadskogo pr., Moscow, 119454, Russia); Senior Process Engineer, Institute of Pharmaceutical Technologies (of. 1, 21, Skolkovskoe sh., Moscow, 121353, Russia). E-mail: elizaweta__@mail.ru. ResearcherID H-9402-2013, RSCI SPIN-code 7112-7197, <https://orcid.org/0000-0001-8560-7060>

Alexey V. Panov, Can. Sci. (Chem.), Associate Professor, Department of Biotechnology and Industrial Pharmacy, M.V. Lomonosov Institute of Fine Chemical Technologies, MIREA – Russian Technological University (78, Vernadskogo pr., Moscow, 119454, Russia); Director of Science, Institute of Pharmaceutical Technologies (of. 1, 21, Skolkovskoe sh., Moscow, 121353, Russia). E-mail: panov@mirea.ru. Scopus Author ID 59339673200, RSCI SPIN-code 5369-3083, <https://orcid.org/0000-0002-1603-143X>

Об авторах

Мошков Герман Дмитриевич, аспирант, кафедра биотехнологии и промышленной фармации, Институт тонких химических технологий им. М.В. Ломоносова, ФГБОУ ВО «МИРЭА – Российский технологический университет» (119454, Россия, Москва, пр-т Вернадского, д. 78). E-mail: hdmannihalation@gmail.com. <https://orcid.org/0009-0009-0598-6992>

Нормов Андрей Максимович, лаборант, кафедра биотехнологии и промышленной фармации, Институт тонких химических технологий им. М.В. Ломоносова, ФГБОУ ВО «МИРЭА – Российский технологический университет» (119454, Россия, Москва, пр-т Вернадского, д. 78); технолог производственного отдела, АО «Институт фармацевтических технологий» (121353, Россия, Москва, Сколковское ш., д. 21, оф. 1). E-mail: a.m.normov@ipt.ru.com. <https://orcid.org/0009-0004-7720-6530>

Шняк Елизавета Александровна, к.фарм.н., доцент, кафедра биотехнологии и промышленной фармации, Институт тонких химических технологий им. М.В. Ломоносова, ФГБОУ ВО «МИРЭА – Российский технологический университет» (119454, Россия, Москва, пр-т Вернадского, д. 78); старший инженер-технолог, АО «Институт фармацевтических технологий» (121353, Россия, Москва, Сколковское ш., д. 21, оф. 1). E-mail: elizaweta__@mail.ru. ResearcherID H-9402-2013, SPIN-код РИНЦ 7112-7197, <https://orcid.org/0000-0001-8560-7060>

Панов Алексей Валерьевич, к.х.н., доцент, кафедра биотехнологии и промышленной фармации, Институт тонких химических технологий им. М.В. Ломоносова, ФГБОУ ВО «МИРЭА – Российский технологический университет» (119454, Россия, Москва, пр-т Вернадского, д. 78); директор по науке, АО «Институт фармацевтических технологий» (121353, Россия, Москва, Сколковское ш., д. 21, оф. 1). E-mail: panov@mirea.ru. Scopus Author ID 59339673200, SPIN-код РИНЦ 5369-3083, <https://orcid.org/0000-0002-1603-143X>

Translated from Russian into English by H. Moshkov

Edited for English language and spelling by Thomas A. Beavitt

Synthesis and processing of polymers
and polymeric composites
Синтез и переработка полимеров и композитов
на их основе

UDC 541.14:535.31

<https://doi.org/10.32362/2410-6593-2025-20-4-310-323>

EDN QWUHUW



RESEARCH ARTICLE

Aging effects on polystyrene thin films containing high aromatic moiety compounds under UV irradiation

Shahad M. Hussain¹, Ahmed Ahmed¹, Mohammed Kadhom², Dina S. Ahmed³, Shams S. Hameed⁴, Omar G. Mousa⁵, Ahmed A. Ahmed⁶, Muna Bufaroosha⁷✉, Rahimi Yusop⁸, Emad Yousif¹✉

¹ Department of Chemistry, College of Science, Al-Nahrain University, Baghdad, Iraq

² Department of Environment, College of Energy and Environmental Science, Al-Karkh University of Science, Baghdad, Iraq

³ Department of Chemical Industries, Institute of Technology-Baghdad, Middle Technical University, Baghdad, Iraq

⁴ General Directorate of Education Baghdad, Karkh 1, Ministry of Education, Baghdad, Iraq

⁵ General Directorate of Education Baghdad, Resafa 1, Ministry of Education, Baghdad, Iraq

⁶ Polymer Research Unit, College of Science, Mustansiriyah University, Baghdad, Iraq

⁷ Department of Chemistry, College of Science, United Arab Emirates University, Al-Ain, United Arab Emirates

⁸ School of Chemical Sciences and Food Technology, Faculty of Science and Technology, Universiti Kebangsaan Malaysia, Bangi, Selangor, Malaysia

✉ Corresponding authors, e-mail: Dr. Muna Bufaroosha, muna.bufaroosha@uaeu.ac.ae,
Dr. Emad Yousif, emad.yousif@nahrainuniv.edu.iq

Abstract

Objectives. Exposure to ultraviolet (UV) radiation initiates a photo-oxidative degradation process in plastics that causes broken chemical bonds, weight loss, and weakened crosslinking, as well as the formation of free radicals and release of volatile substances. The work aims to study the influence of UV radiation on polystyrene films containing low concentrations of highly aromatic Schiff bases.

Methods. Utilizing the described casting technique, polystyrene films containing a small quantity of strong highly aromatic Schiff bases were produced. These films were then subjected to 300 h of UV irradiation. Following irradiation, analyses were conducted on the infrared spectra, weight loss, and surface morphology of the polystyrene.

Results. The surface of the sheets was initially smooth and free of wrinkles. However, following irradiation, remarkable morphological changes were observed as the surface became more uneven. Intentional perforations and imperfections introduced into the examined surfaces were used to indicate the degradation of the polymer matrices.

Conclusions. Highly aromatic Schiff bases act as photostabilizers to significantly reduce the extent of photodegradation in polystyrene films when compared to films with no additives.

Keywords

polystyrene films, carbonyl group index, photooxidation, photodegradation, surface roughness, Schiff's foundations

Submitted: 11.09.2024

Revised: 24.02.2025

Accepted: 21.06.2025

For citation

Hussain Sh.M., Ahmed A., Kadhom M., Ahmed D.S., Hameed Sh.S., Mousa O.G., Ahmed A.A., Bufaroosha M., Yusop R., Yousif E. Aging effects on polystyrene thin films containing high aromatic moiety compounds under UV irradiation. *Tonk. Khim. Tekhnol. = Fine Chem. Technol.* 2025;20(4):310–323. <https://doi.org/10.32362/2410-6593-2025-20-4-310-323>

НАУЧНАЯ СТАТЬЯ

Влияние ультрафиолетового облучения на старение тонких пленок полистирола с высоким содержанием ароматических компонентов

Shahad M. Hussain¹, Ahmed Ahmed¹, Mohammed Kadhom², Dina S. Ahmed³, Shams S. Hameed⁴, Omar G. Mousa⁵, Ahmed A. Ahmed⁶, Muna Bufaroosha⁷✉, Rahimi Yusop⁸, Emad Yousif¹✉

¹ Department of Chemistry, College of Science, Al-Nahrain University, Baghdad, Iraq

² Department of Environment, College of Energy and Environmental Science, Al-Karkh University of Science, Baghdad, Iraq

³ Department of Chemical Industries, Institute of Technology-Baghdad, Middle Technical University, Baghdad, Iraq

⁴ General Directorate of Education Baghdad, Karkh 1, Ministry of Education, Baghdad, Iraq

⁵ General Directorate of Education Baghdad, Resafa 1, Ministry of Education, Baghdad, Iraq

⁶ Polymer Research Unit, College of Science, Mustansiriyah University, Baghdad, Iraq

⁷ Department of Chemistry, College of Science, United Arab Emirates University, Al-Ain, United Arab Emirates

⁸ School of Chemical Sciences and Food Technology, Faculty of Science and Technology, Universiti Kebangsaan Malaysia, Bangi, Selangor, Malaysia

✉ Авторы для переписки, e-mail: Dr. Muna Bufaroosha, muna.bufaroosha@uaeu.ac.ae,
Dr. Emad Yousif, emad.yousif@nahrainuniv.edu.iq

Аннотация

Цели. Воздействие ультрафиолетового (УФ) излучения инициирует процесс фотоокислительной деградации пластмасс, сопровождающийся разрушением химических связей, выделением летучих веществ, как следствие, потерей массы, а также образованием свободных радикалов. Цель работы — установление влияния УФ-излучения на полистирольные пленки, содержащие низкие концентрации оснований Шиффа с расширенной цепью сопряжений.

Методы. С использованием технологии литья получены пленки из полистирола, содержащие небольшое количество оснований Шиффа с расширенной цепью сопряжений. Прослежено влияние УФ-облучения полученных пленок (время воздействия — 300 ч) на их строение, изученное методом инфракрасной спектроскопии, массу и морфологию поверхности.

Результаты. Изначально гладкая и не содержащая дефектов поверхности полистирольная пленка после облучения претерпела значительные морфологические изменения и становилась неровной. Сделан вывод о разрушении полимерной матрицы.

Выводы. Показано, что основания Шиффа с расширенной цепью сопряжений действуют как фотостабилизаторы, обеспечивающие уменьшение степени фотодеградации пленок из полистирола по сравнению с системами, не содержащими добавок этих соединений.

Ключевые слова

пленки из полистирола, индекс карбонильной группы, фотоокисление, фотодеградация, шероховатость поверхности, основания Шиффа

Поступила: 11.09.2024

Доработана: 24.02.2025

Принята в печать: 21.06.2025

Для цитирования

Hussain Sh.M., Ahmed A., Kadhom M., Ahmed D.S., Hameed Sh.S., Mousa O.G., Ahmed A.A., Bufaroosha M., Yusop R., Yousif E. Aging effects on polystyrene thin films containing high aromatic moiety compounds under UV irradiation. *Tonk. Khim. Tekhnol. = Fine Chem. Technol.* 2025;20(4):310–323. <https://doi.org/10.32362/2410-6593-2025-20-4-310-323>

1. INTRODUCTION

Polystyrene (PS), with a molecular weight of 100000 to 400000 is one of the most commonly used thermoplastic polymers [1]. It is derived from styrene polymerization to form either foam or solid final structures. One of its primary benefits lies in its cost-effectiveness due to being based on inexpensive feedstock materials. Furthermore, its low weight and chemical inertness make it impervious to interact with other chemicals, including acids and bases [2]. As documented in previous reports, PS is adaptable to various deposition types [3]. However, it is also non-biodegradable, flammable, and soluble in various chlorinated solvents. Despite these drawbacks, PS has been extensively applied in many commercial products, from simple packaging to intricate engineering tasks [4]. The arrangement of phenyl groups along the polymer chain influences PS's crystallinity [5]. Due to random phenyl group positioning, commercially valuable atactic PS is amorphous, while syndiotactic PS is crystalline with phenyl groups formed alternately on both sides of the polymer chain [1].

The main environmental variables affecting the durability of polymers used in outdoor settings are solar irradiation, weather patterns, temperature, humidity, and pollutants. When these factors are compared, ultraviolet (UV) radiation is generally considered to be the most significant [6]. Due to high oxygen levels and the UV sensitivity of microplastics (MPs), multiple aging processes occur upon their discharge to landfills or the environment. Some of the steps in these processes include direct exposure to UV radiation from the sun, thermo-oxidative breakdown, physical stress, and biodegradation. The high commercial value of atactic PS is due to its amorphous structure, which derives from the randomly positioned phenyl groups. In contrast, syndiotactic PS has an alternating arrangement of phenyl groups along the polymer chain, resulting in a crystalline structure [1].

As a result of aging processes, cracks and fragmentation are developed within plastic polymers [7, 8]. MPs constitute tiny fragments of synthetic polymers discovered in freshwater, marine ecosystems, sediment, and within living organisms. These particles significantly threaten aquatic environments and organisms, causing ecological harm through ecotoxicological pathways [9].

By altering the surface properties of plastic debris, the above-described processes escalate the release of intermediary chemical additives including pigments, antioxidants, flame retardants, stabilizers, and plasticizers. As a consequence of their discharged from MPs, such additives introduce harmful chemicals into marine ecosystems [10]. Moreover, due to their diminutive size, high hydrophobicity, rugged particle

surfaces, and enhanced mobility, MPs can absorb various organic pollutants in aquatic environments. Consequently, there has been a surge in interest in investigating the potential ecotoxicological ramifications of MPs as carriers of pollutants [11]. The present work sets out to demonstrate the efficiency of adding highly aromatic Schiff bases at low concentrations as photostabilizers as a means of mitigating the photodegradation of PS films under extended UV irradiation. This provides another means to enhance the photostability of polymeric materials in addition to those presented previously [12–14]. The described Schiff bases, which function as UV absorbers and stabilizers, can be incorporated into PS to improve its resistance to photodegradation. In order to prevent PS photodecomposition, such stable compounds are required to have a high concentration of heteroatoms and aromatic moieties such as phenyl and heterocycles.

In the present study, we demonstrate the effective use of highly aromatic Schiff bases at low concentrations as photostabilizers to significantly reduce the photodegradation of PS films under 300 h UV exposure. This work contributes to ongoing research on the photostabilization of polymeric materials.

2. MATERIALS AND METHODS

2.1. Chemicals and devices

The PS used in this study was obtained from *Sigma-Aldrich* chemical company (*Gillingham*, United Kingdom). Fourier transform infrared (FTIR) spectra spanning the range of 4000–400 cm^{-1} were acquired using a FT/IR-4200 spectrometer (*Jasco*, Tokyo, Japan). The PS films underwent irradiation at a temperature of 25°C, a maximum wavelength of 365 nm, and an intensity of $6.43 \cdot 10^{-9} \text{ ein/dm}^2\cdot\text{s}$. This irradiation process was conducted using a QUV tester, an accelerated weather meter sourced from the *Q-Panel* company (*Homestead*, FL, USA). The surface of the PS films was analyzed using a *Veeco Instrument* atomic force microscope (AFM) (*Plainview*, NY, USA). Scanning electron microscopy (SEM) was also employed to examine the PS surface. This process, which utilized an *Inspect S50* microscope from the *FEI Company* (*Czechia*, Czech Republic), was operated at an accelerating voltage of 15 kV. Microscopic images of the PS surface were captured using a *Meiji Techno* microscope (Tokyo, Japan). The thickness of the PS films was measured to be approximately 40 μm using a Digital Vernier Caliper 2610 A micrometer from *Vogel GmbH* (*Kevelaer*, Germany). The films were supported using aluminum plate stands with a thickness of 0.6 mm from *Q-Panel* company (*Homestead*, FL, USA).

2.2. Synthesis of the compounds

2.2.1. Synthesis of compound 1

A solution consisting of 5 mL of hydrazine hydrate (*Merck*, Germany) and 10 mL of 0.079 mol methyl benzoate (*Merck*, Germany) was refluxed for 4 h. Following this, 8 mL of ethanol was added, and the mixture was refluxed for an additional hour. After cooling, the product was separated via filtration and left to dry in readiness for the next step [15].

2.2.2. Synthesis of compound 2

3.4 g of benzohydrazide (0.024 mol, *Merck*, Germany) was dissolved in 30 mL of absolute ethanol (*Alfa Chemical Co.*, China) along with 2 g potassium hydroxide (0.035 mol, *Merck*, Germany) and stirred for 15 min. Following this, 2 mL of a 0.033 mol carbon disulfide solution (*Fisher Scientific*, MA, USA) was added and the mixture was continuously stirred for 18 h until it became homogeneous. Subsequently, 10 mL of hydrazine hydrate (*Merck*, Germany) was added to the potassium xanthate (*Merck*, Germany) product. The resulting mixture underwent reflux with stirring, resulting in a homogeneous solution that is associated with the release of hydrogen sulfide gas. The reaction was stopped when the release of hydrogen sulfide ceased (as indicated by the absence of a reaction with lead acetate paper). After filtration, the reaction mixture was diluted with 10 mL of cold water and acidified using concentrated hydrochloric acid (*Alfa Chemical Co.*, China), resulting in the formation of a white precipitate [15].

2.2.3. Synthesis of compound 3

The compound 2 (2 mol, 1 g) was combined with terephthalaldehyde (1 mol, 0.3 g, *Merck*, Germany) in 10 mL of dimethylformamide (DMF, *Alfa Chemical Co.*, China), along with two drops of glacial acetic acid (*Alfa Chemical Co.*, China). The mixture was then refluxed for 7 h. Following this, the solution was cooled to prompt the precipitation of the product, which was then washed with ethanol [15].

2.2.4. Synthesis of compounds 4 and 5

0.5 g of sulfamethoxazole (*Merck*, Germany, to prepare compound 4) or methyl dopa (*Merck*, Germany) to prepare compound 5) along with 0.2 mL triethylamine (0.001 mol) were dissolved in 10 mL of DMF in two 50 mL round bottom flasks each fitted with a magnetic stirring bar. The flask was cooled to 0°C for 30 min while stirring, and then 0.1 mL of 0.001 mol chloroacetyl chloride was slowly added in small portions. The mixture was stirred overnight at room temperature (25°C). Following reaction completion, the mixture was transferred into ice water, filtered, and the product

was washed with water. The yields were purified using ether [16].

2.2.5. Reaction of compound 3 with compounds 4 and 5

Compound 3 was dissolved in 10 mL of DMF in a round bottom flask utilizing 1 mol (0.1 g) of the compound. Following complete dissolution, 2 mol (0.05 g) of K_2CO_3 was added. Subsequently, compounds 4 and 5 were added in a total amount of 4 mol (0.2 g). The mixture was stirred for an extended period and then transferred into a container of ice water. Following this, the mixture was filtered and the resulting solid was allowed to desiccate in readiness for the subsequent reaction [17]. By this means, compounds 6 and 7 were prepared.

2.3. Preparation of PS films

5 gram of PS was stirred in 100 mL of chloroform (*Merck*, Germany) for 90 min at 25°C. Compounds 6 and 7, weighing 25 mg and constituting 0.5% of the total weight, were added to the PS solution. The resulting mixture was stirred for 30 min at 25°C. The homogeneous mixture was then poured onto clean glass slides to a thickness of approximately 40 μm and allowed to dry for 24 h at 25°C.

2.4. Accelerated UV weathering

The films were subjected to 300 h of accelerated UV weathering testing using the QUV tester from *Q-Panel* company (*Homestead*, FL, USA). During each weathering cycle, the films were continuously exposed to UV radiation having a maximum wavelength of 365 nm and intensity of $6.43 \cdot 10^{-9} \text{ ein/dm}^2\cdot\text{s}$. Testing intervals were set at 0, 50, 100, 150, 200, 250, and 300 h of exposure at a temperature of 25°C. After each duration of exposure, every group underwent extraction for measurements.

2.5. Monitoring UV degradation by FTIR spectrophotometry of PS films

Under photolytic conditions, PS degradation occurs, resulting in the generation of small polymer fragments containing carbonyl (C=O) groups. The FTIR spectra of the irradiated PS films were measured at different irradiation durations. The functional group index ($I_{C=O}$) was determined by calculating the absorbance of the functional group ($A_{C=O}$) and the reference peak (A_T) using Eq. (1) [18, 19].

$$I_{C=O} = \frac{A_{C=O}}{A_T} \quad (1)$$

2.6. Weight loss of PS films

The sheets were weighed before irradiation (W_0) and after irradiation at different time intervals (W_t). The estimation of the polymer weight loss percentage due to irradiation was calculated using Eq. (2) [19].

$$\text{Weight loss (\%)} = \frac{W_0 - W_t}{W_0} \times 100. \quad (2)$$

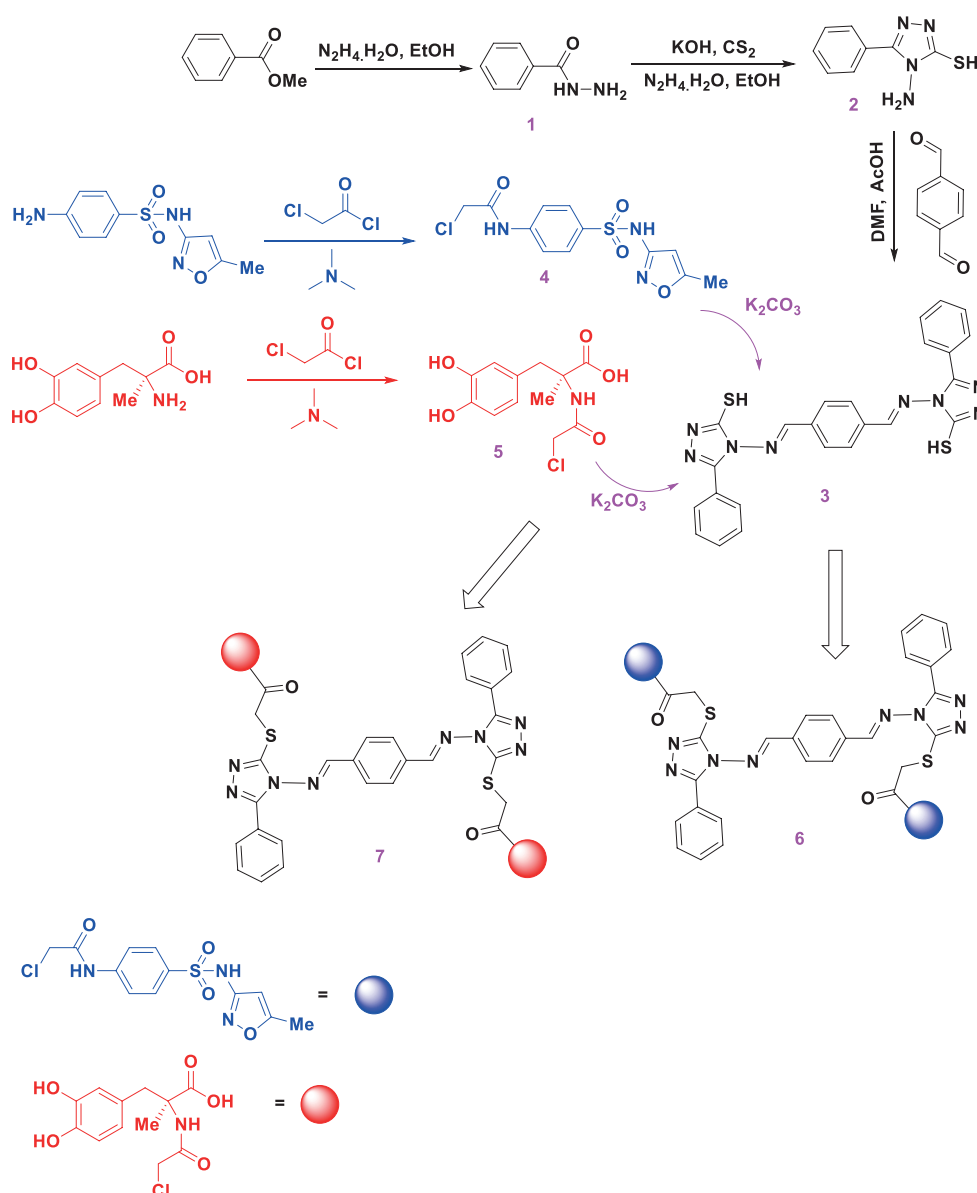
3. RESULTS AND DISCUSSION

This synthesis process yielded compounds 1–7, which were utilized in the fabrication of PS films. The compounds were obtained with yields ranging from 40% to 96% (Scheme). Table 1 presents the physical characteristics of compounds 1 to 7.

Table 1. Physical properties of compounds 1–7

No.	<i>M</i> , wt %	Yield, %	Color	Melting point, °C
1	136.15	50	White	112–114
2	192.24	96	White	200–202
3	482.58	61	Orange	300
4	329.50	40	Orange	110–112
5	287.50	70	Brown	250
6	1069.18	50	Yellow	250
7	985.06	65	Brown	130–131

Compound 1 was synthesized by reacting salt with hydrazine hydrate. The synthesis was confirmed using an FTIR device, which detected a peak at



Scheme. Synthesis of compounds 1–7

1632 cm^{-1} corresponding to the C=N group of the triazole ring. Two distinct stretching vibration bands additionally observed at 3294 and 3189 cm^{-1} were attributed to the NH_2 group. The FTIR spectra of the prepared Schiff base indicated the disappearance of the stretching band of the primary amine NH_2 at 3294 and 3189 cm^{-1} . In contrast, a stretching band at 1657 cm^{-1} , associated with the creation of the imine group $\text{HC}=\text{N}$, appeared. Table 2 shows the FTIR analysis for compounds 2–7, and Fig. 1 shows FTIR spectra for compounds 2–7. Furthermore, Table 3 and Figs. 2 and 3 present the ^1H nuclear magnetic resonance (NMR) and ^{13}C NMR characteristic spectra, respectively, for compounds 2, 3, and 6.

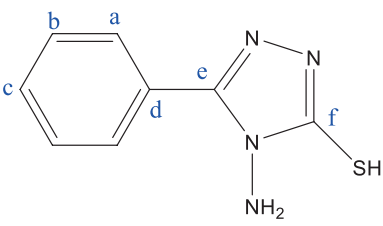
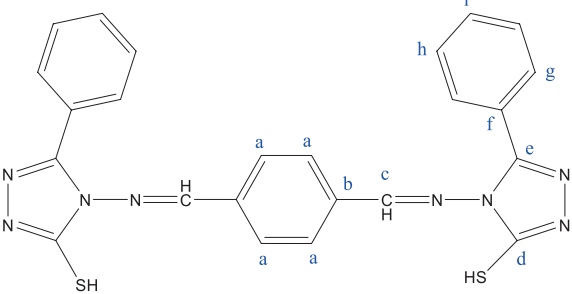
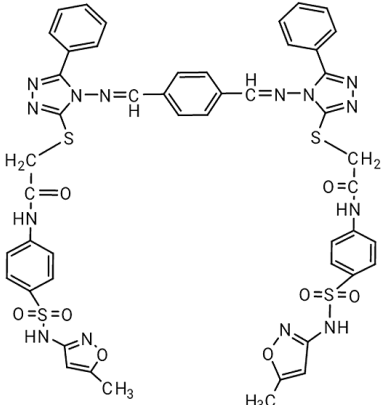
Table 2. FTIR characteristic spectra for compounds 2–7

No.	Frequency numbers, cm^{-1}
2	3294 and 3189 cm^{-1} for asymmetric and symmetric $[\text{NH}_2]$, 3002 cm^{-1} for $[\text{C}-\text{H}]$ aromatic, 2663 cm^{-1} for $[\text{S}-\text{H}]$, 1632 cm^{-1} for $[\text{C}=\text{N}]$, and 662 cm^{-1} for $[\text{C}-\text{S}]$

Table 2. Continued

No.	Frequency numbers, cm^{-1}
3	3067 cm^{-1} for $[\text{C}-\text{H}]$ aromatic, 2932 cm^{-1} for $[\text{C}-\text{H}]$ aliphatic, 2752 cm^{-1} for $[\text{S}-\text{H}]$, 1657 cm^{-1} for $[\text{C}=\text{N}]$, and 688 cm^{-1} for $[\text{C}-\text{S}]$
4	3040 cm^{-1} for $[\text{C}-\text{H}]$ aromatic, 1620 cm^{-1} for $[\text{C}=\text{O}]$ of amide, 3332 cm^{-1} for $[\text{NH}]$, 2982 and 2930 cm^{-1} for $[\text{C}-\text{H}]$ aliphatic, and 715 cm^{-1} for $[\text{C}-\text{Cl}]$
5	1691 cm^{-1} for $[\text{C}=\text{O}]$ of amide, 3050 cm^{-1} for $[\text{C}-\text{H}]$ aromatic, 2983 cm^{-1} $[\text{C}-\text{H}]$ aliphatic, 1655 cm^{-1} for $[\text{C}=\text{N}]$, and 763 cm^{-1} for $[\text{C}-\text{Cl}]$
6	1612 cm^{-1} for $[\text{C}=\text{N}]$ of Schiff base, 1518 cm^{-1} for $[\text{C}=\text{N}]$ of triazole ring, 1661 cm^{-1} for $[\text{C}=\text{O}]$ of amide, 1149 cm^{-1} for symmetric $[\text{S}=\text{O}]$, 1302 cm^{-1} for asymmetric $[\text{S}=\text{O}]$, 3058 cm^{-1} for $[\text{C}-\text{H}]$ aromatic, 2965 and 2931 cm^{-1} $[\text{C}-\text{H}]$ aliphatic
7	1613 cm^{-1} for $[\text{C}=\text{N}]$ of Schiff base, 1502 cm^{-1} for $[\text{C}=\text{N}]$ of triazole ring, 1663 cm^{-1} for $[\text{C}=\text{O}]$ of amide, 3051 cm^{-1} for $[\text{C}-\text{H}]$ aromatic, 2991 and 2931 cm^{-1} $[\text{C}-\text{H}]$ aliphatic

Table 3. ^1H NMR and ^{13}C NMR characteristic spectra for compounds [2, 3, and 6]

No.	Structure	Chemical shift, ppm
2		^1H NMR shows: δ = (7.5 ppm, 8.05 ppm, m) for protons at the aromatic ring, (5.9 ppm, s) for NH_2 , and (10 ppm, s) for SH ^{13}C NMR shows: δ = (166.8 ppm) for carbon at f, (149.4 ppm) at e, and (128, 128.4, 128.9, and 130.4 ppm) for carbons at a, b, c, and d
3		^1H NMR shows: δ = (8.02 ppm, s) for protons at aromatic ring that bonded to $\text{C}=\text{N}$, (8.3 ppm, s) for $\text{HC}=\text{N}$, (14.4 ppm, s) for $\text{S}-\text{H}$, and (7.65, 7.66, and 8.06 ppm, m) for protons at aromatic ring bonded to 1,2,4-triazole ^{13}C NMR shows: δ = (162 ppm) for carbon at c, (165 ppm) for carbon at d, (148.7 ppm) for carbon at e, and (129.3, 135.5, 130.7, 128.4, and 129.2 ppm) for carbons at aromatic rings (a, b, f, g, h)
6		^1H NMR shows: δ = (8.01 ppm, s) for protons at aromatic ring bonded to $\text{C}=\text{N}$, (8.3 ppm, s) for $\text{HC}=\text{N}$, (4.04 ppm, s) for CH_2 , (2.3 ppm, s) for CH_3 , and (7.5–8.1 ppm, m) for protons at aromatic rings

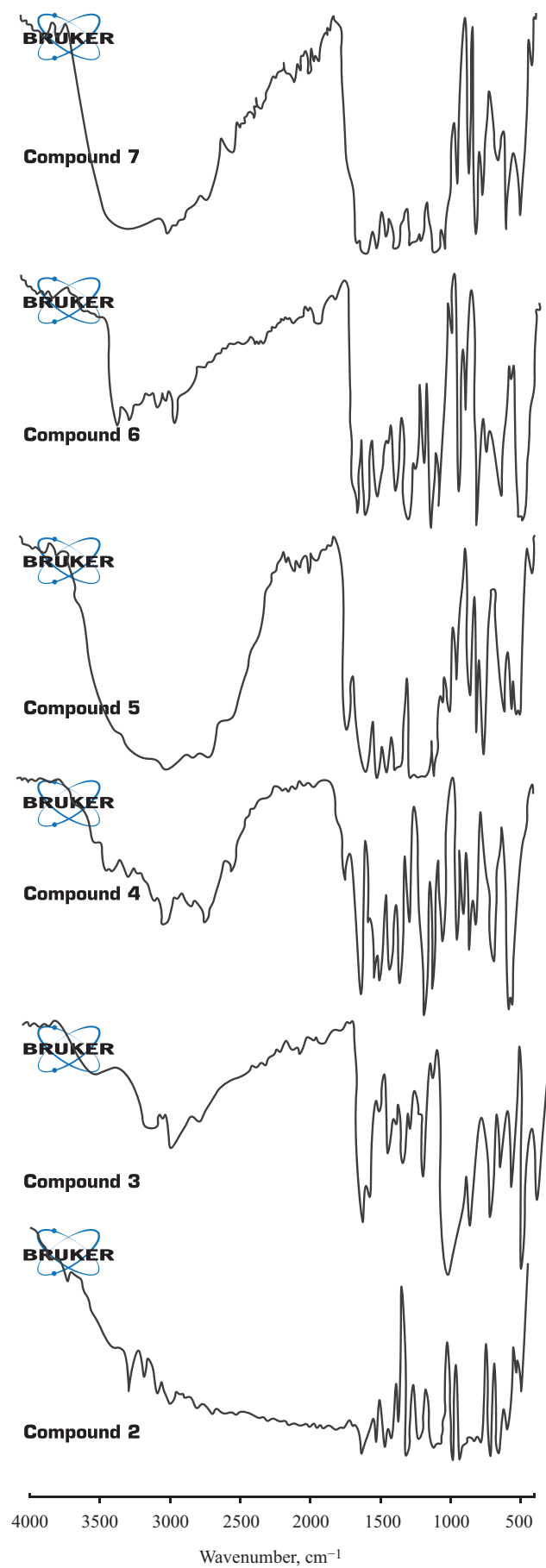


Fig. 1. FTIR for compounds 2–7

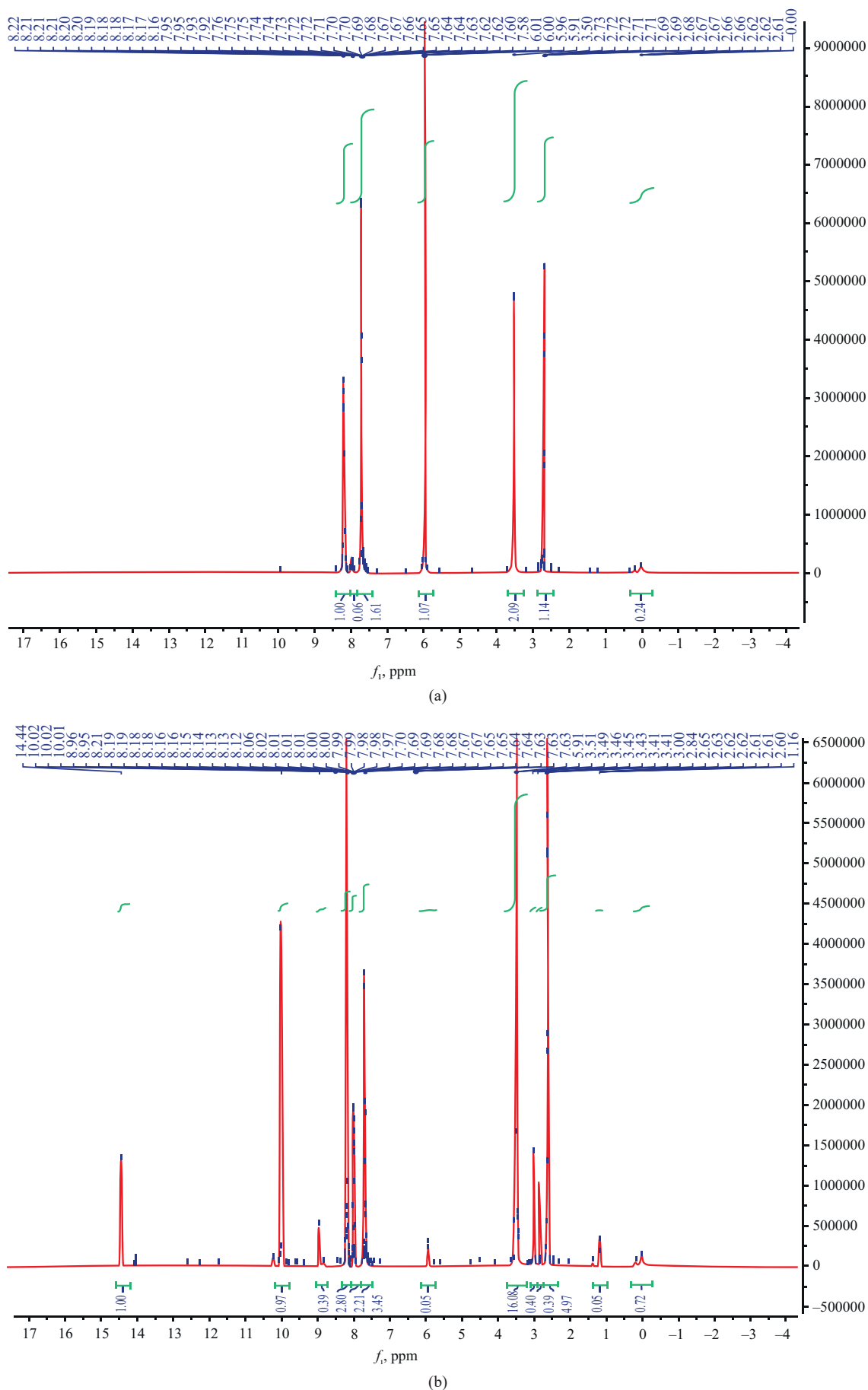


Fig. 2. ^1H NMR for (a) compound 2 and (b) compound 3

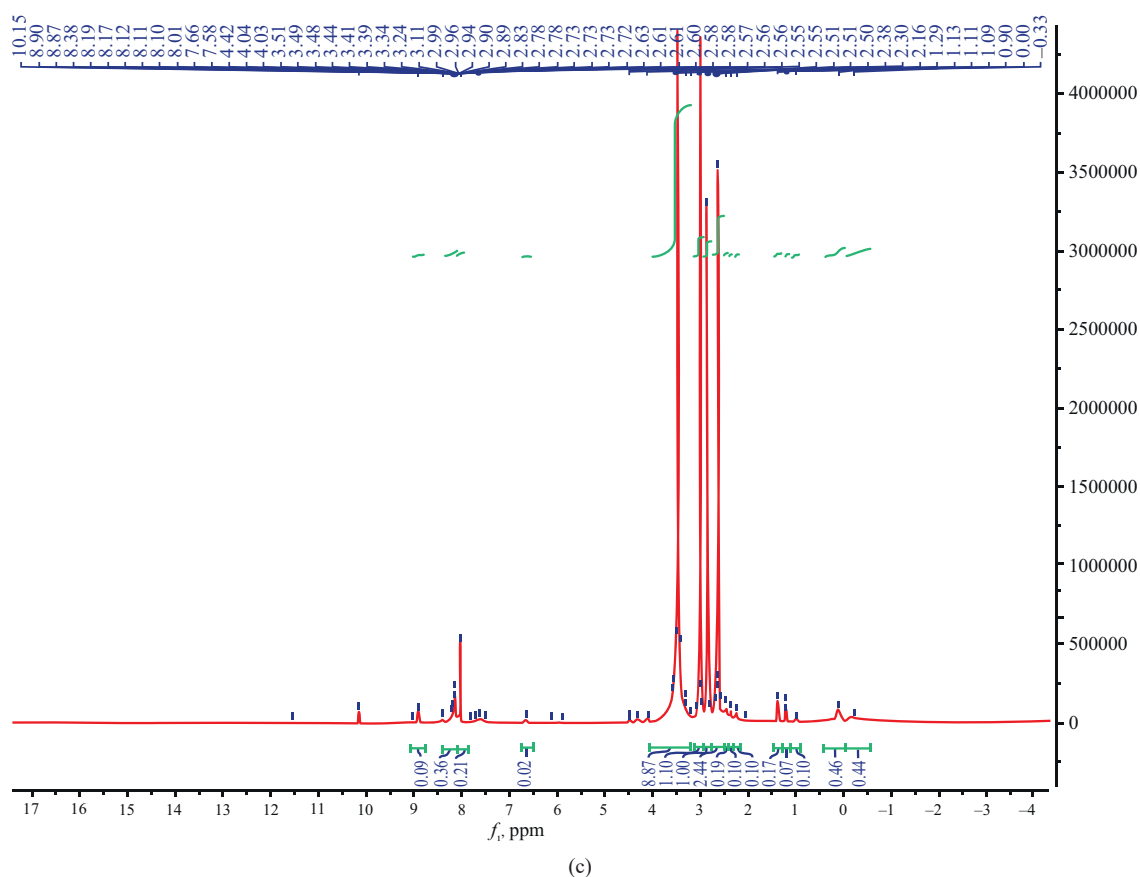


Fig. 2. Continued. ^1H NMR for (c) compound 6

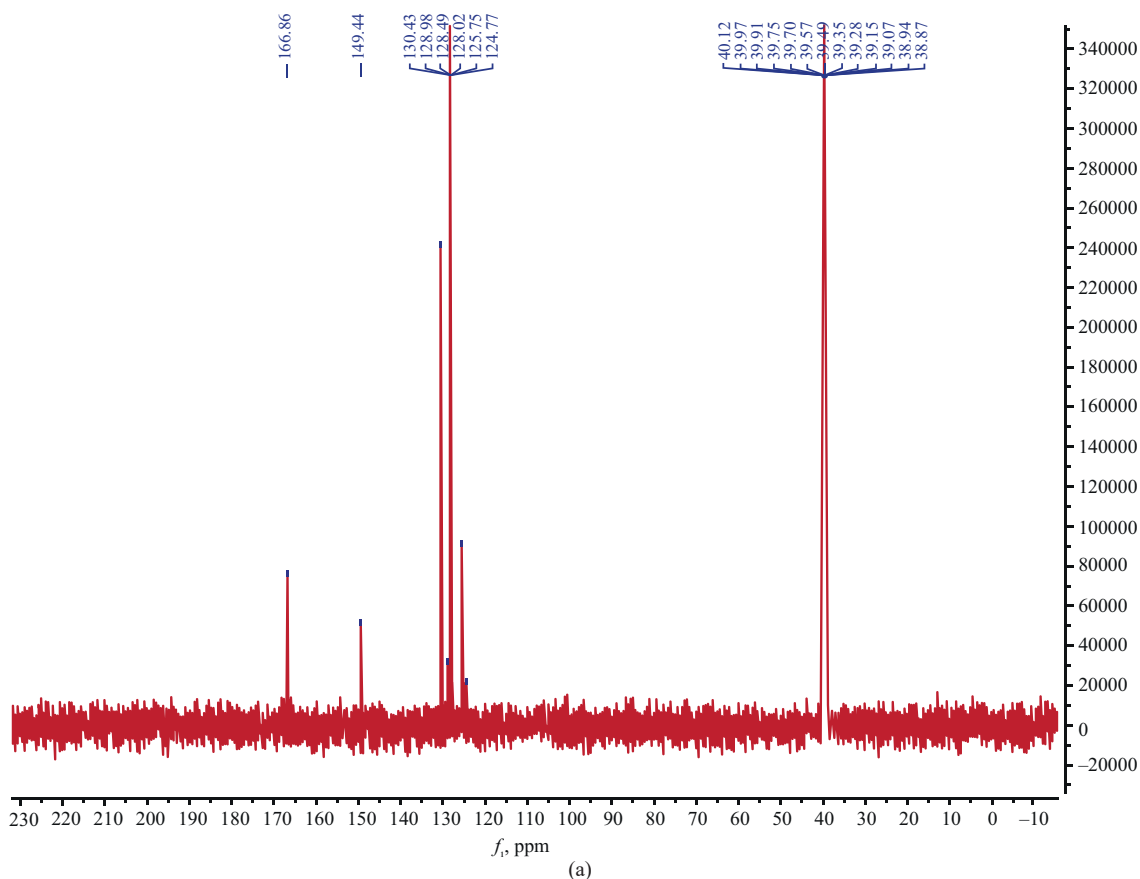
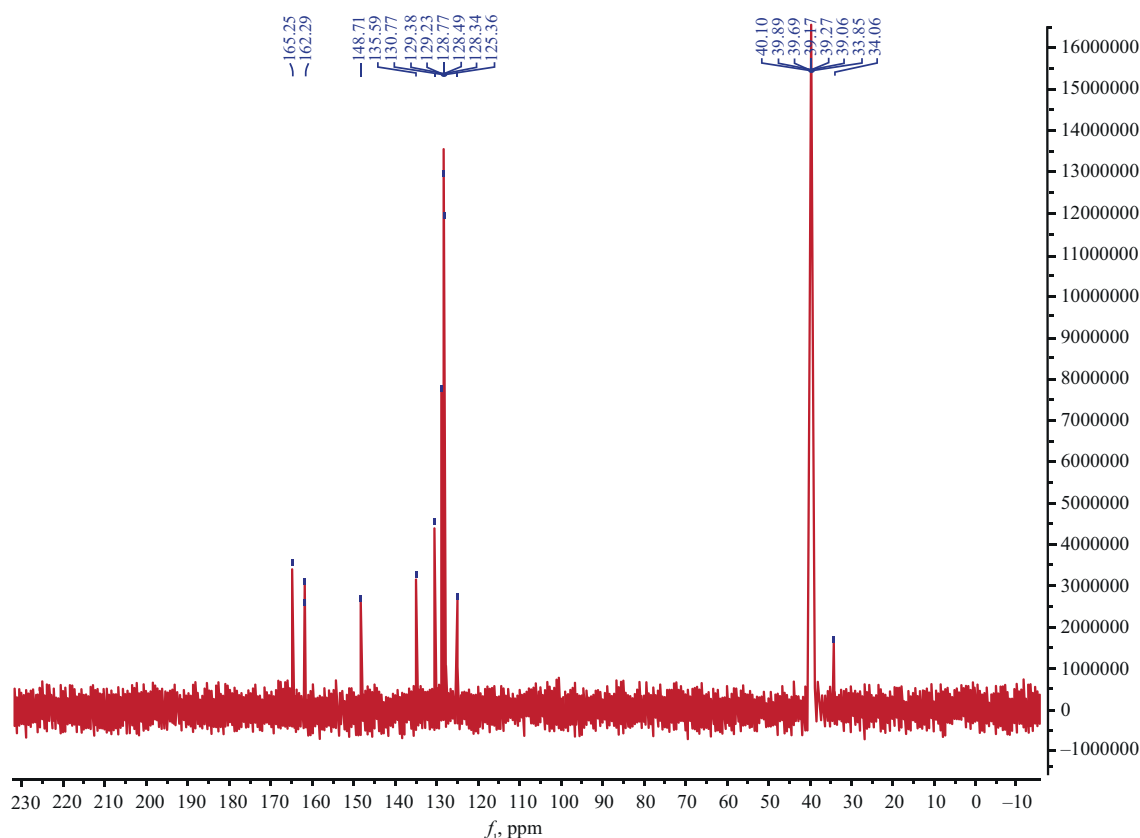


Fig. 3. ^{13}C NMR for (a) compound 2



(b)

Fig. 3. Continued. ^{13}C NMR for (b) compound 3

3.1. Chemical structure changes

The aging of polymer materials entails irreversible alterations in their characteristics due to exposure to light, heat, ambient air, oxygen, and sun rays. A heightened overall impact of weathering occurs due to the combination of multiple agents in aging processes. Photodegradation of polymers involves both crosslinking and chain scission reactions to significantly alter their physical properties. FTIR spectroscopy has been successfully employed to analyze the chemical changes occurring during the UV irradiation period as a means of understanding photooxidation processes [20]. The carbonyl group index ($I_{\text{C=O}}$) was determined using Eq. (1). The intensity of the signal corresponding to the absorption of the C=O group at 1720 cm^{-1} was significantly higher following irradiation as compared to before. Figure 4 illustrates the variations observed in $I_{\text{C=O}}$ as the irradiation time ranged from 0 to 300 h. In contrast with the blank PS film, films containing compounds 6 and 7 (0.5 wt %) exhibited reduced carbonyl group indices after irradiation. The results demonstrated the successful utilization of these compounds, particularly compound 6, to enhance the photostability of the PS films.

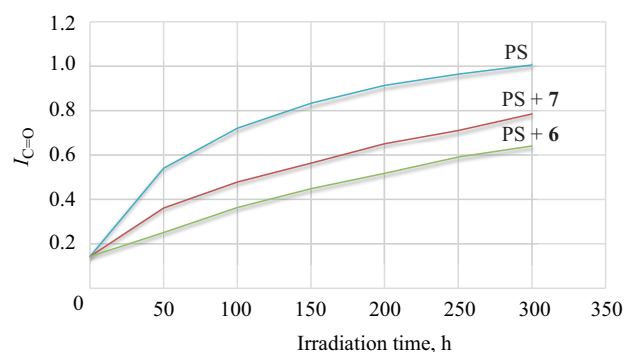


Fig. 4. Carbonyl index during UV exposure

3.2. Weight loss of PS films

When subjected to high temperatures and prolonged UV exposure, polystyrene undergoes a rapid color change from colorless to yellow and gradually becomes more brittle. This results in the formation of tiny fragments and a reduction in overall polymer weight [21]. The weight loss of PS films exposed to UV irradiation for a maximum of 300 h was determined using Eq. (2). Figure 5 illustrates the changes in the weight of the PS material after exposure to radiation for 300 h. The polymer experienced significantly greater weight loss in

the blank PS film compared to the PS films containing compounds **6** and **7**. Compound **6** exhibited the lowest weight loss.

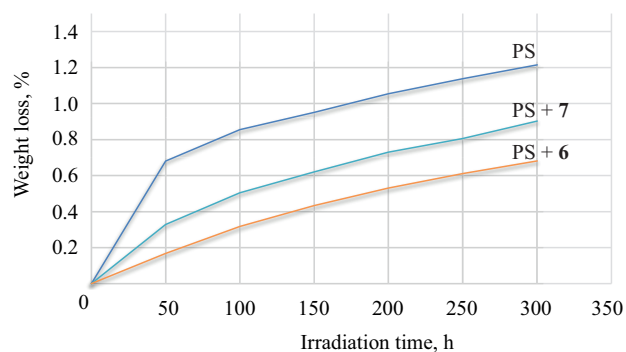


Fig. 5. Weight loss percent during UV exposure

3.3. Morphology analysis

An SEM study was conducted on the surface of PS films to identify any alterations caused by photooxidation in the various samples. The surface of the films was initially smooth and devoid of wrinkles. However, significant morphological changes were observed following irradiation as the surface of the films became more uneven [22]. Intentional perforations and imperfections were additionally incorporated into the surfaces under investigation to reveal the degradation of the polymer matrices. Typically, the evaluated specimens grew more fragile after being exposed to 300 h of irradiation (Fig. 6).

AFM is a commonly used method for studying the surface structure of polymeric materials [23, 24]. Figure 7 shows the AFM images of the PS film

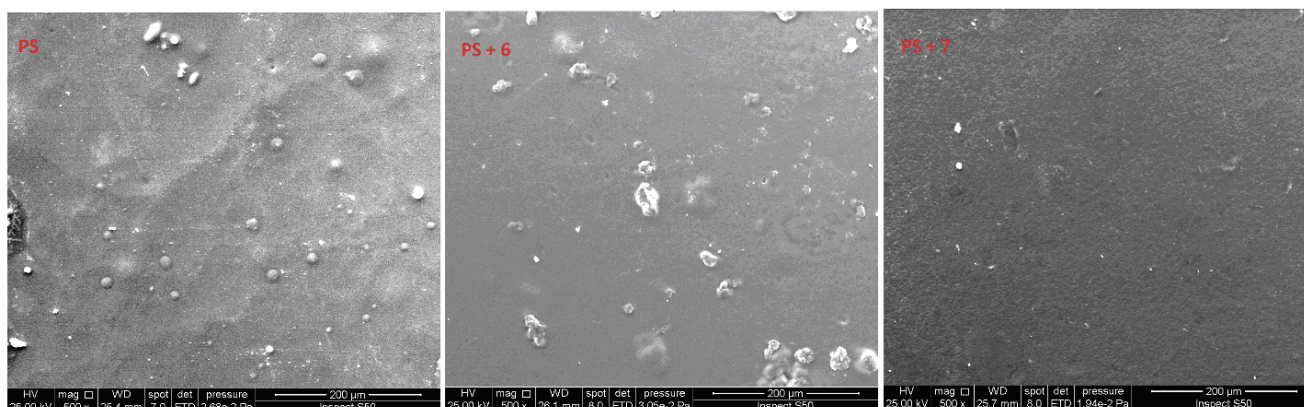


Fig. 6. SEM micrographs of PS films after 300 h of UV exposure

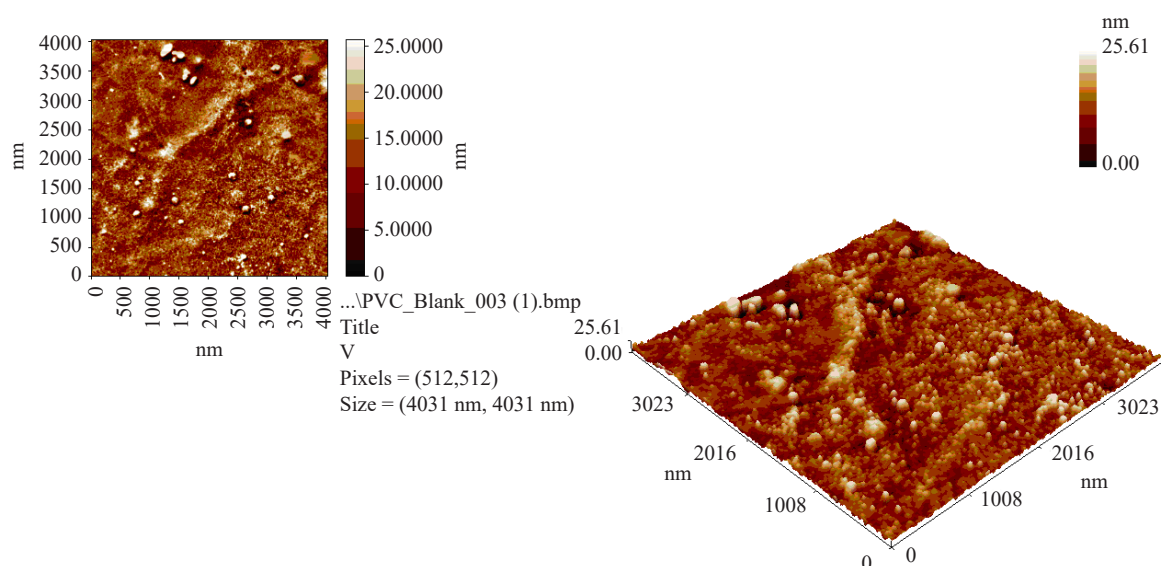


Fig. 7. AFM images for PS blank film after 300 h of UV exposure

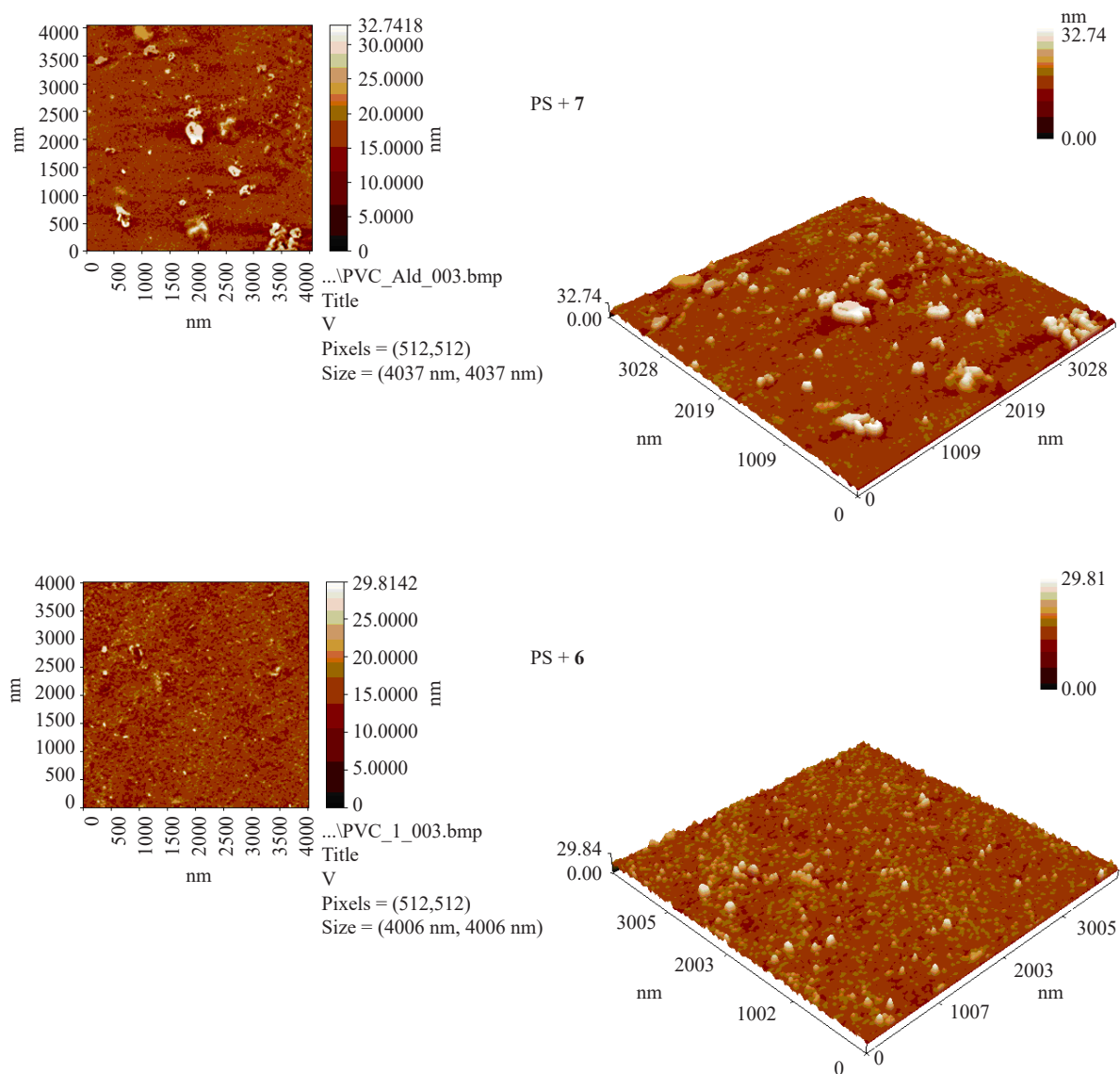


Fig. 8. AFM images for PS films after 300 h of UV exposure

without any compounds, while the PS film with compounds **6** and **7** after exposure to radiation for 300 h are depicted in Fig. 8. The presence of black specks can be attributed to residue originating from the PS matrix. The surface of the PS film containing compound **6** after irradiation exhibited a smooth texture.

4. CONCLUSIONS

This study investigated the effects of aging on PS thin films containing highly aromatic Schiff bases under UV irradiation. The analysis of the performance using FTIR spectroscopy, weight loss measurements, and morphology testing revealed several key findings. Photostabilization by the synthesized aromatic compounds, especially components **6** and **7**, reduced PS film photodegradation after 300 h of UV exposure. FTIR spectroscopy revealed a decrease in carbonyl

group indices in films containing these compounds, which indicates a reduction in photo-oxidative degradation compared to the blank PS film. Moreover, weight loss measurements corroborated these findings by showing significantly lower weight loss in films with compounds **6** and **7**. In addition to the photostabilization effects, morphological analyses via SEM and AFM showed that films containing the aromatic compounds had smoother surfaces and fewer cracks. These results highlight the potential of highly aromatic Schiff bases for use as photostabilizers to reduce PS film photodegradation and increase UV film durability and longevity.

Acknowledgments

The authors thank the Department of Chemistry at Al-Nahrain University for partially supporting this work.

Authors declare no conflicts of interest.

REFERENCES

1. Maul J., Frushour B.G., Kontoff J.R., Eichenauer H., Ott K.-H., Schade C. Polystyrene and Styrene Copolymers. In: *Ullmann's Encyclopedia of Industrial Chemistry*. Weinheim, Germany: Wiley-VCH; 2007. V. 29. P. 475–522. https://doi.org/10.1002/14356007.a21_615.pub2
2. Gary J.E. *Polystyrene: Properties, Performance and Applications*. New York, USA: Nova Science Publishers Inc.; 2011. 188 p.
3. Lynwood C. *Polystyrene: Synthesis, Characteristics and Applications*. New York, USA: Nova Science Publishers Inc.; 2014. 318 p.
4. Wünsch J.R. *Polystyrene: Synthesis, Production and Applications*. Shropshire, UK: Rapra Technology Ltd.; 2000. 176 p.
5. De Rosa C., Auriemma F. Structure and physical properties of syndiotactic polypropylene: A highly crystalline thermoplastic elastomer. *Prog. Polym. Sci.* 2006;31(2):145–237. <https://doi.org/10.1016/j.progpolymsci.2005.11.002>
6. Hussein I.A. Rheological investigation of the influence of molecular structure on natural and accelerated UV degradation of linear low density polyethylene. *Polym. Degrad. Stab.* 2007;92(11):2026–2032. <https://doi.org/10.1016/j.polymdegradstab.2007.07.021>
7. Zhao H., Li R.K.Y. A study on the photo-degradation of zinc oxide (ZnO) filled polypropylene nanocomposites. *Polymer.* 2006;47(9):3207–3217. <https://doi.org/10.1016/j.polymer.2006.02.089>
8. Andrady A.L. The plastic in microplastics: A review. *Mar. Pollut. Bull.* 2017;119(1):12–22. <https://doi.org/10.1016/j.marpolbul.2017.01.082>
9. Burrows S.D., Frustaci S., Thomas K.V., Galloway T. Expanding exploration of dynamic microplastic surface characteristics and interactions. *TrAC Trends Anal. Chem.* 2020;130:115993. <https://doi.org/10.1016/j.trac.2020.115993>
10. Xu S., Ma J., Ji R., Pan K., Miao A.J. Microplastics in aquatic environments: Occurrence, accumulation, and biological effects. *Sci. Total Environ.* 2020;703:134699. <https://doi.org/10.1016/j.scitotenv.2019.134699>
11. Kedzierski M., D'Almeida M., Magueresse A., Le Grand A., Duval H., César G., Sire O., Bruzaud S., Le Tilly V. Threat of plastic ageing in marine environment. Adsorption/desorption of micropollutants. *Mar. Pollut. Bull.* 2018;127:684–694. <https://doi.org/10.1016/j.marpolbul.2017.12.059>
12. Alsayed R., Ahmed D.S., Husain A., Al-Baidhani M., Al-Mashhadani M., Rashad A.A., Bufaroosha M., Yousif E. Silicon-carbide (SiC) nanocrystal as technology and characterization and its applications in photo-stabilizers of Teflon. *Mater. Sci. Energy Technol.* 2023;6:166–177. <https://doi.org/10.1016/j.mset.2022.12.001>
13. Ahmed D.S., El-Hiti G.A., Yousif E., Hameed A.S. Polyphosphates as inhibitors for poly(vinyl chloride) photodegradation. *Molecules.* 2017;22(11):1849. <https://doi.org/10.3390/molecules22111849>
14. Ahmed D.S., El-Hiti G.A., Yousif E., Hameed A.S., Abdalla M. New eco-friendly phosphorus organic polymers as gas storage media. *Polymers.* 2017;9(8):336. <https://doi.org/10.3390/polym9080336>
15. Jubie S., Sikdar P., Antony S., Kalirajan R., Gowramma B., Gomathy S., Elango K. Synthesis and biological evaluation of some Schiff bases of [4-(amino)-5-phenyl-4H-1,2,4-triazole-3-thiol]. *Pak. J. Pharm. Sci.* 2011;24(2):109–112.
16. Çimen Z., Akko, S., Kökbudak Z. Reactions of aminopyrimidine derivatives with chloroacetyl and isophthaloyl chlorides. *Heteroatom Chem.* 2018;29(4):e21458. <https://doi.org/10.1002/hc.21458>
17. Liang Y., Peng B. Revisiting Aromatic Claisen Rearrangement Using Unstable Aryl Sulfonium/Iodonium Species: The Strategy of Breaking Up the Whole into Parts. *Acc. Chem. Res.* 2022;55(15):2103–2122.
18. Ghani H., Kadhom M., Husain A.A., Jawad A., Yousif E. Study of Photodecomposition Rate Constant and Surface Morphology of PVC Films Embedded with Tin(IV) Complexes. *Prog. Color Colorants Coat.* 2022;15(4): 319–326. <https://doi.org/10.30509/PCCC.2022.166929.1144>
19. Yousif E., Ahmed D.S., El-Hiti G.A., Alotaibi M.H., Hashim H., Hameed A.S., Ahmed A. Fabrication of novel ball-like polystyrene films containing Schiff base microspheres as photostabilizers. *Polymers.* 2018;10(11):1185. <https://doi.org/10.3390/polym10111185>
20. Ainali N.M., Bikiaris D.N., Lambropoulou D.A. Aging effects on low-and high-density polyethylene, polypropylene and polystyrene under UV irradiation: An insight into decomposition mechanism by Py-GC/MS for microplastic analysis. *J. Anal. Appl. Pyrolysis.* 2021;158:105207. <https://doi.org/10.1016/j.jaap.2021.105207>
21. Chai R.D., Zhang J. Synergistic effect of hindered amine light stabilizers/ultraviolet absorbers on the poly(vinyl chloride)/powder nitrile rubber blends during photodegradation. *Polym. Eng. Sci.* 2013;53(8):1760–1769. <https://doi.org/10.1002/pen.23432>
22. Omer R.M., Al-Tikrity E.T., El-Hiti G.A., Alotibi M.F., Ahmed D.S., Yousif E. Porous aromatic melamine Schiff bases as highly efficient media for carbon dioxide storage. *Processes.* 2019;8(1):17. <https://doi.org/10.3390/pr8010017>
23. Ye X., Pi H., Guo S. A novel route for preparation of PVC sheets with high UV irradiation resistance. *J. Appl. Polym. Sci.* 2010;117(5):2899–2906. <https://doi.org/10.1002/app.32214>
24. Yaseen A.A., Yousif E., Al-Tikrity E.T., El-Hiti G.A., Kariuki B.M., Ahmed D.S., Bufaroosha M. FTIR, weight, and surface morphology of poly (vinyl chloride) doped with tin complexes containing aromatic and heterocyclic moieties. *Polymers.* 2021;13(19):3264. <https://doi.org/10.3390/polym13193264>
25. Yousif E., Ahmed D.S., El-Hiti G.A., Alotaibi M.H., Hashim H., Hameed A.S., Ahmed A. Fabrication of novel ball-like polystyrene films containing Schiff base microspheres as photostabilizers. *Polymers.* 2018;10(11):1185. <https://doi.org/10.3390/polym10111185>

About the Authors

Shahad M. Hussain, Instructor, Department of Chemistry, College of Science, Al-Nahrain University, Baghdad, Iraq. E-mail: shahad.muhammed@nahrainuniv.edu.iq. Scopus Author ID 57834372700, <https://orcid.org/0009-0006-9029-535X>

Ahmed Ahmed, Dr. Sci., Professor, Department of Chemistry, College of Science, Al-Nahrain University, Baghdad, Iraq. E-mail: ahmed.ahmed@nahrainuniv.edu.iq. Scopus Author ID 57199491761, <https://orcid.org/0000-0003-2526-1015>

Mohammed Kadhom, Assistant Professor, Department of Environment, College of Energy and Environmental Science, Al-Karkh University of Science, Baghdad, Iraq. E-mail: kadhom@kus.edu.iq. Scopus Author ID 57192541622, <https://orcid.org/0000-0001-9222-7955>

Dina S. Ahmed, PhD Lecturer, Department of Chemical Industries, Institute of Technology-Baghdad, Middle Technical University, Baghdad, Iraq. E-mail: dina_saadi@mtu.edu.iq. Scopus Author ID 57195275055, <https://orcid.org/0000-0003-2205-4061>

Shams S. Hameed, Instructor, General Directorate of Education Baghdad, Karkh 1, Ministry of Education, Baghdad, Iraq. E-mail: shamshameed94@gmail.com. Scopus Author ID 59541622400, <https://orcid.org/0009-0001-2380-3151>

Omar G. Mousa, Instructor, General Directorate of Education Baghdad, Resafa 1, Ministry of Education, Baghdad, Iraq. E-mail: omarchemistry1987@gmail.com. Scopus Author ID 57221945577, <https://orcid.org/0000-0002-3596-6249>

Ahmed A. Ahmed, Dr. Sci., Professor, Polymer Research Unit, College of Science, Mustansiriyah University, Baghdad, Iraq. E-mail: dr_ahmedabd@uomustansiriyah.edu.iq. Scopus Author ID 57446216800, <https://orcid.org/0000-0001-7114-2418>

Muna Bufaroosha, PhD, Associate Professor, Department of Chemistry, College of Science, United Arab Emirates University, Al-Ain, United Arab Emirates. E-mail: muna.bufaroosha@uaeu.ac.ae. Scopus Author ID 57216961114, <https://orcid.org/0000-0003-4799-3356>

Rahimi Yusop, Dr. Sci., Professor, School of Chemical Sciences and Food Technology, Faculty of Science and Technology, Universiti Kebangsaan Malaysia, Bangi, Selangor, Malaysia. E-mail: rahimi@ukm.edu.my. Scopus Author ID 36994895800, <https://orcid.org/0000-0002-8843-8677>

Emad Yousif, Dr. Sci., Professor, Department of Chemistry, College of Science, Al-Nahrain University, Baghdad, Iraq. E-mail: emad.yousif@nahrainuniv.edu.iq. Scopus Author ID 26533612800, <https://orcid.org/0000-0003-1458-4724>

*The text was submitted by the authors in English
and edited for English language and spelling by Thomas A. Beavitt*

Chemistry and technology of inorganic materials
Химия и технология неорганических материалов

UDC 546.62+535.376

<https://doi.org/10.32362/2410-6593-2025-20-4-324-343>

EDN KEDCJH




REVIEW ARTICLE

Aluminum oxynitrides doped with rare-earth and transition metal ions

Nailya S. Akhmadullina¹, Aleksey V. Ishchenko²

¹ A.A. Baikov Institute of Metallurgy and Material Science, Russian Academy of Sciences, Moscow, 119991 Russia

² Ural Federal University, Yekaterinburg, 620062 Russia

 Corresponding author, e-mail: nakhmadullina@mail.ru

Abstract

Objectives. The work set out to summarize the results of the studies of aluminum oxynitrides (AIONs) doped with rare earth (REM) and transition metals (TM) and to highlight the main effects of REM and TM dopants on the formation, phase composition, and optical properties of the AION.

Results. The presented analysis of the literature data includes the results of our own studies of the AION doped with REM and TM ions. The influence of REM and TM additives on the formation of AION and its phase composition, as well as optical properties, was considered.

Conclusions. It is clearly shown that the doping with REM and TM ions enhances the formation of pure AION phase via high-temperature synthesis from oxide and nitride. The oxynitride matrix exhibits reducing properties with respect to both REM and TM. Doping with the REM ions leads to the emergence of luminescent properties in the visible range, while doping with TM ions affects the band gap in AION as a semiconductor. The solubility limits of all metals in the AION matrix do not exceed 1–2 at. % vs Al. Concentration quenching of luminescence is observed at REM contents from 0.1 to 0.5 at. %.

Keywords

aluminum oxynitride, rare earth metals, transition metals, phase composition, solubility, luminescence

Submitted: 02.10.2024

Revised: 27.01.2025

Accepted: 15.06.2025

For citation

Akhmadullina N.S., Ishchenko A.V. Aluminum oxynitrides doped with rare-earth and transition metal ions. *Tonk. Khim. Tekhnol. = Fine Chem. Technol.* 2025;20(4):324–343. <https://doi.org/10.32362/2410-6593-2025-20-4-324-343>

ОБЗОР

Оксинитриды алюминия, легированные ионами редкоземельных и переходных металлов

Н.С. Ахмадуллина¹, А.В. Ищенко²

¹ Институт металлургии и материаловедения им. А.А. Байкова, Российская академия наук, Москва, 119991 Россия

² Уральский федеральный университет им. первого Президента России Б.Н. Ельцина, Екатеринбург, 620062 Россия

✉ Автор для переписки, e-mail: nakhmadullina@mail.ru

Аннотация

Цели. Обобщить результаты исследований и сформулировать основные закономерности влияния ионов редкоземельных (РЗМ) и переходных металлов (ПМ) на формирование, фазовый состав и оптические свойства оксинитрида алюминия (алона).

Результаты. Проведен анализ литературных данных, включая результаты собственных исследований авторов, касающихся алонов, легированных ионами РЗМ и ПМ. Рассмотрено влияние добавок РЗМ и ПМ на формирование алона и его фазовый состав и оптические свойства.

Выводы. Установлено, что введение ионов РЗМ и ПМ способствует образованию фазы алона при высокотемпературном синтезе из оксида и нитрида алюминия. Оксинитридная матрица проявляет восстановительные свойства как в отношении РЗМ, так и ПМ. Легирование ионами РЗМ приводит к получению материалов, обладающих люминесцентными свойствами в видимом диапазоне. Легирование ионами ПМ влияет на ширину запрещенной зоны алона как полупроводника. Пределы растворимости всех металлов в матрице алона не превышают 1–2 ат. % относительно алюминия. Концентрационное тушение люминесценции наблюдается при содержании РЗМ от 0.1 до 0.5 ат. %.

Ключевые слова

оксинитрид алюминия, редкоземельные металлы, переходные металлы, фазовый состав, растворимость, люминесценция

Поступила: 02.10.2024

Доработана: 27.01.2025

Принята в печать: 15.06.2025

Для цитирования

Ахмадуллина Н.С., Ищенко А.В. Оксинитриды алюминия, легированные ионами редкоземельных и переходных металлов. *Тонкие химические технологии*. 2025;20(4):324–343. <https://doi.org/10.32362/2410-6593-2025-20-4-324-343>

INTRODUCTION

Aluminum oxide in its trigonal modification $\alpha\text{-Al}_2\text{O}_3$, also known as corundum, has found wide application due to its thermal and chemical resistance, as well as desired physical and mechanical characteristics of hardness and strength [1]. The next generation material in relation to aluminum oxide is aluminum oxynitride, otherwise called AlON. AlON has been known since about 1960–1970, when the phase diagram of the pseudo-binary $\text{AlN}\text{--}\text{Al}_2\text{O}_3$ system was fully described [2–5]. The classical phase diagram of this system, which is constructed under the assumption that the atmosphere is a nitrogen current, was first presented in [6]. According to these data, AlON is a solid solution in the $\text{AlN}\text{--}\text{Al}_2\text{O}_3$ system with a rather wide region of homogeneity. The $\gamma\text{-AlON}$ phase has a spinel-type crystal structure (space group $Fd\bar{3}m$). As a phase of variable composition $\text{Al}_{64+x/3}\text{O}_{32-x}\text{N}_x$ ($0 < x < 8$), it is usually considered in the model of constant anions, as proposed by

McCauley [3]. Its stoichiometric composition in this case (at $x = 5$) is defined by the formula $\text{Al}_{23}\text{O}_{27}\text{N}_5$ ($5\text{AlN}\cdot 9\text{Al}_2\text{O}_3$). In this model, it is assumed that the anionic positions are completely occupied by oxygen and nitrogen in the crystal lattice of the spinel phase, while the cationic positions are occupied by aluminum and contain vacancies. Comparatively recent quantum-chemical modeling has confirmed the assumption of this type of structure as the most probable [7]. The indicated composition corresponds to the content of AlN 35.7 mol % and Al_2O_3 64.3 mol %. Another frequently attributed composition, which is described by the formula $\text{Al}_5\text{O}_6\text{N}$ ($\text{AlN}\cdot 2\text{Al}_2\text{O}_3$), corresponds to the content of AlN 33.3 mol % and Al_2O_3 66.7 mol %. The exact composition depends on the initial components and the method of synthesis. In addition to $\gamma\text{-AlON}$ in the system, there are a number of mixed oxide-nitride phases in which aluminum nitride predominates and which are thus considered as AlN polytypes: 27R ($7\text{AlN}\cdot \text{Al}_2\text{O}_3$), 21R ($5\text{AlN}\cdot \text{Al}_2\text{O}_3$), 12H ($4\text{AlN}\cdot \text{Al}_2\text{O}_3$) and others

(symbols R and H denote rhombohedral and hexagonal phases, respectively). On the other hand, there are oxynitride phases of composition $\text{Al}_{11}\text{O}_{15}\text{N}$ (ϕ' -AlON, $\text{AlN} \cdot 5\text{Al}_2\text{O}_3$) and $\text{Al}_{27}\text{O}_{39}\text{N}$ (ϕ -AlON, $\text{AlN} \cdot 13\text{Al}_2\text{O}_3$).

Among all these phases, it is γ -AlON that inherits the high thermal and chemical stability and strength of corundum, adding to them resistance to high-speed loading, due to which it has attracted the attention of researchers over the last five decades [8, 9]. Among the many applications of alumina are the production of transparent ceramics [5] and its use as a phosphor matrix for the fabrication of light-emitting diodes (LEDs), including white light-emitting diodes (WLEDs) [10], which currently demonstrate longer lifetimes, higher light output and lower power consumption as compared to other light sources, as well as being more environmentally friendly [11–13]. Currently, commercially available WLEDs can be fabricated by combining an InGaN chip with emission in the blue range of the spectrum and a yellow phosphor $\text{Y}_3\text{Al}_5\text{O}_{12}$ (YAG:Ce) phosphor [14]. However, this type of WLED has a low color rendering index and high correlated color temperature (CCT) due to the lack of sufficient emission in the red region [15, 16]. To solve this problem, WLEDs based on tri-color phosphors and LEDs emitting in the near ultraviolet (UV) region have been developed. This approach is considered to be the most promising because due to the excellent color rendering and low CCT demonstrated by WLEDs at high efficiency [17, 18]. The search for new luminescent materials that provide luminescence in the red, blue and green spectral regions is relevant.

AlON in powder form is usually obtained by reaction between AlN and Al_2O_3 powders with some additives. This reaction can be accomplished by plasma arc synthesis, carbothermal reduction, or self-propagating high-temperature synthesis [5, 19–21]. For fabrication, the resulting AlON powder is molded and sintered at temperatures $>1850^\circ\text{C}$ for a long time in a nitrogen atmosphere (by pressureless sintering) and by hot pressing, hot isostatic pressing, or reaction sintering [22]. The use of transient liquid-phase sintering, in which the material moves from the liquid/solid state region to the solid solution region as the liquid reacts with and is incorporated into the AlON phase as it compacts, has also been investigated [5, 23].

Aluminum oxynitrides doped with REM ions

Aluminum oxynitride can be doped with various metal ions to impart certain properties. Doping with REM ions is used to improve physical and mechanical properties, as well as to impart luminescent properties to AlON. In particular, the incorporation of Y^{3+} and

La^{3+} ions into AlON contributes to the densification of the material at the sintering stage [24–30]. Martin *et al.* used 0.5 wt % Y_2O_3 as a sintering additive to densify and enhance the homogeneity at the microstructure level of AlON by hot pressing [25]. Similarly, Wang *et al.* prepared transparent AlON ceramics (2 mm thick) using 0.12 wt % Y_2O_3 and 0.09 wt % La_2O_3 as sintering additives, achieving a transmittance of $\sim 84\%$ at 1100 nm for a 4.2 mm thick sample after hot isostatic pressing for 2 h at 1900°C [26]. Nevertheless, this ceramic is characterized by large grains because at this temperature, grain growth is not only due to compaction but also stimulated by additives [27]. The developed method was further improved [29], and transparent AlON ceramics with similar characteristics were obtained with lower content of sintering additives—0.08 wt % Y_2O_3 and 0.02 wt % La_2O_3 . Addition of extra 0.2 wt % MgO allowed obtaining compact material from AlON powder by pressureless sintering at 1900°C for 24 h, and the relative density of the obtained sample amounted to 99.9% [30]. Jin *et al.* also sintered AlON without pressure using 0.08 wt % Y_2O_3 , 0.025 wt % La_2O_3 , and 0.1 wt % MgO as additives. The resulting 1 mm thick sample had a transmittance of $\sim 81\%$ at a wavelength of 1100 nm [25].

The inclusion of other REMs into the composition of AlON, as well as certain TMs, primarily Mn^{2+} , is used to impart luminescent properties to the sample [31, 32]. Doping with Eu^{2+} ions allows the preparation of blue-green light phosphors. Kikkawa *et al.* [33] reported the synthesis of AlON: Eu^{2+} phosphors via ammonia nitriding of aluminum oxide prepared from aluminum nitrate by sol–gel method with the addition of europium nitrate. The synthesis included nitriding steps, which were carried out at 1200 – 1500°C , and post-annealing in a nitrogen current at 1700°C . Powders with Eu^{2+} content of 1 and 3 mol % showed two maxima in the photoluminescence (PL) spectrum at 475 and 520 nm, whose source was presumably the EuAl_2O_4 phase. Subsequently, co-alloyed phosphors of the composition AlON:3% Eu^{2+} /10% Mg^{2+} were obtained by solid-phase synthesis directly from commercial Al_2O_3 and AlN powders by firing in a nitrogen current at 1800°C [34]. The obtained phosphors exhibited a broad emission band in the PL spectra in the range of 430–620 nm with a maximum around 490 nm at the excitation wavelength of 310 nm. It was clarified that the main europium-containing phase in the samples of AlON doped with Eu^{2+} ions is the europium aluminate phase of the composition $\text{EuAl}_{12}\text{O}_{19}$. Samples with similar composition and properties with Eu^{2+} content of 0.6% and 0.8% were prepared by carbothermal reductive nitriding of aluminum oxide [35]. The obtained samples were effectively excited by UV light with a wavelength of

350–410 nm and had an emission band in the PL spectrum with a maximum around 495 nm. The authors also determined the dynamic characteristics of luminescence and studied the dependence of luminescence intensity in the temperature range from 80 to 500 K. The effect of thermal quenching of luminescence was observed in the range of 200–500 K. Similar results were obtained in [36]. $\text{AlON}:x\%\text{Eu}$ ($x = 0.25\text{--}1.00$) phosphors showed two main emission bands in the PL spectrum with maxima at 410 and 475 nm. The intensity of the 475 nm band reached a plateau at $x = 0.25\%$ and above, probably due to reaching the solubility limit of the Eu^{2+} ion in the AlON matrix. The intensity of the 410 nm band increased linearly with increasing Eu^{2+} content, which was mainly due to the contribution of the $\text{EuAl}_{12}\text{O}_{19}$ phase.

In previous works, we carried out detailed studies of pulsed cathodoluminescence (PCL) as well as PL for a wide range of luminophores based on AlN doped with REM ions. A synthesis method based on the interaction of amorphous highly dispersed Al_2O_3 with AlN in a pressureless nitrogen current at a temperature of 1600–1750°C was developed. Amorphous highly dispersed Al_2O_3 was prepared by controlled hydrolysis of aluminum isopropoxide $\text{Al}(\text{OiPr})_3$ in an isopropanol–water mixture in the presence of citric acid with the addition of magnesium acetate (Mg^{2+} content is <1 at. % relative to aluminum) followed by drying and annealing in air. The use of Al_2O_3 obtained in this way avoids the need for increased nitrogen pressure (a small current of N_2 at a pressure of 1 atm is sufficient) to achieve a decrease in the synthesis temperature by a value from 100 to 350°C, as well as to reduce the time of high-temperature processing to 1–2 h. Furthermore, the doping ion (or ions) can be introduced in the form of water- or organosoluble compounds at the stage of aluminum isopropoxide synthesis, allowing, in some cases, to solve the problem of poor homogenization of the mixture at low contents of doping ions. Using the developed method, AlON doped with Eu^{2+} , Ce^{3+} [37] and Tb^{3+} ions [38], as well as those doped with $\text{Eu}^{2+}/\text{Ce}^{3+}$, $\text{Eu}^{2+}/\text{Tb}^{3+}$, and $\text{Ce}^{3+}/\text{Tb}^{3+}$ ion pairs, were synthesized [39].

Eu^{2+} and Ce^{3+} doped AlON were prepared by two methods: using as a source of REM ions the corresponding oxides added to a mixture of amorphous highly dispersed Al_2O_3 and AlN, and the use of REM acetylacetonates for doping Al_2O_3 , which was further subjected to high-temperature sintering in a nitrogen current in a mixture with AlN [37]. The Eu^{2+} content varied in the range of 0.025–1.0 at. % and Ce^{3+} content varied in the range of 0.025–0.2 at. %. The annealing was carried out at 1600°C for 2 h. All obtained AlON:REM samples are mixtures of aluminum oxynitride $\text{Al}_5\text{O}_6\text{N}$, corundum $\alpha\text{-Al}_2\text{O}_3$ and impurities AlN and REM aluminates. The content of these phases depends on the concentration and nature

of the alloying ions and the synthesis procedure. When AlON:REM is obtained directly from Al_2O_3 , AlN, and Eu_2O_3 or CeO_2 at all concentrations of REM ions, the content of impurity phases does not exceed 5–7 vol %. On the contrary, in the case of pre-doping of Al_2O_3 with REM acetylacetonates at low concentrations of Eu^{2+} and Ce^{3+} , the phases of Al_2O_3 and AlN are minor, but they cannot be considered as impurity phases, since their content reaches tens of vol %. When the concentrations of Eu^{2+} and Ce^{3+} increase to a certain level (0.2 and 0.1 at. %, respectively), the content of minor phases sharply decreases. For the series obtained using Eu_2O_3 and CeO_2 , the lowest impurity content is observed at close Eu^{2+} and Ce^{3+} contents, respectively, and the impurity content is markedly lower compared to the series obtained using $\text{Eu}(\text{acac})_3$ and $\text{Ce}(\text{acac})_3$. With further increase in Eu^{2+} and Ce^{3+} concentrations, the formation of REM aluminates $\text{EuAl}_{12}\text{O}_{19}$ and $\text{CeAl}_{11}\text{O}_{18}$ is observed. The formation of $(\text{REM})\text{Al}_x\text{O}_y$ is usually accompanied by an increase in AlN content. It can be assumed that the figurative point shifts to the region of ternary systems $\text{AlON} + \text{CeAl}_{11}\text{O}_{18}/\text{EuAl}_{12}\text{O}_{19} + \text{AlN}$ as a result of Al_2O_3 consumption for the formation of $(\text{REM})\text{Al}_x\text{O}_y$.

The PCL spectra of the series samples obtained using Eu_2O_3 and $\text{Eu}(\text{acac})_3$ are presented in Fig. 1. For both series, broad bands of complex shape with maximum in the range of 422–505 nm are observed depending on the Eu^{2+} concentration and precursor type. The highest intensity in both series is exhibited by samples with Eu^{2+} content of 0.5 at. %. The PCL spectra of samples with Eu^{2+} concentration of 0.4, 0.5, and 1.0 at. % have a flat top due to saturation of the photodetector during measurement (Fig. 1a).

The PCL spectra of the series samples prepared using Eu_2O_3 show pronounced $d \rightarrow f$ -luminescence bands of Eu^{2+} with a maximum in the region of 495–510 nm at Eu^{2+} concentrations from 0.4 to 1.0 at. % (Fig. 1a). When the Eu^{2+} concentration increases from 0.025 to 1.0 at. %, the maximum of the luminescence band undergoes a bathochromic shift due to the increase in the Eu^{2+} luminescence intensity against the background of the intrinsic broadband luminescence bands of AlON and impurities $\alpha\text{-Al}_2\text{O}_3$ [40] and AlN [41], whose maxima lie in the range of 400–420 nm. The PCL spectra of a series of samples obtained using $\text{Eu}(\text{acac})_3$ differ from those discussed above (Fig. 1b). The emission intensity of the samples prepared using $\text{Eu}(\text{acac})_3$ is lower than for the samples synthesized using Eu_2O_3 . With increasing Eu^{2+} concentration, the highest luminescence intensity is observed at an Eu^{2+} ion content of 0.5 at. %, as for the samples prepared using Eu_2O_3 ; however, the $d \rightarrow f$ -luminescence bands of Eu^{2+} appear as a broad band shoulder with a maximum around 450 nm. The latter

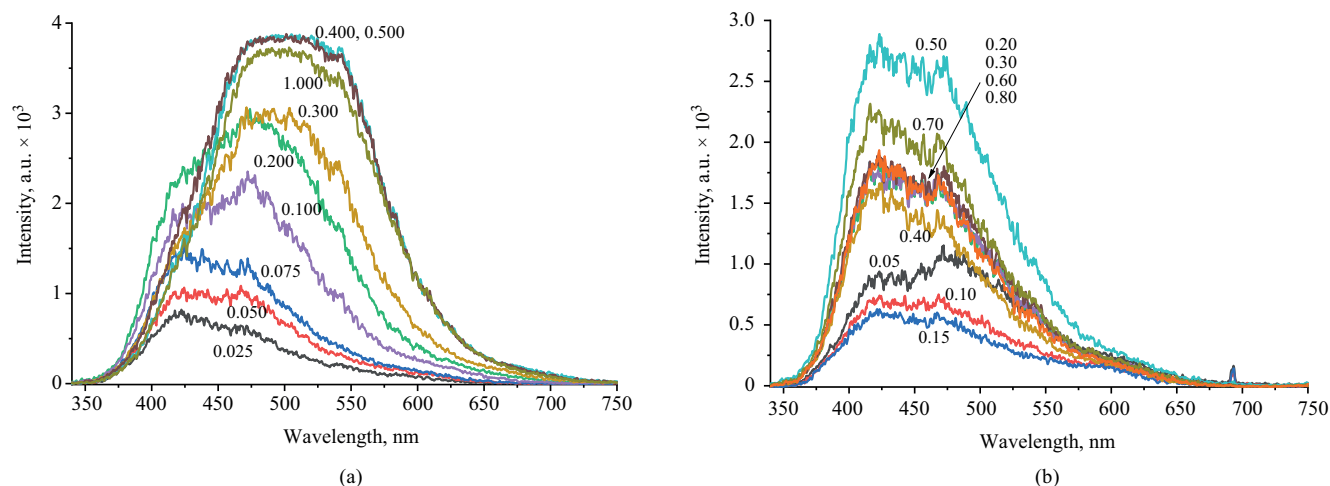


Fig. 1. Pulsed cathodoluminescence (PCL) spectra of Eu^{2+} -doped AlON prepared with Eu_2O_3 (a) and $\text{Eu}(\text{acac})_3$ (b). The concentration in at. % of Eu ions is shown near the curves (reprinted from [37])

may be due to defects in the crystal structure of $\text{Al}_5\text{O}_6\text{N}$, which are vacancies in the anionic sublattice and O_N^- and $(\text{V}_{\text{Al}}-\text{O}_\text{N})$ -type centers [42]. It is also contributed by the intrinsic emission of impurities $\alpha\text{-Al}_2\text{O}_3$ [40] and AlN [41].

The PCL spectra of a series of samples obtained using Eu_2O_3 at Eu^{2+} content less than 0.1 at. % and those of all samples obtained using $\text{Eu}(\text{acac})_3$ can be described as the sum of emission bands of AlN (400, 475, and 600 nm [41]) and F-centers in $\alpha\text{-Al}_2\text{O}_3$ (410–420 nm) [40]. It can be assumed that similar defects exist in $\text{Al}_5\text{O}_6\text{N}$.

A comparatively recent theoretical study of the geometrical and electronic structure and its relation to the optical properties of $\gamma\text{-AlON}$ doped with Eu^{2+} ions has been performed [43]. The calculations were performed using the CASTEP software package¹. The model of permanent anions was used for the AlON structure [3]. Eu^{2+} anions can occupy one of 4 possible positions: tetrahedral positions $\text{V}_{\text{Al}}\text{O}_4$ and $\text{V}_{\text{Al}}\text{O}_3\text{N}$ and octahedral positions $\text{V}_{\text{Al}}\text{O}_6$ and $\text{V}_{\text{Al}}\text{O}_5\text{N}$. Calculations have shown that for Eu^{2+} ions the octahedral positions of $\text{V}_{\text{Al}}\text{O}_5\text{N}$ are preferable. The lattice parameters and primitive cell volume of $\text{Eu}_x\text{Al}_{23-x}\text{O}_{27}\text{N}_5$ increase with increasing Eu^{2+} content. In the calculated absorption spectrum of PL $\text{Al}_{23}\text{O}_{27}\text{N}_5$ doped with Eu^{2+} , an intense band in the range 275–425 nm with a maximum at 335 nm was observed, which was attributed to electronic transitions $4f^7 \rightarrow 4f^65d^1$ in the Eu^{2+} ion, and the position of which agrees quite well with the experimental data. However, it should be taken into account that calculations in the framework of the density functional theory lead to a

systematic underestimation of the optical gap width. In this case, the calculations gave a value of 4.03 eV for the unalloyed AlON, while the experimentally determined value is 6.2–6.5 eV [44, 45].

The PCL spectra of a series of samples obtained using CeO_2 and $\text{Ce}(\text{acac})_3$ [37] are shown in Figs. 2a and 2b. For both series, a broad band of complex shape with a maximum around 450 nm is observed. The highest luminescence intensity is achieved for the samples with 0.1–0.15 at. % Ce^{3+} in the series of samples obtained using CeO_2 and for the sample with 0.125 at. % Ce^{3+} in the series of samples obtained using $\text{Ce}(\text{acac})_3$ (Fig. 2c and 2d). In the spectra of the samples obtained using CeO_2 , a pronounced $\text{Ce}^{3+} d \rightarrow f$ -luminescence band with a maximum around 450 nm is observed at a Ce^{3+} content of 0.1–0.2 at. %. At the same time, for the samples obtained using CeO_2 having Ce^{3+} content less than 0.1 at. %, the PCL spectra are similar to those of the series samples obtained using Eu_2O_3 and $\text{Eu}(\text{acac})_3$, with Eu^{2+} content less than 0.1 at. %. This means that the luminescence centers in all these samples are of the same nature.

In general, the highest PCL intensity is observed for Eu^{2+} -doped samples, in particular, at a Eu^{2+} content of 0.5 at. %. The PCL intensity of Ce^{3+} doped samples is significantly lower (up to an order of magnitude). The use of oxides as a source of REM ions gives better results as compared to the use of the corresponding acetylacetonate complexes.

It should be noted that Ce^{3+} is rarely used as an independent luminescence activator in oxynitride matrices; however it is much more often used as a

¹ <https://www.castep.org/>. Accessed June 11, 2025.

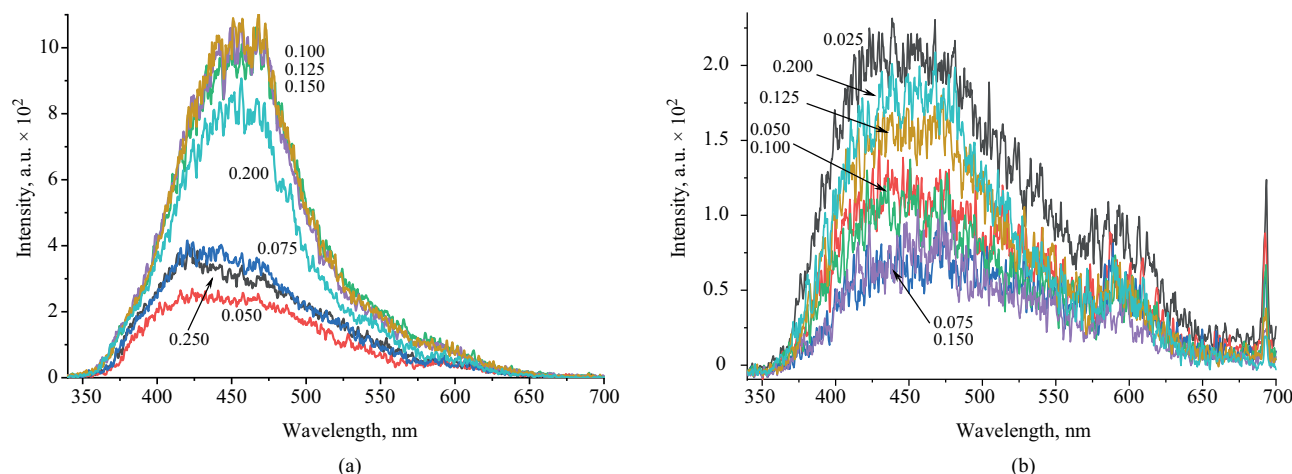


Fig. 2. PCL spectra of Ce³⁺-doped AlONs prepared with CeO₂ (a) and Ce(acac)₃ (b). The concentration in at. % of Ce ions is shown near the curves (reprinted from [37])

sensitizer, primarily for Eu²⁺ and Tb³⁺ ions (see below). Photoluminescent and radioluminescent properties of AlON doped with Ce³⁺ ions are described in [46]. AlON, whose composition is described by the authors as AlO_{0.86}N_{0.43}:Ce_x, where $x = 0.005, 0.01$, was obtained by firing mixtures of Al₂O₃ and AlN with the addition of Y₂O₃ as a sintering additive and CeO₂ in a nitrogen current at 1780°C for 2 h. Transparent samples were obtained by cold isostatic pressing of the obtained powder followed by sintering at 1900°C. The excitation spectra of the samples show a PL absorption band with a maximum around 325 nm and the emission spectra show a band with a maximum around 405 nm. Ionization scintillation in the obtained samples was confirmed using a ¹³⁷Cs (661 keV) radiation source; however, the large width of the forbidden zone and insufficient Ce³⁺ concentration, according to the authors, lead to a low light output. In general, the obtained results confirm the low efficiency of Ce³⁺ ions as luminescence activators in AlON. The actual composition of aluminum oxynitride is not clear from the work, since the composition of AlO_{0.86}N_{0.43} does not correspond to either γ -AlON or one of the other phases described in the pseudo-binary system AlN–Al₂O₃. Moreover, the claimed composition does not correspond to the given loadings of initial components either.

Active studies into the luminescent properties of AlONs doped with Tb³⁺ ions have been focused on obtaining phosphors with luminescence in the green region of the spectrum. Being an effective luminescence activator, Tb³⁺ is most often used in pair with some sensitizer, typically Ce³⁺. The reason is the high cost of terbium, which, in many cases, makes its independent use economically unfeasible. Thus, [47] studied the properties of AlONs doped with Tb³⁺

(as well as co-doped with Tb³⁺ and Ce³⁺) prepared by reductive nitriding of mixtures of Al₂O₃, CeO₂, and Tb₄O₇ oxides and aluminum nitride AlN. The authors found that in AlON:Ce³⁺ samples the concentration quenching of photoluminescence starts at Ce³⁺ concentration above 1 at. %, while for Tb³⁺ the critical concentration is 0.5 at. %. In the absorption spectra of AlON:Tb³⁺, two main bands at 270 and 300 nm are observed, corresponding to the spin-resolved transition $4f^8 \rightarrow 4f^7 5d^1$ in the Tb³⁺ ion. There are 4 narrow intense bands in the emission spectrum corresponding to the transitions from the ⁵D₄ level to the ⁷F₆ (485 nm), ⁷F₅ (543 nm), ⁷F₄ (580 nm), and ⁷F₃ (619 nm) levels in the Tb³⁺ ion.

We also synthesized AlONs doped with ions Tb³⁺ [38]. Samples with Tb³⁺ content from 0.025 to 0.5 at. % relative to aluminum were obtained by two-hour roasting in a nitrogen current of mixtures of amorphous highly dispersed Al₂O₃, AlN, and Tb₂O₃. The study of the phase composition of the obtained samples showed that AlON is the main phase in all cases. In samples with Tb³⁺ content of 0.025, 0.1, and 0.5 at. %, a nitrogen-enriched AlON phase of Al₇O₃N₅ composition is identified (in insignificant amounts). At Tb³⁺ content of 0.1 at. % and more, the formation of impurity quantities of phases of corresponding perovskite TbAlO₃ and garnet Tb₃Al₅O₁₂ aluminates is noted.

The PCL and PL spectra of the obtained AlON samples doped with Tb³⁺ ions with terbium content from 0.025 to 0.5 at. % are presented in Fig. 3. At a Tb³⁺ content of 0.025 at. %, two broad bands with maxima around 400 and 595 nm are observed in the Fourier-transform infrared spectra, which can be attributed to the luminescence of defects in the impurity phase of AlN [41]. In other samples, the AlN content is lower

(or it is not identified at all), and the described bands are not detected in the PCL spectra.

In the PCL spectra of all other AlON:Tb^{3+} samples, a series of bands corresponding to the intra-center electronic $f \rightarrow f$ transitions in Tb^{3+} ions are observed, having maxima around 380, 415, 438, 457, 488, 541, 586, and 621 nm. In particular, the bands with maxima around 488, 541, 586, and 621 nm correspond to $^5\text{D}_4 \rightarrow ^7\text{F}_J$ transitions, $J = 6, 5, 4$, and 3 , respectively, while the bands with maxima around 380, 415, 438, and 457 nm correspond to $^5\text{D}_3 \rightarrow ^7\text{F}_J$ transitions, $J = 6, 5, 4$, and 3 [48, 49]. The band with a maximum at about 541 nm corresponding to the $^5\text{D}_4 \rightarrow ^7\text{F}_5$ transition has the highest intensity in the PCL spectra, while the band with a maximum at about 457 nm corresponding to the $^5\text{D}_3 \rightarrow ^7\text{F}_3$ transition is extremely weakly expressed. The maximum

integrated luminescence intensity of AlON:Tb^{3+} samples is achieved at a Tb^{3+} ion concentration of 0.2–0.4 at. %.

The PL emission spectra of AlON:Tb^{3+} samples show all the bands recorded in the PCL spectra (Figs. 3b and 3c), as well as an additional unresolved PCL band having a maximum around 470 nm, which can be attributed to the $^4\text{D}_5 \rightarrow ^7\text{F}_5$ transition. The PL excitation spectra (PLE) reveal a number of bands with maxima around 220, 230, 260, and 285 nm, which can be attributed to the $4f^8 \rightarrow 4f^7 5d^1$ transitions in Tb^{3+} ions.

In the PL emission spectra, the probabilities of the $^5\text{D}_4 \rightarrow ^7\text{F}_J$ and $^5\text{D}_3 \rightarrow ^7\text{F}_J$ electronic transitions differ as a function of the excitation wavelength (Fig. 3b, curves 1 and 2). The PLE spectra also behave in a similar way. When the PLE spectra are recorded for the 543 and 415 nm bands, the profile of the spectra changes. The band

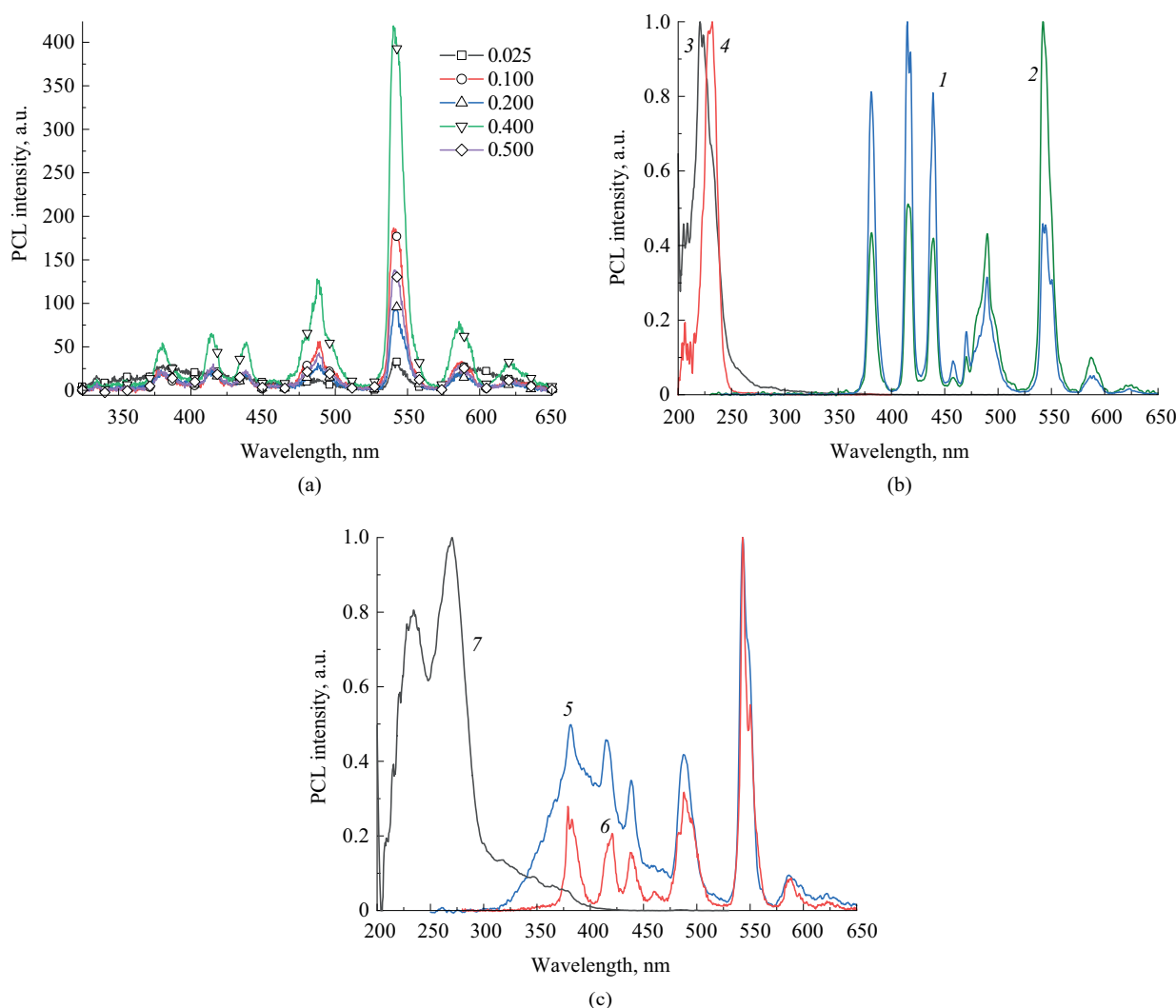


Fig. 3. (a) PCL emission spectra of $\text{Al}_5\text{O}_6\text{N:Tb}^{3+}$ samples with a Tb^{3+} content ranging from 0.025 at. % to 0.5 at. %; (b) photoluminescence (PL) and photoluminescence excitation (PLE) spectra of an $\text{Al}_5\text{O}_6\text{N:Tb}^{3+}$ sample with a Tb^{3+} content of 0.1 at. % (1 and 2 are the PL spectra upon excitation at 231 and 220 nm; 3 and 4 are the PLE spectra for luminescence bands at 543 and 415 nm); (c) PL and PLE spectra of an $\text{Al}_5\text{O}_6\text{N:Tb}^{3+}$ sample with a Tb^{3+} content of 0.4 at. % (5 and 6 are the PL spectra upon excitation at 233 and 270 nm; 7 is the PLE spectrum for the luminescence band at 543 nm) (reprinted from [38])

with a maximum around 220 nm becomes dominant in the PLE spectra for the $^5D_4 \rightarrow ^7F_J$ transitions, while for the $^5D_3 \rightarrow ^7F_J$ transitions the band has a maximum around 230 nm (Fig. 3b, curves 3 and 4).

The PL and PLE spectra of samples with high Tb^{3+} content have some differences. Thus, the PLE spectrum of the AlON:0.4 at.% Tb sample (Fig. 3c, curve 7) is also caused by the $4f^8 \rightarrow 4f^7 5d^1$ transition (spin-allowed transition $^7F_6 \rightarrow ^7D_J$) in Tb^{3+} ions, but differs by the presence of an intense excitation band with a maximum around 270 nm, which is related to the spin-allowed transition $^7F_6 \rightarrow ^9D_J$, and a broad structureless region in the range of 300–400 nm. The narrow bands in the PL spectra of AlON:0.4 at. % Tb are also due to the $^5D_4 \rightarrow ^7F_J$ and $^5D_3 \rightarrow ^7F_J$ transitions in Tb^{3+} ions. The broad band with a maximum near 400 nm may belong to the intrinsic luminescence of AlON or the luminescence of the AlN impurity [50], which begin to be effectively excited below 250 nm. The above-mentioned differences in the PL and PLE spectra of AlON: Tb^{3+} samples with low and high content of Tb^{3+} ions can be related to the effect of cross-relaxation of electronic excitations ($^5D_3, ^7F_6 \rightarrow ^5D_4, ^7F_0$) [48, 50] between nearby Tb^{3+} ions in the AlON matrix.

Ions of other rare earth metals have not generally been used as dopants for aluminum oxynitrides until recently. In 2009–2012, a team of authors from the Shanghai Institute of Ceramics described the ap-conversion of infrared (IR) radiation at 980 nm in AlON doped with Er^{3+} ions with addition of Mg^{2+} [51, 52]. AlONs with Er^{3+} content up to 3.0 mol % were studied. The obtained samples showed intense green and red luminescence with maxima in the PL spectra around 548 and 666 nm, which are the result of $^4S_{3/2}/^2H_{11/2} \rightarrow ^4I_{15/2}$ and $^4F_{9/2} \rightarrow ^4I_{15/2}$ transitions, respectively. By varying the doping concentration of Er^{3+} ions, the predominant color of the phosphors can be tuned due to the cross relaxation like $^4F_{7/2} \rightarrow ^4F_{9/2}$ and $^4F_{9/2} \leftarrow ^4I_{11/2}$. Upon co-doping with Er^{3+} , Mg^{2+} , broadening of the bands in the PL spectra was observed [51]. According to X-ray phase analysis (XRD) data, the solubility of Er^{3+} ions in the AlON matrix increased with the addition of Mg^{2+} , and band broadening was observed in the PL spectra. The intensity of the red emission band increased with increasing Mg^{2+} content up to 0.6 mol %, and decreased with further addition of Mg^{2+} . The authors propose that the introduction of Mg^{2+} up to a certain limit facilitates the introduction of Er^{3+} into the AlON lattice and lowers its symmetry due to the formation of oxygen vacancies, leading to the enhancement of red emission due to energy transfer. When the critical concentration of Mg^{2+} is reached, the effect of luminescence quenching on the formed defects begins to prevail.

AlONs doped only with Er^{3+} ions were obtained in [53]. The authors noted the dual role of erbium as a sintering additive (in the form of Er_2O_3) and a fluorescence activator. Upon excitation with 980 nm radiation, the previously described green and red bands, as well as a band with a maximum around 845 nm corresponding to the transition $^4S_{3/2}/^2H_{11/2} \rightarrow ^4I_{13/2}$, were observed in the PL spectra. In the IR emission spectra of AlON: Er^{3+} , an intense band with a maximum at 1534 nm corresponding to the $^4I_{13/2} \rightarrow ^4I_{15/2}$ transition due to the radiation-free $^4I_{11/2} \rightarrow ^4I_{13/2}$ transition and AP-conversion emission at 845 nm was observed.

The study of AlONs doped with ions of a wide range of REMs, including Sc, La, Pr, Sm, Gd, Dy, Er, and Yb, was performed several years ago at Yeungnam University (Republic of Korea). All the above elements were used in the form of the corresponding nitrates as well as oxides as sintering additives to obtain transparent AlONs [54]. The authors used the ratio $Al_2O_3:AlN = 9:2.503$ instead of 9:5 to increase sinterability by creating additional cation vacancies, metals were introduced in the amount of 0.2 wt %. Two-stage sintering under nitrogen pressure up to 2 atm at temperatures of 1610–1650°C and 1940°C allowed obtaining single-phase samples γ -AlON. The highest efficiency was demonstrated by Pr in the form of nitrate. Unfortunately, no measurements of optical properties were made by the authors, but relatively recently the same team studied the photoluminescent properties of AlON samples doped with Sm and Yb ions, albeit to a very limited extent [55]. In the PL excitation spectra of AlON: Sm^{3+} , a main band with a maximum around 340 nm was observed, which is due to the $4f^6 \rightarrow 4f^5 5d^1$ transition, while in the emission spectra, narrow bands with maxima around 690 (main band), 700, and 730 nm appear corresponding to the $^5D_0 \rightarrow ^7F_J$ transitions, where $J = 0.1$ and 2, respectively. In the PL excitation spectra of AlON: Yb^{3+} there is one band with a maximum at about 333 nm, due to the $^1S_0 \rightarrow ^7F_{7/2} T_{2g}$ transition, to which corresponds a band in the emission spectrum with a maximum at about 435 nm, arising from the reverse transition. Thus, AlON: Sm^{3+} phosphors belong to red light phosphors, while those of AlON: Yb^{3+} correspond to blue light phosphors.

The doping of oxynitride materials with two REM ions simultaneously has recently attracted increasing interest. If the material is doped with two different REM ions, one of them plays the role of an activator providing light emission, while the other plays the role of a sensitizer promoting absorption of excitation light. Efficient energy transfer between the two types of metal ions is also important for the sensitizing effect. Typically, energy transfer occurs through dipole-dipole or dipole-quadrupole interactions. The Eu^{2+}/Ce^{3+} pair is often used for co-doping nitride materials due to the emission

band of Ce^{3+} overlapping sufficiently with the excitation band of Eu^{2+} . For example, $\text{SrSi}_2\text{O}_2\text{N}_2$ doped with Eu^{2+} and Ce^{3+} ions ($\text{SrSi}_2\text{O}_2\text{N}_2:x\text{Eu}^{2+},y\text{Ce}^{3+}$; $x = 0\text{--}0.04$, $y = 0\text{--}0.04$) exhibits green-yellow luminescence in the PL spectra with a maximum around 540 nm [56, 57].

We have obtained samples of AlONs doped with Eu^{2+} and Ce^{3+} ions of the composition $\text{Al}_5\text{O}_6\text{N}:x\text{Eu}^{2+},y\text{Ce}^{3+}$; $x = 0.25$; $y = 0.01, 0.025, 0.04$, and 0.08 ; $y = 0.025$; $x = 0.1, 0.25, 0.4$, and 0.8 [39]. The main phase of the samples, which are almost single phase, can be described as $\text{Al}_5\text{O}_6\text{N}$; trace amounts of $\alpha\text{-Al}_2\text{O}_3$ and AlN are also present. A broad non-elemental band is observed in the PCL spectra (Figs. 4a and 4b). The band maximum is located at ~ 405 nm with a shoulder in the range of 450–550 nm. The band is approximated by two bands—

a narrower band with a maximum around 401 nm, which corresponds to the $5d \rightarrow 4f$ transitions in Ce^{3+} ions, and a broader band with a maximum around 447 nm, which corresponds to the $5d \rightarrow 4f$ transitions in Eu^{2+} ions.

The position of the band maximum in the PCL spectra depends weakly on the Eu^{2+} ion content, while the integrated luminescence intensity varies with the Eu^{2+} and Ce^{3+} content. At an Eu^{2+} content of 0.25 at. %, the highest intensity is observed at a Ce^{3+} content of 0.04 at. %. On the other hand, at a fixed Ce^{3+} content of 0.025 at. %, the highest intensity is observed at an Eu^{2+} content of 0.1 at. %. An increase in Eu^{2+} content leads to a decrease in the intensity of both Eu^{2+} and Ce^{3+} bands. Conversely, increasing the Ce^{3+} content decreases the intensity of Eu^{2+} band and increases the intensity of

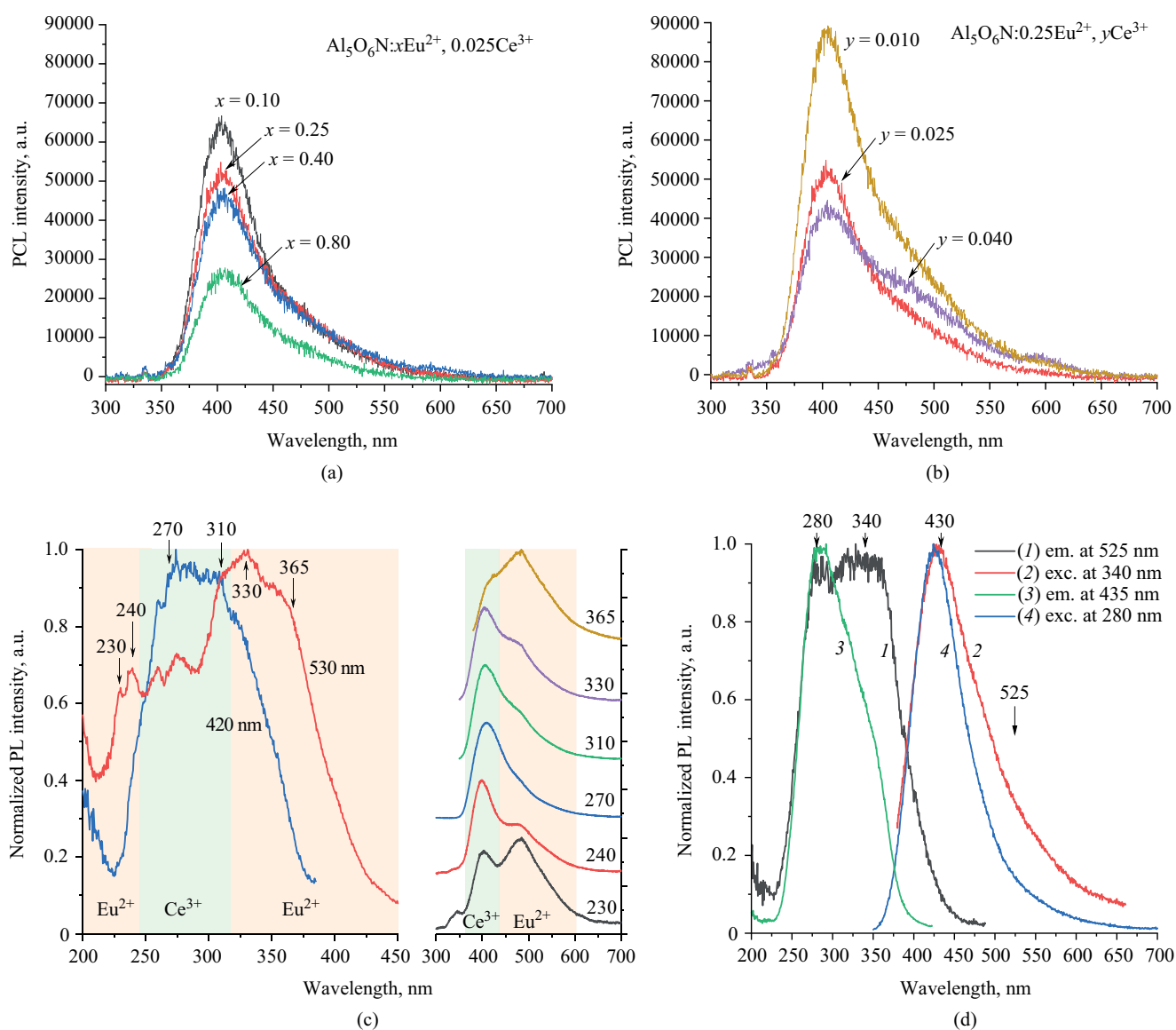


Fig. 4. (a) PCL spectra of samples $\text{Al}_5\text{O}_6\text{N}:x\text{Eu}^{2+},y\text{Ce}^{3+}$; $x = 0.1, 0.25, 0.4, 0.8$; $y = 0.025$; (b) PCL spectra of samples $\text{Al}_5\text{O}_6\text{N}:x\text{Eu}^{2+},y\text{Ce}^{3+}$; $x = 0.25$; $y = 0.01, 0.025, 0.04$; (c) PLE and PL spectra of $\text{Al}_5\text{O}_6\text{N}:0.25\text{Eu}^{2+},0.01\text{Ce}^{3+}$ sample; (d) PL and PLE spectra of $\text{Al}_5\text{O}_6\text{N}:0.25\text{Eu}^{2+},0.04\text{Ce}^{3+}$ sample (reprinted from [39])

Ce³⁺ band, thus also increasing the total luminescence intensity.

Three bands distinguished in the PLE spectra (Fig. 4c) correspond to the excitation of different bands of the PL spectra (Fig. 4d). The ~405 nm PL band is effectively excited in the range of 245–320 nm. The broad band with a maximum of 455 nm is more efficiently excited below 245 nm, as well as in the range of 320–450 nm. The shape of the PLE spectra of the sample with Ce³⁺ content of 0.04 at. % differs from the samples with Ce³⁺ content of 0.01 at. %. The relative intensities of the excitation band at 280 nm and the PL band at 405 nm are maximal for Al₅O₆N:0.25Eu²⁺,0.04Ce³⁺. Analysis of the PL and PLE spectra allows us to conclude that the observed bands belong to the $5d \rightarrow 4f$ transitions in Eu²⁺ and Ce³⁺ ions. This is confirmed by earlier results for AlONs doped with REM ions of the same species [35, 37, 58–60]. However, the maximum of the Ce³⁺ excitation band in the samples obtained by us is shifted compared to that for the band in the Ce³⁺ spectrum presented in [60] due to the possible energy transfer Ce³⁺ → Eu²⁺. Thus, in this case, a sensitizing effect of Ce³⁺ with respect to Eu²⁺ is observed. Presumably, the main energy transfer pathway is the radiation-free dipole-dipole interaction, possibly with some contribution from dipole-quadrupole interactions.

More recently, a series of blue-light phosphors γ -AlON:yCe³⁺,xEu²⁺ ($y = 0$ –0.025, $x = 0$ –0.01) were prepared in a similar way and their photoluminescence was studied [61]. The effect of sensitization of Eu²⁺ ions by Ce³⁺ ions was also demonstrated for them; the energy transfer from Ce³⁺ to Eu²⁺ is confirmed by a significant overlap between the emission spectrum of γ -AlON:0.025Ce³⁺ ($\lambda_{\text{ex}} = 285$ nm) and the excitation spectrum of γ -AlON:0.004Eu²⁺ ($\lambda_{\text{em}} = 400$ nm). As described above, the energy transfer is mainly due to radiation-free dipole-dipole interactions. The critical energy transfer distance was determined as 25.45 Å from concentration quenching of luminescence. The presented results showed that γ -AlON:Eu²⁺,Ce³⁺ phosphors can be considered as promising candidates for the role of the blue component in full-spectrum warm WLEDs.

Ce³⁺ is also quite frequently used as a sensitizer for Tb³⁺. In [59], the phosphor Al₅O₆N:0.5%Ce³⁺,0.67%Tb³⁺ was obtained by nitriding cinders prepared from nitrates of the corresponding metals. In its PL emission spectrum obtained under excitation with light at 275 nm, 4 main bands with maxima around 485, 540, 580, and 625 nm were observed, which correspond to $^5D_4 \rightarrow ^7F_J$ transitions in Tb³⁺ ions, where $J = 6, 5, 4$, and 3 , respectively. The intensity of the band with a maximum around 540 nm for the Al₅O₆N:0.5%Ce³⁺,0.67%Tb³⁺ sample was found to be 10 times higher than that for the Al₅O₆N:0.67%Tb³⁺ sample. Increasing the Tb³⁺ content to 1 mol % did

not lead to an increase in the intensity of the bands in the emission spectrum; moreover, at a Tb³⁺ content of 3 mol %, it decreased by a factor of five. Thus, Ce³⁺ has been shown to be an effective sensitizer for Tb³⁺. The main mechanism of energy transfer seems to be dipole-dipole interactions.

Similar results were obtained in [47]. Additionally, it was shown that the energy transfer efficiency exceeds 98% at a Tb³⁺ content of 3 mol %, although concentration quenching leads to a decrease in the overall emission.

Tb³⁺ can also be sensitized by Eu²⁺, such as in Al₅O₆N:0.2Eu²⁺,xTb³⁺ ($x = 0$ –0.5) [62]. Although the energy transfer efficiency did not exceed 25%, the reason for this was most likely due to the low total dopant ion content. The main mechanism of energy transfer is radiation-free dipole-dipole interactions at a critical transfer distance of 6.49 Å. The materials are green light phosphors, whose PL emission spectra obtained under excitation with light at 330 nm are the sum of spectra due to Eu²⁺ and Tb³⁺ ions.

We also studied the PL and PCL spectra of AlON:xTb³⁺,yCe³⁺ samples ($x = 0.4\%$, $y = 0.01$ –0.08%), which were prepared by a similar AlON:xEu²⁺,yCe³⁺ method [39]. According to XRD data, all samples contain Al₅O₆N as the major phase; the minor phases present in impurity amounts are represented by some other AlON polymorphs (Al₈O₃N₆, Al₁₁O₁₅N, etc.). Terbium and cerium aluminates were not detected.

The PCL and PLE/PL spectra of Al₅O₆N:xTb³⁺,yCe³⁺ samples are shown in Fig. 5. The emission spectra show narrow bands with maxima around 380, 415, 439, 460, 472, 485, 540, 582, and 620 nm, which correspond to the in-center $f \rightarrow f$ transitions in Tb³⁺ ions. As in the case of AlONs doped only with Tb³⁺ ions [38], the bands with maxima around 485, 540, 582, and 620 nm correspond to $^5D_4 \rightarrow ^7F_J$ transitions, $J = 6, 5, 4, 4$, and 3 , while the 380, 415, 439, 460, and 472 nm bands correspond to $^5D_3 \rightarrow ^7F_J$ transitions, $J = 6, 5, 4, 3$, and 2 [48, 49]. The high intensity band of $^5D_3 \rightarrow ^7F_J$ transitions is observed in the PL spectra only under selective excitation as has been shown earlier for Al₅O₆N:Tb³⁺ phosphors [38]. The $^5D_4 \rightarrow ^7F_5$ transition band at 542 nm has the highest intensity in the PCL spectra. Broad bands of $d \rightarrow f$ transitions in Ce³⁺ ions were not observed. Increasing the Ce³⁺ content leads to an increase in the integrated intensity of the bands related to Tb³⁺. The totality of these facts clearly indicates an effective radiation-free energy transfer from Ce³⁺ to Tb³⁺.

AlON:xTb³⁺,yEu²⁺ ($x = 0.4\%$, $y = 0.1$ –0.8%) samples were also obtained. As in all other cases, no reduction of Tb³⁺ was observed at complete reduction of Eu³⁺ to Eu²⁺. All AlON:xTb³⁺,yEu²⁺ samples contain Al₅O₆N as the main phase and corundum as an impurity. In addition, some amount of EuAl₁₂O₁₉ phase is present in

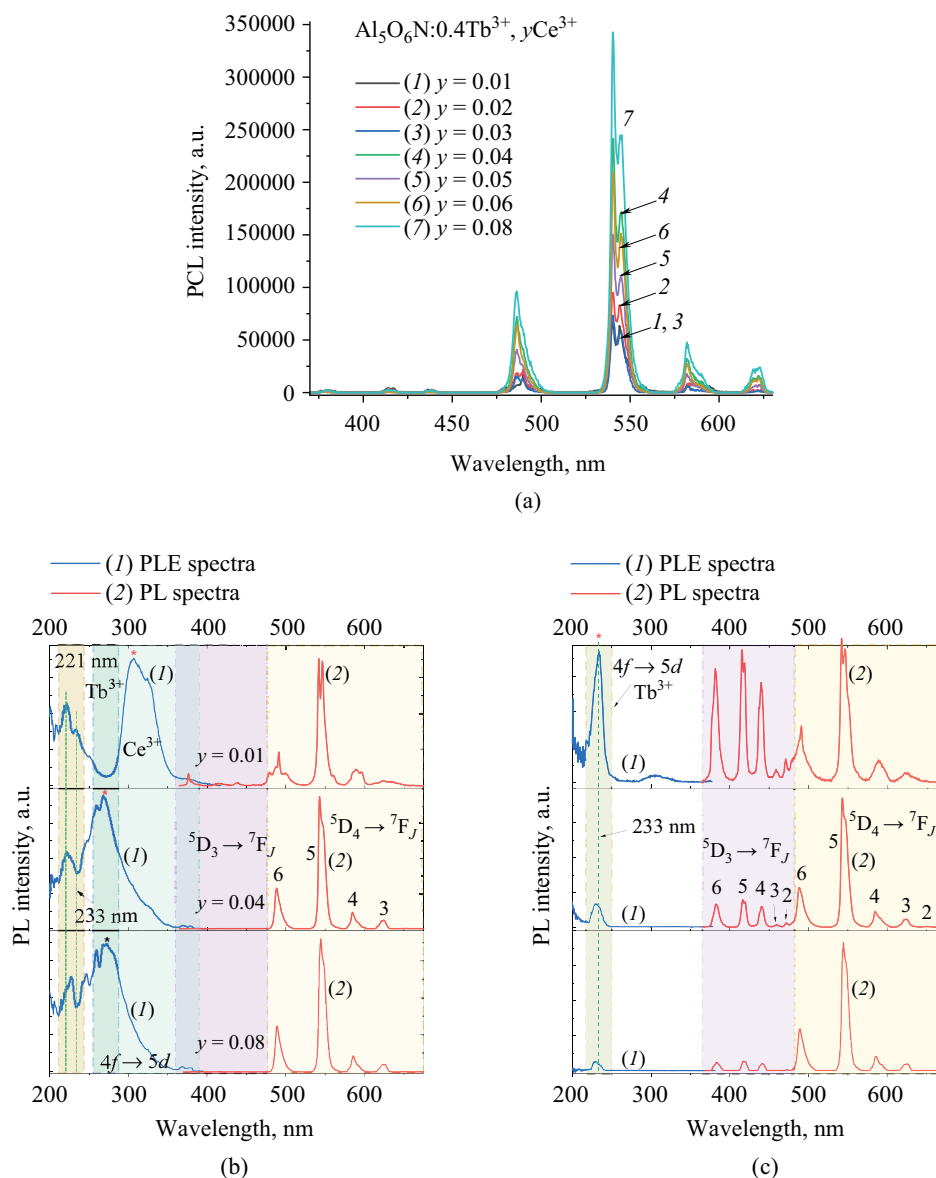


Fig. 5. (a) PCL spectra of $\text{Al}_5\text{O}_6\text{N}:x\text{Tb}^{3+},y\text{Ce}^{3+}$ samples; PLE (b) and PL (c) spectra of $\text{Al}_5\text{O}_6\text{N}:x\text{Tb}^{3+},y\text{Ce}^{3+}$ samples (reprinted from [39])

the $\text{AlON}:x\text{Tb}^{3+},y\text{Eu}^{2+}$ samples, indicating incomplete dissolution of Eu^{2+} in the AlON matrix.

The PCL spectra of $\text{Al}_5\text{O}_6\text{N}:x\text{Tb}^{3+},y\text{Eu}^{2+}$ are presented in Fig. 6. The observed narrow bands, which have maxima around 415, 437, 485, 540, 582, and 620 nm, are associated with the intra-center $f \rightarrow f$ transitions in Tb^{3+} ions as described above. The band with a maximum around 380 nm observed for the $\text{AlON}:\text{Tb}^{3+}/\text{Ce}^{3+}$ samples is not represented here due to overlap with a broad asymmetric band with a maximum around 410 nm and a half-width of 66 nm, which is associated with $d \rightarrow f$ transitions in Eu^{2+} . The integrated luminescence intensity due to Tb^{3+} ions depends very weakly on the Eu^{2+} concentration. At the same time, concentration quenching of Eu^{2+} luminescence is

observed; the maximum intensity is reached at Eu^{2+} content of 0.3 at. %.

The PL and PLE spectra recorded in the fluorescence mode mainly consist of broad bands that are related to the $4f \leftrightarrow 5d$ transitions in Eu^{2+} (Fig. 6b). The band in the PLE spectra is the sum of two bands with maxima around 260 and 300 nm. Two broad bands with maxima around 395 and 455 nm are observed in the PL spectra. The PL spectra recorded in the phosphorescence mode (Fig. 6c) consist of narrow bands associated with $f \rightarrow f$ transitions in Tb^{3+} as described above. The broad bands attributed to Eu^{2+} are not observed. The broad band in the range of 250–400 nm PLE in the phosphorescence spectra, which is attributed to the $4f \rightarrow 5d$ transitions in Eu^{2+} , clearly indicate the energy transfer of $\text{Eu}^{2+} \rightarrow \text{Tb}^{3+}$,

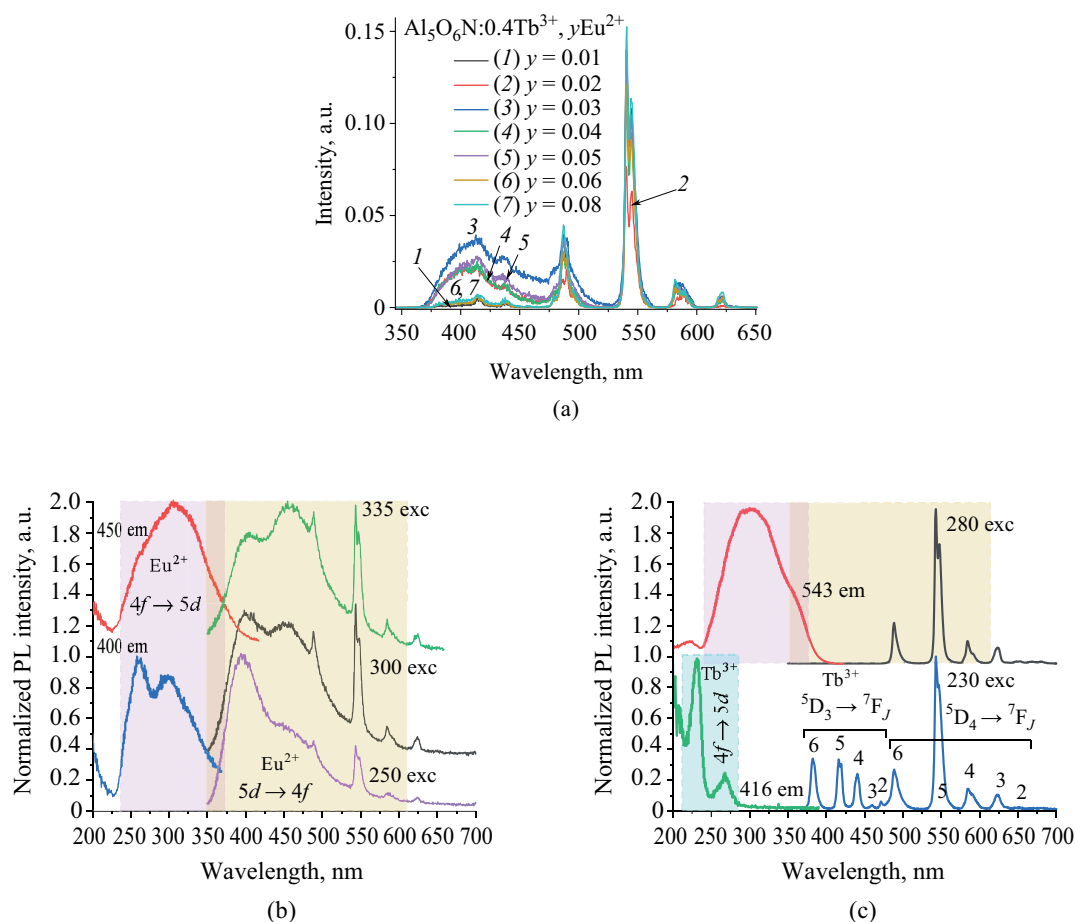


Fig. 6. (a) PCL spectra of samples $\text{Al}_5\text{O}_6\text{N}:0.4\text{Tb}^{3+}, y\text{Eu}^{2+}$; PL and PLE spectra for $\text{Al}_5\text{O}_6\text{N}:0.4\text{Tb}^{3+}/0.3\text{Eu}^{2+}$ sample recorded in fluorescence (b) and phosphorescence (c) modes (reprinted from [39])

albeit at a reduced transfer efficiency. The probable reason for this is that the total concentration of Tb^{3+} and Eu^{2+} ions exceeds the concentration limit of quenching in contrast to the $\text{Al}_5\text{O}_6\text{N}:\text{Tb}^{3+}, \text{Ce}^{3+}$ samples.

Concluding this section, it should be noted that the developed method allows easy and reproducible preparation of AIONs doped with both one and two different types of REM ions, which can be used as luminophores. The obtained materials exhibit intense cathodo- and photoluminescence over a wide wavelength range, which can be tuned by varying the dopant or dopant ions as well as their content in the AION matrix. Sensitization and concentration quenching effects are observed for the obtained samples, which should be taken into account when selecting the optimal composition for particular applications.

Aluminum oxynitrides doped with TM ions

Until recently, data on aluminum oxynitride-based systems containing TM ions were very limited. The exception was AIONs doped with manganese

ions [31, 63–66], which are green light phosphors having a narrow emission band. A characteristic view of the PLE and PL spectra of $\gamma\text{-AlON}:x\text{Mn}^{2+}$ ($x = 0.03\text{--}0.15$) samples obtained by firing of Al_2O_3 , AlN, and MnCO_3 mixtures with the addition of oxides or carbonates of alkaline earth and alkali metals for charge compensation is presented in [31]. The spectral characteristics of all samples are very similar except for the fluorescence intensity. The PLE spectrum ($\lambda_{\text{em}} = 510$ nm) consists of several bands with maxima at 340, 360, 380, 424, and 445 nm [31], which correspond to transitions from the main level $^6\text{A}_1$ to the $^4\text{T}_2(^4\text{P})$, $^4\text{E}(^4\text{G})$, $^4\text{T}_2(^4\text{E}(^4\text{G}), ^4\text{A}(^4\text{G}))$, and $^4\text{T}_2(^4\text{G})$ levels, respectively. Since all these transitions are spin- and parity forbidden, the intensities of the corresponding bands in the PLE and PL spectra are also reduced. The PL spectrum shows a narrow band with a maximum at 510 nm ($\lambda_{\text{ex}} = 445$). The narrow band in the green region of the spectrum is characteristic of the Mn^{2+} ion due to the $^4\text{T}_1(^4\text{G}) \rightarrow ^6\text{A}_1$ transition. Furthermore, the intensities of the bands in the PL spectrum monotonically increase with increasing Mn^{2+} content to reach a maximum at $x = 0.07$, after

which concentration quenching of luminescence is observed. In general, the distance between Mn^{2+} ions decreases with increasing x , which leads to a decrease in the radiative transition rate and an increase in the rate of non-radiative transitions due to cross-relaxation. The calculated critical distance between manganese ions was 8.3 Å, which is significantly larger than the distance allowing exchange interactions (5 Å). Analysis of the dependence of $\lg I/x$ on $\lg x$ (where I is the luminescence intensity, x is the activator content) showed that the most probable mechanism of energy transfer is dipole-dipole interactions.

The first report on Cr^{3+} -doped AlONs appeared in 2020 in [67]. Powders $\gamma\text{-AlON}:\text{Cr}^{3+}$ with Cr^{3+} content from 0.25 to 1.25 mol % were obtained by high-temperature roasting of the corresponding oxides and AlN in nitrogen atmosphere. The powders of the obtained materials consist of homogeneous particles of hexagonal shape with the size from 50 to 100 nm. According to XRD data they represent $\gamma\text{-Al}_5\text{O}_6\text{N}$, no impurity phases were observed. According to X-ray photoelectron spectroscopy (XPS) data, chromium is present in the form of Cr^{3+} ions in the octahedral environment of oxygen atoms, i.e., it either replaces aluminum in the corresponding positions or occupies $\text{V}_{\text{Al}}\text{O}_6$ vacancies. Two broad intense bands with maxima around 430 and 588 nm are observed in the PLE spectra, which can be attributed to the $d \rightarrow d$ transitions ${}^4\text{A}_2({}^2\text{F}) \rightarrow {}^4\text{T}_1({}^4\text{F})$ and ${}^4\text{A}_2({}^2\text{F}) \rightarrow {}^4\text{T}_2({}^4\text{F})$, respectively.

The narrow intense band in the PL emission spectrum ($\lambda_{\text{ex}} = 588$ nm) with a maximum at 693 nm is attributed to the ${}^2\text{E}({}^2\text{G}) \rightarrow {}^4\text{A}_2({}^4\text{F})$ transition, while the broad band with a maximum at 720 nm is presumably due to defects in the AlON matrix.

More recently, we have investigated AlONs doped with titanium [68], cobalt [69], and iron [70] ions. As well as samples of AlONs doped with REM ions, these were prepared by high-temperature roasting of mixtures of amorphous highly dispersed aluminum oxide Al_2O_3 and AlN in a nitrogen current under 1 atm pressure for 2 h at 1750°C. In the case of cobalt, the aluminum oxide was pre-doped using $\text{Co}(\text{OAc})_2 \cdot 4\text{H}_2\text{O}$ [33]. In the case of titanium and iron, the corresponding oxides were added directly to the mixture of Al_2O_3 and AlN. The TM content ranged from 0.01 to 5.0 at. % relative to aluminum.

According to XRD data, all titanium-doped AlN samples are almost pure $\gamma\text{-Al}_5\text{O}_6\text{N}$ [68]. Samples with 0.05–0.2 at. % of titanium contain AlN (less than 2 vol %) as an impurity. Samples with titanium content of 0.5 at. % and more contain TiN as an impurity, whose content increases with increasing total titanium content. Interestingly, even a sample with 0.05 at. % titanium does not contain corundum as an impurity phase.

Typically, to suppress the formation of corundum in the synthesis of $\gamma\text{-AlON}$, Mg^{2+} ions are incorporated in the amount from 0.5 to 10 at. %. It can be concluded that titanium effectively promotes the formation of the $\gamma\text{-Al}_5\text{O}_6\text{N}$ phase, having a solubility limit in the AlON matrix ranging from 0.2 to 0.5 at. %. According to the RFES data, titanium ions occupy octahedral positions in the AlON structure to form $[\text{TiN}_6]$, $[\text{TiO}_x\text{N}_{6-x}]$, and $[\text{TiO}_6]$ links, which are quantitatively correlated as 39:38:23. Titanium nitride TiN, as measured by Raman spectroscopy, probably forms a thin film on the surface of the AlON particles.

In the absorption spectra in the UV-visible range of $\text{AlON}:\text{Ti}^{3+}$ samples, which are obtained by the computational method using the Kubelka–Munk expression [71] from diffuse reflectance spectra, an absorption band with a maximum around 255 nm is observed. This is typical for AlON and associated with electronic transitions in defects such as V_{Al} [72]. The presence of a pronounced fundamental absorption edge in the absorption spectra formed a basis for estimating the optical width of the forbidden zone E_g by the Tautz method [73] with subsequent correction of the absorption spectra. It was found that E_g varies from 5.68 to 5.72 eV when the titanium content changes.

The PCL spectra of all samples can be represented by the sum of four luminescence bands with maxima at 393, 483, 602, and 765 nm (Fig. 7). The bands with maxima around 393 and 483 nm probably belong to intrinsic defects of the type of electroneutral complexes $[\text{V}_{\text{Al}}^{'''}\text{--}3\text{O}_{\text{N}}^{\bullet}]$. The latter are destroyed by X-ray irradiation and form charged defect states $\text{V}_{\text{Al}}^{'''}$, $3\text{O}_{\text{N}}^{\bullet}$, $[\text{V}_{\text{Al}}^{'''}\text{--}\text{O}_{\text{N}}^{\bullet}]^{2-}$ and $[\text{V}_{\text{Al}}^{'''}\text{--}2\text{O}_{\text{N}}^{\bullet}]^{-}$ [72]. The electronic transitions arising from these defects are manifested by several emission bands in the spectra of non-stoichiometric AlON compounds. However, the nature of intrinsic luminescence in AlON is still debatable. It is interesting to note that the intensity of these bands decreases with increasing titanium content. Apparently, this is due, at least in part, to a decrease in the number of intrinsic defects.

The narrower bands with maxima at 602 and 765 nm can be attributed to defects due to the presence of impurities. Compounds containing Mn^{2+} ions are often found as an uncontrolled impurity in AlN, which causes the appearance of a red luminescence band with a maximum around 600 nm [74]; a small amount of AlN is also determined by XRD in the studied samples. As for the band with a maximum around 765 nm, this can be attributed either to Ti^{3+} ions in the Al_2O_3 matrix [75], whose phase is also defined as impurity, or to Fe^{2+} ions, which can also be active in this part of the spectrum [76, 77].

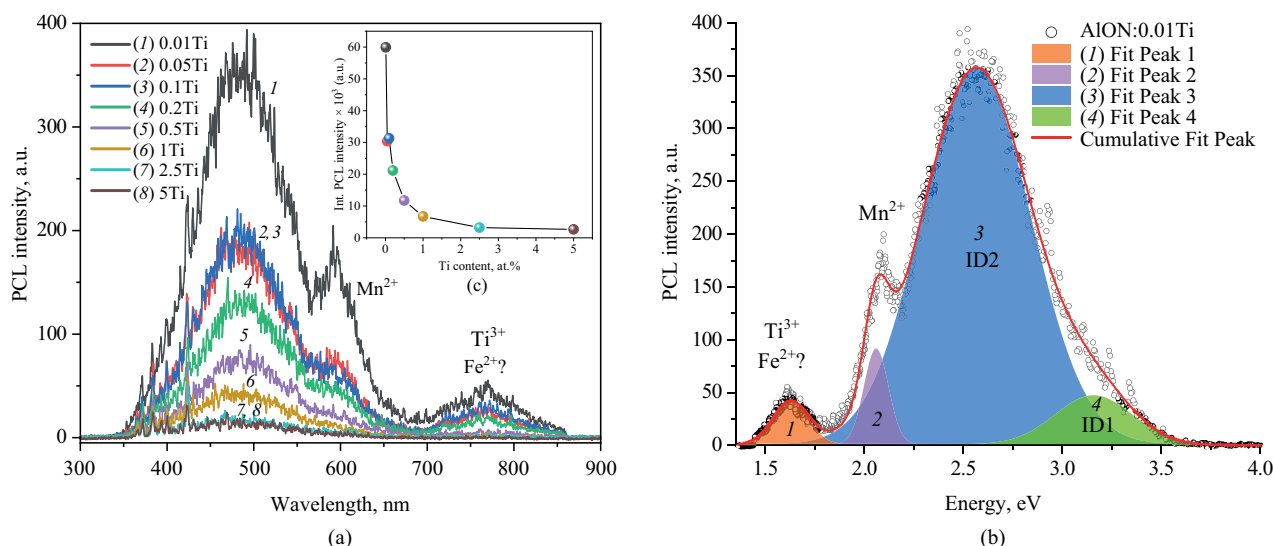


Fig. 7. (a) PCL spectra of the AlON:Ti samples; (b) decomposition of PCL spectrum of AlON:0.01Ti by 4 Gaussian bands; (c) dependence of integral PCL intensity on the total titanium content (reprinted from [68])

The pronounced tendency with increased titanium content to decrease the total luminescence intensity of AlON, as well as each of the bands separately, is probably due to the formation of an increasing amount of TiN on the surface of AlON particles, which has high absorption in the UV- and visible parts of the spectrum [78].

AlON:Co samples were obtained by high-temperature firing of mixtures of amorphous highly dispersed aluminum oxide Al_2O_3 pre-doped with Co ions. $\text{Co}(\text{OAc})_2 \cdot 4\text{H}_2\text{O}$ and AlN in a nitrogen current under 1 atm pressure at 1750°C for 2 h as the starting material [69]. The cobalt content ranged from 0.01 to 5.0 at. % relative to aluminum.

In all AlON:Co samples, the $\text{Al}_5\text{O}_6\text{N}$ phase is the main phase according to XRD data. The samples with cobalt content from 0.01 to 0.5 at. % contain a small admixture of AlN. In samples with cobalt content of 1.0 and 2.5 at. %, a new impurity phase is detected, which becomes the only impurity in the AlON:5.0%Co sample. However, it was not possible to identify this phase. Corundum as an impurity phase was not detected even at the minimum cobalt content (0.01 at. %), as in the case of titanium ion doping.

The study of AlON:Co samples by XRD showed that the spectra of Al 2p and O 1s fully coincide with those of AlON:Ti samples. The spectra of the ground level N 1s show several peaks. The main peak (396.5 eV) appears to correspond to the Al–N bond [79], although this is shifted towards lower bond energies. A similar low-energy shift has been observed previously for numerous systems containing Me–N–O type bonds, such as Ti–N–O [80]. The second peak may be due to the formation of Co–N bonds.

As in the case of AlON:Ti, the optical bandgap width in AlON:Co samples was estimated by the Tautz method with subsequent correction of the absorption spectra. The E_g value varied from 5.72 to 5.84 eV when the cobalt content was varied.

The PCL spectra of the prepared AlON:Co samples are shown in Fig. 8. Three broad luminescence bands with maxima around 476, 595–600, and 750–760 nm are observed for all the samples. The AlON:0.05%Co sample exhibits the brightest luminescence. With increasing cobalt concentration, the intensity of all the bands decreases. The band with a maximum around 480–500 nm can be attributed to defects in the $[\text{V}_{\text{Al}}^{\text{III}}-\text{3O}_{\text{N}}^{\bullet}]$ type structure, and the bands with maxima around 600 and 765 nm to impurity emission centers of Mn^{2+} and Ti^{3+} or Fe^{2+} , respectively, as in the case of titanium-doped samples [68, 72].

AlON: Fe^{3+} samples were obtained by high-temperature roasting of mixtures of amorphous highly dispersed aluminum oxide Al_2O_3 , AlN, and Fe_2O_3 in a nitrogen current under a pressure of 1 atm for 2 h at a temperature of 1750°C [70]. The Fe^{3+} content ranged from 0.01 to 5.0 at. % relative to aluminum. The diffractograms of the obtained samples show that the main reflections correspond to the $\text{Al}_5\text{O}_6\text{N}$ phase with a small admixture of AlN. Besides AlN, an additional phase was present in all samples, which could not be identified. The total content of AlN and unidentified phase did not exceed 5 vol %. As in the case of doping with Ti and Co ions, the minimum iron content (0.01 at. %) already allows the formation of the $\alpha\text{-Al}_2\text{O}_3$ phase to be suppressed.

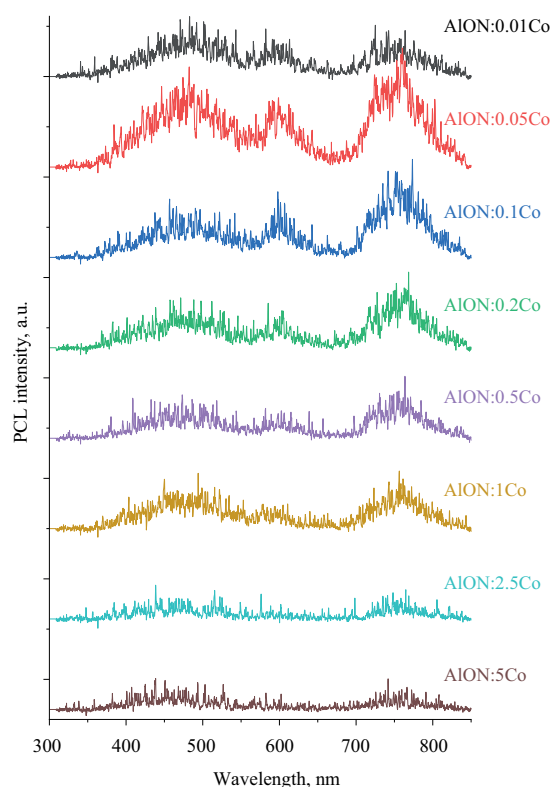
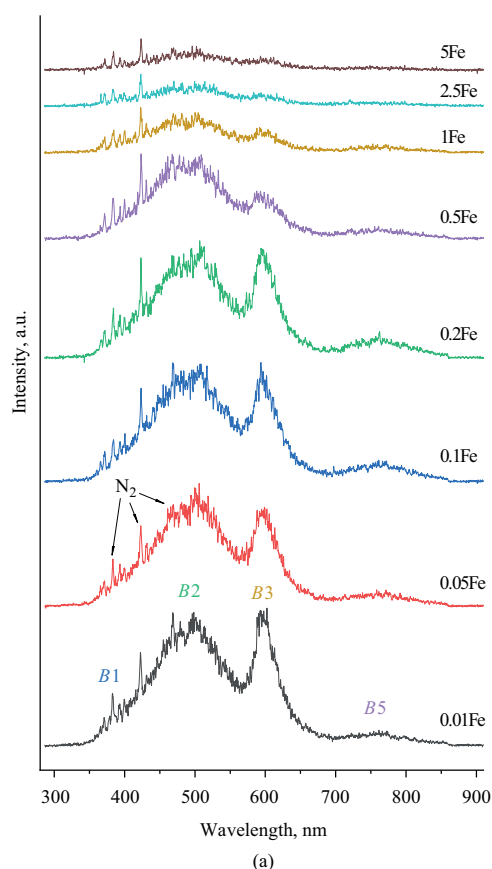


Fig. 8. PCL spectra of AlON: $x\%$ Co, $x = 0.01$ – 5.00 (reprinted from [69])



The optical bandgap width in AlON:Fe samples as evaluated by the Tautz method with correction of absorption spectra showed values in the range of 5.76–5.88 eV. The PCL spectra of AlON:Fe³⁺ samples (Fig. 9) contain broad luminescence bands with maxima around 495, 595, and 760 nm. The sample with the minimum iron content, AlON:0.01%Fe, has the most intense emission. The PCL spectra can be approximated by four bands with maxima around 398, 492, 602, and 738 nm. The band with maximum around 398 nm refers to radiative transitions in AlN [72]. The band with maximum around 492 nm is a consequence of emission of defects of the $[V_{Al}^{III}-3O_N^{\bullet}]$ type. The bands with maxima around 602 and 738 nm appear to be related to the emission of impurity ions (possibly Mn²⁺ and others).

The results of the studies of AlONs doped with TM ions allowed us to determine the state of TM ions in AlON matrices along with the solubility limits, as well as the influence of the nature and concentration of TM on the optical bandwidth and luminescent properties, which in the case of AlON:Ti, AlON:Co, and AlON:Fe are determined, first of all, by defects in the intrinsic structure of the AlONs.

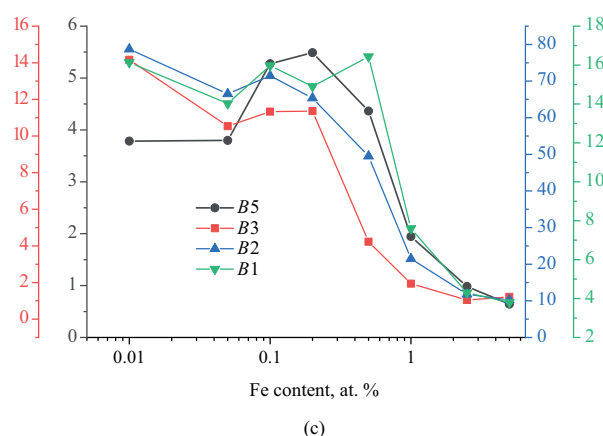
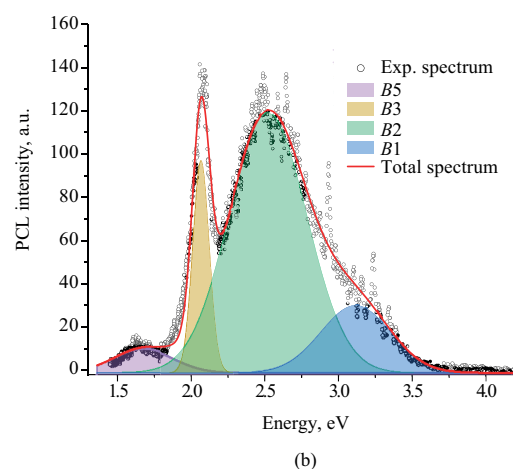


Fig. 9. (a) PCL spectra of AlON:Fe samples; (b) decomposition of PCL spectrum of AlON:0.01Fe by 4 Gaussian bands; (c) dependence of the intensity of B1, B2, B3, and B5 bands on the total iron content (reprinted from [70])

CONCLUSIONS

AlONs, in particular γ -AlON, whose composition is usually described by the formula $\text{Al}_{23}\text{O}_{27}\text{N}_5$ or $\text{Al}_5\text{O}_6\text{N}$, are promising materials not only for the manufacture of high-strength glasses, but also for use as matrices of phosphors. The main methods for producing aluminum oxynitrides include direct high-temperature interaction of aluminum oxide and nitride, direct nitriding and carbothermal reduction-nitriding. AlONs are doped with REM and TM ions both to improve sinterability and increase physical and mechanical characteristics, as well as to impart certain optical properties. To date, there is information on the use of oxides and other compounds of Mg, Y, La, Sc, La, Pr, Sm, Gd, Dy, Er, and Yb as sintering additives. Conversely, Eu^{2+} , Tb^{3+} , and Mn^{2+} , and in some cases Ce^{3+} , Er^{3+} , Sm^{3+} , Yb^{3+} , and Cr^{3+} , are

more commonly used to impart luminescent properties. Double doping with $\text{Eu}^{2+}/\text{Ce}^{3+}$, $\text{Tb}^{3+}/\text{Eu}^{2+}$, and $\text{Tb}^{3+}/\text{Ce}^{3+}$ ions can be used to adjust the luminescence color of the phosphor, as well as to reduce the content of terbium, one of the most expensive REMs, in phosphors due to the sensitization effect. Although doping with Ti, Co, and Fe ions does not impart luminescent properties, it facilitates the synthesis and processing of AlONs.

Acknowledgments

The work was carried out within the framework of State Assignment No. 075-00319-25-00.

Authors' contributions

N.S. Akhmadullina—generalization of data on synthesis and phase composition, preparation of the manuscript.

A.V. Ishchenko—summarizing data on luminescent properties.

Authors declare no conflicts of interest.

REFERENCES

1. Abyzov A.M. Aluminum oxide and alumina ceramics (Review). Part 1. Properties of Al_2O_3 and industrial production of dispersed Al_2O_3 . *Novye ognepropy = New Refractories*. 2019;1:16–23 (in Russ.). <https://doi.org/10.17073/1683-4518-2019-1-16-23>
2. Yamaguchi G., Yanagida H. Study on the reductive spinel – a new spinel formula $\text{AlN}-\text{Al}_2\text{O}_3$ instead of the previous one Al_3O_4 . *Bull. Chem. Soc. Jap.* 1959;32(11):1264–1265. <https://doi.org/10.1246/bcsj.32.1264>
3. McCauley J.W. A simple model for aluminum oxynitride spinels. *J. Am. Ceram. Soc.* 1978;61(7–8):372–373. <https://doi.org/10.1111/j.1151-2916.1978.tb09336.x>
4. McCauley J.W., Corbin N.D. Phase relations and reaction sintering of transparent cubic aluminum oxynitride spinel (ALON). *J. Am. Ceram. Soc.* 1979;62(9–10):476–479. <https://doi.org/10.1111/j.1151-2916.1979.tb19109.x>
5. McCauley J.W., Patel P., Chen M., Gilde G., Strassburger E., Paliwal B., Dandekar D.P. ALON: a brief history of its emergence and evolution. *J. Eur. Ceram. Soc.* 2009;29(2):223–236. <https://doi.org/10.1016/j.jeurceramsoc.2008.03.046>
6. McCauley J.W., Corbin N.D. High Temperature Reactions and Microstructures in the Al_2O_3 -AlN System. In: Riley F.L. (Ed.). *Progress in Nitrogen Ceramics. NATO ASI Series*. Springer; 1983. V. 65. P. 111–118. https://doi.org/10.1007/978-94-009-6851-6_8
7. Batyrev I.G., Taylor D.E., Gazonas G.A., McCauley J.W. Density functional theory and evolution algorithm calculations of elastic properties of AlON. *J. Appl. Phys.* 2014;115(2):023505. <https://doi.org/10.1063/1.4859435>
8. Swab J.J., LaSalvia J.C., Gilde G.A., Patel P.J., Motyka M.J. Transparent armor ceramics: Alon and spinel. *Ceram. Eng. Sci. Proc.* 1999;20(4):79–84. <https://doi.org/10.1002/9780470294574.ch10>
9. Maguire E.A., Rawson J.K., Tustison R.W. Aluminum oxynitride's resistance to impact and erosion. In: *SPIE's 1994 Int. Symposium on Optics, Imaging, and Instrumentation. Proc. SPIE*. 1994;2286:26–32. <https://doi.org/10.1117/12.187372>
10. Kargin Yu.F., Akhmadullina N.S., Solntsev K.A. Ceramic Materials and Phosphors Based on Silicon Nitride and SiALON. *Inorg. Mater.* 2014;50(13):1325–1342. <https://doi.org/10.1134/S0020168514130032>
11. Shang M., Geng D., Yang D., Kang X., Zhang Y., Lin J. Luminescence and energy transfer properties of $\text{Ca}_2\text{Ba}_3(\text{PO}_4)_3\text{Cl}$ and $\text{Ca}_2\text{Ba}_3(\text{PO}_4)_3\text{Cl}:\text{A}$ ($\text{A} = \text{Eu}^{2+}/\text{Ce}^{3+}/\text{Dy}^{3+}/\text{Tb}^{3+}$) under UV and low-voltage electron beam excitation. *Inorg. Chem.* 2013;52(6):3102–3112. <https://doi.org/10.1021/ic3025759>
12. Liu H., Luo Y., Mao Z., Liao L., Xia Z. A novel single-composition trichromatic white-emitting $\text{Sr}_{3.5}\text{Y}_{6.5}\text{O}_2(\text{PO}_4)_{1.5}(\text{SiO}_4)_{4.5}:\text{Ce}^{3+}/\text{Tb}^{3+}/\text{Mn}^{2+}$ phosphor: synthesis, luminescent properties and applications for white LEDs. *J. Mater. Chem. C*. 2014;2(9):1619–1627. <https://doi.org/10.1039/C3TC32003K>
13. Lin C.C., Liu R.S. Advances in phosphors for light-emitting diodes. *J. Phys. Chem. Lett.* 2011;2(11):1268–1277. <https://doi.org/10.1021/jz2002452>
14. Yamamoto H. White LED phosphors: the next step. *Proc. SPIE*. 2010;7598:08–14. <https://doi.org/10.1117/12.843536>
15. Bachmann V., Ronda C., Meijerink A. Temperature quenching of yellow Ce^{3+} luminescence in YAG:Ce. *Chem. Mater.* 2009;21(10):2077–2084. <http://dx.doi.org/10.1021/cm8030768>
16. Setlur A.A. Phosphors for LED-based solid-state lighting. *Electrochem. Soc. Interface*. 2009;18(4):32–36. <http://dx.doi.org/10.1149/2.F040941F>
17. Xia Z.G., Wang X.M., Wang Y.X., Liao L.B., Jing X.P. Synthesis, structure, and thermally stable luminescence of Eu^{2+} -doped $\text{Ba}_2\text{Ln}(\text{BO}_3)_2\text{Cl}$ ($\text{Ln} = \text{Y}$, Gd and Lu) host compounds. *Inorg. Chem.* 2011;50(20):10134–10142. <https://doi.org/10.1021/ic200988w>
18. Zhu G., Wang Y., Ci Z., Liu B., Shi Y., Xin S. $\text{Ca}_5\text{La}_5(\text{SiO}_4)_3(\text{PO}_4)_2\text{O}_2:\text{Ce}^{3+},\text{Mn}^{2+}$: A color-tunable phosphor with efficient energy transfer for white light-emitting diodes. *J. Electrochem. Soc.* 2011;158:J236–J242. <https://doi.org/10.1149/1.3595434>

19. Fukuyama H., Nakao W., Susa M., Nagata K. New synthetic method of forming aluminum oxynitride by plasma arc melting. *J. Am. Ceram. Soc.* 1999;82(6):1381–1387. <https://doi.org/10.1111/j.1151-2916.1999.tb01927.x>
20. Rafaniello W., Cutler I.B. Preparation of sinterable cubic aluminum oxynitride by the carbothermal nitridation of aluminum-oxide. *J. Am. Ceram. Soc.* 1981;64(10):128–C128. <https://doi.org/10.1111/j.1151-2916.1981.tb10232.x>
21. Zientara D., Bučko M.M., Lis J. ALON-based materials prepared by SHS technique. *J. Eur. Ceram. Soc.* 2007;27(2–3): 775–779. <https://doi.org/10.1016/j.jeurceramsoc.2006.04.008>
22. Wang S.F., Zhang J., Luo D.W., Gua F., Tang D.Y., Dong Z.L., Kong L.B. Transparent ceramics: Processing, materials and applications. *Prog. Sol. State Chem.* 2013;41:20–54. <https://doi.org/10.1016/j.progsolidstchem.2012.12.002>
23. Patel P.J., Gilde G., McCauley J.W. The role of gas pressure in transient liquid phase sintering of aluminum oxynitride (Alon). *Cer. Eng. Sci. Proc.* 2003;24(3):425–431. <https://doi.org/10.1002/9780470294802.ch61>
24. Martin C., Cales B. Synthesis and Hot Pressing Of Transparent Aluminum Oxynitride. In: *SPIE 1989 Technical Symposium on Aerospace Sensing. Proc. SPIE*; 1989. V. 1112. P. 20–24. <https://doi.org/10.1117/12.960759>
25. Jin X., Gao L., Sun J., Liu Y., Gui L. Highly Transparent ALON Pressurelessly Sintered from Powder Synthesized by a Novel Carbothermal Nitridation Method. *J. Am. Ceram. Soc.* 2012;95(9): 2801–2807. <https://doi.org/10.1111/j.1551-2916.2012.05253.x>
26. Wang J., Zhang F., Chen F., Zhang J., Zhang H., Tian R., Wang Z., Liu J., Zhang Z., Chen S., Wang S. Effect of Y_2O_3 and La_2O_3 on the sinterability of γ -ALON transparent ceramics. *J. Eur. Ceram. Soc.* 2015;35(1):23–28. <https://doi.org/10.1016/j.jeurceramsoc.2014.07.016>
27. Tsukuma K. Transparent $MgAl_2O_4$ Spinel Ceramics Produced by HIP Post-Sintering. *J. Ceram. Soc. Jap.* 2006;114(1334): 802–806. <https://doi.org/10.2109/jcersj.114.802>
28. Chen F., Zhang F., Wang J., Zhang H., Tian R., Zhang J., Zhang Z., Sun F., Wang S. Microstructure and optical properties of transparent aluminum oxynitride ceramics by hot isostatic pressing. *Scripta Mater.* 2014;81:20–23. <https://doi.org/10.1016/j.scriptamat.2014.02.009>
29. Chen F., Zhang F., Wang J., Zhang H., Tian R., Zhang Z., Wang S. Hot isostatic pressing of transparent ALON ceramics with Y_2O_3/La_2O_3 additives. *J. Alloys Compd.* 2015;650: 753–757. <https://doi.org/10.1016/j.jallcom.2015.08.028>
30. Zhang J., Lei J., Shi Y., Xie J., Lei F., Zhang L. Effect of Y_2O_3 , La_2O_3 and MgO Co-Doping on Densification, Microstructure and Properties of ALON Ceramics. *J. Ceram. Sci. Tech.* 2017;8(1):177–182. <https://dx.doi.org/10.4416/JCST2016-00114>
31. Dong Q., Yang F., Cui J., Tian Y., Liu S., Du F., Peng J., Ye X. Enhanced narrow green emission and thermal stability in γ -ALON:Mn²⁺,Mg²⁺ phosphor via charge compensation. *Ceram. Int.* 2019;45(9): 11868–11875. <https://doi.org/10.1016/j.ceramint.2019.03.069>
32. Thi M.H.N., Le P.X. Utilizing a strait-range green phosphor γ -ALON: Mn,Mg for the task of achieving a super-broad hue gamut display. *Indones. J. Electr. Eng. Comput. Sci.* 2022;27(2): 748–753. <http://doi.org/10.11591/ijeecs.v27.i2.pp748-753>
33. Kikkawa S., Hatta N., Takeda T. Preparation of Aluminum Oxynitride by Nitridation of a Precursor Derived from Aluminum–Glycine Gel and the Effects of the Presence of Europium. *J. Am. Ceram. Soc.* 2008;91(3):924–928. <https://doi.org/10.1111/j.1551-2916.2007.02213.x>
34. Yin L., Xu X., Hao L., Xie W., Wang Y., Yang L., Yang X. Synthesis and photoluminescence of Eu²⁺–Mg²⁺ co-doped γ -ALON phosphors. *Mater. Lett.* 2009;63(17):1511–1513. <https://doi.org/10.1016/j.matlet.2009.04.002>
35. Zhang F., Chen S., Chen J.F., Zhang H.L., Li J., Liu X.J., Wang S.W. Characterization and luminescence properties of ALON:Eu²⁺ phosphor for white-emitting-diode illumination. *J. Appl. Phys.* 2012;111(8):083532. <https://doi.org/10.1063/1.4705404>
36. Zhang L., Luo H., Zhou L., Liu Q., Li J., Zhang W. Preparation of γ -aluminum oxynitride phosphor with Eu doping by direct nitridation in ammonia and postannealing. *J. Am. Ceram. Soc.* 2018;101(8):3299–3308. <https://doi.org/10.1111/jace.15494>
37. Akhmadullina N.S., Lysenkov A.S., Ashmarin A.A., Baranchikov A.E., Ishchenko A.V., Yagodin V.V., Shul'gin B.V., Kargin Yu.F. Synthesis and luminescence properties of Eu²⁺- and Ce³⁺-doped ALONs. *Ceram. Int.* 2016;42(1):286–293. <https://doi.org/10.1016/j.ceramint.2015.08.107>
38. Akhmadullina N.S., Ishchenko A.V., Yagodin V.V., et al. Synthesis and Luminescence Properties of Tb³⁺-Doped Aluminum Oxynitride. *Inorg. Mater.* 2019;55(12):1223–1229. <http://dx.doi.org/10.1134/S002016851912001X> [Original Russian Text: Akhmadullina N.S., Ishchenko A.V., Yagodin V.V., Lysenkov A.S., Sirotinkin V.P., Kargin Yu.F., Shulgin B.V. Synthesis and Luminescence Properties of Tb³⁺-Doped Aluminum Oxynitride. *Neorganicheskie materialy*. 2019;55(12):1298–1304 (in Russ.). <https://doi.org/10.1134/S0002337X19120017>]
39. Akhmadullina N.S., Ishchenko A.V., Lysenkov A.V., Shishilov O.N., Kargin Yu.F. Synthesis and luminescence properties of Eu²⁺/Ce³⁺, Ce³⁺/Tb³⁺ and Eu²⁺/Tb³⁺ co-doped ALONs. *J. Alloys Compd.* 2021;887:161410. <https://doi.org/10.1016/j.jallcom.2021.161410>
40. Zorenko Y., Zorenko T., Voznyak T., Mandowski A., Xia Q., Batentschuk M., Friedrich J. Luminescence of F⁺ and F centers in Al₂O₃-Y₂O₃ oxide compounds. *IOP Conf. Ser.: Mater. Sci. Eng.* 2010;15:012060. <http://dx.doi.org/10.1088/1757-899X/15/1/012060>
41. Trinkler L., Berzina B. Localised transitions in luminescence of AlN ceramics. *Radiat. Meas.* 2014;71:232–236. <https://doi.org/10.1016/j.radmeas.2014.02.016>
42. Weinstein I.A., Vokhmintsev A.S., Spiridonov D.M. Thermoluminescence kinetics of oxygen-related centers in AlN single crystals. *Diam. Relat. Mater.* 2012;25:59–62. <https://doi.org/10.1016/j.diamond.2012.02.004>
43. Zhang X., Li Z., Zeng Q. First-principles calculation on the electronic structure and optical properties of Eu²⁺ doped γ -ALON phosphor. *Ceram. Int.* 2018;44(2):1461–1466. <https://doi.org/10.1016/j.ceramint.2017.10.044>
44. French R.H. Electronic band structure of Al₂O₃, with comparison to ALON and AlN. *J. Am. Ceram. Soc.* 1990;73(3):477–489. <https://doi.org/10.1111/j.1151-2916.1990.tb06541.x>
45. Thomas M.E., Tropf W.J., Gilbert S.L. Vacuum-ultraviolet characterization of sapphire ALON, and spinel near the band gap. *Opt. Eng.* 1993;32(6):1340–1343. <https://doi.org/10.1117/12.135837>
46. Chen C.-F., Yang P., King G., Tegtmeier E.L. Processing of Transparent Polycrystalline ALON:Ce³⁺ Scintillators. *J. Am. Ceram. Soc.* 2016;99(2):424–430. <https://doi.org/10.1111/jace.13986>
47. Hu W.-W., Zhu Q.-Q., Hao L.-Y., Xu X., Agathopoulos S. Luminescence properties and energy transfer in Al₅O₆N:Ce³⁺,Tb³⁺ phosphors. *J. Luminesc.* 2014;149:155–158. <https://doi.org/10.1016/j.jlumin.2014.01.010>
48. Cavalli E., Boutinaud P., Mahiou R., Bettinelli M., Dorenbos P. Luminescence Dynamics in Tb³⁺-Doped CaWO₄ and CaMoO₄ Crystals. *Inorg. Chem.* 2010;49(11):4916–4921. <https://doi.org/10.1021/ic902445c>

49. Baklanova Y.V., Maksimova L.G., Denisova T.A., Tyutyunnik A.P., Zubkov V.G. Synthesis and Luminescence Properties of Tb^{3+} and Dy^{3+} Doped $Li_7La_3Hf_2O_{12}$ with Tetragonal Garnet Structure. *Opt. Mater.* 2019;87:122–126. <https://doi.org/10.1016/j.optmat.2018.04.041>
50. Han B., Liang H., Huang Y., Tao Y., Su Q. Vacuum Ultraviolet–Visible Spectroscopic Properties of Tb^{3+} in $Li(Y,Gd)(PO_3)_4$: Tunable Emission, Quantum Cutting, and Energy Transfer. *J. Phys. Chem. C* 2010;114(14):6770–6777. <https://doi.org/10.1021/jp100755d>
51. Zhang F., Wang S.W., Liu X.J., An L.Q., Yuan X.Y. Upconversion luminescence in Er-doped γ -AlON ceramic phosphors. *J. Appl. Phys.* 2009;105(9):093542. <https://doi.org/10.1063/1.3125516>
52. Zhang F., Chen S., Zhang H.L., Li J., Yang Y., Zhou G.H., Liu X.J., Wang S.W. Upconversion Luminescence of γ -AlON:Er $^{3+}$ Phosphors with Mg $^{2+}$ Co-Doping. *J. Am. Ceram. Soc.* 2012;95(1):27–29. <https://doi.org/10.1111/j.1551-2916.2011.04916.x>
53. Wang Y., Xie X., Qi J., Wang S., Wei N., Lu Z., Chen X., Lu T. Bifunctional behavior of Er $^{3+}$ ions as the sintering additive and the fluorescent agent in Er $^{3+}$ single doped γ -AlON transparent ceramics. *J. Lumin.* 2016;175:203–206. <https://doi.org/10.1016/j.jlumin.2016.02.039>
54. Tsabit A.M., Kim M.-D., Yoon D.-H. Effects of various rare-earth additives on the sintering and transmittance of γ -AlON. *J. Eur. Ceram. Soc.* 2020;40(8):3235–3243. <https://doi.org/10.1016/j.jeurceramsoc.2020.03.027>
55. Tsabit A.M., Chung W.J., Lee H., Yoon D.-H. Fabrication and photoluminescence of γ -AlON:Sm and Yb. *J. Am. Ceram. Soc.* 2022;42(4):1348–1353. <https://doi.org/10.1016/j.jeurceramsoc.2021.12.015>
56. Liu R.S., Liu Y.H., Bagkar N.C., Hu S.F., Enhanced luminescence of $SrSi_2O_2N_2:Eu^{2+}$ phosphors by codoping with Ce $^{3+}$, Mn $^{2+}$, and Dy $^{3+}$ ions. *Appl. Phys. Lett.* 2007;91(6):061119. <http://dx.doi.org/10.1063/1.2768916>
57. Song X., Fu R., Agathopoulos S., He H., Zhao X., Li R., Luminescence and energy transfer mechanism in $SrSi_2O_2N_2:Ce^{3+}$, Eu^{2+} phosphors for white LEDs. *J. Electrochem. Soc.* 2010;157(2):J34–J38. <https://doi.org/10.1149/1.3270491>
58. Jian X., Wang H., Lee M.-H., Tian W., Chen G.-Z., Chen W.-Q., Ji W.-W., Xu X., Yin L.-J. Insight the Luminescence Properties of AlON: Eu, Mg Phosphor under VUV Excitation. *Mater.* 2017;10(7):723. <https://doi.org/10.3390/ma10070723>
59. Deng L., Lei J., Shi Y., Lin T., Ren Y., Xie J., Photoluminescence of Tb^{3+}/Ce^{3+} co-doped aluminum oxynitride powders. *Mater. Lett.* 2011;65(4):769–771. <https://doi.org/10.1016/j.matlet.2010.11.027>
60. Wu Q., Li Y., Wang X., Zhao Z., Wang C., Li H., Mao A., Wang Y. Novel optical characteristics of Eu^{2+} doped and Eu^{2+} , Ce $^{3+}$ co-doped $LiSi_2N_3$ phosphors by gas-pressed sintering. *RSC Adv.* 2014;4(73):39030–39036. <https://doi.org/10.1039/C4RA05502K>
61. Chen L., Du F., Liang Y., Zhu Y., Xiao Y., Peng J. A study on photoluminescence and energy transfer of γ -AlON:Ce $^{3+}$, Eu^{2+} phosphors for application in full-visible-spectrum LED lighting. *Displays.* 2022;71:102147. <https://doi.org/10.1016/j.displa.2021.102147>
62. Zhang J., Ma C., Wen Z., Du M., Long J., Ma R., Yuan X., Li J., Cao Y. Photoluminescence and energy transfer properties of Eu^{2+} and Tb^{3+} co-doped gamma aluminum oxynitride powders. *Opt. Mater.* 2016;58:290–295. <https://doi.org/10.1016/j.optmat.2016.05.048>
63. Xie R.-J., Hirosaki N., Liu X.-J., Takeda T., Li H.-L. Crystal Structure and Photoluminescence of Mn $^{2+}$, Mg $^{2+}$ Codoped Gamma Aluminum Oxynitride (γ -AlON): A Promising Green Phosphor for White Light-Emitting Diode. *Appl. Phys. Lett.* 2008;92(20):201905. <https://doi.org/10.1063/1.2920190>
64. Kitaura M., Harima A., Xie R.-J., Takeda T., Hirosaki N., Ohnishi A., Sasaki M. Electron Spin Resonance Study on Local Structure of Manganese Ions Doped in Gamma-Aluminum Oxynitride Phosphors. *J. Light & Vis. Env.* 2012;36(1):6–9. <https://doi.org/10.2150/jlve.36.6>
65. Hao L., Miao X., Li K., Zhong J., Tu B., Yang Z., Wang H. Structural and Luminescent Properties of $Mg_{0.25-x}Al_{2.57}O_{3.79}N_{0.21-x}Mn^{2+}$ Green-Emitting Transparent Ceramic Phosphor. *J. Wuhan Univ. Technol.-Mat. Sci. Edit.* 2024;39(3):533–540. <https://doi.org/10.1007/s11595-024-2909-3>
66. Zhou X., Chen S., Zhang C., Huang X., Lu K., Qi L., Lu T. Mn $^{2+}$ /Mg $^{2+}$ co-doped AlON ceramic with ultra-narrowband green emission combining high transparency toward a wide gamut backlight application. *Opt. Lett.* 2024;49(9):2245–2248. <https://doi.org/10.1364/OL.520495>
67. Liu L., Zhang J., Wang X., Hou W., Liu X., Xu M., Yang J., Liang B. Preparation and fluorescence properties of a Cr $^{3+}$: γ -AlON powder by high temperature solid state reaction. *Mater. Lett.* 2020;258:126811. <https://doi.org/10.1016/j.matlet.2019.126811>
68. Ishchenko A.V., Akhmadullina N.S., Leonidov I.I., Sirotinkin V.P., Skvortsova L.G., Shishilov O.N., Zhidkov I.S., Kukharensko A.I., Kargin Yu.F. Synthesis and spectroscopic properties of aluminum oxynitride doped with 3d-metal ions: The case of γ -AlON:Ti. *J. Alloys Compd.* 2023;934:167792. <https://doi.org/10.1016/j.jallcom.2022.167792>
69. Ishchenko A.V., Akhmadullina N.S., Leonidov I.I., Sirotinkin V.P., Skvortsova L.G., Mandrygina D.A., Shishilov O.N., Zhidkov I.S., Kukharensko A.I., Weinstein I.A., Kargin Yu.F. Synthesis, phase composition, electronic and spectroscopic properties of cobalt-doped aluminum oxynitride. *Physica B: Condens. Matter.* 2024;695:416593. <https://doi.org/10.1016/j.physb.2024.416593>
70. Ishchenko A.V., Akhmadullina N.S., Pastukhov D.A., et al. Phase composition and optical properties of Fe-doped aluminum oxynitride. *Inorg. Mater.* 2024;60(3):859–866. <https://doi.org/10.1134/S002016852470119X> [Original Russian Text: Ishchenko A.V., Akhmadullina N.S., Pastukhov D.A., Leonidov I.I., Sirotinkin V.P., Lysenkov A.S., Shishilov O.N., Kargin Yu.F. Phase composition and optical properties of Fe-doped aluminum oxynitride. *Neorganicheskie materialy.* 2024;60(3):322–330 (in Russ.).]
71. Kubelka P., Munk F. Ein beitrag zur optik der farbanstriche. *Z. Tech. Phys.* 1931;12:593–601.
72. Du X., Yao S., Jin X., Chen H., Li W., Liang B. Radiation damage and luminescence properties of gamma aluminum oxynitride transparent ceramic. *J. Phys. D.: Appl. Phys.* 2015;48(34):345104. <https://doi.org/10.1088/0022-3727/48/34/345104>
73. Tauc J. Optical properties and electronic structure of amorphous Ge and Si. *Mater. Res. Bull.* 1968;3(1):37–46. [https://doi.org/10.1016/0025-5408\(68\)90023-8](https://doi.org/10.1016/0025-5408(68)90023-8)
74. Xu J., Cherepy N.J., Ueda J., Tanabe S. Red persistent luminescence in rare earth- free AlN:Mn $^{2+}$ phosphor. *Mater. Lett.* 2017;206:175–177. <https://doi.org/10.1016/j.matlet.2017.07.015>
75. Zorenko Y., Zorenko T., Voznyak T., Nizhankovskiy S., Krivonosov E., Danko A., Puzikov V., Comparative study of the luminescence of $Al_2O_3:Ti$ and Al_2O_3 crystals under VUV synchrotron radiation excitation. *Opt. Mater.* 2013;35(12):2053–2055. <https://doi.org/10.1016/j.optmat.2012.10.044>

76. Gaffney E.S. Spectra of tetrahedral Fe^{2+} in MgAl_2O_4 . *Phys. Rev. B.* 1973;8:3484–3486. <https://doi.org/10.1103/PhysRevB.8.3484>
77. Basyrova L., Bukina V., Balabanov S., Belyaev A., Drobotenko V., Dymshits O., Alekseeva I., Tsenter M., Zapalova S., Khubetsov A., Zhilin A., Volokitina A., Vitkin V., Mateos X., Serres J.M., Camy P., Loiko P. Synthesis, structure and spectroscopy of $\text{Fe}^{2+}:\text{MgAl}_2\text{O}_4$ transparent ceramics and glass-ceramics. *J. Lumin.* 2021;236:118090. <https://doi.org/10.1016/j.jlumin.2021.118090>
78. Thi Le T.-L., Nguyen L.T., Nguyen H.-H., Van Nghia N., Vuong N.M., Hieu H.N., Van Thang N., Le V.T., Nguyen V.H., Lin P.-C., Yadav A., Madarevic I., Janssens E., Van Bui H., Ngoc L.L.T. Titanium nitride nanodonuts synthesized from natural ilmenite ore as a novel and efficient thermoplasmonic material. *Nanomaterials.* 2021;11(1):76. <https://doi.org/10.3390/nano11010076>
79. Tabora J.A.P., Landázuri H.R., Londoño L.P.V. Correlation Between Optical, Morphological, and Compositional Properties of Aluminum Nitride Thin Films by Pulsed Laser Deposition. *IEEE Sens. J.* 2016;16(2):359–364. <https://doi.org/10.1109/JSEN.2015.2466467>
80. Prieto P., Kirby R.E. X-ray photoelectron spectroscopy study of the difference between reactively evaporated and direct sputter-deposited TiN films and their oxidation properties. *J. Vac. Sci. Technol. A.* 1995;13(6):2819–2826. <https://doi.org/10.1116/1.579711>

About the Authors

Nailya S. Akhmadullina, Cand. Sci. (Chem.), Senior Researcher, Laboratory of Physical and Chemical Analysis of the Ceramic Materials, A.A. Baikov Institute of Metallurgy and Material Science of the Russian Academy of Sciences (49, Leninskii pr., Moscow, 119991, Russia). E-mail: nakhmadullina@mail.ru. Scopus Author ID 26432528700, ResearcherID M-7540-2018, RSCI SPIN-code 4892-2471, <https://orcid.org/0000-0002-5662-1223>

Aleksy V. Ishchenko, Cand. Sci. (Phys.-Math.), Associate Professor, Senior Researcher, Department of Experimental Physics, Ural Federal University (19, Mira pr., Yekaterinburg, 620062, Russia). E-mail: a-v-i@mail.ru. Scopus Author ID 57195266830, RSCI SPIN-code 3652-5774, <https://orcid.org/0000-0002-9883-6652>

Об авторах

Ахмадуллина Наиля Сайфулловна, к.х.н., старший научный сотрудник, лаборатория физико-химического анализа керамических материалов, ФГБУН «Институт металлургии и материаловедения им. А.А. Байкова Российской академии наук» (119991, Россия, Москва, Ленинский пр., д. 49). E-mail: nakhmadullina@mail.ru. Scopus Author ID 26432528700, ResearcherID M-7540-2018, SPIN-код РИНЦ 4892-2471, <https://orcid.org/0000-0002-5662-1223>

Ищенко Алексей Владимирович, к.ф.-м.н., доцент, старший научный сотрудник, кафедра экспериментальной физики, ФГАОУ ВО «Уральский федеральный университет имени первого Президента России Б.Н. Ельцина» (620062, Россия, Екатеринбург, пр. Мира, д. 19). E-mail: a-v-i@mail.ru. Scopus Author ID 57195266830, SPIN-код РИНЦ 3652-5774, <https://orcid.org/0000-0002-9883-6652>

Translated from Russian into English by H. Moshkov

Edited for English language and spelling by Thomas A. Beavitt

Chemistry and technology of inorganic materials
Химия и технология неорганических материалов

UDC 546.03, 54.057

<https://doi.org/10.32362/2410-6593-2025-20-4-344-356>

EDN PPMBCCK



RESEARCH ARTICLE

Cr-substituted M-type hexaferrite solid solutions with high level of substitution

Alena R. Zykova¹, Andrey I. Kovalev¹✉, Darya P. Sherstyuk¹, Vladimir E. Zhivulin¹,
Sergey V. Taskaev², Denis A. Vinnik^{1,3,4}

¹ Laboratory of Single Crystal Growth, South Ural State University National Research University, Chelyabinsk, 454080 Russia

² Chelyabinsk State University, Chelyabinsk, 454001 Russia

³ Moscow Institute of Physics and Technology (State University), Dolgoprudny, 141700 Russia

⁴ St. Petersburg State University, St. Petersburg, Peterhof, 198504 Russia

✉ Corresponding author, e-mail: kovalev-andrey-i@mail.ru

Abstract

Objectives. This study aims to synthesize strontium hexaferrites having a high level of chromium substitution ($\text{SrFe}_{12-x}\text{Cr}_x\text{O}_{19}$, $x = 0-6$) and investigate their structural, morphological, and magnetic properties.

Methods. The synthesis was carried out using the solid-phase reaction method at a temperature of 1400°C. The impact of chromium substitution for iron on the phase, structure, morphology, and magnetic characteristics was studied using powder X-ray diffraction (XRD), scanning electron microscopy (SEM), energy-dispersive X-ray spectroscopy, and vibrating-sample magnetometry.

Results. XRD analysis confirmed the development of single-phase samples having a hexagonal space group $P6_3/\text{mmc}$. An increase in Cr concentration leads to a decrease in unit cell parameters, due to the smaller ionic radius of Cr^{3+} . The surface morphology of the samples consists of bulk crystallites a few microns in length. Substitution with Cr results in decreased saturation and remanent magnetization.

Conclusions. Pure samples of Cr-substituted strontium hexaferrite were synthesized. The linear dependence of the investigated structural parameters on the Cr concentration confirms the Cr substitution into the hexaferrite solid solution by Vegard's law. In addition to structural parameters, magnetic characteristics were obtained for hexaferrite solid solutions. Saturation and remanent magnetization dependencies were shown to significantly decrease with Cr concentration, while coercive force varies in a complex dependence on Cr concentration. The sample with $x = 1$ has the highest product of coercive force and saturation magnetization, indicating its suitability for permanent magnet application.

Keywords

strontium hexaferrites, structure, XRD, SEM, DSC, vibrating-sample magnetometry

Submitted: 18.11.2024

Revised: 24.01.2025

Accepted: 23.05.2025

For citation

Zykova A.R., Kovalev A.I., Sherstyuk D.P., Zhivulin V.E., Taskaev S.V., Vinnik D.A. Cr-substituted M-type hexaferrite solid solutions with high level of substitution. *Tonk. Khim. Tekhnol. = Fine Chem. Technol.* 2025;20(4):344–356. <https://doi.org/10.32362/2410-6593-2025-20-4-344-356>

НАУЧНАЯ СТАТЬЯ

Твердые растворы гексаферритов М-типа с высокой степенью замещения Cr

А.Р. Зыкова¹, А.И. Ковалев¹✉, Д.П. Шерстюк¹, В.Е. Живулин¹, С.В. Таскаев², Д.А. Винник^{1,3,4}

¹ Южно-Уральский государственный университет (национальный исследовательский университет), Челябинск, 454080 Россия

² Челябинский государственный университет, Челябинск, 454001 Россия

³ Московский физико-технический институт (национальный исследовательский университет), Долгопрудный, 141700 Россия

⁴ Санкт-Петербургский государственный университет, Санкт-Петербург, Петергоф, 198504 Россия

✉ Автор для переписки, e-mail: kovalev-andrey-i@mail.ru

Аннотация

Цели. Работа нацелена на синтез стронциевых гексаферритов с высокой степенью замещения железа хромом и исследование их структурных, термических, морфологических и магнитных свойств.

Методы. Синтез образцов проводился по твердофазному методу при температуре 1400°C. Влияние замещения железа хромом на фазовый состав, структуру, морфологию и магнитные характеристики синтезированных гексаферритов исследовано методами рентгеновской дифракции, сканирующей электронной микроскопии, энергодисперсионной рентгеновской спектроскопии и вибрационной магнитометрии.

Результаты. Анализ методом рентгеновской дифракции показал, что полученные образцы однофазные и соответствуют гексагональной структуре с пространственной группой $R\bar{6}_3/mmc$. С ростом концентрации хрома размеры элементарной ячейки уменьшаются, что происходит из-за меньшего ионного радиуса иона Cr^{3+} . Морфология поверхности образцов показывает присутствие крупных частиц, размером в несколько микрон. Замещение железа хромом приводит к снижению остаточной намагниченности и намагниченности насыщения.

Выводы. Однофазные образцы Cr-замещенных стронциевых гексаферритов получены твердофазным методом. Структурные параметры образцов линейно зависят от концентрации Cr, что подтверждает замещение хромом в твердых растворах гексаферритов из-за соблюдения правила Вегарда. В дополнение к структурным параметрам, изучены магнитные характеристики твердых растворов. Для остаточной намагниченности и намагниченности насыщения наблюдается значительное снижение с ростом концентрации Cr. Коэрцитивная сила носит сложный характер зависимости от концентрации Cr. Образец со степенью замещения $x = 1$ обладает наибольшим произведением намагниченности насыщения и коэрцитивной силы, что подчеркивает его применимость в качестве постоянного магнита.

Ключевые слова

гексаферриты стронция, структура, рентгеновская дифракция, сканирующая электронная микроскопия, дифференциальная сканирующая калориметрия, вибрационная магнитометрия

Поступила: 18.11.2024

Доработана: 24.01.2025

Принята в печать: 23.05.2025

Для цитирования

Zykova A.R., Kovalev A.I., Sherstyuk D.P., Zhivulin V.E., Taskaev S.V., Vinnik D.A. Cr-substituted M-type hexaferrite solid solutions with high level of substitution. *Tonk. Khim. Tekhnol. = Fine Chem. Technol.* 2025;20(4):344–356. <https://doi.org/10.32362/2410-6593-2025-20-4-344-356>

INTRODUCTION

Ferrites are an important class of materials, playing a significant role in magnetic applications and high frequency electronics [1–5]. Among them, a subclass of M-type hexagonal ferrites has attracted the research attention due to their unique properties: a Curie temperature of about 450°C, a high corrosion resistance, low production costs, a magnetocrystalline anisotropy of 17.5 kOe, and low dielectric loss [6–9]. Barium

hexaferrite ($BaFe_{12}O_{19}$) was the first investigated M-type hexaferrite. This material was used in permanent magnet manufacturing along with strontium hexaferrite ($SrFe_{12}O_{19}$), which is more easily manufacturable, as well as offering higher coercivity (H_c) and remanence magnetization (M_r), which are important permanent magnet characteristics [10].

Barium and strontium hexaferrites are still used for permanent magnet manufacturing, however,

due to the interest in the M-type hexagonal ferrites structure, proposed hexaferrite applications include photocatalysis [11, 12] and electromagnetic interference shielding [13–15]. Many different hexaferrite solid solutions have been synthesized and investigated using various methods. Mono- or polysubstituted $\text{BaFe}_{12}\text{O}_{19}$ with Sr [16], Al [17], Ca [18], Ti [19], Mn [20], Ni [21], Gd [22], Cr [23], etc. atoms have been reported, as well as high entropy solid solutions [24–26].

In the scientific literature on hexaferrite, relatively few works have focused on partially Cr^{3+} substituted barium hexaferrite [27–32]. From analyzing these sources, it can be seen that Cr^{3+} substituted barium hexaferrite was earlier synthesized by sol–gel [27–31] and solid-state [32] methods. In the works [27–29], the level of Cr^{3+} substitution (x) varies from 0.25 to 1, while the synthesis temperature lies in the range from 850 to 1000°C. However, the obtained samples were subject to impurity constraints, consisting not only in the target $\text{BaCr}_x\text{Fe}_{(12-x)}\text{O}_{19}$ phase, but also in $\alpha\text{-Fe}_2\text{O}_3$ [27] and Cr_2O_3 [28, 29]. In work [28], the authors were able to obtain single-phase samples of $\text{BaCr}_x\text{Fe}_{(12-x)}\text{O}_{19}$ with $x(\text{Cr}) = 0.1\text{--}0.8$. An increase in Cr concentration was shown to lead to lower saturation magnetization and higher coercive force values. Single-phase samples were also obtained in [31], where $x(\text{Cr}) = 0, 0.5, 1.0, 2.0$. The synthesis of pure barium hexaferrite with $x(\text{Cr}) = 2$ by the solid-state method was reported in the work [32]; the synthesis process was carried out for 3 h at a temperature of 1300°C.

Concluding the literature review, it becomes clear that the synthesis of single-phase of partially Cr-substituted barium hexaferrite remains problematic. Meanwhile, strontium hexaferrite has not been investigated in terms of Cr substitution. At the same time, an interest in Cr-substituted hexaferrites could be identified in the analyzed publications.

The present study set out to obtain single-phase samples of M-type Sr hexaferrites $\text{SrFe}_{(12-x)}\text{Cr}_x\text{O}_{19}$ with x from 0 to 6 and investigate their magnetic, structural, and morphological properties.

MATERIALS AND METHODS

Sample preparation

The samples were prepared using solid-state synthesis. Iron oxide (Fe_2O_3), chromium oxide (Cr_2O_3), and strontium carbonate (SrCO_3) were used as initial components for synthesis. All of the components were reagent-grade (*Reahim*, Russia). They were weighed at a given stoichiometric ratio and ground in an agate mortar (*Rushim*, Russia). Table 1 shows the chemical formula of the samples as well as the mass content of the initial components.

Table 1. Compositions of the initial mixture

No.	Chemical formula	Mass ratio of the initial components, g		
		SrCO_3	Fe_2O_3	Cr_2O_3
1	$\text{SrFe}_{11.5}\text{Cr}_{0.5}\text{O}_{19}$	1.3374	8.3183	0.3442
2	$\text{SrFe}_{11}\text{Cr}_1\text{O}_{19}$	1.3398	7.9706	0.6897
3	$\text{SrFe}_{10.5}\text{Cr}_{1.5}\text{O}_{19}$	1.3421	7.6216	1.0363
4	$\text{SrFe}_{10}\text{Cr}_2\text{O}_{19}$	1.3445	7.2714	1.3842
5	$\text{SrFe}_{9.5}\text{Cr}_{2.5}\text{O}_{19}$	1.3468	6.9199	1.7332
6	$\text{SrFe}_9\text{Cr}_3\text{O}_{19}$	1.3492	6.5673	2.0836
7	$\text{SrFe}_{8.5}\text{Cr}_{3.5}\text{O}_{19}$	1.3516	6.2133	2.4351
8	$\text{SrFe}_8\text{Cr}_4\text{O}_{19}$	1.3539	5.8582	2.7879
9	$\text{SrFe}_{7.5}\text{Cr}_{4.5}\text{O}_{19}$	1.3563	5.5017	3.1419
10	$\text{SrFe}_7\text{Cr}_5\text{O}_{19}$	1.3587	5.1441	3.4972
11	$\text{SrFe}_{6.5}\text{Cr}_{5.5}\text{O}_{19}$	1.3612	4.7851	3.8537
12	$\text{SrFe}_6\text{Cr}_6\text{O}_{19}$	1.3636	4.4249	4.2116

After grinding, the mixture was pressed into tablets with a diameter of 8 mm and a height of 5 mm using a hydraulic laboratory press FFMP-15T (*KARALTAY*, Russia) and a metal mold with a force of 5 t/cm².

The samples were placed on a platinum substrate and sintered in a self-made tube furnace with silicon carbide heaters. Solid-state synthesis lasted for 5 h at 1400°C.

Phase, structural, microstructural, and elemental analysis

The samples obtained through chemical reaction were studied via powder X-ray diffraction (XRD) analysis (Ultima IV powder diffractometer with $\text{CuK}\alpha$ radiation, *Rigaku*, Japan), scanning electron microscopy (SEM), and elemental microanalysis.

The phase content and cell parameters were studied at 25°C. The unit cell parameters were calculated by the Rietveld method using the PDXL software (*Rigaku*, Japan) application. The chemical composition and microstructure images were examined using the scanning electron microscope JEOL JSM-7001F (*JEOL*, Japan) with an energy dispersive X-ray fluorescence spectrometer Oxford INCA X-max 80 (United Kingdom).

Histograms of the distribution of grain sizes were created by using ImageJ (*National Institutes of Health, USA*) and Origin (*OriginLab Corporation, USA*) software.

Magnetic analysis methods

In order to determine the magnetic parameters, a Quantum Design PPMS® VersaLab vibrating-sample magnetometer (USA) with a magnetic field strength up to 30 kOe at temperatures from 50 to 300 K was used.

RESULTS AND DISCUSSION

XRD analysis

The phase composition and unit cell parameters of the samples were determined through powder X-ray diffraction. Figure 1 shows the XRD patterns of single-phase samples. The red strips represent the data for unsubstituted strontium hexaferrite $\text{SrFe}_{12}\text{O}_{19}$ [33]. Figure 1 shows that the reflections in the XRD patterns of the samples correspond to pure $\text{SrFe}_{12}\text{O}_{19}$ from the ICDD® database¹ with the hexagonal space group $\text{P6}_3/\text{mmc}$. On the presented magnified capture of XRD patterns (Fig. 2), it can be clearly observed that the peak positions are shifting to the higher 2θ angle with the introduction of Cr into the hexaferrite.

Unit cell parameters for each obtained solid solution were obtained by indexing the XRD patterns (Table 2).

When Fe in strontium hexaferrite is substituted with Cr, the values of unit cell parameters monotonically decreasing with x (Fig. 3). Since the ionic radius

Table 2. Unit cell parameters of the obtained solid solutions

Sample composition	Cell sizes		c/a	Cell volume V , \AA^3
	a , \AA	c , \AA		
$\text{SrFe}_{12}\text{O}_{19}$ [34]	5.8840	23.0500	3.9174	690.403
$\text{SrFe}_{12}\text{O}_{19}$	5.881(2)	23.049(9)	3.9192	690.43(5)
$\text{SrFe}_{11.5}\text{Cr}_{0.5}\text{O}_{19}$	5.875(3)	23.015(1)	3.9174	687.8867(1)
$\text{SrFe}_{11}\text{Cr}_1\text{O}_{19}$	5.874(3)	23.007(1)	3.9167	687.441(6)
$\text{SrFe}_{10.5}\text{Cr}_{1.5}\text{O}_{19}$	5.870(4)	22.983(5)	3.9153	685.746(2)
$\text{SrFe}_{10}\text{Cr}_2\text{O}_{19}$	5.868(1)	22.968(1)	3.9141	684.897(2)
$\text{SrFe}_{9.5}\text{Cr}_{2.5}\text{O}_{19}$	5.864(4)	22.944(2)	3.9126	683.281(1)
$\text{SrFe}_9\text{Cr}_3\text{O}_{19}$	5.858(2)	22.930(3)	3.9143	681.519(4)
$\text{SrFe}_{8.5}\text{Cr}_{3.5}\text{O}_{19}$	5.858(8)	22.919(6)	3.9124	681.102(2)
$\text{SrFe}_8\text{Cr}_4\text{O}_{19}$	5.857(6)	22.875(3)	3.9055	679.748(1)
$\text{SrFe}_{7.5}\text{Cr}_{4.5}\text{O}_{19}$	5.853(1)	22.843(6)	3.9028	677.627(1)
$\text{SrFe}_7\text{Cr}_5\text{O}_{19}$	5.852(2)	22.828(3)	3.9009	677.075(1)
$\text{SrFe}_{6.5}\text{Cr}_{5.5}\text{O}_{19}$	5.847(1)	22.794(2)	3.8984	674.858(2)
$\text{SrFe}_6\text{Cr}_6\text{O}_{19}$	5.845(8)	22.776(3)	3.8966	673.849(7)

of Cr^{3+} (0.615 \AA , CN = 6) is smaller than that of Fe^{3+} (0.645 \AA , CN = 6)², the unit cell and its parameters decrease with x .

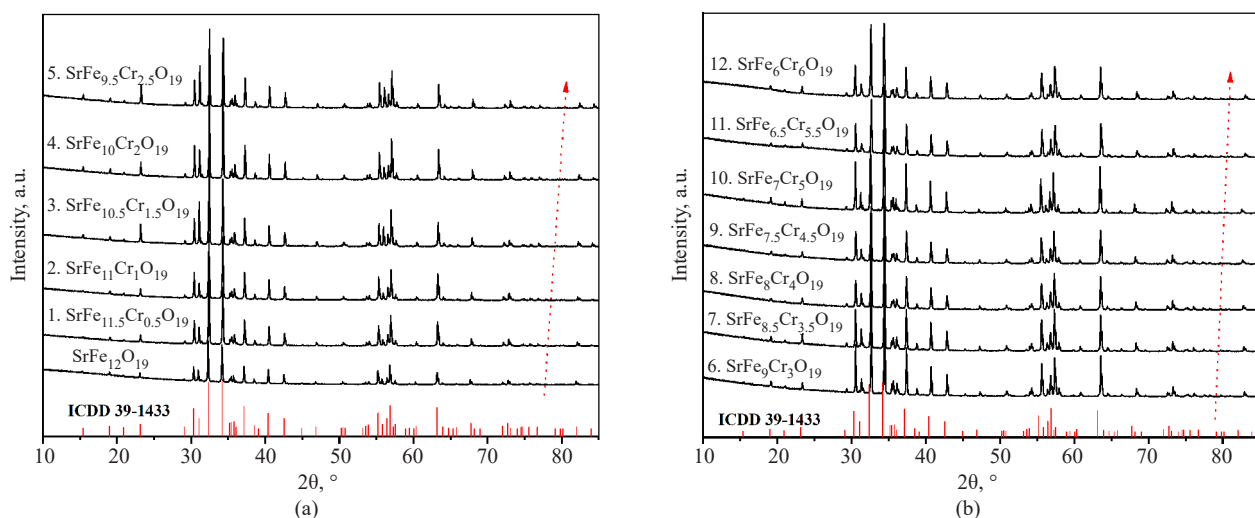


Fig. 1. XRD patterns of $\text{SrFe}_{12-x}\text{Cr}_x\text{O}_{19}$ system: (a) $x = 0-2.5$; (b) $x = 3-6$

¹ The International Centre for Diffraction Data (ICDD®). <https://www.icdd.com/>. Accessed July 15, 2024.

² Imperial College London, Radii for All Species. <http://abulafia.mt.ic.ac.uk/shannon/radius.php>. Accessed July 15, 2024.

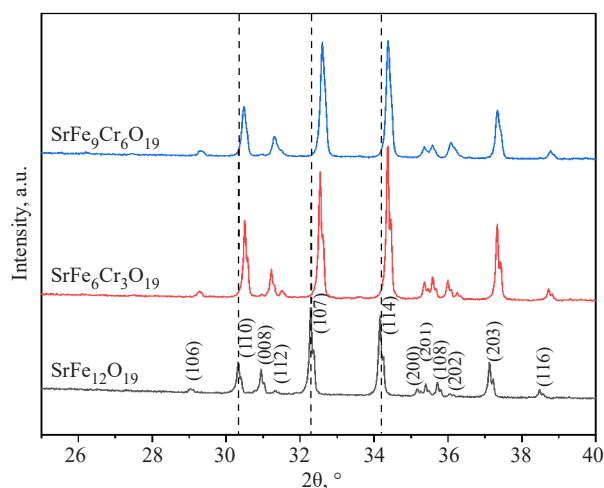


Fig. 2. XRD patterns of $\text{SrFe}_{12-x}\text{Cr}_x\text{O}_{19}$ system ($x = 0, 3, 6$) magnified image

The linear dependence indicates Vegard's law, which confirms the formation of the substitutional solid solutions.

Surface morphology and elemental composition

The surface morphology of the samples is represented by a multitude of differently oriented crystallites merged together, some of them showing hexagonal morphology. Figures 4a–4l show SEM images of each sample.

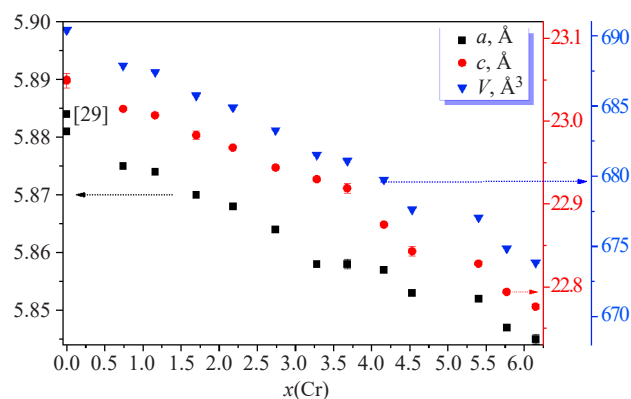


Fig. 3. Dependence of the unit cell parameters a , c , and V on x in $\text{SrFe}_{(12-x)}\text{Cr}_x\text{O}_{19}$

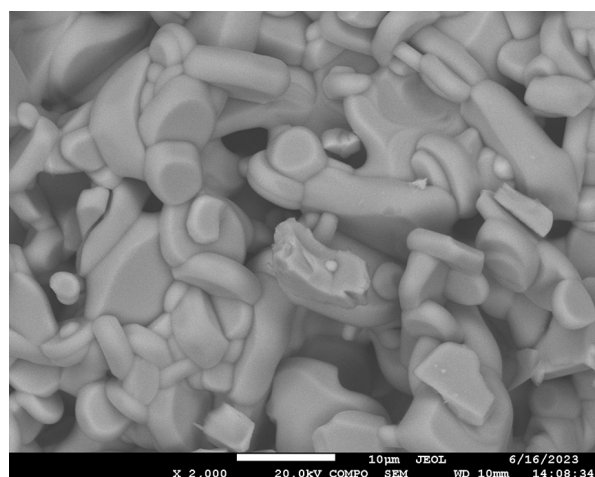
From the particle size distribution shown in the histograms, it is evident that particle size is not strongly dependent on the degree of Cr substitution. However, among all the samples, the sample with $x = 6$ stands out; at this rate of substitution, a maximum of $9.4 \mu\text{m}$ is observed. Results of elemental analysis are presented at Table 3.

Magnetic properties

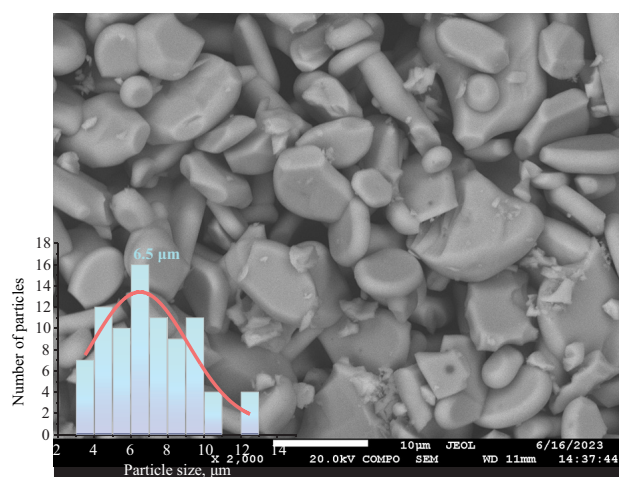
Hysteresis loops for $\text{SrFe}_{(12-x)}\text{Cr}_x\text{O}_{19}$ ($x = 0–6$) solid solutions are shown in Figs. 5 and 6. By visually analyzing the hysteresis loops, we can conclude that Cr concentration (x) increases the coercive force (H_c), while residual magnetization (M_r) and saturation magnetization (M_s) both decrease.

Table 3. Elemental composition of the samples

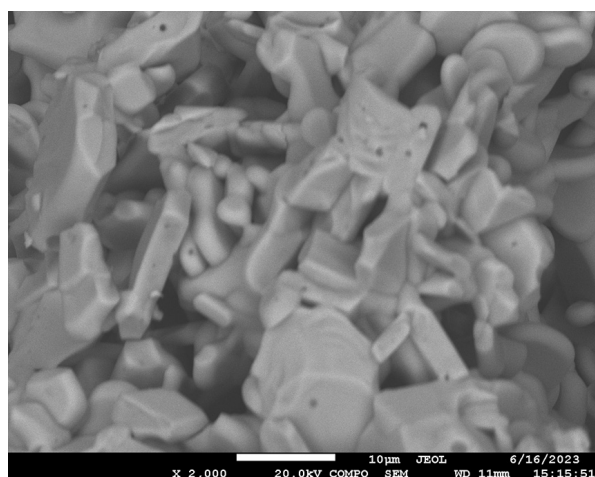
No.	Theoretical chemical formula	Elemental composition of the obtained samples, At. %			Resulting chemical formula
		Sr	Fe	Cr	
1	$\text{SrFe}_{11.5}\text{Cr}_{0.5}\text{O}_{19}$	1.00	11.26	0.74	$\text{SrFe}_{11.26}\text{Cr}_{0.74}\text{O}_{19}$
2	$\text{SrFe}_{11}\text{Cr}_1\text{O}_{19}$	1.00	10.84	1.16	$\text{SrFe}_{10.84}\text{Cr}_{1.16}\text{O}_{19}$
3	$\text{SrFe}_{10.5}\text{Cr}_{1.5}\text{O}_{19}$	1.00	10.30	1.70	$\text{SrFe}_{10.30}\text{Cr}_{1.70}\text{O}_{19}$
4	$\text{SrFe}_{10}\text{Cr}_2\text{O}_{19}$	1.00	9.82	2.18	$\text{SrFe}_{9.82}\text{Cr}_{2.18}\text{O}_{19}$
5	$\text{SrFe}_{9.5}\text{Cr}_{2.5}\text{O}_{19}$	1.00	9.26	2.74	$\text{SrFe}_{9.26}\text{Cr}_{2.74}\text{O}_{19}$
6	$\text{SrFe}_9\text{Cr}_3\text{O}_{19}$	1.00	8.72	3.28	$\text{SrFe}_{8.72}\text{Cr}_{3.28}\text{O}_{19}$
7	$\text{SrFe}_{8.5}\text{Cr}_{3.5}\text{O}_{19}$	1.00	8.32	3.68	$\text{SrFe}_{8.32}\text{Cr}_{3.68}\text{O}_{19}$
8	$\text{SrFe}_8\text{Cr}_4\text{O}_{19}$	1.00	7.84	4.16	$\text{SrFe}_{7.84}\text{Cr}_{4.16}\text{O}_{19}$
9	$\text{SrFe}_{7.5}\text{Cr}_{4.5}\text{O}_{19}$	1.00	7.47	4.53	$\text{SrFe}_{7.47}\text{Cr}_{4.53}\text{O}_{19}$
10	$\text{SrFe}_7\text{Cr}_5\text{O}_{19}$	1.00	6.60	5.40	$\text{SrFe}_{6.60}\text{Cr}_{5.40}\text{O}_{19}$
11	$\text{SrFe}_{6.5}\text{Cr}_{5.5}\text{O}_{19}$	1.00	6.23	5.77	$\text{SrFe}_{6.23}\text{Cr}_{5.77}\text{O}_{19}$
12	$\text{SrFe}_6\text{Cr}_6\text{O}_{19}$	1.00	5.85	6.15	$\text{SrFe}_{5.85}\text{Cr}_{6.15}\text{O}_{19}$



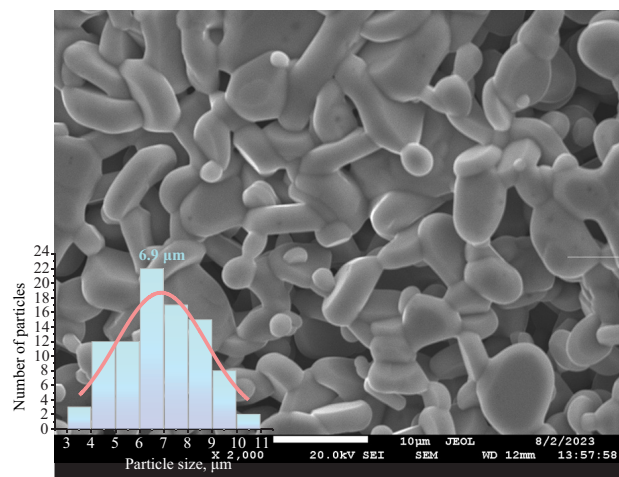
(a)



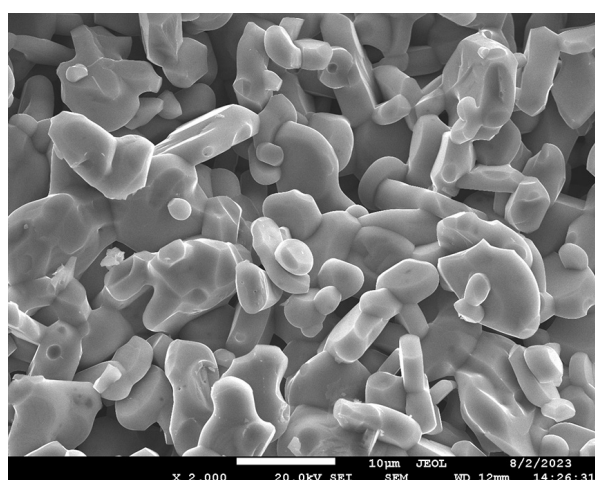
(b)



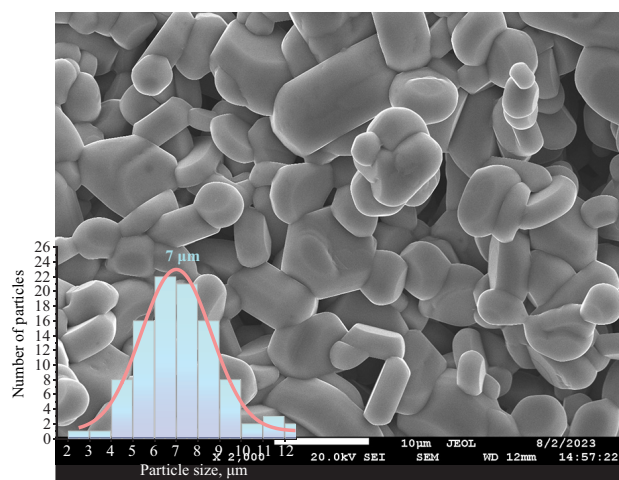
(c)



(d)

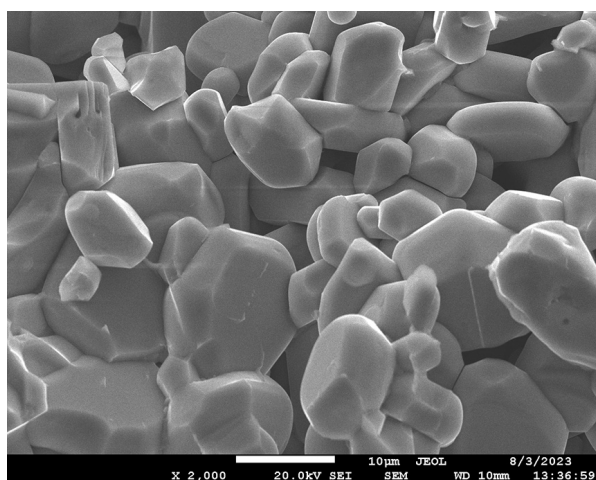


(e)

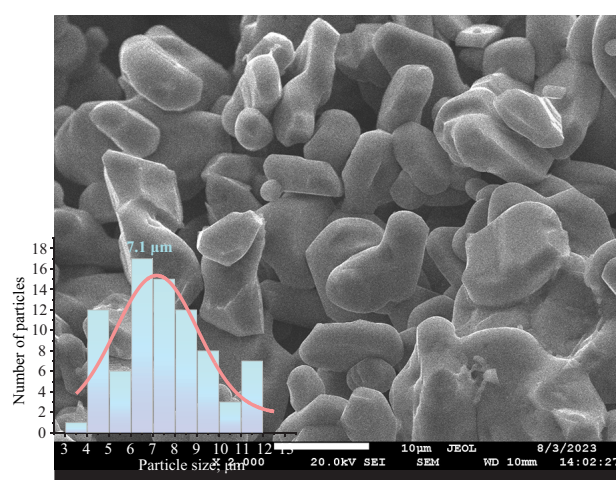


(f)

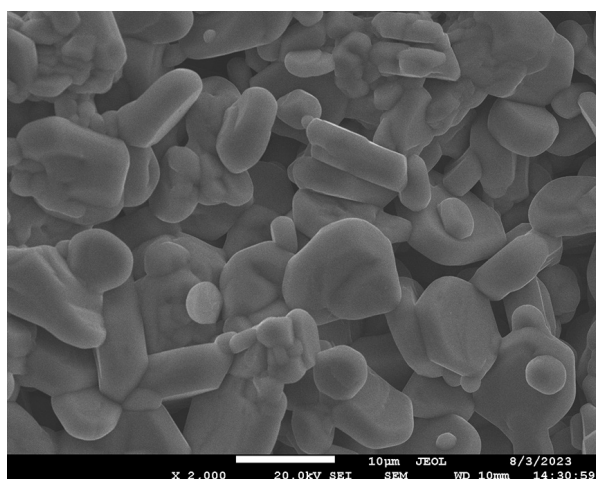
Fig. 4. SEM images of $\text{SrFe}_{(12-x)}\text{O}_{19}$ ceramic samples. x = (a) 0.5; (b) 1.0; (c) 1.5; (d) 2.0; (e) 2.5; (f) 3.0



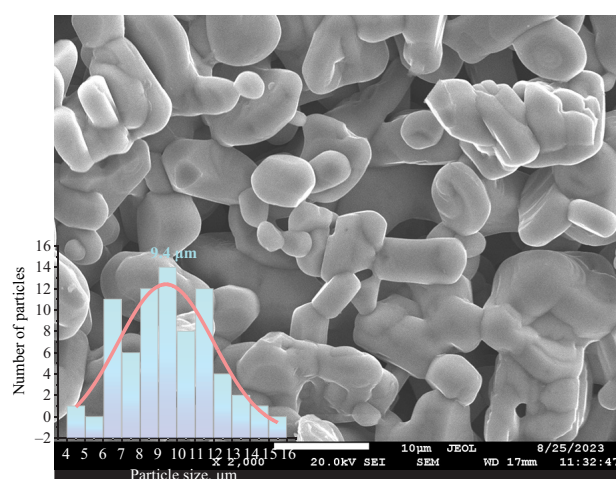
(g)



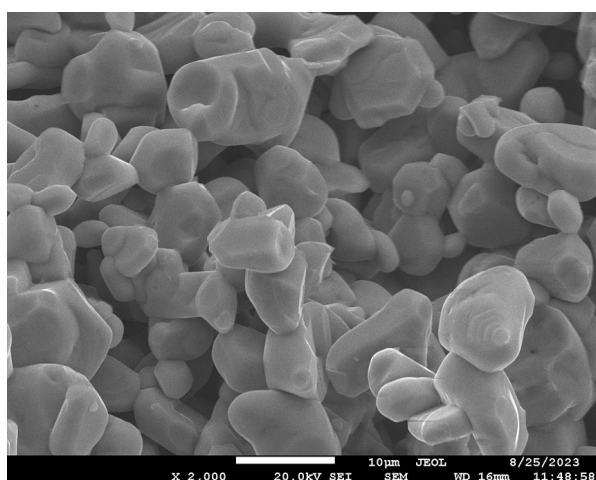
(h)



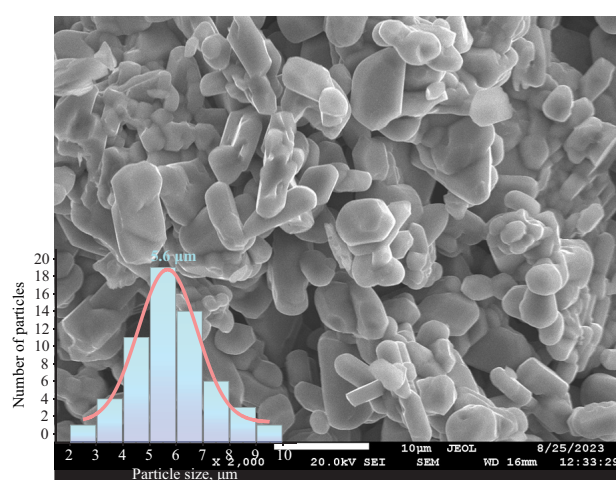
(i)



(j)



(k)



(l)

Fig. 4. SEM images of $\text{SrFe}_{(12-x)}\text{O}_{19}$ ceramic samples. x = (g) 3.5; (h) 4.0; (i) 4.5; (j) 5.0; (k) 5.5; (l) 6.0

While this correlates with the data given in [28], the coercive force values for $\text{BaFe}_{11.5}\text{Cr}_{0.5}\text{O}_{19}$ and $\text{SrFe}_{11.5}\text{Cr}_{0.5}\text{O}_{19}$ are not similar at the same level of substitution; this dissimilarity may be attributed to the coercive force being influenced by the nature of the bivalent ion. Since applying 30 kOe to the samples did not cause saturation or the magnetization value to keep increasing, the law to approach saturation was applied. According to the Stoner–Wohlfarth model, M_s can be determined by plotting magnetization (M) against $1/H^2$ (Eq. 1) and then extrapolating the linear plot to a zero value of $1/H^2$ (Fig. 7).

The effective magnetic anisotropy constant (K_{eff}) can also be determined from this graph by calculating the slope value to determine parameter B (Eq. 2). From this parameter, the value of the magnetic anisotropy field (H_a) can be derived (Eq. 3).

$$M = M_s \cdot \left(1 - \frac{B}{H^2}\right), \quad (1)$$

$$K_{\text{eff}} = M_s \cdot \sqrt{\frac{15B}{4}}, \quad (2)$$

$$H_a = 2 \cdot \frac{K_{\text{eff}}}{M_s}. \quad (3)$$

The values of M_r and H_c are determined from hysteresis loops (Figs. 5 and 6). The values of M_s are presented in Table 4; K_{eff} and H_a values are presented in Table 5. With a temperature decrease, H_c decreases but M_s and M_r increase. M_s and M_r linearly depend on the Cr concentration (Figs. 9 and 10). H_c does not fit perfectly to the linear dependence, but demonstrates a more complicated fit. This could be caused by the complex Cr^{3+} ion substitution for Fe^{3+} ions in different Wyckoff positions.

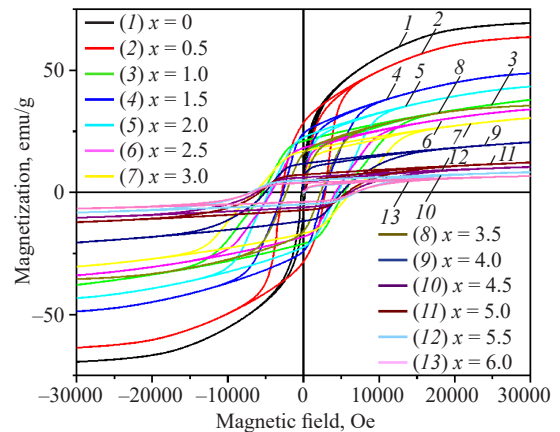


Fig. 5. Hysteresis loops of $\text{SrFe}_{(12-x)}\text{Cr}_x\text{O}_{19}$ ($x = 0.5\text{--}6.0$) for solid solutions at 300 K

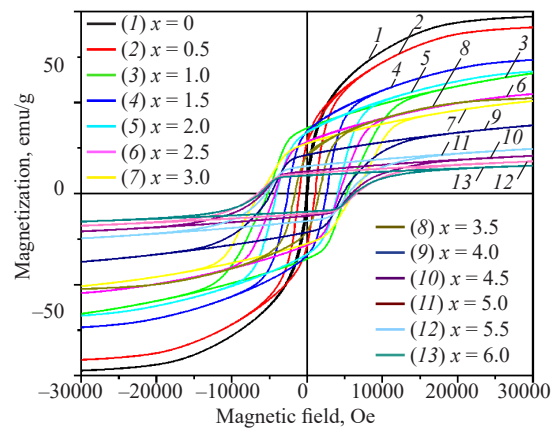


Fig. 6. Hysteresis loops of $\text{SrFe}_{(12-x)}\text{Cr}_x\text{O}_{19}$ ($x = 0.5\text{--}6.0$) solid solutions at 50 K

Table 4. Magnetic parameters of $\text{SrFe}_{(12-x)}\text{Cr}_x\text{O}_{19}$ ($x = 0\text{--}6$) solid solutions

x (Cr)	300 K			50 K		
	M_s , emu/g	M_r , emu/g	H_c , Oe	M_s , emu/g	M_r , emu/g	H_c , Oe
0	67.90	21.03	610	99.76	5.95	95
0.5	66.14	28.49	2868	94.19	28.69	1105
1.0	41.04	21.02	5414	71.25	35.90	5245
1.5	51.93	24.09	2683	77.30	34.00	2553
2.0	46.48	22.44	4514	71.41	33.36	4050
2.5	36.58	18.19	4204	58.61	28.33	4247
3.0	32.79	16.85	6491	54.68	27.47	6216
3.5	37.27	15.97	2282	54.32	20.66	1596
4.0	22.18	11.74	5061	40.46	21.22	4804
4.5	11.33	6.09	6201	22.44	12.23	5935
5.0	13.34	7.26	5771	26.59	15.05	5537
5.5	9.12	4.91	7037	19.20	11.12	6575
6.0	7.37	3.89	6800	16.73	9.93	6278

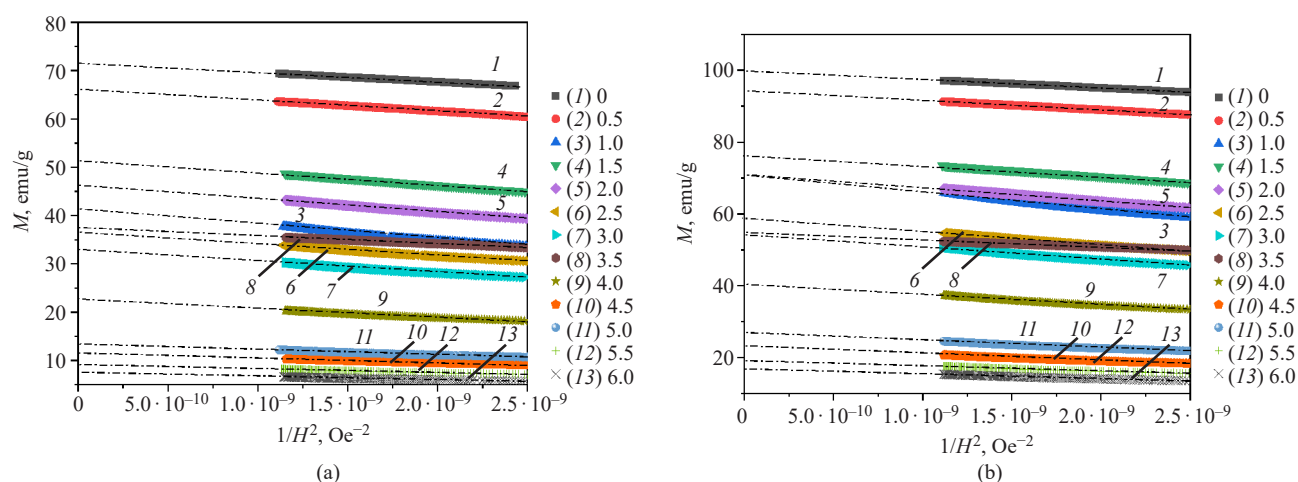


Fig. 7. Dependencies of magnetization on the magnetic field for (a) 300 K; (b) 50 K

An analysis of field cooling (FC) magnetization curves (Fig. 8) reveals a mostly linear growth of magnetization with cooling. However, the sample with $x = 0.5$ shows a nonlinear dependence with a peak. This could be related to the redistribution of the resulting magnetic moment due to complex Cr^{3+} ion substitution.

Table 5. Parameters of magnetic anisotropy $\text{SrFe}_{(12-x)}\text{Cr}_x\text{O}_{19}$ ($x = 0-6$), solid solutions

x (Cr)	300 K		50 K	
	$K_{\text{eff}} \cdot 10^{-6}$ emu/g·Oe	H_a , Oe	$K_{\text{eff}} \cdot 10^{-6}$ emu/g·Oe	H_a , Oe
0	0.70	20756	0.94	18773
0.5	0.75	22742	0.96	20465
1.0	0.69	33399	1.17	32900
1.5	0.74	28618	1.00	25908
2.0	0.71	30736	1.03	28783
2.5	0.59	31991	0.90	30756
3.0	0.53	32504	0.88	32028
3.5	0.47	25024	0.60	22055
4.0	0.37	33543	0.67	33051
4.5	0.20	34696	0.38	33550
5.0	0.23	34999	0.44	33395
5.5	0.17	36561	0.33	33964
6.0	0.14	37108	0.29	34377

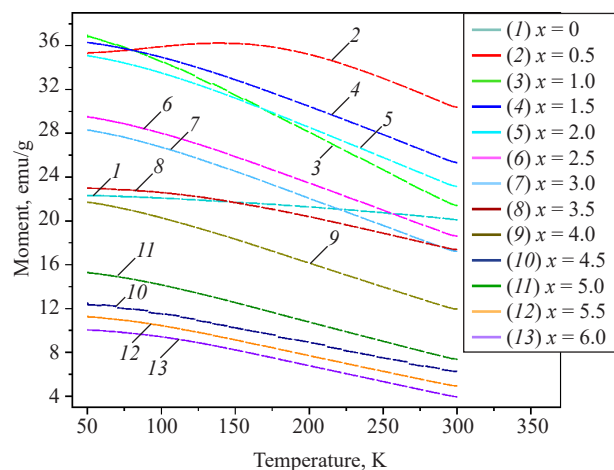


Fig. 8. Field cooling at 500 Oe magnetization curves of $\text{SrFe}_{(12-x)}\text{Cr}_x\text{O}_{19}$ ($x = 0-6$), solid solutions

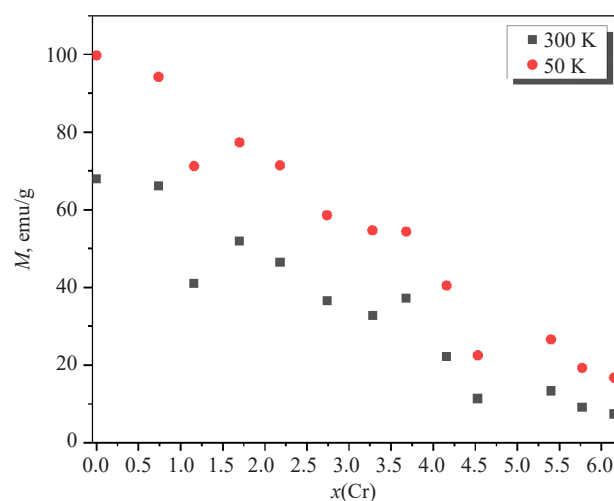


Fig. 9. Dependence of saturation magnetization (M_s) on Cr content at 50 and 300 K

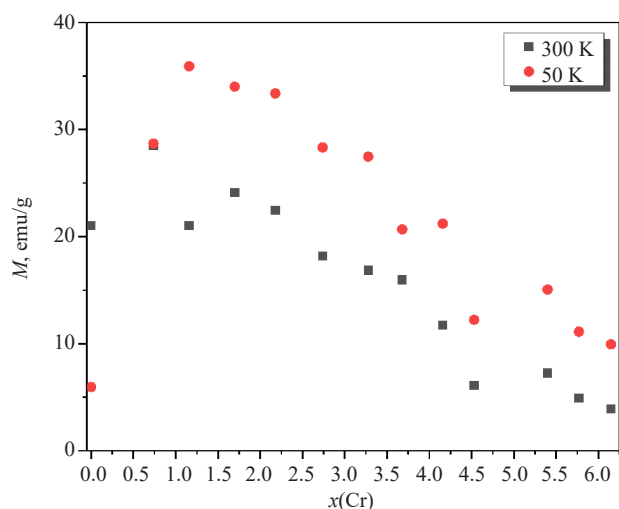


Fig. 10. Dependence of remanent magnetization (M_r) on Cr content at 50 and 300 K

The replacement of Fe by Cr in hexaferrite strontium leads to complex changes in the magnetic structure, which ultimately reduces the saturation magnetization of the material. This change can be explained in terms of the replacement of Fe^{3+} (5 μB) ions by less magnetic Cr^{3+} (3 μB) ions in octahedral and tetrahedral positions, which results in a decrease in the total magnetic moment per unit volume of material to weaken exchange interactions.

CONCLUSIONS

$\text{SrFe}_{(12-x)}\text{Cr}_x\text{O}_{19}$ solid solutions with x up to 6 were synthesized using the ceramic method. Average crystallite sizes varied from 5.6 to 9.4 μm . The purity of the samples was verified using XRD analysis: all obtained samples consists only of crystal

structure, which is isomorphic to magnetoplumbite. The linear dependence of the investigated structural parameters a , c , and V on the Cr concentration confirms the incorporation of Cr into the hexaferrite solid solution according to Vegard's law. In addition to structural parameters, magnetic characteristics were obtained for hexaferrite solid solutions. A trend for M_s and M_r dependencies to significantly decrease with Cr concentration is observed. Coercive force shows a complex dependence on Cr concentration. The sample with $x = 1$ has the highest product of M_s and H_c , indicating its high magnetic potential and suitability for use in the manufacture of permanent magnets. Samples with high Cr substitution ($x = 5.5$, 6.0) possess the highest H_c values, which is a favorable parameter for high-frequency applications; however, additional investigation on other parameters is needed. Cr substituted ferrites can be utilized at high-frequency electronic or sensor production.

Acknowledgments

The study was supported by the Russian Science Foundation (project No. 24-29-20187, <http://rscf.ru/project/24-29-20187>).

Authors' contributions

A.R. Zykova—conceptualization, formal analysis, funding acquisition, investigation, methodology, supervision.

A.I. Kovalev—formal analysis, investigation.

D.P. Sherstyuk—formal analysis, investigation.

V.E. Zhivulin—methodology, resources.

S.V. Taskaev—formal analysis, investigation.

D.A. Vinnik—conceptualization, methodology, project administration, resources, supervision.

The authors declare no conflict of interest.

REFERENCES

1. Khudaysh L., Ahmed I.A., Ejaz S.R., Khan S.A., Haleem Y.A., Ibrahim M.M., Ali M., Farid H.M.T., El-Bahy Z.M. Analysis of cerium substitution in Co–Sr based spinel ferrites for high frequency application. *J. Rare Earths*. 2023;42(9):1755–1763. <https://doi.org/10.1016/j.jre.2023.10.013>
2. He D., Xu Z., Wang K., Wu P., Cui J., Qiao L., Wang T. The regulation of high-frequency magnetic properties of NiZnCo ferrite for miniaturized antenna application. *J. Magn. Magn. Mater.* 2023;588(15):171449. <https://doi.org/10.1016/j.jmmm.2023.171449>
3. El Yaagoubi M., Schrödl M., Schwegler D., Münster B. Development of hard ferrite filled thermoplastic elastomers for the production of permanent magnets. *Sensors Actuators A Phys.* 2022;333(1):113224. <https://doi.org/10.1016/j.sna.2021.113224>
4. Waki T., Nakai S., Tabata Y., Nakamura H. Role of oxygen potential in dopant solubility in ferrite magnets: Enhanced Zn solubility and magnetization in La–Zn co-substituted magnetoplumbite-type strontium ferrite. *Mater. Res. Bull.* 2023;168:112470. <https://doi.org/10.1016/j.materresbull.2023.112470>
5. Icin K., Akyol S., Alptekin F., Yıldız A., Sünbül S.E., Ergin İ., Öztürk S. A comparative study of the correlation among the phase formation, crystal stability and magnetic properties of $\text{SrFe}_{12-x}\text{M}_x\text{O}_{19}$ ($\text{M}=\text{Al}^{3+}$, Cr^{3+} and Mn^{3+} , $x = 0\text{--}0.5$) ferrite permanent magnets. *J. Solid State Chem.* 2023;324:124126. <https://doi.org/10.1016/j.jssc.2023.124126>

6. Hashim M., Salih S.J., Ismail M.M., Ahmed A., Meena S.S., Gaikwad A.A., Jotania R.B., Kumar S., Ravinder D., Kumar R., Imran A., Batoo K.M., Shirsath S.E. Effect of lightly substituted samarium ions on the structural, optical, magnetic and dielectric properties of the sonochemically synthesized M-type Sr-hexaferrite nanoparticles. *Phys. B: Condens. Matter.* 2024;681:415840. <https://doi.org/10.1016/j.physb.2024.415840>
7. Rambabu C., Aruna B., Shanmukhi P.S.V., Gnana Kiran M., Murali N., Mammo T. Wegayehu, Parajuli D., Choppa P., Himakar P., Lakshmi Narayana P.V. Effect of $\text{La}^{3+}/\text{Cu}^{2+}$ and $\text{La}^3/\text{Ni}^{2+}$ substitution on the synthesis, magnetic and dielectric properties of M-type $\text{Sr}_{1-x}\text{La}_x\text{Fe}_{12-x}\text{M}_x\text{O}_{19}$ ($\text{M} = \text{Cu}$ and Ni) hexaferrite. *Inorg. Chem. Commun.* 2024;159:111753.
8. Gorbachev E.A., Lebedev V.A., Kozlyakova E.S., Alyabyeva L.N., Ahmed A., Cervellino A., Trusov L.A. Tuning the microstructure, magnetostatic and magnetodynamic properties of highly Al-substituted M-type Sr/Ca hexaferrites prepared by citrate-nitrate auto-combustion method. *Ceram. Int.* 2023;49(16): 26411–26419. <https://doi.org/10.1016/j.ceramint.2023.05.177>
9. Yao Y., Hreka I.A., Tishkevich D.I., Zubar T.I., Turchenko V.A., Lu S., Silibin M.V., Migas D.B., Sayyed M.I., Trukhanov S.V., Trukhanov A.V. Correlation of the chemical composition, phase content, structural characteristics and magnetic properties of the Bi-substituted M-type hexaferrites. *Ceram. Int.* 2023;49(22): 37009–37016. <https://doi.org/10.1016/j.ceramint.2023.09.033>
10. Pullar R.C. Hexagonal ferrites: A review of the synthesis, properties and applications of hexaferrite ceramics. *Prog. Mater. Sci.* 2012;57(7):1191–1334. <https://doi.org/10.1016/j.pmatsci.2012.04.001>
11. Chandel M., Ghosh B.K., Moitra D., Ghosh N.N. Barium Hexaferrite ($\text{BaFe}_{12}\text{O}_{19}$) Nanoparticles as Highly Active and Magnetically Recoverable Catalyst for Selective Epoxidation of Styrene to Styrene Oxide. *J. Nanosci. Nanotechnol.* 2018;18(5):3478–3483. <https://doi.org/10.1166/jnn.2018.14625>
12. Khaliq N., Bibi I., Majid F., Sultan M., Amami M., Iqbal M. Zn and Mn doped $\text{Ba}_{1-x}\text{Zn}_x\text{Fe}_{12-y}\text{Mn}_y\text{O}_{19}$ as highly photoactive under visible light with enhanced electrochemical and dielectric properties. *Mater. Sci. Semicond. Process.* 2022;139:106324. <https://doi.org/10.1016/j.mssp.2021.106324>
13. Danish M., ul Islam M., Ahmad F., Madni M.N., Jahangeer M. Synthesis of M-type hexaferrite reinforced graphene oxide composites for electromagnetic interference shielding. *J. Phys. Chem. Solids.* 2024;185:111783. <https://doi.org/10.1016/j.jpcs.2023.111783>
14. Gunanto Y.E., Izaak M.P., Sitompul H., Adi W.A. Composite Paint based on Barium-Strontium-Hexaferrite as an Absorber of Microwaves at X-band Frequency. *Mater. Today Proc.* 2019;13(1):1–4. <https://doi.org/10.1016/j.matpr.2019.03.177>
15. Chakradhary V.K., Akhtar M.J. Highly coercive strontium hexaferrite nanodisks for microwave absorption and other industrial applications. *Compos. Part B: Eng.* 2020;183:107667. <https://doi.org/10.1016/j.compositesb.2019.107667>
16. Trukhanov A.V., Turchenko V.A., Kostishin V.G., Damay F., Porcher F., Lupu N., Bozzo B., Fina I., Polosan S., Silibin M.V., Salem M.M., Tishkevich D.I., Trukhanov S.V. The origin of the dual ferroic properties in quasi-centrosymmetrical $\text{SrFe}_{12-x}\text{In}_x\text{O}_{19}$ hexaferrites. *J. Alloys Compd.* 2021;886:161249. <https://doi.org/10.1016/j.jallcom.2021.161249>
17. Wang X., Yan H., Zhao S., Liu S., Chang H. Modifiable natural ferromagnetic resonance frequency and strong microwave absorption in $\text{BaFe}_{12-y-2x}\text{Al}_x\text{Sn}_x\text{Mn}_x\text{O}_{19}$ M-type hexaferrite. *J. Magn. Magn. Mater.* 2023;586:171159. <https://doi.org/10.1016/j.jmmm.2023.171159>
18. Yousaf M., Nazir S., Hayat Q., Akhtar M.N., Akbar M., Lu Y., Noor A., Zhang J.-M., Shah M.A.K.Y., Wang B. Magneto-optical properties and physical characteristics of M-type hexagonal ferrite ($\text{Ba}_{1-x}\text{Ca}_x\text{Fe}_{11.4}\text{Al}_{0.6}\text{O}_{19}$) nanoparticles (NPs). *Ceram. Int.* 2021;47(8):11668–11676. <https://doi.org/10.1016/j.ceramint.2021.01.006>
19. Jyotsna K., Phanjoubam S. Improved magnetoelectric coupling of Co–Ti substituted barium hexaferrite at room temperature and related electrical investigations. *Mater. Chem. Phys.* 2024;317: 129186. <https://doi.org/10.1016/j.matchemphys.2024.129186>
20. Dongquoc V., Park S.-Y., Jeong J.-R., Tu B.D., Huong Giang D.T., Dang N.T., Phan T.L. Electronic structure, and dielectric, magnetic and reflection-loss behaviors of $\text{BaFe}_{12-x}\text{Mn}_x\text{O}_{19}$ ($0 < x \leq 2$) hexaferrites. *J. Magn. Magn. Mater.* 2023;588(8):171486.
21. Cheon S.J., Choi J.R., Lee S., Lee J.I., Lee H. Frequency tunable Ni–Ti-substituted Ba–M hexaferrite for efficient electromagnetic wave absorption in 8.2–75 GHz range. *J. Alloys Compd.* 2024;976:173019. <https://doi.org/10.1016/j.jallcom.2023.173019>
22. Hashhash A., Hassen A., Baleidy W.S., Refai H.S. Impact of rare-earth ions on the physical properties of hexaferrites $\text{Ba}_{0.5}\text{Sr}_{0.5}\text{RE}_{0.6}\text{Fe}_{11.4}\text{O}_{19}$, ($\text{RE} = \text{La}, \text{Yb}, \text{Sm}, \text{Gd}, \text{Er}, \text{Eu}$, and Dy). *J. Alloys Compd.* 2021;873:159812. <https://doi.org/10.1016/j.jallcom.2021.159812>
23. Atif M., Hanif Alvi M., Ullah S., Ur Rehman A., Nadeem M., Khalid W., Ali Z., Guo H. Impact of strontium substitution on the structural, magnetic, dielectric and ferroelectric properties of $\text{Ba}_{1-x}\text{Sr}_x\text{Fe}_{11}\text{Cr}_1\text{O}_{19}$ ($x = 0.0\text{--}0.8$) hexaferrites. *J. Magn. Magn. Mater.* 2020;500:166414. <https://doi.org/10.1016/j.jmmm.2020.166414>
24. Zhivulin V.E., Trofimov E.A., Zaitseva O. V., Sherstyuk D.P., Cherkasova N.A., Taskaev S.V., Vinnik D.A., Alekhina Y.A., Perov N.S., Naidu K.C.B., Elsaedy H.I., Khandaker M.U., Tishkevich D.I., Zubar T.I., Trukhanov A.V., Trukhanov S.V. Preparation, phase stability, and magnetization behavior of high entropy hexaferrites. *IScience.* 2023;26(7):107077. <https://doi.org/10.1016/j.isci.2023.107077>
25. Yao Y., Zhivulin V.E., Zykova A.R., Cherkasova N.A., Vinnik D.A., Trofimov E.A., Gudkova S.A., Zaitseva O.V., Taskaev S.V., Alyabyeva L.N., Gorshunov B.P., Gurchenko A.A., Lu S., Trukhanov S.V., Trukhanov A.V. High entropy $\text{BaFe}_{12-x}(\text{Ti}/\text{Mn}/\text{Ga}/\text{In})_x\text{O}_{19}$ ($x = 1\text{--}7$) oxides: Correlation of the composition, entropy state, magnetic characteristics, and terahertz properties. *Ceram. Int.* 2023;49(19):31549–31558. <https://doi.org/10.1016/j.ceramint.2023.07.106>
26. Luo X., Huang S., Huang R., Hong J., Yuan S., Shu Z., Zhao L., Lu C., Jin H. Rare-earth high-entropy magnetoplumbite structure hexaluminates ($\text{La}_{1/5}\text{Nd}_{1/5}\text{Sm}_{1/5}\text{Eu}_{1/5}\text{Gd}_{1/5}$) $\text{MAl}_{11}\text{O}_{19}$ ($\text{M} = \text{Mg}, \text{Zn}$) for thermal barrier coating applications with enhanced mechanical and thermal properties. *Ceram. Int.* 2024;50(12): 21281–21288. <https://doi.org/10.1016/j.ceramint.2024.03.237>
27. Qiu J., Wang Y., Gu M. Effect of Cr substitution on microwave absorption of $\text{BaFe}_{12}\text{O}_{19}$. *Mater. Lett.* 2006;60(21–22): 2728–2732. <https://doi.org/10.1016/j.matlet.2006.01.079>
28. Ounnunkad S., Winotai P. Properties of Cr-substituted M-type barium ferrites prepared by nitrate–citrate gel-autocombustion process. *J. Magn. Magn. Mater.* 2006;301(2):292–300. <https://doi.org/10.1016/j.jmmm.2005.07.003>
29. Dhage Vinod N., Mane M.L., Babrekar M.K., Kale C.M., Jadhav K.M. Influence of chromium substitution on structural and magnetic properties of $\text{BaFe}_{12}\text{O}_{19}$ powder prepared by sol–gel auto combustion method. *J. Alloys Compd.* 2011;509(12):4394–4398. <https://doi.org/10.1016/j.jallcom.2011.01.040>

30. Qiu J., Gu M., Shen H. Microwave absorption properties of Al- and Cr-substituted M-type barium hexaferrite. *J. Magn. Magn. Mater.* 2005;295(3):263–268. <https://doi.org/10.1016/j.jmmm.2005.01.018>
31. Kumar S., Supriya S., Kar M. Correlation between temperature dependent dielectric and DC resistivity of Cr substituted barium hexaferrite. *Mater. Res. Express.* 2017;4:126302. <https://doi.org/10.1088/2053-1591/aa9a51>
32. Bashkurov L.A., Kostyushko Yu.L. Formation of Ferrite-Cromites $\text{BaFe}_{10}\text{Cr}_2\text{O}_{19}$ and $\text{BaFe}_{10}\text{Cr}_2\text{O}_{19}$ in the Solid-Phase reaction of Fe_2O_3 and Cr_2O_3 with barium or strontium carbonate. *Russ. J. Appl. Chem.* 2005;78:351–355. <http://doi.org/10.1007/s11167-005-0294-z>
- [Original Russian Text: Bashkurov L.A., Kostyushko Yu.L. Formation of Ferrite-Cromites $\text{BaFe}_{10}\text{Cr}_2\text{O}_{19}$ and $\text{BaFe}_{10}\text{Cr}_2\text{O}_{19}$ in the Solid-Phase reaction of Fe_2O_3 and Cr_2O_3 with barium or strontium carbonate. *Zhurnal Prikladnoi Khimii.* 2005;78(3):357–361 (in Russ.).]
33. Wong-Ng W., McMurdie H.F., Paretzkin B., Kuchinski M.A., Dragoo A.L. Standard X-Ray Diffraction Powder Patterns of Fourteen Ceramic Phases. *Powder Diffr.* 1988;3(4):246–254. <https://doi.org/10.1017/S0885715600013579>
34. Obradors X., Solans X., Collomb A., Samaras D., Rodriguez J., Pernet M., Font-Altaba M. Crystal structure of strontium hexaferrite $\text{SrFe}_{12}\text{O}_{19}$. *J. Solid State Chem.* 1988;72(2): 218–224. [https://doi.org/10.1016/0022-4596\(88\)90025-4](https://doi.org/10.1016/0022-4596(88)90025-4)

About the Authors

Alena R. Zykova, Cand. Sci. (Chem.), Researcher, Crystal Growth Laboratory, South Ural State University (National Research University) (76, Lenina pr., Chelyabinsk, 454080, Russia). E-mail: zykovaar@susu.ru. Scopus Author ID 57203743055, RSCI SPIN-code 4777-5816, <https://orcid.org/0000-0001-6333-5551>

Andrey I. Kovalev, Postgraduate Student, Department of Materials Science, Physical and Chemical Properties of Materials, South Ural State University (National Research University) (76, Lenina pr., Chelyabinsk, 454080, Russia). E-mail: kovalev-andrey-i@mail.ru. Scopus Author ID 59364557200, RSCI SPIN-code 4221-8845, <https://orcid.org/0009-0003-4773-1687>

Darya P. Sherstyuk, Postgraduate Student, Department of Materials Science, Physical and Chemical Properties of Materials, South Ural State University (National Research University) (76, Lenina pr., Chelyabinsk, 454080, Russia). E-mail: sherstiukd@susu.ru. Scopus Author ID 57208630693, RSCI SPIN-code 1013-4917, <https://orcid.org/0000-0002-8461-9761>

Vladimir E. Zhivulin, Cand. Sci. (Phys.-Math.), Head of the Crystal Growth Laboratory, South Ural State University (National Research University) (76, Lenina pr., Chelyabinsk, 454080, Russia). E-mail: zhivulinve@mail.ru. Scopus Author ID 57044766800, ResearcherID U-50003-2019, RSCI SPIN-code 6282-2773, <https://orcid.org/0000-0002-4389-8936>

Sergey V. Taskaev, Dr. Sci. (Phys.-Math.), Rector, Chelyabinsk State University (129, Brat'ev Kashirinykh ul., Chelyabinsk, 454001, Russia). E-mail: tsv@csu.ru. Scopus Author ID 55886287900, ResearcherID AAU-9890-2021, RSCI SPIN-code 4131-9937, <https://orcid.org/0000-0001-6352-2816>

Denis A. Vinnik, Dr. Sci. (Chem.), Professor, Department of Materials Science, Physical and Chemical Properties of Materials, South Ural State University (National Research University) (76, Lenina pr., Chelyabinsk, 454080, Russia); Leading Researcher-Head of the Laboratory of Semiconductor Oxide Materials, Institute of Quantum Technologies, Moscow Institute of Physics and Technology (9, Institutskii per., Dolgoprudnyi, Moscow oblast, 141700, Russia); Professor, Institute of Chemistry, St. Petersburg University (7–9, Universitetskaya nab., St. Petersburg, 199034, Russia). E-mail: vinnikda@susu.ru. Scopus Author ID 24451310100, ResearcherID K-1594-2013, RSCI SPIN-code 5971-1044, <https://orcid.org/0000-0002-5190-9834>

Об авторах

Зыкова Алена Романовна, к.х.н., научный сотрудник, лаборатория роста кристаллов, ФГАОУ ВО «Южно-Уральский государственный университет (национальный исследовательский университет) (454080, Россия, Челябинск, пр-т Ленина, д. 76). E-mail: zykovaar@susu.ru. Scopus Author ID 57203743055, SPIN-код РИНЦ 4777-5816, <https://orcid.org/0000-0001-6333-5551>

Ковалев Андрей Игоревич, аспирант, кафедра «Материаловедение и физико-химия материалов», ФГАОУ ВО «Южно-Уральский государственный университет (национальный исследовательский университет) (454080, Россия, Челябинск, пр-т Ленина, д. 76). E-mail: kovalev-andrey-i@mail.ru. Scopus Author ID 59364557200, SPIN-код РИНЦ 4221-8845, <https://orcid.org/0009-0003-4773-1687>

Шерстюк Дарья Петровна, аспирант, кафедра «Материаловедение и физико-химия материалов», ФГАОУ ВО «Южно-Уральский государственный университет (национальный исследовательский университет) (454080, Россия, Челябинск, пр-т Ленина, д. 76). E-mail: sherstiukd@susu.ru. Scopus Author ID 57208630693, SPIN-код РИНЦ 1013-4917, <https://orcid.org/0000-0002-8461-9761>

Живулин Владимир Евгеньевич, к.ф.-м.н., заведующий лабораторией роста кристаллов, ФГАОУ ВО «Южно-Уральский государственный университет (национальный исследовательский университет) (454080, Россия, Челябинск, пр-т Ленина, д. 76). E-mail: zhivulinve@mail.ru. Scopus Author ID 57044766800, ResearcherID U-50003-2019, SPIN-код РИНЦ 6282-2773, <https://orcid.org/0000-0002-4389-8936>

Таскаев Сергей Валерьевич, д.ф.-м.н., ректор, ФГБОУ ВО «Челябинский государственный университет» (454001, Челябинск, ул. Братьев Кашириных, д. 129). E-mail: tsv@csu.ru. Scopus Author ID 55886287900, ResearcherID AAU-9890-2021, SPIN-код РИНЦ 4131-9937, <https://orcid.org/0000-0001-6352-2816>

Винник Денис Александрович, д.х.н., профессор РАН, профессор кафедры «Материаловедение и физико-химия материалов», ФГАОУ ВО «Южно-Уральский государственный университет (национальный исследовательский университет) (454080, Россия, Челябинск, пр-т Ленина, д. 76); ведущий научный сотрудник, заведующий лабораторией полупроводниковых оксидных материалов, Институт квантовых технологий, ФГАОУ ВО «Московский физико-технический университет (национальный исследовательский университет)» (141701, Россия, Московская обл., г. Долгопрудный, Институтский пер., д. 9); профессор, Институт химии, ФГБОУ ВО «Санкт-Петербургский государственный университет» (199034, Россия, Санкт-Петербург, Университетская наб., д. 7-9). E-mail: vinnikda@susu.ru. Scopus Author ID 24451310100, ResearcherID K-1594-2013, SPIN-код РИНЦ 5971-1044, <https://orcid.org/0000-0002-5190-9834>

*The text was submitted by the authors in English and
edited for English language and spelling by Thomas A. Beavitt*

Analytical methods in chemistry and chemical technology
Аналитические методы в химии и химической технологии

UDC 54.04, 544.032.72, 544.032.76, 544.353.21

<https://doi.org/10.32362/2410-6593-2025-20-4-357-371>

EDN QNESUI



RESEARCH ARTICLE

Interaction of poly(diallyldimethylammonium chloride) with inorganic acids

Yaroslava N. Golubeva✉, Alexander V. Krylov✉, Tatyana A. Chebotareva

MIREA – Russian Technological University (M.V. Lomonosov Institute of Fine Chemical Technologies), Moscow, 119454 Russia

✉ Corresponding authors, e-mail: Yaroslava N. Golubeva, golubeva.ya.n@gmail.com; Alexander V. Krylov, allylnmr@yandex.ru

Abstract

Objectives. The study set out to investigate the state of poly(*N,N*-diallyl-*N,N*-dimethylammonium chloride) (polyDADMAC) in aqueous solutions and the exchange reactions of polyelectrolyte anions with anions of inorganic acids, as well as to assess the effect of the acidity, basicity, and nature of H_nX_m acids on the state of the polymer-colloidal complex (PCC) in aqueous solutions.

Methods. Potentiometry, dynamic light scattering, infrared spectroscopy, and nuclear magnetic resonance spectroscopy methods were used.

Results. The main factors affecting the state of the polyDADMAC polyelectrolyte in aqueous solutions were determined along with the characteristics of exchange processes involving anions of inorganic acids. The polymer electrolyte polyDADMAC is shown to exist in an aqueous solution in the form of impermeable polymer coils, representing polymer solvent-separated ion pairs. The Cl^- anion of the polyelectrolyte is exchanged for the OH^- ion of water or the X^{n-} anions of inorganic acids to form PCCs with polymer chain links and various counteranions. The exchange of the anions takes place mainly on the surface of the polymer coil, which limits the degree of substitution of anions and depends on the strength, nature, and basicity of the H_nX_m acids. A relationship was found between the degree of substitution of the X^{n-} anions of the polymer coil and the strength of the resulting PCC with the enthalpy of solvation of inorganic acids H_nX_m .

Conclusions. The polymer electrolyte polyDADMAC exists in an aqueous solution in the form of impermeable polymer coils, which are represented by polymer solvent-separated ion pairs. The exchange of the Cl^- anion of the polyelectrolyte for the OH^- ion of water or the X^{n-} anions of inorganic acids results in the formation of PCCs with polymer chain links and various counteranions. The exchange of the anions, which takes place on the surface of the polymer coil, mainly involves the OH^- anion of the polyelectrolyte. A relationship was identified between the state of polymer coils of polyDADMAC, the degree of substitution of anions with different pK_a , and the degree of acid solvation. The degree of substitution of the X^{n-} anions of acids, which decreases with a decrease in the strength of the H_nX_m acid and the charge of the resulting anion in the series $HClO_4 > HCl > HNO_3 > HBF_4 > HSO_4^- > H_2PO_4^-$, is characterized by a significant change in the size of the coil of the slow mode of motion of the PCC polyelectrolyte. Here, the increased diffusion coefficient from $3.0 \cdot 10^{-13}$ to $1.3 \cdot 10^{-10} \text{ cm}^2/\text{s}$ corresponds to a decrease in the degree of association of the links of the polymer coil of PCC in the same series. The degree of substitution of the X^{n-} anions of the polymer coil and the strength of the forming PCC decrease symbatically with a decrease in the degree of solvation of inorganic acids in water.

Keywords

polyDADMAC, potentiometric titration, IR spectroscopy, NMR spectroscopy, dynamic light scattering, polyelectrolyte chlorine anion exchange, inorganic acids, polymer-colloidal complexes, diffusion of polymer coils

Submitted: 26.10.2024

Revised: 27.03.2025

Accepted: 16.06.2025

For citation

Golubeva Ya.N., Krylov A.V., Chebotareva T.A. Interaction of poly(diallyldimethylammonium chloride) with inorganic acids. *Tonk. Khim. Tekhnol. = Fine Chem. Technol.* 2025;20(4):357–371. <https://doi.org/10.32362/2410-6593-2025-20-4-357-371>

НАУЧНАЯ СТАТЬЯ

Взаимодействие полидиметилдиаллиламмоний хлорида с неорганическими кислотами

Я.Н. Голубева✉, А.В. Крылов✉, Т.А. Чеботарева

МИРЭА – Российский технологический университет (Институт тонких химических технологий им. М.В. Ломоносова), Москва, 119454 Россия

✉ Авторы для переписки, e-mail: Я.Н. Голубева, golubeva.ya.n@gmail.com; А.В. Крылов, allylnmr@yandex.ru

Аннотация

Цели. Исследовать состояние поли-*N,N*-диметил-*N,N*-диаллиламмоний хлорида (ПДМДААХ) в водных растворах и реакции обмена анионов полиэлектролита с анионами неорганических кислот; оценить влияние кислотности, основности и природы кислот H_nX_m на состояние полимер-коллоидного комплекса в водных растворах.

Методы. Использовались методы потенциометрии, динамического светорассеяния, инфракрасной спектроскопии и спектроскопии ядерного магнитного резонанса.

Результаты. Установлены основные закономерности, влияющие на состояние полиэлектролита ПДМДААХ в водных растворах и характеристики обменных процессов с участием анионов неорганических кислот. Показано, что полимерный электролит ПДМДААХ находится в водном растворе в форме непротекаемых полимерных клубков, представляющих собой полимерные сольватно-разделенные ионные пары. Установлено наличие обмена аниона Cl^- полиэлектролита на ион OH^- воды или анионы X^{n-} неорганических кислот с образованием полимер-коллоидных комплексов (ПКК) со звеньями полимерной цепи, содержащих различные противоионы. Обмен анионов протекает преимущественно на поверхности полимерного клубка, что ограничивает степень замещения анионов и зависит от силы, природы и основности кислот H_nX_m . Установлена связь степени замещения анионов X^{n-} полимерного клубка и прочности образующегося ПКК с энтальпией сольватации неорганических кислот H_nX_m .

Выводы. Установлено, что полимерный электролит ПДМДААХ находится в водном растворе в форме непротекаемых полимерных клубков, представляющих собой полимерные сольватно-разделенные ионные пары. Результатом обмена аниона Cl^- полиэлектролита на ион OH^- воды или анионы X^{n-} неорганических кислот является образование ПКК со звеньями полимерной цепи, содержащих различные противоионы. Обмен анионов протекает на поверхности полимерного клубка и преимущественно с участием аниона OH^- полиэлектролита. Установлена связь между состоянием полимерных клубков ПДМДААХ, степенью замещения анионов с различным rK_a и степенью сольватации кислот. Степень замещения анионов кислот X^{n-} уменьшается с понижением силы кислоты H_nX_m и зарядом образующегося аниона в ряду $HClO_4 > HCl > HNO_3 > HBF_4 > HSO_4^- > H_2PO_4^-$ и характеризуется существенным изменением размеров клубка медленной моды движения полиэлектролита ПКК, для которых величина коэффициента диффузии увеличивается от $3.0 \cdot 10^{-13}$ до $1.3 \cdot 10^{-10}$ см²/с, что соответствует уменьшению степени ассоциации звеньев полимерного клубка ПКК в том же ряду. Степень замещения анионов X^{n-} полимерного клубка и прочность образующегося ПКК симбатно уменьшается с понижением степени сольватации неорганических кислот в воде.

Ключевые слова

ПДМДААХ, потенциометрическое титрование, ИК-спектроскопия, ЯМР-спектроскопия, динамическое светорассеяние, обмен анионов хлора полиэлектролита, неорганические кислоты, полимер-коллоидные комплексы, диффузия полимерных клубков

Поступила:	26.10.2024
Доработана:	27.03.2025
Принята в печать:	16.06.2025

Для цитирования

Голубева Я.Н., Крылов А.В., Чеботарева Т.А. Взаимодействие полидиметилдиаллиламмоний хлорида с неорганическими кислотами. *Тонкие химические технологии.* 2025;20(4):357–371. <https://doi.org/10.32362/2410-6593-2025-20-4-357-371>

INTRODUCTION

As an ionic liquid, the polymer electrolyte poly(*N,N*-diallyl-*N,N*-dimethylammonium chloride) (polyDADMAC) (Fig. 1) has wide practical, including biological, applications as a coagulant/flocculant in water treatment facilities (for example, in polyelectrolyte VPK-402), or as part of polymer inorganic hybrid materials based on it [1, 2].

The transition to the use of gel or polymer inorganic hybrid materials [3–5] leads to the demand for coagulants having higher molecular weights and larger molecular sizes for increasing treatment efficiency in comparison with conventional inorganic coagulating salts [5]. Polymer inorganic hybrid materials are also noted to be more resistant to temperature and pH in wastewater treatment technology [4].

Polyelectrolytes based on polymeric quaternary ammonium compounds (QACs) are used as effective biocidal agents in medicine, biology [6], and the food industry [1], as well as in the method of layer-by-layer assembly of polymer layers on the surface of metal hydroxides [1].

The water-soluble cationic polyelectrolyte VPK-402, which is used for natural and waste water treatment, is currently the only polyDADMAC-based product currently manufactured in the Russian city of Sterlitamak. This is a fairly viscous, opaque substance with a relatively high molecular weight of 250–350 kDa. Any addition of acids or salts to the solution of the polymer leads to its salting out, as confirmed experimentally in the present work. The product used in this work, which has a molecular weight of 20–70 kDa and offers high biocidal and penetrating activity, is recommended for use in medicine, disinfectology (disinfectant VOLAVELA) and agriculture (*Matritsa Rosta* agent, protected by a patent of the Russian Federation [7]). The manufacturer of the agents is *Penta Tekhnologii* (Russia), a developer and manufacturer of biologically active environmentally friendly high-molecular compounds, in partnership with and under the direction of whom this work was carried out.

PolyDADMAC is widely used in agriculture as an effective surfactant that exhibits structuring and moisturizing effects on the soil. This beneficial effect is due to the ability of the polyelectrolyte to dissociate to increase osmotic pressure and, consequently, the filling of soil capillaries with water. PolyDADMAC also exhibits good transport properties for the delivery of nutrients and salts along plant stems [8].

An important role in the efficiency of coagulants/flocculants is played by the size of counteranions. It is asserted [9, 10] that the replacement of the small

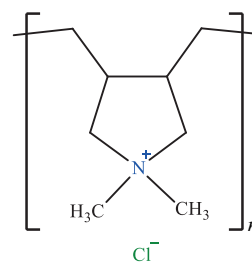


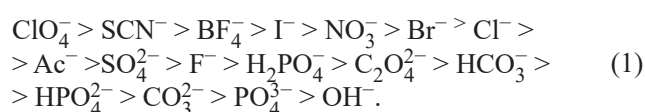
Fig. 1. Structure of poly(*N,N*-diallyl-*N,N*-dimethylammonium chloride) (polyDADMAC)

ions Cl^- and SO_4^{2-} with a bulky inorganic anion (for example, the silicate ion SiO_3^{2-}) in the composition of polymer inorganic hybrid materials leads to the formation of an inorganic polymer-colloidal complex (PCC) having a larger molecular structure. This leads to an increase in the aggregation capacity of the coagulant along with a simultaneous decrease in its concentration. The inclusion of polyDADMAC [8] or polyacrylamide [9] in the composition of organic–inorganic hybrid materials improves the ability of dispersed particles to aggregate via a bridge mechanism.

Apart from studies into the use of styrene–divinylbenzene copolymer anion-exchange resins AN-31, AV-17-8chS, and AV-2-8chS with grafted ammonium groups (NH_3^+ , $\text{N}(\text{CH}_3)_3^+$) to remove a number of inorganic anions from aqueous media [11, 12], there are virtually no literature data on the effect of the size and nature of counteranions X^{n-} on the degree of substitution of Cl^- anions in polymeric QACs.

Many more studies have investigated the exchange of anions in mono-ammonium compounds, which are widely used in the anion-exchange extraction of nonferrous and rare-earth metals [11–13]. The efficiency of extraction is largely determined by the accessibility of the cationic center N^+ . For example, it was determined that anion-exchange extraction of hydrophilic double charged anions with higher QACs, such as trinonyl octadecylammonium bromide (TNODA), occurs insignificantly, which is due to the steric accessibility of the exchange center [13–15].

The values of the constants for the exchange of X^{n-} anions for the standard Cl^- anion in a two-phase water–toluene system were determined [15–17], which made it possible to expand the Hofmeister series for anions:



The obtained series of exchange efficiency shows confirms that the exchange constant in the series for a multiply charged anion decreases with increasing ion

charge. This has been explained in terms of a change in the solvation of X^{n-} by water molecules and, as a consequence of this, a decrease in pK_a for anions with the same name at the central atom [13, 18]:



A study into the ion-exchange equilibria of X^{n-} anions at the ammonium center of TNODA in reactions of extraction from an aqueous medium into toluene confirms that the position of anions in the exchange series is determined not only by the strength pK_a of the corresponding acids H_nX_m , but also by the energies of hydration of the acid anions [13, 18]. For strong and medium-strength mineral acids, the difference in the free energies of hydration of anions dominates over the difference in the free energies of solvation of the nitrogen center N^+ . This is confirmed by the linear correlation of the dependence of the ion exchange constant $\ln K(X^{n-}/2Cl^-)$ in the two-phase water–toluene system on the energy of hydration of X^{n-} anions in water.

The noticeable difference of the absolute values of the equilibrium constants from those calculated using the Eigen–Dancy–Ramsey–Fuoss theory is explained by the difference in ion association [19]. More specifically, this proceeds according to the formation of solvent-separated ion pairs (SSIPs) in the aqueous and organic phases [14]. An increase in the strength of SSIPs with a decrease in the anion size leads to an increase in the ion exchange constants $K(An^{2-}/2Cl^-)$.

The reactivity of organic electrolytes can be varied by combining different cations or anions. Electrolytes have been developed that consist of large organic asymmetric

cations such as 1,3-dialkylimidazolium, 1-alkylpyridinium, 1-alkylpyrazolium, and tetraalkylammonium cations and the anions HF_2^- , $HCOO^-$, CH_3COO^- [20], BF_4^- , PF_6^- , $CF_3SO_3^-$ or $N(SO_2CF_3)_2^-$ [21, 22], 1-ethyl-3-methylimidazoline chloroaluminate (EMImAlCl₄) [20].

However, despite their wide practical application, fewer studies have been carried out into aqueous solutions of QACs and polymeric QACs as compared to the exchange of anions at ammonium centers in organic solvents.

The high hydrophilicity of charged quaternary ammonium groups of polyDADMAC promotes high solubility of the polymer in water; moreover, its solutions exhibit properties of strong polyelectrolytes [1].

All solvents, which differ in their thermodynamic qualities in terms of their interaction with a polymer, can be divided into thermodynamically “good”, “ideal”, and “bad”. This determination is carried out according to the preferred polymer–solvent interaction in a “good” solvent or a polymer–polymer interaction in a “bad” solvent. In a thermodynamically “good” solvent, a linear macromolecule tends to adopt the conformation of the so-called swollen polymer coil (Fig. 2a); as the salinity of the medium increases, the coil contracts (Fig. 2b).

In “bad” solvents or in the presence of inorganic salts, polymer coils are observed to contract and adopt a more compact globule conformation [19, 23]. A similar effect of polymer coil contraction, which should also be observed upon introduction of low-molecular inorganic and organic salts (Me_nX_m) (Fig. 2b), will be determined by both the concentration of the polyelectrolyte and the acidity pK_a of the salt-forming acids (H_nX_m). An equally

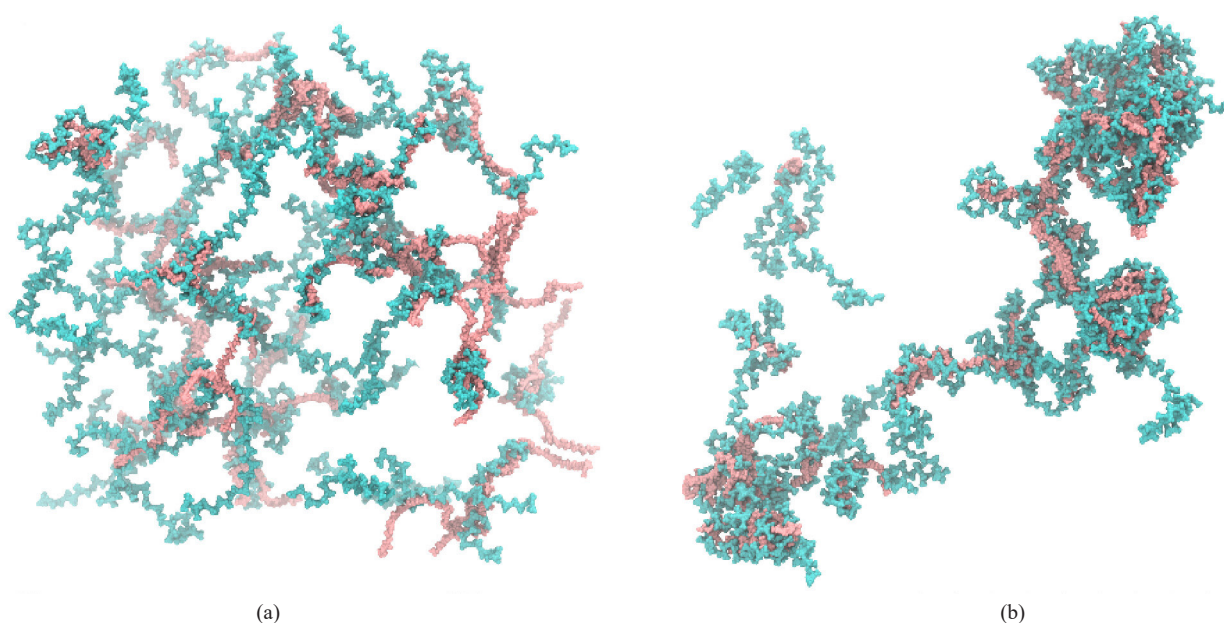


Fig. 2. Conformation of the polyDADMAC coil (0.3 M) as determined by the molecular dynamics method in the OPLS (Optimized Potential for Liquid Simulations) force field (water molecules are omitted for clarity) (a) in a salt-free system or (b) with 2 M KBr [22]

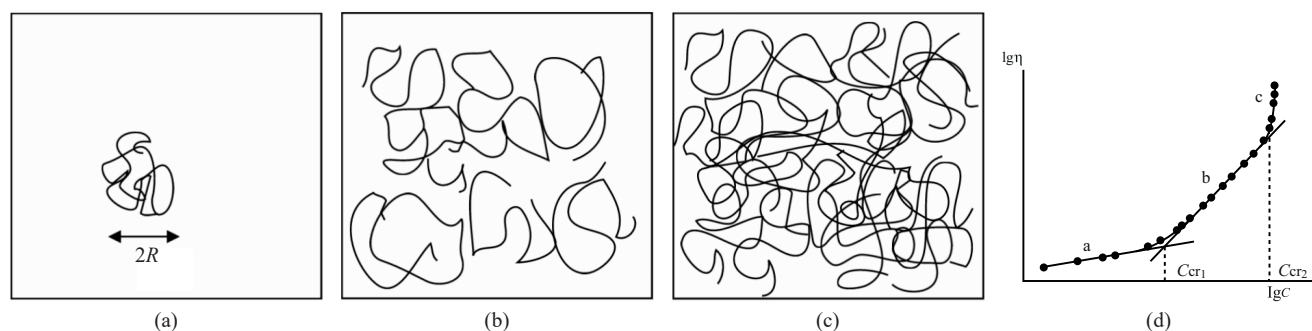


Fig. 3. Schemes of (a) dilute, (b) semi-dilute, and (c) concentrated solutions. (d) Dependence $\lg \eta = f(\lg C)$. $2R$ is a hydrodynamic diameter of the folded polymer chain

important role in the conformation of the polymer coil is played by the ionic strength of the medium, as was described in the literature [20, 24–27] and confirmed in our work.

In “ideal” (theta) solvents, the coil has a conformation of a coil obeying Gaussian statistics.

It is reported [26] that a 1 M NaCl aqueous solution and the Mark–Kuhn–Houwink equation correspond to the conditions of the theta solvent according to the equation:

$$[\eta] = 1.12 \cdot 10^{-4} M_w^{0.82}, \quad (3)$$

where $[\eta]$ is the characteristic viscosity of the polymer chain with the molecular weight M_w .

It is also necessary to take into account the dependence of the state of the polymer molecule on its concentration [24]. The characteristic viscosity $[\eta]$ determined in a given concentration range characterizes the density of filling the solution with segments (loops) of macromolecules or the concentration at which the overlap of polymer blobs occurs. The limiting concentrations of the transition from dilute (C^*) to semi-dilute (C^{**}) to concentrated (C^{***}) solution depend on the molecular weight M_w , the concentration of the polyelectrolyte, and the quality of the solvent, which in turn determine the volume of the polymer coil (Fig. 3). Thus when the solution is concentrated, the structure of the polyelectrolyte solution changes from the content of “polymer in water” to “water in polymer”.

Since the polymer concentration is quite low in the case of dilute solutions, the polymer chains exist separately from each other. Here polymer–polymer interaction plays a minor role; thus, for such solutions the M_w of polyDADMAC is determined in most studies using Mark–Kuhn–Houwink equation (3).

It has been confirmed that the crossover points C^* , C^{**} , and C^{***} (Fig. 3d) are fairly well determined for this polyelectrolyte on the dependence $\lg \eta = f(\lg C)$ and that the crossover point values shift toward higher values with increasing salt concentration [24, 26]. The size of the polymer coil also exhibits this tendency.

EXPERIMENTAL

Equipment and methods for sample preparation

Initial substances. The initial aqueous solution of polyDADMAC having a polymer mass fraction of $\omega = 52\%$ and a viscosity of 25000 mPa·s was obtained by homoallylic condensation of *N,N*-diallyl-*N,N*-dimethylammonium chloride in the presence of analytical grade ammonium persulfate (Scharlab, Spain) in the Laboratory of the Department of Physical Chemistry at the MIREA – Russian Technological University according to the published procedure [7]. The M_w of the polyelectrolyte sample, which was estimated using equation (3) taking into account the content of inorganic salts, was approximately ~20–25 kDa. The estimated value of M_w can be considered approximate, since, as will be shown below, the state of the polymer in the solution changes as acids or salts of inorganic acids are added to the aqueous solution. PolyDADMAC solutions were prepared using distilled water H_2O of the first category with a specific electrical conductivity of 4–5 $\mu S/cm$ in accordance with GOST R 58144-2018¹.

For the study, polyDADMAC solutions with concentrations in the range of 0.06–0.3 M (0.67–3.35 wt %) were selected, i.e., semi-dilute solutions, in which both small polymer coils without entanglement and large coils with entanglement can be expected [22, 23].

¹ GOST R 58144-2018. National Standard of the Russian Federation. Distilled water. Specifications. Moscow: Standartinform; 2018. https://meganorm.ru/mega_doc/norm/gost-r_gosudarstvennyj-standart/10/gost_r_58144-2018_natsionalnyy_standart_rossiyskoy.html. Accessed June 11, 2025.

Taking into account a high pH sensitivity of the polyelectrolyte, the initial polyelectrolyte solution was prestandardized by treatment with the solid anion exchanger AV-17-8chS (*Smoly*, Russia) in the OH form to pH 12. For brevity, let us denote the alkaline form polyDADMA–OH. To obtain polyDADMA–OH, the solid anion exchanger AV-17-8chS was initially treated with a 3 M NaOH solution in a glass beaker for 60 min. Next, the anion exchanger was repeatedly washed with water until a neutral pH to remove residual alkali and chlorine anion salts. To the obtained anion exchanger AV-17-8chS in the OH form, a solution of polyDADMAC was added and stirred for 60 min until reaching pH 12. The concentration of the obtained polyDADMA–OH solution was refined gravimetrically using the dried residue of the solution in a vacuum drying oven.

Reagents. The following acids were selected. Monoprotic acids: perchloric acid (pure, 60%); hydrochloric acid (chemically pure, 35%); nitric acid (chemically pure, 65%); tetrafluoroboric acid (pure, 40%); sulfamic acid (pure, 99.5%). Polyprotic acids: sulfuric acid (special pure, 93.5%); orthophosphoric acid (pure, 85%); periodic acid (pure, 98%); boric acid (pure, 99%) (all by *CHIMMED*, Russia). Acid titers were controlled by the titer of the alkali of the state standard sample (standard titer, 0.5 N, *CHIMMED*, Russia).

^1H nuclear magnetic resonance (NMR) spectra were recorded with an AVHD600 NMR pulsed broadband Fourier spectrometer with a superconducting magnet (*Bruker BioSpin AG*, USA). Strongly adsorbed water molecules in polyDADMAC make it difficult to record NMR due to requiring dissolution of the polymer in D_2O . A specially developed technique was used to transfer polyDADMAC from an aqueous solution to a D_2O solution. A solution of the polyDADMAC polyelectrolyte sample in H_2O (2 mL) was placed in a 15-mL glass vial and concentrated in a CentriVap 7310031 tabletop concentrator (*Labconco Corporation*, USA) with a built-in RV5 pump (*Edwards*, United Kingdom) with a gradient increase in temperature to 55°C. As evaporation proceeded, a new portion of the sample was added. After evaporation until the formation of a dry residue, the resulting polyelectrolyte was immediately dissolved in deuterated water (99.8 wt %) to record ^1H NMR spectra. At higher temperatures, the polyelectrolyte decomposed with the appearance of a characteristic odor of methylamines, which is consistent with the published data [27].

Infrared (IR) spectra of the samples in liquid and solid forms were recorded with an Agilent Cary 630 FTIR spectrometer (*Agilent*, USA) by the attenuated total internal reflection method in the range of 4000–350 cm^{-1}

at a spectral resolution of $<2\text{ cm}^{-1}$. The IR spectra were processed using the Agilent MicroLab software.

The solid samples of polyDADMAC and polymer complexes based on it were obtained by drying in a BV-50 vacuum drying oven (*Being*, China) for 180 min at a temperature of 80°C. The use of solid samples after using the CentriVap concentrator is impossible due to the active absorption of water vapor by the dehydrated polyelectrolyte sample.

Dynamic light scattering (DLS) spectra were recorded with a Photocor Compact-Z analyzer (*Fotokor*, Russia). The power of the 638-nm thermostable semiconductor laser was 25 mW. The particle sizes in concentrated and low-transparency systems were measured by the backscattering method at an angle of 160° at a constant temperature of 25°C. The signals were analyzed by a built-in Photocor FC correlator for auto- and cross-correlation measurements. The DLS spectra were processed by the DynaLS software package (*Fotokor*).

Potentiometric titration was carried out in an ATP-02 automatic titrator (Russia) with an IT ESC 10601.7 combined glass electrode in the measurement range of pH 0–12. The limiting reference absolute error of measuring pH is 0.03. In all experiments, polyDADMA–OH solutions were titrated, and acid solutions were titrants. The corresponding PCCs were conventionally denoted as polyDADMA–X, where X is a fully substituted anion of the titrant acid.

Data of **polyDADMAC** analyses. ^1H NMR (600 MHz, D_2O) δ , ppm: 3.91–3.77 (2H, $\text{N}^+(\text{CH}_2)_2$), 3.40–3.10 (6H, $\text{N}^+(\text{CH}_3)_2$), 2.67–2.24 (2H, *cis/trans*-CH), 1.57–1.00 (4H, *iso/sindio/a* CHCH_2). IR (1 wt %, H_2O): 3328, 2357, 2327, 2115, 1995, 1632, 706, 674 cm^{-1} . IR (52 wt %, H_2O): 3360, 2950, 2871, 2322, 2096, 1997, 1917, 1634, 1472, 1420, 1101, 1000, 959, 875, 674 cm^{-1} . IR (96 wt %, H_2O): 3362, 3019, 2933, 2866, 2706, 2113, 1995, 1636, 1472, 1457, 1418, 1386, 1252, 1093, 989, 961, 911, 877, 836 cm^{-1} .

RESULTS AND DISCUSSION

The state of polyDADMAC in D_2O was analyzed by ^1H NMR spectroscopy. The symmetry of the relatively flat five-membered heterocyclic rings of the polymer component gives rise to *cis*- and *trans*-isomers of polymeric QAS as confirmed by a double set of broadened signals of proton-containing groups. The ratio of *cis/trans*-isomers is 4.5 : 1.

IR spectroscopy was carried out for solutions with different concentrations of polyDADMAC from 1 to 52 wt % and dried samples with a content of 96 wt %. The IR spectrum of dilute aqueous solutions of polyDADMAC (Fig. 4) presents mainly broadened

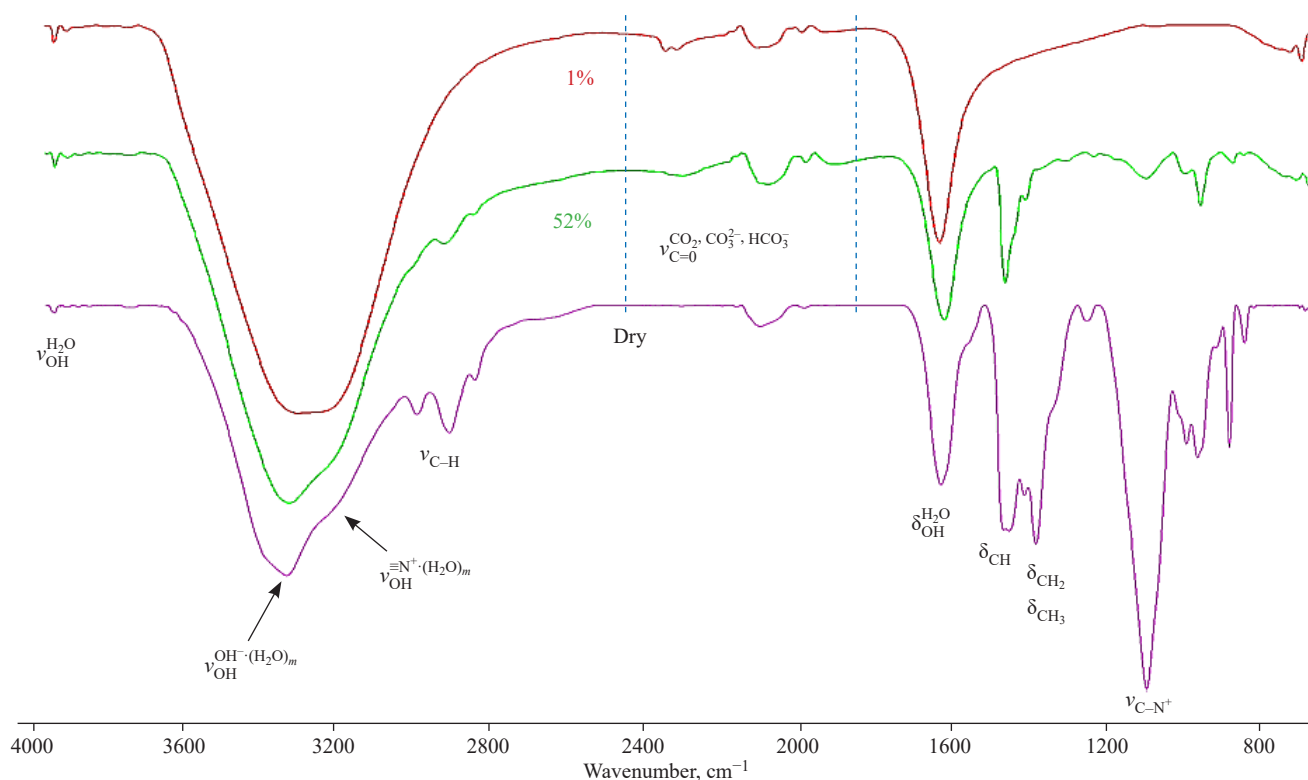


Fig. 4. IR spectra of polyDADMAC solutions of various concentrations from 1 to 96 wt %

overlapping signals of stretching vibrations in the range of $\nu = 3650\text{--}3050\text{ cm}^{-1}$ and bending vibrations of water $\delta_{\text{H}_2\text{O}} = 1635\text{--}1640\text{ cm}^{-1}$ shows almost no polyDADMAC vibration bands due to the overlap with the H_2O bands.

It should be noted that, even for a virtually completely dried sample, the IR spectrum is dominated by the vibration bands of adsorbed water. As can be seen from Fig. 4, the band of stretching vibrations is divided into two signals characteristic of a strongly adsorbed phase in the form of SSIP and free water, which agrees with the published data [19].

The vibration bands of the polyelectrolyte become clearly distinguishable for a concentrated aqueous sample (52 wt %), i.e., in the region of the “water-in-polymer” system, or for dried samples (≈ 96 wt %).

The stretching vibrations of the C–H bond occur at $\nu = 2937\text{ cm}^{-1}$ and $\delta = 1470$ and 1370 cm^{-1} in the CH_2 groups and the terminal CH_3 groups of the polymer chain. The stretching vibrations of the C–N^+ bond are characterized by an intense vibration band with a maximum at $\nu = 1080\text{ cm}^{-1}$.

We may also note the occurrence of vibration bands in the range of $2100\text{--}2200\text{ cm}^{-1}$ due to the presence of carbonate and bicarbonate ions bound to the polyelectrolyte, which agrees with the previously obtained data [28] and confirms the possibility of using polyDADMAC solutions for gas treatment.

The results obtained suggest that the exchange of Cl^- anions for OH^- ions of water for the monomer and polymer occurs according to the schemes shown in Figs. 5 and 6, respectively, which should be manifested in both monomeric and polymeric QASs.

According to the proposed scheme and as confirmed in the present work, monomeric and polymeric QASs are pH-sensitive and can be titrated in both acidic and alkaline media.

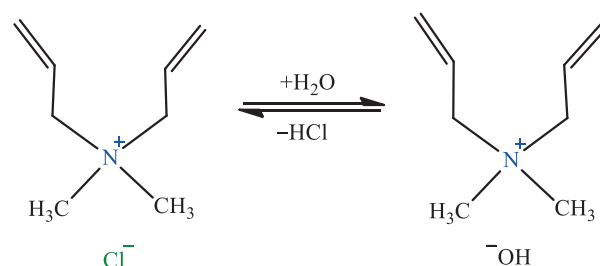


Fig. 5. Scheme of anion exchange at ammonium N^+ centers in polyDADMAC in water

Figure 7 illustrates the results of acid–base titration of monomeric and polymeric QASs separately with hydrochloric acid and sodium hydroxide. The curves of titration with acid and alkali at polyelectrolyte concentrations of 2.7, 5.4, and 10.8 wt % are combined

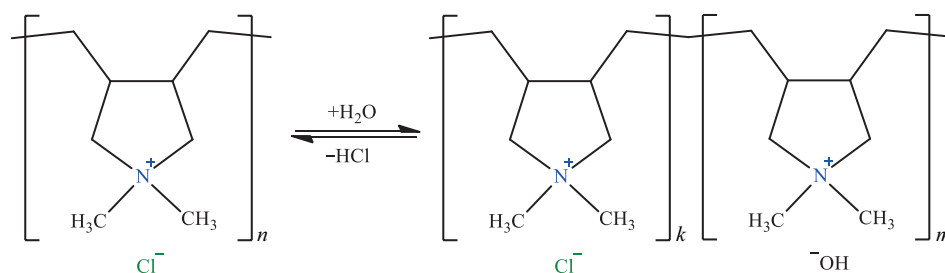


Fig. 6. Scheme of anion exchange at ammonium N^+ centers in polyDADMAC in water ($n = k + m$)

into a common graph (Fig. 7b). In contrast to the monomer, for which equilibrium between the chloride and hydroxide forms of QAS is observed (Fig. 5), in the case of polymeric QASs (Fig. 7), in the polyelectrolyte molecule, equilibrium is achieved between the polymer units containing different counterions Cl^- and OH^- .

As can be seen from Fig. 7, the titration curves have a typical sigmoid shape with a single pH step, which confirms the proposed anion exchange schemes (Figs. 5 and 6). The equivalence point (EP) for QASs virtually corresponds to a ratio of equivalents n_{eq} of ~ 1 and shows that all monomer anions are accessible for titration.

A different picture is observed in the case of polyDADMAC, for which the EP shifts from the alkaline to the acidic region: $pH_{EP} = 7.75, 6.16,$ and 5.24 as the polymer concentration is increased from 2.7 and 5.4 to 10.8 wt %, respectively, which confirms the pH sensitivity of the polyelectrolyte according to the scheme (Fig. 6). At the same time, the number of HCl equivalents remains virtually unchanged after quadrupling the polyelectrolyte concentration and is $n_{eq} \approx 0.032$. This result confirms that the polyelectrolyte in the solution exists in the form of an impermeable polymer coil,

and only a part of the anions located on the surface is accessible for exchange.

This state of the polyelectrolyte can be characterized as a PCC. Since the equilibrium distribution of counterions Cl^- or OH^- in the PCC between the polyDADMAC units or the ratio of units $k : m$ (Fig. 6) will depend on the nature of the exchanging anion, a change in the size of the polymer coil occurs, which we confirmed by the DLS method.

In the DLS spectra of the initial polyDADMAC (Fig. 8a) and the polymer treated with an anion exchanger (PDMDAA- OH) (Fig. 8b), three modes of polymer coil motion are observed: fast (F), intermediate (I), and slow (S).

Depending on the concentration of the polyelectrolyte, three to five modes of motion can appear in the DLS spectrum [22, 23]. The diffusion coefficients D of the fast and slow modes of motion of the macromolecular coils depend linearly on the polymer concentration C_p [23, 24]:

$$D = D_0(1 + K_D C_p), \quad (4)$$

where D_0 is the diffusion coefficient as $C_p \rightarrow 0$ and the diffusion coefficient constant K_D is determined by the balance of bulk and hydrodynamic interactions. Whereas

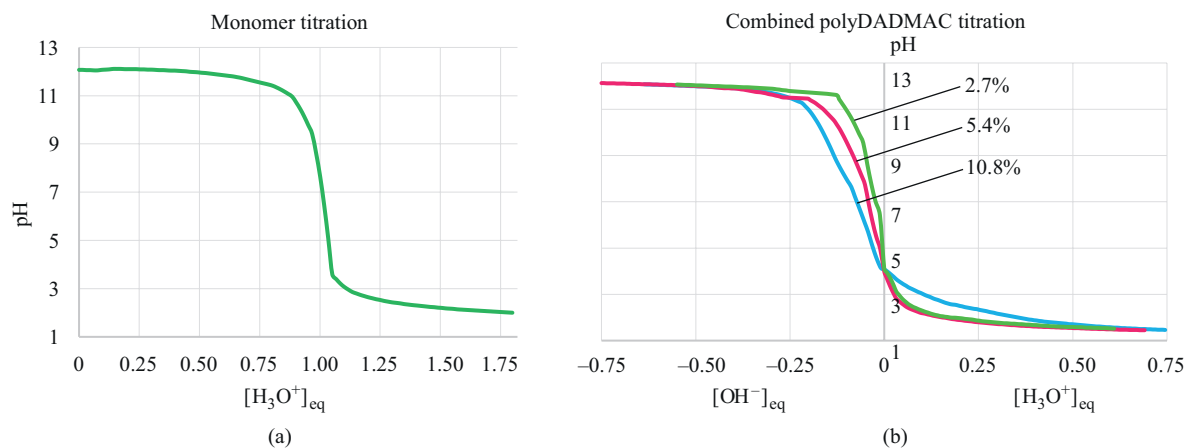


Fig. 7. (a) Titration curve of the monomer and (b) the full titration curve of the 0.3 M polyelectrolyte with 0.1 M NaOH and 0.1 M HCl. $[H_3O^+]_{eq} = n(HCl)/n(\text{polyDADMAC})$; $[OH^-]_{eq} = n(NaOH)/n(\text{polyDADMAC})$

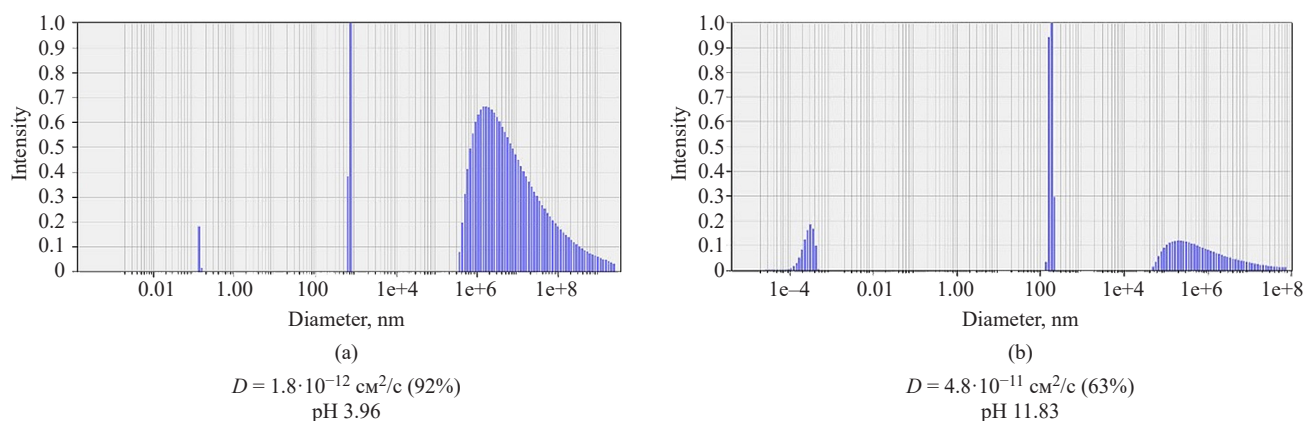


Fig. 8. Dynamic light scattering (DLS) spectra of the initial 0.3 M polyDADMAC and the treated 0.3 M polyDADMA–OH

the slow mode characterizes the agglomeration or contraction of the polymer chain into a polymer coil, the nature of the fast mode remains somewhat unclear [23]. Table presents the diffusion coefficients of the slow mode of motion for PCCs with various inorganic acids. The slow mode of motion (S) is of the greatest interest since it reaches micron sizes and is contained in the maximum amount (Table).

As will be shown, the state of polyDADMAC and the number of modes of motion of polymer coils significantly depend on the nature of the X^{n-} anion.

The DLS spectra of the acidic form polyDADMAC and alkaline form polyDADMA–OH of the polyelectrolyte (Fig. 8) differ noticeably in content and diffusion coefficients of the slow mode S_1 of the polymer coils. This confirms the influence of the anion

Table. Results of potentiometric titration and DLS data on polyDADMA–OH + H_nX_m system

Acid	n_{eq}	pH _{EP}	F (EP), %	S (EP), %	D_S (EP) · 10 ¹¹ , cm ² /s	pK _a (H _n X)	ΔH_s , kJ/mol
–*	–	11.83*	8.2*	63.3*	4.80*	–	–
HClO ₄ **	0.359	4.69	50.2	48.9	0.03	–15.20	–88.41
HCl	0.205	4.75	22.7	75.0	13	–5.60	–74.52
HNO ₃	0.188	6.26	35.9	47.7	7.1	–1.64	–32.90
HBF ₄	0.087	7.36	1.9	97.1	58	–0.44	–
NH ₂ SO ₃ H	0.250	5.65	3.1	77.6	15	1.00	–
H ₂ SO ₄	0.048	7.67	66.3	28.6	0.68	–3.0 / 1.9	–76.73
H ₃ PO ₄	0.067 / 0.162	8.89 / 4.43	17.4	74.8	3.3	2.14 / 7.20 / 12.37	–10.71
H ₃ BO ₃	0.077 / 0.296	10.79 / 9.21	33.6	26.7	14	9.24 / 12.40 / 13.30	20.05
H ₅ IO ₆	0.184 / 0.336	8.64 / 4.76	64.9	20.4	6.1	3.29 / 8.31 / 11.60	–

Note:

* Data for 0.3 M polyDADMA–OH solution.

** A white precipitate is formed.

$n_{eq} = n(H_nX)/n(\text{polyDADMA–OH})$.

ΔH_s is the heat of H_nX_m solvation in water.

pH_{EP} is the pH value at the EP of the titration curve.

D_S (EP) are the diffusion coefficients of the slow mode at the EP, cm²/s.

nature and acidity on the aggregation of the polyelectrolyte.

Whereas the fraction of the slow mode S decreases from 92.0 to 63.3%, the polyDADMA–OH solution is characterized by a narrower molecular weight distribution and an increase in the contribution of the fast mode of motion (F) from 1.0 to 8.2%. This is apparently due to a change in the size of the polymer coil involving an increase in the fraction of units containing OH[−] anions. The diffusion coefficient of the mode S is observed to quadruple. At the same time, adsorption of some larger aggregates on the anion exchanger cannot be ruled out.

As inorganic acids and salts, substances differing in strength (pK_a) and heat of solvation of H_nX_m in water (ΔH_s) were selected. Table presents the results of potentiometric titration and DLS data on the polyDADMA–OH + H_nX_m system for EPs.

As can be seen from Table, the degree of substitution of polyelectrolyte anions for acid anions H_nX_m does not exceed $n_{eq} = 0.184\text{--}0.336$. This confirms that polyDADMAC in solution exists in the form of an impermeable polymer coil and that only a part of the anions located on the surface of the polymer coil is accessible for exchange. In this case, the result of exchange for the X^{m-} anion is the presence of 3 types of links in the polyelectrolyte structure (Fig. 9).

In the case of HClO₄, the titration of the system yields an insoluble white precipitate at the EP having an extremely low value of the diffusion coefficient of the slow mode of motion S with D_S (EP) = $3 \cdot 10^{-13}$ cm²/s. While the EP on the titration curve symbatically shifts from the acidic to the alkaline region from pH_{EP} 4.69 to 7.36, the degree of substitution of anions of monoprotic strong acids (n_{eq}) increases with increasing strength of the H_nX_m acid: HClO₄ > HCl > HNO₃ > HBF₄. The obtained result from the point of view of acid–base equilibrium shows that the exchange reaction of the acid anion X^{n-} occurs predominantly with the participation of the OH[−] anion of the polyelectrolyte. An exception is the amino-substituted acid NH₂SO₃H with a low $pK_a(H_nX) = 1$ value in the series of inorganic acids; however, this is capable of additional protonation at the amino group during titration.

The low value of $n_{eq} = 0.048$ for the strong dibasic acid H₂SO₄ and simultaneous shift of the pH of 7.67 to the alkaline region can be explained in terms of an exchange reaction that predominantly forms the HSO₄[−] anion with $pK_a = 1.9$. A similar effect is observed for other polyprotic acids.

The triprotic acids H₃PO₄ and H₃BO₃ and the polyprotic periodic acid H₅IO₆ are characterized by two pH steps; here, despite the inverse relationship $pK_a(H_2X^-) < pK_a(H_3X)$, the degree of substitution at the second stage increases ($n_{eq}(H_2X^{2-}) > n_{eq}(X^{3-})$) with a decrease in the ion charge. This observed phenomenon agrees with the published data [13, 18] on the efficiency of anion exchange in the Hofmeister series. Thus, a change in the nature of the anion affects not only the degree of substitution, but also the state of the polymer coil (Fig. 10).

With a decrease in the acid strength pK_a in the acid series, the diffusion coefficient D_S (cm²/s) of the slow mode S increases: $3 \cdot 10^{-13}$ (HClO₄), $7.1 \cdot 10^{-11}$ (HNO₃), $1.3 \cdot 10^{-10}$ (HCl), and $5.8 \cdot 10^{-10}$ (HBF₄). This corresponds to a decrease in the degree of association of the units of the polymer coil of PCC in the same series. The high value of the diffusion coefficient D_S of the slow mode for HBF₄ (Table) can also be explained by its partial dissociation in the alkaline medium of polyDADMA–OH into H₃BO₃ and HF to form a PCC with the F[−] anion.

A decrease in the strength pK_a was also found to lead to the occurrence of two to three additional intermediate (I) modes of motion, which are the modes of interaction between the cationic nitrogen N⁺ centers and anions. This argues for the formation of the PCC in the form of SSIP with different values of the diffusion coefficients D of the modes of motion of polymer coils.

In this case, both a broadening and an increase is observed in the contributions of fast (F) and intermediate (I) modes of motion in the series HNO₃ > H₂SO₄ > H₃PO₄ (Fig. 10; Table), which can be explained by the presence of different forms of anions of acidic and neutral salts.

The obtained result confirms that the process of solvation of acid anions X^{n-} by water molecules represents an important additional factor in the exchange

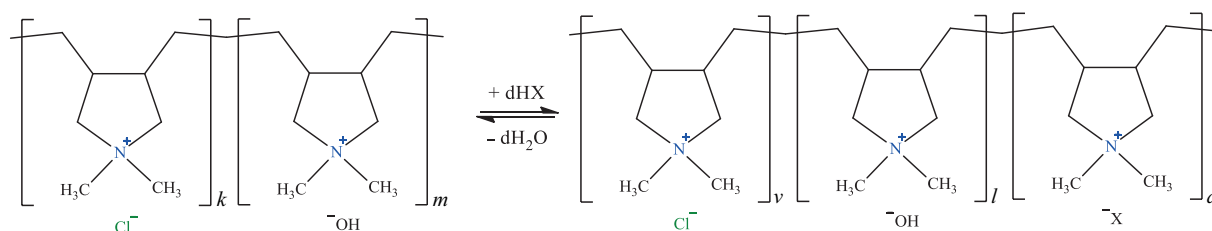


Fig. 9. Scheme of anion exchange at ammonium N⁺ centers of polyDADMAC with H_nX ($k + m = v + l + d$)

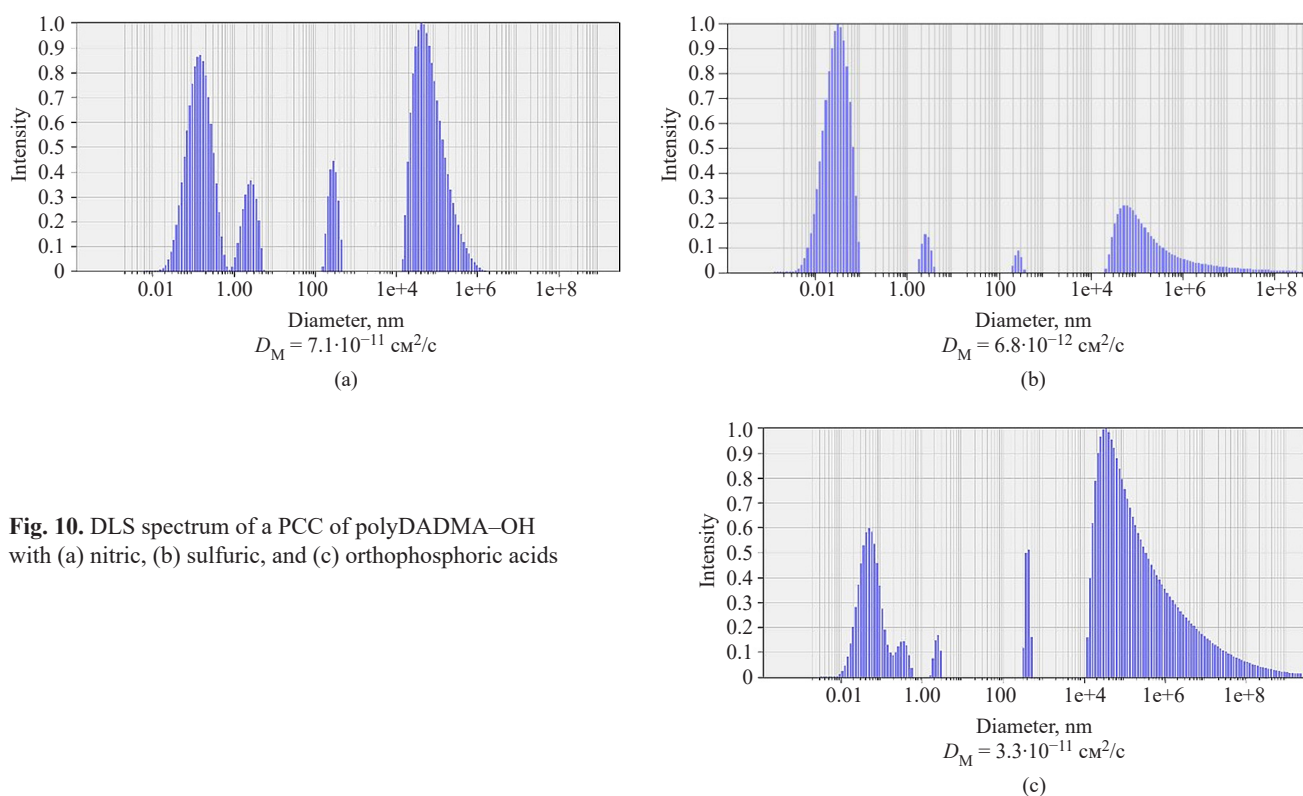


Fig. 10. DLS spectrum of a PCC of polyDADMA–OH with (a) nitric, (b) sulfuric, and (c) orthophosphoric acids

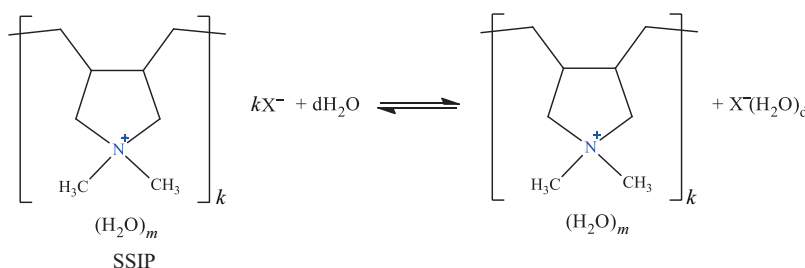


Fig. 11. Scheme of solvation of the solvent-separated ion pair (SSIP) anion: $X^- = \text{ClO}_4^-, \text{Cl}^-, \text{NO}_3^-, \text{BF}_4^-, \text{HSO}_4^-, \text{and } \text{H}_2\text{PO}_4^-$

(Fig. 11), which will affect both the strength of the PCC and the degree of dissociation of SSIP into a polymer cation and solvated anions $X^-(\text{H}_2\text{O})_d$.

In this work, the degree of solvation of the X^{n-} anions is estimated using the heats of dissolution of the H_nX acids. A decrease in the exothermicity of the heat of dissolution of the inorganic acid from $\Delta H_s = -88.4$ to -10.71 kJ/mol of the H_nX acids (Table) leads to a symbatic decrease in the degree of substitution of the X^{n-} anions of the polymer coil from $n_{\text{eq}} = 0.359$ to 0.048 , thus confirming that the solution contains not only SSIP aggregates, but also dissociated forms of the polyelectrolyte. The exceptions to this rule are sulfur-containing acids H_2SO_4 and $\text{NH}_2\text{SO}_3\text{H}$, which form HSO_4^- and NH_2SO_3^- anions during titration.

CONCLUSIONS

The reported DLS, potentiometry, and IR spectroscopy studies confirm that the polymer electrolyte polyDADMAC exists in an aqueous solution in the form of impermeable polymer coils, which are made up of polymer solvent-separated ion pairs (SSIPs). Here, the Cl^- anion of the polyelectrolyte is exchanged for the OH^- ion of water or the X^{n-} anions of inorganic acids to form polymer chain links with various counteranions. The anion exchange, which mainly occurs on the surface of the polymer coil and depends on the strength, nature, and basicity of the H_nX_m acids, serves to limit the degree of anion substitution. The obtained forms of substituted polyelectrolyte can be classified as PCCs.

The substitution of the X^{n-} anions of strong acids in the series $\text{HClO}_4 > \text{HCl} > \text{HNO}_3 > \text{HBF}_4 > \text{H}_2\text{SO}_4, \text{H}_3\text{PO}_4$, which mainly involves the OH^- anion of the polyelectrolyte, decreases with decreasing strength of the HX acid from $n_{\text{eq}} = 0.336$ to 0.07. This also leads to significant changes in the sizes of the slow-mode PCC coil, for which the diffusion coefficient increases from $D = 3.0 \cdot 10^{-13}$ to $1.3 \cdot 10^{-10} \text{ cm}^2/\text{s}$, as well as corresponding to a decrease in the degree of association of the PCC polymer coil links in the same series.

The degree of exchange for polyprotic acids is limited by the formation of mainly monoprotic anions HSO_4^- and H_2PO_4^- corresponding to the first stage of substitution. The fallout from the trend of the influence of the strength of the acids H_3BO_3 and H_5IO_6 is explained by their ability to form polymeric forms of anions in solution, which are stabilized by the polymer matrix of polyDADMAC.

The exchange of anions at the ammonium centers of polymeric QASs is established to be an important factor influencing the degree of solvation of acid anions X^{n-} by water molecules. A decrease in the degree of solvation (ΔH_s) of acids H_nX_m in water symbatically reduces the degree of substitution of X^{n-} anions of the polymer coil, as well as the strength of the forming PCC and its ability to dissociate into a polymer cation and solvated anions $X^-(\text{H}_2\text{O})_d$.

Authors' contributions

Ya.N. Golubeva—conducting research, collecting and processing the material, and writing the text of the article.

A.V. Krylov—development of the concept of scientific work, critical revision with the introduction of valuable intellectual content.

T.A. Chebotareva—reviewing publications on the topic of the article.
The authors declare no conflict of interest.

REFERENCES

- Golubeva Ya.N., Chebotareva T.A., Tokareva A.A., Krylov A.V., Zhеглаты P.V. Prospects the development of urification methods of sludge-lignin deposits of JSC "Baikal Pulp Mill" with polymer electrolytes. *Khimicheskaya bezopasnost' = Chem. Safety Sci.* 2023;7(2):55–73 (in Russ.). <https://doi.org/10.25514/CHS.2023.2.25004>
- Monney I., Buamah R., Donkor E.A., et al. Treating waste with waste: the potential of synthesized alum from bauxite waste for treating car wash wastewater for reuse. *Environ. Sci. Pollut. Res.* 2019;26(13):12755–12764. <https://doi.org/10.1007/s11356-019-04730-0>
- Xin-Hui Su C., Tow Teng T., Morad N. Optimization of the Coagulation-Flocculation of Reactive Dye Wastewater Using Novel Inorganic-Organic Hybrid Polymer. *Iranica J. Energy Environ.* 2016;7(1):31–38.
- Abujazar M., Karaağaç S.U., Bashir M.J.K., et al. Recent advancement in the application of hybrid coagulants in coagulation-flocculation of wastewater: A review. *J. Cleaner Product.* 2022;345:131–133. <https://doi.org/10.1016/j.jclepro.2022.131133>
- Kabanov V.A. From synthetic polyelectrolytes to polymer-subunit vaccines. *Pure Appl. Chem.* 2004;76(9):1659–1677. <https://doi.org/10.1351/pac200476091659> [Original Russian Text: Kabanov V.A. From synthetic polyelectrolytes to polymer-subunit vaccines. *Vysokomolekulyarnye soedineniya. Seriya A.* 2004;46(5):759–782 (in Russ.).]
- Tokareva A.A., Krylov A.V., Bondareva A.M., Chebotareva T.A., Zhеглаты P.V. Integrated approaches to the treatment of highly polluted wastewater. *Khimicheskaya bezopasnost' = Chem. Safety Sci.* 2023;7(1):81–92 (in Russ.). <https://doi.org/10.25514/CHS.2023.1.24006>
- Zhеглаты P.V., Bobrova I.V., Krylov A.V., Nosik N.N., Nosik D.N. *New Virucidal Agents Containing Complex Based on Polypyrrolidinium Polymers*: RF Pat. 2782065. Publ. 21.10.2022 (in Russ.).
- Kristianto H., Rahman H., Prasetyo S., et al. Removal of Congo red aqueous solution using *Leucaena leucocephala* seed's extract as natural coagulant. *Appl. Water Sci.* 2019;9:88. <https://doi.org/10.1007/s13201-019-0972-2>

СПИСОК ЛИТЕРАТУРЫ

- Голубева Я.Н., Чеботарева Т.А., Токарева А.А., Крылов А.В., Жеглаты П.В. Перспективы разработки методов очистки коллоидных осадков шлам – лигнина ОАО «Байкальского целлюлозного комбината» полимерными электролитами. *Химическая безопасность.* 2023;7(2):55–73. <https://doi.org/10.25514/CHS.2023.2.25004>
- Monney I., Buamah R., Donkor E.A., et al. Treating waste with waste: the potential of synthesized alum from bauxite waste for treating car wash wastewater for reuse. *Environ. Sci. Pollut. Res.* 2019;26(13):12755–12764. <https://doi.org/10.1007/s11356-019-04730-0>
- Xin-Hui Su C., Tow Teng T., Morad N. Optimization of the Coagulation-Flocculation of Reactive Dye Wastewater Using Novel Inorganic-Organic Hybrid Polymer. *Iranica J. Energy Environ.* 2016;7(1):31–38.
- Abujazar M., Karaağaç S.U., Bashir M.J.K., et al. Recent advancement in the application of hybrid coagulants in coagulation-flocculation of wastewater: A review. *J. Cleaner Product.* 2022;345:131–133. <https://doi.org/10.1016/j.jclepro.2022.131133>
- Кабанов В.А. От синтетических полиэлектролитов к полимер-субъединичным вакцинам. *Высокомолекулярные соединения. Серия А.* 2004;46(5):759–782.
- Токарева А.А., Крылов А.В., Бондарева А.М., Чеботарева Т.А., Жеглаты П.В. Комплексные подходы к очистке сложно загрязненных сточных вод. *Химическая безопасность.* 2023;7(1):81–92. <https://doi.org/10.25514/CHS.2023.1.24006>
- Жеглаты П.В., Боброва И.В., Крылов А.В., Носик Н.Н., Носик Д.Н. *Новые вирулицидные средства, содержащие комплекс на основе полипирролидиниевых полимеров*: пат. 2782065 РФ. Заявка № 2021105431; заявл. 03.03.2021; опубл. 21.10.2022.
- Kristianto H., Rahman H., Prasetyo S., et al. Removal of Congo red aqueous solution using *Leucaena leucocephala* seed's extract as natural coagulant. *Appl. Water Sci.* 2019;9:88. <https://doi.org/10.1007/s13201-019-0972-2>

9. Zhao Y.X., Gao B.Y., Shon H., *et al.* Coagulation characteristics of titanium (Ti) salt coagulant compared with aluminum (Al) and iron (Fe) salts. *J. Hazardous Mater.* 2011; 185(2–3):1536–1542. <https://doi.org/10.1016/j.jhazmat.2010.10.084>
10. Nesterov Yu.V. *Ionity i ionoobmen. Sorbtsionnaya tekhnologiya pri dobyche urana i drugikh metallov metodom podzemnogo vyshchelachivaniya (Ionites and Ion Exchange. Sorption Technology in the Extraction of Uranium and Other Metals by Underground Leaching)*. Moscow: Atomredmetzoloto; 2007. 480 p. (in Russ.).
11. Matveichuk Yu.V., Stanishevskii D.V. Anion-Exchange Extraction of Doubly Charged Anions by Higher Quaternary Ammonium Salts with Different Steric Accessibility of the Exchange Center. *J. Anal. Chem.* 2020;75(6):711–716. <https://doi.org/10.1134/S1061934820040097>
[Original Russian Text: Matveichuk Yu.V., Stanishevskii D.V. Anion-Exchange Extraction of Doubly Charged Anions by Higher Quaternary Ammonium Salts with Different Steric Accessibility of the Exchange Center. *Zhurnal analiticheskoi khimii.* 2020;75(6):496–501 (in Russ.). <https://doi.org/10.31857/S0044450220040106>]
12. Kuzmin V.I., Gudkova N.V., Kuzmin D.V., *et al.* Effect of solvation-dehydration of quaternary ammonium base salts in the organic phase on the selectivity of anion-exchange extraction. *Sep. Sci. Technol.* 2023;58(7):1283–1294. <https://doi.org/10.2139/ssrn.3967023>
13. Egorov V.V., Rakhman'ko E.M., Pomelenok E.V., *et al.* Effect of the steric accessibility of the exchange site in long-chain quaternary ammonium salts on the anion-exchange extraction of divalent ions. *Russ. J. Phys. Chem.* 2006;80(6):969–973. <https://doi.org/10.1134/S0036024406060239>
[Original Russian Text: Egorov V.V., Rakhman'ko E.M., Pomelenok E.V., Okaev E.B. Effect of the steric accessibility of the exchange site in long-chain quaternary ammonium salts on the anion-exchange extraction of divalent ions. *Zhurnal fizicheskoi khimii.* 2006;80(6):1104–1109 (in Russ.).]
14. Merenbloom S.I., Flick T.G., Daly M.P., *et al.* Effects of select anions from the Hofmeister series on the gas-phase conformations of protein ions measured with traveling-wave ion mobility spectrometry/mass spectrometry. *J. Am. Soc. Mass Spectrom.* 2011;22(11):1978–1990. <https://doi.org/10.1007/s13361-011-0238-1>
15. Xie W.J., Liu C.W., Yang L.J., *et al.* On the molecular mechanism of ion specific Hofmeister series. *Sci. China Chem.* 2014;57(1):36–47. <https://doi.org/10.1007/s11426-013-5019-1>
16. Tsyganov A.R., Rakhman'ko E.M., Starobinets G.L. Anion exchange extraction of acid dyes with triononyloctadecylammonium salts. *Izvestiya AN BSSR. Seriya khimicheskikh nauk = Proceedings of Academy of Sciences of BSSR. Chemical Series.* 1980;2:61–66 (in Russ.).
17. Egorov V.V., Rakhman'ko E.M., Okaev E.B., Pomelenok E.V., Nazarov V.A. Effects of ion association of lipophilic quaternary ammonium salts in ion-exchange and potentiometric selectivity. *Talanta.* 2004;63(1):119–130. <https://doi.org/10.1016/j.talanta.2003.11.019>
18. Tager A.A. *Fiziko-khimiya polimerov (Physico-Chemistry of Polymers)*. Moscow: Nauchnyi mir; 2007. 573 p. (in Russ.).
19. Anouti M., Caillon-Caravanier M., Le Floch C. Alkylammonium-Based Protic Ionic Liquids. II. Ionic Transport and Heat-Transfer Properties: Fragility and Ionicity Rule. *J. Phys. Chem. B.* 2008;112(31):9412–9416. <https://doi.org/10.1021/jp803489n>
9. Zhao Y.X., Gao B.Y., Shon H., *et al.* Coagulation characteristics of titanium (Ti) salt coagulant compared with aluminum (Al) and iron (Fe) salts. *J. Hazardous Mater.* 2011;185(2–3):1536–1542. <https://doi.org/10.1016/j.jhazmat.2010.10.084>
10. Нестеров Ю.В. *Иониты и ионообмен. Сорбционная технология при добыче урана и других металлов методом подземного выщелачивания*. М.: ОАО «Атомредметзолото»; 2007. 480 с.
11. Матвейчук Ю.В., Станишевский Д.В. Анионообменная экстракция двузарядных анионов растворами высших четвертичных аммониевых солей с различной стерической доступностью обменного центра. *Журн. аналит. химии.* 2020;75(6):496–501. <https://doi.org/10.31857/S0044450220040106>
12. Kuzmin V.I., Gudkova N.V., Kuzmin D.V., *et al.* Effect of solvation-dehydration of quaternary ammonium base salts in the organic phase on the selectivity of anion-exchange extraction. *Sep. Sci. Technol.* 2023;58(7):1283–1294. <https://doi.org/10.2139/ssrn.3967023>
13. Егоров В.В., Рахманько Е.М., Помеленок Е.В., Окаев Е.Б. Влияние стерической доступности обменного центра высших четвертичных аммониевых солей на анионообменную экстракцию двухзарядных ионов. *Журн. физ. химии.* 2006;80(6):1104–1109.
14. Merenbloom S.I., Flick T.G., Daly M.P., *et al.* Effects of select anions from the Hofmeister series on the gas-phase conformations of protein ions measured with traveling-wave ion mobility spectrometry/mass spectrometry. *J. Am. Soc. Mass Spectrom.* 2011;22(11):1978–1990. <https://doi.org/10.1007/s13361-011-0238-1>
15. Xie W.J., Liu C.W., Yang L.J., *et al.* On the molecular mechanism of ion specific Hofmeister series. *Sci. China Chem.* 2014;57(1):36–47. <https://doi.org/10.1007/s11426-013-5019-1>
16. Цыганов А.Р., Рахманько Е.М., Старобинец Г.Л. Анионообменная экстракция кислотных красителей солями тринионлоктадециламмония. *Вестн. АН БССР. Серия химич. наук.* 1980;2:61–66.
17. Egorov V.V., Rakhman'ko E.M., Okaev E.B., Pomelenok E.V., Nazarov V.A. Effects of ion association of lipophilic quaternary ammonium salts in ion-exchange and potentiometric selectivity. *Talanta.* 2004;63(1):119–130. <https://doi.org/10.1016/j.talanta.2003.11.019>
18. Тегер А.А. *Физико-химия полимеров*. М.: Научный мир; 2007. 573 с.
19. Anouti M., Caillon-Caravanier M., Le Floch C. Alkylammonium-Based Protic Ionic Liquids. II. Ionic Transport and Heat-Transfer Properties: Fragility and Ionicity Rule. *J. Phys. Chem. B.* 2008;112(31):9412–9416. <https://doi.org/10.1021/jp803489n>
20. Wilkes J.S. A short history of ionic liquids-from molten salts to neoteric solvents. *Green Chem.* 2002;4(2):73–80. <https://doi.org/10.1039/B110838G>
21. Pernak J., Legosz B., Walkiewicz F., Klejdysz T., Borkowsky A., Chrzanowski L. Ammonium ionic liquids with anion of natural origin. *RSC Adv.* 2015;5(80):65471–65480. <https://doi.org/10.1039/C5RA11710K>
22. Eneh C.L., Nixon K., Lalwani S.M., *et al.* Solid-Liquid-Solution Phases in Poly(diallyldimethylammonium) / Poly(acrylic acid) Polyelectrolyte Complexes at Varying Temperatures. *Macromolecules.* 2024;57(5):2363–2375. <https://doi.org/10.1021/acs.macromol.4c00258>
23. Есакова А.С., Лаптинская Т.В., Литманович Е.А. Диффузия полидiallyлдиметиламмония хлорида в водных растворах с добавленной солью. *Вестник Московского университета. Серия 3. Физика. Астрономия.* 2010;2:50–56.

20. Wilkes J.S. A short history of ionic liquids-from molten salts to neoteric solvents. *Green Chem.* 2002;4(2):73–80. <https://doi.org/10.1039/B110838G>
21. Pernak J., Legosz B., Walkiewicz F., Klejdysz T., Borkowsky A., Chrzanowski L. Ammonium ionic liquids with anion of natural origin. *RSC Adv.* 2015;5(80):65471–65480. <https://doi.org/10.1039/C5RA11710K>
22. Eneh C.L., Nixon K., Lalwani S.M., et al. Solid-Liquid-Solution Phases in Poly(diallyldimethylammonium) / Poly(acrylic acid) Polyelectrolyte Complexes at Varying Temperatures. *Macromolecules.* 2024;57(5):2363–2375. <https://doi.org/10.1021/acs.macromol.4c00258>
23. Esakova A.S., Laptinskaya T.V., Litmanovich E.A. Diffusion of polydiallyldimethylammonium chloride in aqueous solutions with added salt. *Moscow University Physics Bulletin.* 2010;65(2):119–125. <https://doi.org/10.3103/S0027134910020098>
[Original Russian Text: Esakova A.S., Laptinskaya T.V., Litmanovich E.A. Diffusion of polydiallyldimethylammonium chloride in aqueous solutions with added salt. *Vestnik Moskovskogo universiteta. Seriya 3. Fizika. Astronomiya.* 2010;2:50–56 (in Russ.).]
24. Litmanovich E.A., Orleneva A.P., Korolev B.A., Kasaikin V.A., Kulichikhin V.G. Dynamics of the polymer chain in aqueous and salt-containing aqueous solutions of poly(dimethyl diallylammonium chloride). *Polym. Sci. Ser. A.* 2000;42(6):689–693.
[Original Russian Text: Litmanovich E.A., Orleneva A.P., Korolev B.A., Kasaikin V.A., Kulichikhin V.G. Dynamics of the polymer chain in aqueous and salt-containing aqueous solutions of poly(dimethyl diallylammonium chloride). *Vysokomolekulyarnye soedineniya. Seriya A.* 2000;42(6):1035–1041 (in Russ.).]
25. Marcelo G., Tarazona M. P., Saiz E. Solution properties of poly(diallyldimethylammonium chloride) (PDDA). *Polymer.* 2005;46(8):2584–2594. <https://doi.org/10.1016/j.polymer.2005.01.078>
26. Litmanovich E.A., Kasaikin V.A., Zezin A.B., Kabanov V.A. Effect of the concentration of poly-(N,N'-diallyldimethylammonium chloride) in a solution on the self-organization in its mixtures with sodium dodecyl sulfate. *Doklady Physical Chemistry.* 2000;373(1–3):121–124.
[Original Russian Text: Litmanovich E.A., Kasaikin V.A., Zezin A.B., Kabanov V.A. Effect of the concentration of poly-(N,N'-diallyldimethylammonium chloride) in a solution on the self-organization in its mixtures with sodium dodecyl sulfate. *Doklady Akademii nauk.* 2000;373(3):350–354 (in Russ.).]
27. Jia X., Zhan X., Gong X., et al. Thermal decomposition mechanism of poly(dimethyldiallylammonium chloride). *Therm. Anal. Calorim.* 2022;147(7):4589–4596. <https://doi.org/10.1007/s10973-021-10860-w>
28. Krylov A.V., Tokareva A. A., Syromyatnikov P.A., Novichkova P.M., Zheglatiy P.V. Abnormal behavior of supramolecular systems based on quaternary ammonium salts and hydroxides in aqueous solutions. *AIP Conf. Proc.* 2022;2390(1):020040. <https://doi.org/10.1063/5.0070097>
24. Литманович Е.А., Орленева А.П., Королёв Б.А., Касаикин В.А., Куличихин В.Г. Динамика полимерной цепи в водных и водно-солевых растворах полидиметил-диаллил-аммоний хлорида. *Высокомолекулярные соединения. Серия А.* 2000;42(6):1035–1041.
25. Marcelo G., Tarazona M. P., Saiz E. Solution properties of poly(diallyldimethylammonium chloride) (PDDA). *Polymer.* 2005;46(8):2584–2594. <https://doi.org/10.1016/j.polymer.2005.01.078>
26. Литманович Е.А., Касаикин В.А., Зезин А.Б., Кабанов В.А. Влияние концентрационного режима раствора поли-(N,N')-диаллилдиметиламмоний хлорида на процессы самоорганизации в его смесях с додецилсульфатом натрия. *Доклады Академии наук.* 2000;373(3):350–354.
27. Jia X., Zhan X., Gong X., et al. Thermal decomposition mechanism of poly(dimethyldiallylammonium chloride). *Therm. Anal. Calorim.* 2022;147(7):4589–4596. <https://doi.org/10.1007/s10973-021-10860-w>
28. Krylov A.V., Tokareva A. A., Syromyatnikov P.A., Novichkova P.M., Zheglatiy P.V. Abnormal behavior of supramolecular systems based on quaternary ammonium salts and hydroxides in aqueous solutions. *AIP Conf. Proc.* 2022;2390(1):020040. <https://doi.org/10.1063/5.0070097>

About the Authors

Yaroslava N. Golubeva, Postgraduate Student, Ya.K. Syrkin Department of Physical Chemistry, M.V. Lomonosov Institute of Fine Chemical Technologies, MIREA – Russian Technological University (78, Vernadskogo pr., Moscow, 119454, Russia). E-mail: golubeva.ya.n@gmail.com. <https://orcid.org/0009-0008-2344-6933>

Alexander V. Krylov, Cand. Sci. (Chem.), Associate Professor, Ya.K. Syrkin Department of Physical Chemistry, M.V. Lomonosov Institute of Fine Chemical Technologies, MIREA – Russian Technological University (78, Vernadskogo pr., Moscow, 119454, Russia). E-mail: allylnmr@yandex.ru. Scopus Author ID 57484351900, RSCI SPIN-code 5633-1360, <https://orcid.org/0000-0002-2389-9026>

Tatyana A. Chebotareva, Master Student, M.V. Lomonosov Institute of Fine Chemical Technologies, MIREA – Russian Technological University (78, Vernadskogo pr., Moscow, 119454, Russia). E-mail: chiebotariova.t@mail.ru. <https://orcid.org/0009-0008-8412-7098>

Об авторах

Голубева Ярослава Николаевна, аспирант, кафедра физической химии им. Я.К. Сыркина, Институт тонких химических технологий им. М.В. Ломоносова, ФГБОУ ВО «МИРЭА – Российский технологический университет» (119454, Россия, Москва, пр-т Вернадского, д. 78). E-mail: golubeva.ya.n@gmail.com. <https://orcid.org/0009-0008-2344-6933>

Крылов Александр Владимирович, к.х.н., доцент, кафедра физической химии им. Я.К. Сыркина, Институт тонких химических технологий им. М.В. Ломоносова, ФГБОУ ВО «МИРЭА – Российский технологический университет» (119454, Россия, Москва, пр-т Вернадского, д. 78). E-mail: allylnmr@yandex.ru. Scopus Author ID 57484351900, SPIN-код РИНЦ 5633-1360, <https://orcid.org/0000-0002-2389-9026>

Чеботарева Татьяна Александровна, магистр, Институт тонких химических технологий им. М.В. Ломоносова, ФГБОУ ВО «МИРЭА – Российский технологический университет» (119454, Россия, Москва, пр-т Вернадского, д. 78). E-mail: chiebotariova.t@mail.ru. <https://orcid.org/0009-0008-8412-7098>

Translated from Russian into English by V. Glyanchenko

Edited for English language and spelling by Thomas A. Beavitt

Analytical methods in chemistry and chemical technology
Аналитические методы в химии и химической технологии

UDC 542.87; 541.49:546.657

<https://doi.org/10.32362/2410-6593-2025-20-4-372-381>

EDN QNZATD



RESEARCH ARTICLE

Rare-earth element complexes with complexones, heparin, and antibiotics in biosystems for use as electrode-active materials in membrane ion-selective electrodes

Timofey V. Kryukov✉, Mariana A. Feofanova, Viktor M. Nikol'skii, Alexandra I. Ivanova, Ivan A. Kaplunov

Tver State University, Tver, 170100 Russia

✉ Corresponding author; e-mail: p528491@yandex.ru

Abstract

Objectives. The creation of ion-selective electrodes (ISEs) based on rare-earth element (REE) complexes in environmentally friendly biosystems is of interest due to the increased relevance of environmental management. The work sets out to study the possibility of using REE complexes for creating ISEs sensitive to cefazolin. The created potentiometric sensors can be used for rapid determination of antibiotics in microvolume samples.

Methods. The work presents the synthesis of electrode-active REE complexes with cefazolin. In order to identify the obtained electrode-active substances and investigate their physicochemical characteristics, the following methods were used: elemental analysis with a scanning electron microscope, infrared spectroscopy, simultaneous thermal analysis, and potentiometry.

Results. Previously unstudied complexes of cerium and lutetium with cefazolin were obtained for use as an electrode-active substance for creating ISEs. The physicochemical characteristics of the complexes were investigated. For the created ISEs, the following characteristics were studied: performance characteristics, the dependence of electrode potentials on the analyte concentration, stability, and the response time of the electrode placed in the sample under study. The created membrane electrodes are stable, have a concentration range of operation of pC 1–3, and can be used in the pH range 4–8. Testing of the selectivity of the ISEs with respect to Na⁺ and K⁺ ions showed that the electrodes are effective even in a thousandfold excess. The performance of the electrodes was tested using model systems.

Conclusions. Novel REE–cefazolin complexes were successfully demonstrated for use as electrode-active substances for the manufacture of membrane ISEs sensitive to cephalosporin antibiotics.

Keywords

coordination compounds of rare-earth elements, complexones, heparin, cefazolin complexes, cephalosporins, ion-selective electrodes

Submitted: 26.11.2024

Revised: 07.03.2025

Accepted: 31.05.2025

For citation

Kryukov T.V., Feofanova M.A., Nikol'skii V.M., Ivanova A.I., Kaplunov I.A. Rare-earth element complexes with complexones, heparin, and antibiotics in biosystems for use as electrode-active materials in membrane ion-selective electrodes. *Tonk. Khim. Tekhnol. = Fine Chem. Technol.* 2025;20(4):372–381. <https://doi.org/10.32362/2410-6593-2025-20-4-372-381>

НАУЧНАЯ СТАТЬЯ

Комплексы редкоземельных элементов в биосистемах с комплексонами, гепарином, антибиотиками для применения в качестве электродактивного вещества мембранных ионселективных электродов

Т.В. Крюков✉, М.А. Феофанова, В.М. Никольский, А.И. Иванова, И.А. Каплунов

Тверской государственный университет, Тверь, 170100 Россия

✉ Автор для переписки, e-mail: p528491@yandex.ru

Аннотация

Цели. В настоящее время остро стоит вопрос сохранения благоприятной экологической обстановки на планете, поэтому интересны работы по созданию ионселективных электродов (ИСЭ) на базе комплексов редкоземельных элементов (РЗЭ) в экологически безопасных биосистемах. Цель работы — изучить возможности использования комплексов РЗЭ для создания ИСЭ с откликом на цефазолин. Создаваемые потенциометрические сенсоры позволяют проводить экспрессное определение антибиотиков в микроробъемных пробах.

Методы. В работе реализован синтез электродактивных комплексов РЗЭ с цефазолином. Для идентификации полученных электродактивных веществ и изучения их физико-химических характеристик использованы элементный анализ с помощью растрового электронного микроскопа, инфракрасная спектроскопия, синхронный термический анализ и потенциометрия.

Результаты. Получены ранее не исследованные комплексы церия и лютеция с цефазолином с целью их использования в качестве электродактивного вещества для создания ИСЭ. Изучены их физико-химические характеристики. Для созданных ИСЭ исследованы их эксплуатационные характеристики, зависимость электродных потенциалов от концентрации аналита, а также изучены стабильность созданных ИСЭ и время отклика сигнала электрода, помещенного в исследуемую пробу. Созданные мембранные электроды стабильны, имеют концентрационный диапазон эксплуатации рС 1–3 и могут быть использованы в диапазоне рН 4–8. Проверка селективности ИСЭ по отношению к ионам Na^+ и K^+ показала, что электроды эффективны даже при их тысячекратном присутствии. Работоспособность электродов проверена на модельных объектах.

Выводы. Показано, что впервые созданные комплексы РЗЭ с цефазолином могут успешно использоваться в качестве электродактивных веществ для изготовления мембранных ИСЭ на цефалоспориновые антибиотики.

Ключевые слова

координационные соединения редкоземельных элементов, комплексоны, гепарин, комплексы цефазолина, цефалоспорины, ионселективные электроды

Поступила: 26.11.2024

Доработана: 07.03.2025

Принята в печать: 31.05.2025

Для цитирования

Крюков Т.В., Феофанова М.А., Никольский В.М., Иванова А.И., Каплунов И.А. Комплексы редкоземельных элементов в биосистемах с комплексонами, гепарином, антибиотиками для применения в качестве электродактивного вещества мембранных ионселективных электродов. *Тонкие химические технологии*. 2025;20(4):372–381. <https://doi.org/10.32362/2410-6593-2025-20-4-372-381>

INTRODUCTION

The rapid development of the chemistry of complex compounds of rare-earth elements (REEs) has resulted in the accumulation of a large body of factual material on the physicochemical properties of the created complexes and their areas of application based on their unique properties. The individuality of individual representatives of REEs was first noted by Dmitri Mendeleev as “one of the true strengtheners of the Periodic Law” [1].

Today, environmental management is the focus of much attention. Therefore, studies on REE complexation processes in various biosystems are of particular interest, for example, when used in environmentally friendly complexones derivatives of succinic acid (CDSA). To minimize the negative impact of humans on the environment, not only are the methods of REE extraction and separation being improved, but also the various methods for their secondary utilization. The use of iminodisuccinic acid for the extraction of some REEs by adsorption was described [2]. In passing, attention should also be paid to the inverse problem involving the patented synthesis of iminodisuccinic acid using lanthanide catalysts [3].

Combined with the fact that these ligands in natural conditions are capable of rapid decomposition and do not accumulate in waste [4–7], the unique ability of CDSA to exhibit high complexing properties has found them a wide range of applications, including in “green chemistry” [8–11]. Of interest are the results of studying lanthanide complexes with biuret [12].

The introduction of REE ions into biosystems (for example, the human body) significantly increases the effectiveness of blood anticoagulants such as heparin. In investigating the complexation of heparin with REE, we conducted a thermochemical study of neodymium complexes with heparin. The dehydration of the Nd complex with heparin, which already begins at a temperature of 40°C, continues up to 190°C. Following dehydration at 190°C and up to 420°C, the glycosidic bond and carbon skeleton of heparin are decomposed. At a temperature of 400–450°C, some of the combustion products combine with neodymium to form $\text{Nd}_2(\text{SO}_4)_3$. During further decomposition (above 600°C), this is decomposed to neodymium oxysulfate $\text{Nd}_2\text{O}_2\text{SO}_4$ [13]. The lanthanide atoms are shown to be coordinated by heparin through carboxylate, hydroxyl, sulfonate, and aminosulfonate groups at a denticity of 4 [14].

The present paper presents the results of studying the processes of complexation of REEs with antibiotics, in particular, with cefazolin. It was previously shown that cefazolin in REE metal complexes is bidentate [15] due to the formation of coordination bonds through the amide and carboxylate groups.

Research into novel antibacterial agents is in demand due to their potential uses in the chemical and pharmaceutical industries. While antibiotics represent a widespread group of medicinal compounds, identifying their potential hazards to human health is one of the urgent problems of modern analytical chemistry. Diverse areas in which it is necessary to determine and control the content of antibiotics include pharmaceuticals, biological fluids of the human and animal body, food products, and wastewater from pharmaceutical enterprises [16].

Cephalosporin antibiotics are typically studied by spectroscopic, chromatographic, electrochemical, and other methods. The main methods used for determining cephalexin, cefuroxime, and cefixime in medicinal and biological media are chromatography [17, 18], spectroscopy [19], and voltammetry [20, 21]. However, such methods generally require expensive equipment, reagents, and qualified operators; moreover, they take a long time to complete and do not allow for rapid determination of antibiotic content in clinical and biochemical laboratories. Conversely, potentiometric sensors have shown the possibility of rapid determination of active substances even in microvolume samples [16, 22]. The rapid determination of antibiotics in biological fluids and dosage forms of drugs is necessary for studying physiological and biochemical processes occurring in the body, as well as for ensuring effective drug controls.

It has been established that molecules with antimicrobial activity are necessarily amphiphilic, i.e., also include hydrophobic regions [23]. The low water solubility of sufficiently hydrophobic REE complexes with cefazolin permits their use as an electrode-active substance in the manufacture of membrane ion-selective electrodes (ISEs) sensitive to cephalosporin antibiotics.

Thus, the present work is aimed at developing a new direction of research of the physicochemical characteristics of REE complexes with cefazolin to establish the possibility of creating ISEs sensitive to cefazolin.

EXPERIMENTAL

The potentiometric characteristics of the REE complexes with cefazolin were determined and the pH of the medium was monitored using an I-160MP ion meter (*Izmeritel'naya Tekhnika*, Moscow, Russia). The electrode response time was measured with a stopwatch. To record IR spectra, samples were prepared in the form of tablets with KBr (reagent grade, *Baza No. 1 Khimreaktivov*, Russia). The spectra of the samples containing 2 mg of the test substance per 200 mg of KBr were recorded with an Alpha Fourier transform infrared spectrometer (*Bruker*, Germany) in the range of 4000–400 cm^{-1} . Simultaneous

thermal analysis of the samples was performed with an STA 449 F3 Jupiter simultaneous thermal analyzer (*Netzsch Group*, Germany) in an air atmosphere. Elemental chemical analysis of the samples was carried out with a JEOL JSM-6610LV scanning electron microscope equipped with an Oxford INCA energy dispersive spectrometer (*Oxford Instruments*, United Kingdom).

An ISE sensitive to cefazolin was created using cefazolin sodium salt (NaCzl, *Deko*, Moscow, Russia). The exact concentrations of REE chlorides solutions prepared from reagents of chemical purity grade (*Khimkraft*, Russia) were established by complexometric titration [24].

Electrode-active substances were obtained by mixing aqueous solutions of cerium or lutetium chloride and sodium cefazolin in a molar ratio of 1 : 4. Next, the resultant substances were separated by centrifugation and dried at room temperature (20°C) in a desiccator over a layer of silica gel. The thus obtained samples were stored in a desiccator over a layer of silica gel in a closed cabinet to avoid exposure to light. The stock solution of cefazolin having a concentration of 0.1 M was prepared by dissolving a weighed sample to form a basis for additional solutions obtained by dilution. Membranes were prepared using S-70 polyvinyl chloride (PVC, *SAYANKHIMPLAST*, Russia), dioctyl phthalate (DOP, *Khimprom-M*, Russia), and cyclohexanone (*Baza No. 1 Khimreaktivov*, Russia). The created ion-selective membranes contained 1 wt % electroactive substance, 1 wt % DOP, and 98 wt % PVC.

Before the experiment, the ISEs were soaked for 1 h in a 0.01 M cefazolin solution. The electrode potentials were recorded in the following electrochemical cell:

Ag	AgCl	Cefazolin solution (0.01 M) + + KCl solution (0.1 M)	Ion-selective membrane	Test solution	Saturated KCl solution	AgCl	Ag
----	------	---	------------------------	---------------	------------------------	------	----

Table. Results of elemental analysis

Sample	Molecular formula	Elemental composition	C, %	N, %	O, %	S, %	Me, %
CeCzl ₃	C ₄₂ H ₄₂ CeN ₂₄ O ₁₂ S ₉	Calculated	33.51	22.34	12.76	19.15	9.30
		Found	34.94	22.34	13.05	19.72	9.36
LuCzl ₃	C ₄₂ H ₄₂ LuN ₂₄ O ₁₂ S ₉	Calculated	31.68	21.11	15.07	18.12	10.99
		Found	31.66	21.07	15.05	18.09	10.95

RESULTS AND DISCUSSION

Table presents the calculated and experimentally determined elemental compositions of the metal complex. On the basis of the obtained data, the inner sphere of the metal complex can be unambiguously determined, with the exception of hydrogen atoms, which cannot be detected by X-ray electron microprobe analysis.

According to the obtained data, the samples do not contain sodium and chlorine. The composition of the inner sphere of the metal complex was established to correspond to the molar ratio [metal] : [ligand] = 1 : 3.

The similarity of the obtained spectra when comparing the IR spectra of pure sodium salt and synthesized compounds (Fig. 1) confirms that the interaction of cefazolin sodium salt with REE cations does not cause changes in the chemical structure of cefazolin.

Interpretation of the IR spectrum of cefazolin sodium salt showed that the broad band at 3430 cm⁻¹ corresponds to vibrations of the hydroxyl group, which participates in the formation of hydrogen bonds with coordinated water molecules [25, 26].

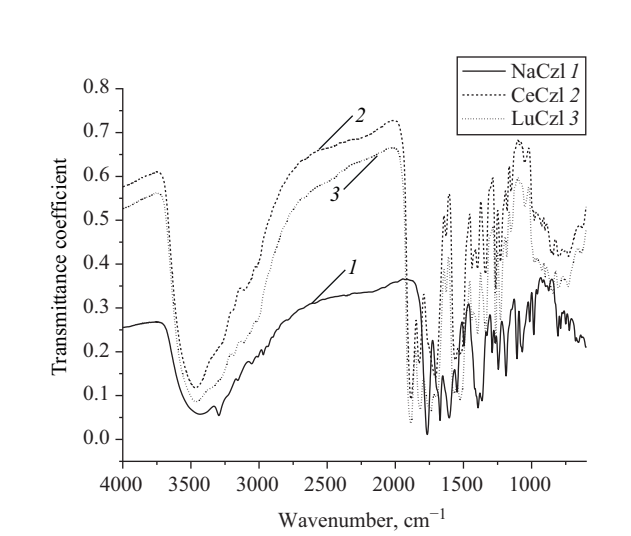


Fig. 1. IR spectra of (1) cefazolin, (2) cerium metal complex, and (3) lutetium metal complex

According to the published research data [26, 27], the carboxyl group is characterized by a wavenumber of 1761 cm^{-1} , while the band at 1680 cm^{-1} corresponds to the amide group C=O . These wavenumbers of the characteristic absorption bands of the carboxyl and amide groups of cefazolin agree with the data given in an earlier work [19]; here, the shift of the band at 1545 cm^{-1} for symmetric stretching vibrations of the carboxyl group is noted to imply coordination through this group. We consequently assigned the band at 1490 cm^{-1} to vibrations of C=C of the aromatic structure. The bands at 1241 , 1183 , 1100 , and 1062 cm^{-1} characterize vibrations of the CN group.

The presented spectra of our samples show a shift of the hydroxyl group band (3439 cm^{-1}), a shift of the amide C=O vibration band (1681 cm^{-1}), and a shift of the symmetrical stretching vibration band of the carboxyl group (1566 cm^{-1}).

Since no significant shifts of the CN vibration bands were found, it can be concluded that nitrogen atoms do not participate in the coordination.

The coincidence of the $\nu(\text{C-S-C})$ stretching vibration bands in both the sodium salt (669 cm^{-1}) and the metal complexes (670 cm^{-1}) of the thiazole ring indicates that the sulfur atom does not participate in the complexation process. A similar picture was also observed in the spectrum of the lutetium metal complex.

Taking into account the shifts of the absorption bands of the amide and carboxylate groups, we conclude that

cefazolin is coordinated bidentately through the amide and carboxylate groups.

Figure 2 presents the results of thermal analysis of CeCzl (thermogravimetry (TG) and differential scanning calorimetry (DSC) curves). The mass loss in the temperature range from 39 to 120°C is due to the evaporation of the adsorption and crystallization water: the mass change in this range was 1.48% , while the mass change in the range from 100 to 120°C was 0.31% . The peak at 222.7°C corresponds to the destruction of the metal complex structure and oxidation of the ligand [15].

The evaluation of ISE stability confirmed that potential drift remains approximately constant, amounting to $2\text{--}5\text{ mV/day}$. According to the stopwatch, the response time is about 45 s for $10^{-1}\text{--}10^{-3}\text{ M}$ solutions. Figure 3 depicts the dependence graphs of the ISE potentials on the cefazolin concentration both for membranes with the cerium metal complex and those used with the lutetium metal complex.

In the range of negative decimal logarithms of concentrations of pC $1\text{--}3$, the experimental points are described by a straight-line equation. The linear portion of the electrode function indicates the possibility of practical use of the ISE for determining cefazolin. We also took into account that the operation of the electrode can be affected by both the pH of the medium and the presence of accompanying cations. The selectivity coefficients for Na^+ and K^+ ($1.5 \cdot 10^{-3}$ and $1.4 \cdot 10^{-3}$, respectively) were

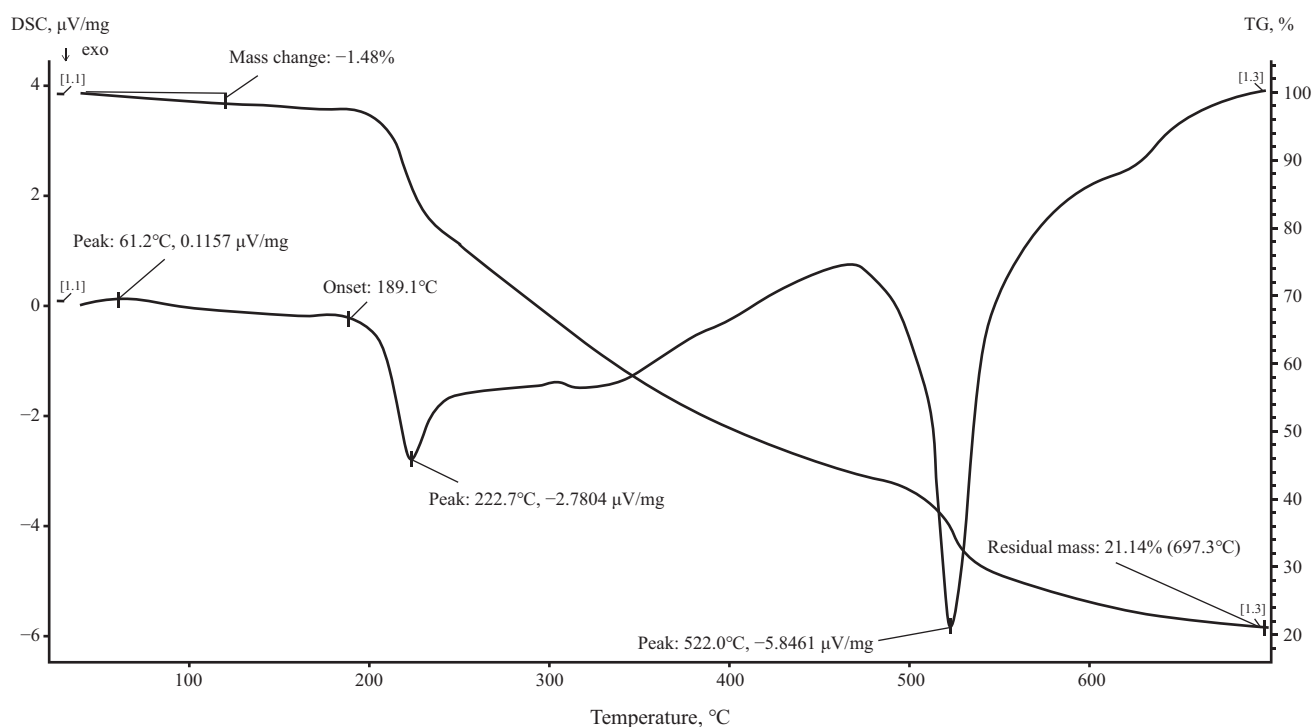


Fig. 2. TG/DSC curves of CeCzl sample

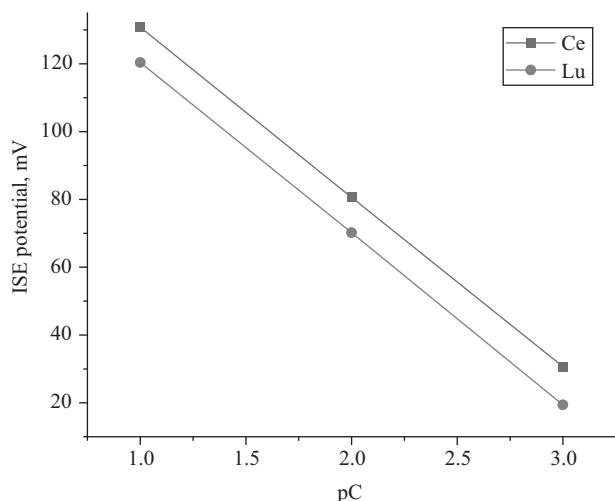


Fig. 3. Dependence of the ISE potentials of (1) the metal complex of cerium and (2) the metal complex of lutetium on the cefazolin concentration

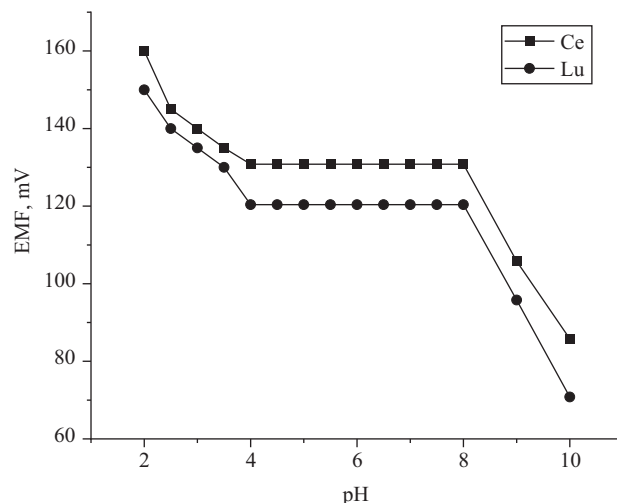


Fig. 4. Dependence of the electromotive force (EMF) of the cell with ISE on the pH of the cefazolin solution

determined by the mixed solution method. The electrode potential is shown to be independent of the acidity of the medium in the pH range of 4–8 at a cefazolin concentration of 0.1 M.

Figure 4 illustrates the dependence of the electromotive force (emf) of the created ISEs on the pH of the cefazolin solution. As can be seen from the figure, the ISE potential is independent of the pH of the solutions in the range of 4–8.

This indicates that the created ISEs have a fairly high stability. However, at $\text{pH} \leq 4$ and $\text{pH} \geq 8$, jumps in the electrode potential are observed, indicating a nonlinear change in the concentration of the antibiotic in an alkaline and acidic medium, which is typical for most ISEs [28].

CONCLUSIONS

The conducted studies confirm that ISEs in which the electrode-active substances are REE complexes with cefazolin are promising for use in determining antibiotics

in microvolume samples. The created membrane electrodes demonstrate stability, have a concentration range of operation of pC 1–3, and can be used in the pH range of 4–8. Testing of the selectivity of the ISEs with respect to Na^+ and K^+ ions demonstrated that the electrodes are effective even when used in thousandfold excess. The performance of the electrodes was tested on model objects.

Acknowledgments

The research was carried out using the resources of the Center for Collective Use of the Tver State University.

Authors' contributions

T.V. Kryukov—experiments, collecting and processing the research materials.

M.A. Feofanova—idea, general guidance.

V.M. Nikol'skii—research concept, scientific editing.

A.I. Ivanova—performing experiments, selecting the optimal conditions for experiments.

I.A. Kaplunov—scientific consulting at all stages of work.

The authors declare no conflict of interest.

REFERENCES

1. Mendeleev D.I. *Osnovy khimii (Fundamentals of Chemistry)*. V. 2. Moscow: Gosizdat; 1928. 771 p. (in Russ.).
2. Burdzy K., Ju Y., Kołodyńska D. Iminodisuccinic acid (IDHA) as an effective biodegradable complexing agent in the adsorption process of La(III), Nd(III) and Ho(III) ions. *Chem. Eng. J.* 2023;461:142059. <https://doi.org/10.1016/j.cej.2023.142059>
3. Aksela R., Rissanen J. *Method for Producing of Chelating Agents*: RF Pat. 2551285. Publ. 20.07.2015 (in Russ.).

СПИСОК ЛИТЕРАТУРЫ

1. Менделеев Д.И. *Основы химии*. Т. 2. М.: Госиздат; 1928. 771 с.
2. Burdzy K., Ju Y., Kołodyńska D. Iminodisuccinic acid (IDHA) as an effective biodegradable complexing agent in the adsorption process of La(III), Nd(III) and Ho(III) ions. *Chem. Eng. J.* 2023;461:142059. <https://doi.org/10.1016/j.cej.2023.142059>
3. Аксела Р., Риссанен Ю. *Способ получения смеси хелатирующих агентов*: пат. 2551285 РФ. Заявка № 2012154341/04; заявл. 20.07.2014; опубл. 20.07.2015. Бюл. № 14.

4. Cokesa Z., Knackmuss H.J., Rieger P.G. Biodegradation of all stereoisomers of the EDTA substitute iminodisuccinate by *Agrobacterium tumefaciens* BY6 requires an epimerase and a stereoselective C-N lyase. *Appl. Environ. Microbiol.* 2004;70(7):3941–3947. <https://doi.org/10.1128/AEM.70.7.3941-3947.2004>
5. Hyvönen H., Aksela R. Complexation of some environmentally friendly carboxylic acid ligands with La^{3+} ion in aqueous solution. *J. Coord. Chemistry.* 2012;65(19):3352–3362. <https://doi.org/10.1080/00958972.2012.708741>
6. Hyvönen H., Aksela R. Complexation of some environmentally friendly carboxylic acid ligands with La^{3+} ion in aqueous solution. *J. Coord. Chemistry.* 2012;65(19):3352–3362. <https://doi.org/10.1080/00958972.2012.708741>
7. Smirnova T. I., Khizhnyak S.D., Nikol'skii V.M., et al. Degradation of complexons derived from succinic acid under UV radiation. *Rus. J. Appl. Chem.* 2017;90(4):507–511. <https://doi.org/10.1134/S1070427217040024> [Original Russian Text: Smirnova T.I., Khizhnyak S.D., Nikol'skii V.M., Khalyapina Ya.M., Pakhomov P.M. Degradation of complexons derived from succinic acid under UV radiation. *Zhurnal Prikladnoi Khimii.* 2017;90(4):406–411 (in Russ.).]
8. Lucena J.J., Sentís J.A., Villén M., Lao T., Pérez-Sáez M. IDHA chelates as a micronutrient source for green bean and tomato in fertigation and hydroponics. *Agron. J.* 2008;100(3):813–818. <https://doi.org/10.2134/agronj2007.0257>
9. Aksela R., Peltonen J., Vekman A. *Coated Seeds and Method of Seeds Coatings*: RF Pat. 2345975. Publ. 10.02.2009 (in Russ.).
10. Zelinger A.S., Tolkacheva L.N., Kryukov T.V., Gridchin S.N., Nikol'skii V.M., Smirnova T.I. *Method of Pre-Sowing Seed Treatment to Stimulate Formation of Green Pigments*: RF Pat. 2813322. Publ. 12.02.2024 (in Russ.).
11. Salamatina E.V., Tolkacheva L.N., Nikol'skii V.M., Kryukov T.V., Gridchin S.N., Smirnova T.I. *Method of Increasing Biomass of Cultivated Green Plants by Pre-Sowing Treatment of Seed and Treatment of Seedlings*: RF Pat. 2816872. Publ. 08.04.2024 (in Russ.).
12. Kornilov A.D., Grigoriev M.S., Savinkina E.V. Comparison of the rare earth complexes iodides and polyiodides with biuret. *Fine Chem. Technol.* 2022;17(2):172–181. <https://doi.org/10.32362/2410-6593-2022-17-2-172-181>
13. Skobin M.I., Feofanova M.A., Nikolskiy V.M., Kryukov T.V., Alekseev V.G., Ivanova A.I. Physical and chemical properties, composition and thermal stability of a complex of neodium(III) with heparin. *Russ. J. Phys. Chem. B.* 2022;16(2):329–333. <https://doi.org/10.1134/S1990793122020245> [Original Russian Text: Skobin M.I., Feofanova M.A., Nikolskiy V.M., Kryukov T.V., Alekseev V.G., Ivanova A.I. Physical and chemical properties, composition and thermal stability of a complex of neodium(III) with heparin. *Khimicheskaya Fizika.* 2022;41(4):38–34 (in Russ.). <https://doi.org/10.31857/S0207401X22040100>]
14. Skobin M.I., Feofanova M.A., Kryukov T.V. Theoretical and experimental study of macromolecular nanostructures based on heparin and lanthanoids. *Fiziko-khimicheskie aspekty izucheniya klasterov, nanostruktur i nanomaterialov = Physical and Chemical Aspects of the Study of Clusters, Nanostructures and Nanomaterials.* 2021;13:513–521 (in Russ.). <https://doi.org/10.26456/pcascnn/2021.13.513>
15. Kryukov T.V., Feofanova M.A., Nikolskiy V.M., et al. Synthesis and study of a metal complex of neodium and cefazolin. *Russ. J. Phys. Chem. A.* 2022;96(6):1254–1257. <https://doi.org/10.1134/S0036024422060127>
4. Cokesa Z., Knackmuss H.J., Rieger P.G. Biodegradation of all stereoisomers of the EDTA substitute iminodisuccinate by *Agrobacterium tumefaciens* BY6 requires an epimerase and a stereoselective C-N lyase. *Appl. Environ. Microbiol.* 2004;70(7):3941–3947. <https://doi.org/10.1128/AEM.70.7.3941-3947.2004>
5. Hyvönen H., Aksela R. Complexation of some environmentally friendly carboxylic acid ligands with La^{3+} ion in aqueous solution. *J. Coord. Chemistry.* 2012;65(19):3352–3362. <https://doi.org/10.1080/00958972.2012.708741>
6. Hyvönen H., Aksela R. Complexation of some environmentally friendly carboxylic acid ligands with La^{3+} ion in aqueous solution. *J. Coord. Chemistry.* 2012;65(19):3352–3362. <https://doi.org/10.1080/00958972.2012.708741>
7. Смирнова Т.И., Хижняк С.Д., Никольский В.М., Халыпина Я.М., Пахомов П.М. Деградация комплексонов, производных янтарной кислоты, под действием УФ излучения. *Журн. прикладной химии.* 2017;90(4):406–411.
8. Lucena J.J., Sentís J.A., Villén M., Lao T., Pérez-Sáez M. IDHA chelates as a micronutrient source for green bean and tomato in fertigation and hydroponics. *Agron. J.* 2008;100(3):813–818. <https://doi.org/10.2134/agronj2007.0257>
9. Аксела Р., Пелтонен Я., Векман А. *Покрытые семена и способ нанесения покрытий на семена*: пат. 2345975 РФ. Заявка № 2006101152/13; заявл. 03.06.2004; опубл. 10.02.2009. Бюл. № 4.
10. Зелингер А.С., Толкачева Л.Н., Крюков Т.В., Гридчин С.Н., Никольский В.М., Смирнова Т.И. *Способ предпосевной обработки семян для стимулирования образования зеленых пигментов*: пат. 2813322 РФ. Заявка № 2023120906; заявл. 09.08.2023; опубл. 12.02.2024. Бюл. № 5.
11. Саламатина Е.В., Толкачева Л.Н., Никольский В.М., Крюков Т.В., Гридчин С.Н., Смирнова Т.И. *Способ увеличения биомассы культивируемых зеленых растений с помощью предпосевной обработки семян и обработки всходов*: пат. 2816872 РФ. Заявка № 2023121096; заявл. 11.08.2023; опубл. 08.04.2024. Бюл. № 10.
12. Корнилов А.Д., Григорьев М.С., Савинкина Е.В. Сравнение иодидов и полииодидов комплексов редкоземельных элементов с биуретом. *Тонкие химические технологии.* 2022;17(2):172–181. <https://doi.org/10.32362/2410-6593-2022-17-2-172-181>
13. Скобин М.И., Феофанова М.А., Никольский В.М., Крюков Т.В., Алексеев В.Г., Иванова А.И. Физико-химические характеристики, состав и термическая устойчивость комплекса неодима(III) с гепарином. *Хим. физика.* 2022;41(4):38–34. <https://doi.org/10.31857/S0207401X22040100>
14. Скобин М.И., Феофанова М.А., Крюков Т.В. Теоретическое и экспериментальное исследование макромолекулярных наноструктур на основе гепарина и лантаноидов. *Физико-химические аспекты изучения кластеров, наноструктур и наноматериалов.* 2021;13:513–521. <https://doi.org/10.26456/pcascnn/2021.13.513>
15. Крюков Т.В., Феофанова М.А., Никольский В.М., Алексеев В.Г., Скобин М.И., Иванова А.И. Синтез и исследование металлокомплекса неодима и цефазолина. *Журн. физ. химии.* 2022;96(6):871–874. <https://doi.org/10.31857/S0044453722060139>
16. Кулапина Е.Г., Снесарев С.В. Потенциометрические сенсоры на основе органических ионообменников тетраалкиламмония и комплексов серебра(I) с ампициллином, оксациллином, цефазолином. *Журн. аналит. химии.* 2012;67(2):198–202.

- [Original Russian Text: Kryukov T.V., Feofanova M.A., Nikolskiy V.M., Alekseev V.G., Skobin M.I., Ivanova A.I. Synthesis and study of a metal complex of neodium and cefazolin. *Zhurnal fizicheskoi khimii*. 2022;96(6):871–874 (in Russ.). <https://doi.org/10.31857/S0044453722060139>]
16. Kulapina E.G., Snesarev S.V. Potentiometric sensors based on organic ion exchangers of tetraalkylammonium and silver complexes with ampicillin, oxacillin and cefazolin. *J. Analyt. Chem.* 2012;67(2):163–167. <https://doi.org/10.1134/S1061934811120069>
[Original Russian Text: Kulapina E.G., Snesarev S.V. Potentiometric sensors based on organic ion exchangers of tetraalkylammonium and silver complexes with ampicillin, oxacillin and cefazolin. *Zhurnal analiticheskoi khimii*. 2012;67(2):198–202 (in Russ.).]
 17. Partani P., Gurule S., Khuroo A., Monif T., Bhardwaj S. Liquid chromatography/electrospray tandem mass spectrometry method for the determination of cefuroxime in human plasma: Application to a pharmacokinetic study. *J. Chromatography B: Analytical Technologies in the Biomedical and Life Sciences*. 2010;78(3–4):428–434. <https://doi.org/10.1016/j.jchromb.2009.12.025>
 18. Du Y., Zhai Y., Zhang J., Wu C., Luo C., Sun J., He Z. Development and evaluation of taste-masked dry suspension of cefuroxime axetil for enhancement of oral bioavailability. *Asian J. Pharm. Sci.* 2013;8(5):287–294. <https://doi.org/10.1016/j.ajps.2013.10.001>
 19. Маякова М.Н., Алексеев В.Г., Иванова А.И., Рясенский С.С. Твердые комплексы цинка(II) с цефазолином и цефотаксимом. *Вестник Тверского ГУ. Серия: Химия*. 2015; 3:5–13.
 20. Jain R., Gupta V.K., Jadon N., Radhapyari K. Voltammetric determination of cefixime in pharmaceuticals and biological fluids. *Anal. Biochem.* 2010;407(1):79–88. <https://doi.org/10.1016/j.ab.2010.07.027>
 21. Ojani R., Raoof J.B., Zamani S. A novel voltammetric sensor for amoxicillin based on nickel–curcumin complex modified carbon paste electrode. *Bioelectrochemistry*. 2012;85:44–49. <https://doi.org/10.1016/j.bioelechem.2011.11.010>
 22. Кулагина О.И., Макарова Н.М., Кулагина Е.Г. Потенциометрические сенсоры для определения некоторых цефалоспориновых антибиотиков в биологических и лекарственных средах. *Журн. аналит. химии*. 2015;70(4):399–406. <https://doi.org/10.7868/S004445021504009X>
 23. Короткин М.Д., Филатова С.М., Дениева З.Г., Буданова У.А., Себякин Ю.Л. Синтез производных аминокислот на основе диэтанолamina с симметричными и асимметричными радикалами в гидрофобном домене с потенциальной антимикробной активностью. *Тонкие химические технологии*. 2022;17(1):50–64. <https://doi.org/10.32362/2410-6593-2022-17-1-50-64>
 24. Пришибил Р. *Аналитические применения этилендиамин-тетрауксусной кислоты и родственных соединений*: пер. с англ. М.: Мир; 1975. 534 с.
 25. Сахарова Ю.Г., Борисова Г.М. Термическая устойчивость тиокарбамидных соединений неодима, самария, европия и гадолиния. *Журн. неорг. химии*. 1976;21(1):76–83.
 26. Pedroso T.M., Salgado H.R.N. Methods for Qualitative Analysis of Cefazolin Sodium Raw Material and Pharmaceutical Product. *Phys. Chem.* 2013;3(2):29–38. <https://doi.org/10.5923/j.pc.20130302.01>
 27. Masoud M.S., Ali A.E., Sharaf R.Y. Physicochemical Studies of Some Biologically Active Metal Complexes of Cefazolin Antibiotics. *J. Chem. Pharm. Res.* 2020;12(9):42–52.
 28. Копытин А.В., Турышев Е.С., Мадраимов М.Ш., Кубасов А.С., Жижин К.Ю., Шпигун Л.К., Кузнецов Н.Т. Ионоселективный мембранный электрод для определения октагидротриборат-аниона. *Журн. неорг. химии*. 2023;68(1):10–16. <https://doi.org/10.31857/S0044457X22601432>
 29. Partani P., Gurule S., Khuroo A., Monif T., Bhardwaj S. Liquid chromatography/electrospray tandem mass spectrometry method for the determination of cefuroxime in human plasma: Application to a pharmacokinetic study. *J. Chromatography B: Analytical Technologies in the Biomedical and Life Sciences*. 2010;78(3–4):428–434. <https://doi.org/10.1016/j.jchromb.2009.12.025>
 30. Du Y., Zhai Y., Zhang J., Wu C., Luo C., Sun J., He Z. Development and evaluation of taste-masked dry suspension of cefuroxime axetil for enhancement of oral bioavailability. *Asian J. Pharm. Sci.* 2013;8(5):287–294. <https://doi.org/10.1016/j.ajps.2013.10.001>
 31. Mayakova M.N., Alekseev V.G., Ivanova A.I., Ryasenskii S.S. Solid state complexes of zinc(II) with cefazolin and cefotaxime. *Vestnik Tverskogo gosudarstvennogo universiteta. Seriya: Khimiya = Herald of Tver State University. Series: Chemistry*. 2015;3:5–13 (in Russ.).
 32. Jain R., Gupta V.K., Jadon N., Radhapyari K. Voltammetric determination of cefixime in pharmaceuticals and biological fluids. *Anal. Biochem.* 2010;407(1):79–88. <https://doi.org/10.1016/j.ab.2010.07.027>
 33. Ojani R., Raoof J.B., Zamani S. A novel voltammetric sensor for amoxicillin based on nickel–curcumin complex modified carbon paste electrode. *Bioelectrochemistry*. 2012;85:44–49. <https://doi.org/10.1016/j.bioelechem.2011.11.010>
 34. Kulapina O.I., Makarova N.M., Kulapina E.G. Potentiometric sensors for the determination of some cephalosporin antibiotics in biological fluids and medicinal preparations. *Russ. J. Anal. Chem.* 2015;70(4):477–484. <https://doi.org/10.1134/S1061934815040073>
[Original Russian Text: Kulapina O.I., Makarova N.M., Kulapina E.G. Potentiometric sensors for the determination of some cephalosporin antibiotics in biological fluids and medicinal preparations. *Zhurnal analiticheskoi khimii*. 2015;70(4):399–406 (in Russ.). <https://doi.org/10.7868/S004445021504009X>]
 35. Korotkin M.D., Filatova S.M., Denieva Z.G., Budanova U.A., Sebyakin Y.L. Synthesis of diethanolamine-based amino acid derivatives with symmetric and asymmetric radicals in their hydrophobic domain and potential antimicrobial activity. *Fine Chem. Technol.* 2022;17(1):50–64. <https://doi.org/10.32362/2410-6593-2022-17-1-50-64>
 36. Pribil R. *Analiticheskie primeneniya etilendiamintetraukusnoi kisloty i rodstvennykh soedinenii (Analytical Applications of EDA and Related Compounds)*: transl. from Engl. Moscow: Mir; 1975. 534 p. (in Russ.).
[Pribil R. *Analytical Applications of EDA and Related Compounds*. Oxford: Pergamon Press; 1972. 400 p.]

25. Sakharova Yu.G., Borisova G.M. Thermal stability of neodymium, samarium, europium and gadolinium thiocarbamide compounds. *Zhurnal neorganicheskoi khimii*. 1976;21(1):76–83 (in Russ.).
26. Pedroso T.M., Salgado H.R.N. Methods for Qualitative Analysis of Cefazolin Sodium Raw Material and Pharmaceutical Product. *Phys. Chem.* 2013;3(2):29–38. <https://doi.org/10.5923/j.pc.20130302.01>
27. Masoud M.S., Ali A.E., Sharaf R.Y. Physicochemical Studies of Some Biologically Active Metal Complexes of Cefazolin Antibiotics. *J. Chem. Pharm. Res.* 2020;12(9):42–52.
28. Kopytin A.V., Turyshchev E.S., Madraimov M.Sh., *et al.* Ion-Selective Membrane Electrode for Determination of the Octahydrotriborate Anion. *Russ. J. Inorg. Chem.* 2023;68(1): 6–12. <https://doi.org/10.1134/S0036023622700103>
[Original Russian Text: Kopytin A.V., Turyshchev E.S., Madraimov M.Sh., Kubasov A.S., Zhizhin K.Yu., Shpigun L.K., Kuznetsov N.T. Ion-Selective Membrane Electrode for Determination of the Octahydrotriborate Anion. *Zhurnal neorganicheskoi khimii*. 2023;68(1):10–16 (in Russ.). <https://doi.org/10.31857/S0044457X22601432>]

About the Authors

Timofey V. Kryukov, Leading Engineer, Department of Inorganic and Analytical Chemistry, Tver State University (33, Zhelyabova ul., Tver, 170100, Russia). E-mail: p528491@yandex.ru. Scopus Author ID 57195754947, ResearcherID LQJ-1144-2024, RSCI SPIN-code 4983-3169, <https://orcid.org/0009-0000-4800-7154>

Mariana A. Feofanova, Cand. Sci. (Chem.), Associate Professor, Dean of the Faculty of Chemistry and Technology, Tver State University (33, Zhelyabova ul., Tver, 170100, Russia). E-mail: Feofanova.MA@tversu.ru. Scopus Author ID 14059766600, RSCI SPIN-code 6178-6092, <https://orcid.org/0009-0006-7325-1232>

Viktor M. Nikol'skii, Dr. Sci. (Chem.), Professor, Department of Inorganic and Analytical Chemistry, Tver State University (33, Zhelyabova ul., Tver, 170100, Russia). E-mail: Nikolskiy.VM@tversu.ru. Scopus Author ID 7006483319, ResearcherID B-5217-2014, RSCI SPIN-code 2442-4135, <https://orcid.org/0000-0003-0361-2945>

Alexandra I. Ivanova, Cand. Sci. (Phys.-Math.), Associate Professor, Department of Applied Physics, Faculty of Physics and Technology, Tver State University (33, Zhelyabova ul., Tver, 170100, Russia). E-mail: Ivanova.AI@tversu.ru. Scopus Author ID 36720663600, ResearcherID X-1725-2018, RSCI SPIN-code 4814-6952, <https://orcid.org/0000-0002-5517-2294>

Ivan A. Kaplunov, Dr. Sci. (Eng.), Head of the Department of Applied Physics, Faculty of Physics and Technology, Tver State University (33, Zhelyabova ul., Tver, 170100, Russia). E-mail: Kaplunov.ia@tversu.ru. Scopus Author ID 6602690601, ResearcherID AAH-3551-2019, RSCI SPIN-code 2542-1343, <https://orcid.org/0000-0002-1726-3451>

Об авторах

Крюков Тимофей Владимирович, ведущий инженер, кафедра неорганической и аналитической химии, ФГБОУ ВО «Тверской государственный университет» (170100, Россия, Тверь, ул. Желябова, д. 33). E-mail: p528491@yandex.ru. Scopus Author ID 57195754947, ResearcherID LQJ-1144-2024, SPIN-код РИНЦ 4983-3169, <https://orcid.org/0009-0000-4800-7154>

Феофанова Мариана Александровна, к.х.н., доцент, декан химико-технологического факультета, ФГБОУ ВО «Тверской государственный университет» (170100, Россия, Тверь, ул. Желябова, д. 33). E-mail: Feofanova.MA@tversu.ru. Scopus Author ID 14059766600, SPIN-код РИНЦ 6178-6092, <https://orcid.org/0009-0006-7325-1232>

Никольский Виктор Михайлович, д.х.н., профессор кафедры неорганической и аналитической химии, ФГБОУ ВО «Тверской государственный университет» (170100, Россия, Тверь, ул. Желябова, д. 33). E-mail: Nikolskiy.VM@tversu.ru. Scopus Author ID 7006483319, ResearcherID B-5217-2014, SPIN-код РИНЦ 2442-4135, <https://orcid.org/0000-0003-0361-2945>

Иванова Александра Ивановна, к.ф.-м.н., доцент кафедры прикладной физики физико-технического факультета, ФГБОУ ВО «Тверской государственный университет» (170100, Россия, Тверь, ул. Желябова, д. 33). E-mail: Ivanova.AI@tversu.ru. Scopus Author ID 36720663600, ResearcherID X-1725-2018, SPIN-код РИНЦ 4814-6952, <https://orcid.org/0000-0002-5517-2294>

Каплунов Иван Александрович, д.т.н., заведующий кафедрой прикладной физики физико-технического факультета, ФГБОУ ВО «Тверской государственный университет» (170100, Россия, Тверь, ул. Желябова, д. 33). E-mail: Kaplunov.ia@tversu.ru. Scopus Author ID 6602690601, ResearcherID AАН-3551-2019, SPIN-код РИНЦ 2542-1343, <https://orcid.org/0000-0002-1726-3451>

Translated from Russian into English by V. Glyanchenko

Edited for English language and spelling by Thomas A. Beavitt

Analytical methods in chemistry and chemical technology
Аналитические методы в химии и химической технологии

UDC 543.544.3; 615.03

<https://doi.org/10.32362/2410-6593-2025-20-4-382-398>

EDN GJESKG




RESEARCH ARTICLE

Semiquantitative determination of meldonium and emoxypine in human urine by HPLC–MS/MS after receiving a single therapeutic dose of Brainmax[®] and milk from cows receiving a preventive course of Emidonol[®]

Pavel V. Postnikov¹, Alexander D. Askretkov¹, Andrey V. Polosin¹, Yuliya A. Efimova², Elena S. Mochalova¹

¹ M.V. Lomonosov Moscow State University, National Anti-Doping Laboratory (Institute) (NADL MSU), Moscow, 105005 Russia

² MIREA – Russian Technological University (M.V. Lomonosov Institute of Fine Chemical Technologies), Moscow, 119454 Russia

 Corresponding author; e-mail: drpavelpostnikov@gmail.com

Abstract

Objectives. Emidonol[®] is a veterinary drug used to treat pathological conditions associated with hypoxia in cattle. In addition to meldonium, which is included in the Prohibited List of the World Anti-Doping Agency, the biotransformation product of Emidonol[®] in animals is the antioxidant and antihypoxant emoxypine, which can act as a marker of contamination of food products with the above-mentioned widely known metabolic modulator. The study set out to semiquantitatively determine emoxypine and meldonium levels, as well as to compare the excretion profiles of these substances by high-performance liquid chromatography–tandem mass spectrometry (HPLC–MS/MS) in urine samples of volunteers after receiving a single oral administration of a therapeutic dose of Brainmax[®] and after consuming a large amount of milk from cows that had received a prophylactic course of Emidonol[®].

Methods. Sample preparation of urine samples for the determination of meldonium was carried out using the “dilute and shoot” approach. Enzymatic hydrolysis with β -glucuronidase followed by purification by solid-phase extraction was used to determine emoxypine. Identification of meldonium and emoxypine was carried out by HPLC–MS/MS under conditions of electrospray ionization with registration of positively charged ions in the selective reaction monitoring (SRM) mode for the following transitions and collision energies: for meldonium, 147.1 > 147.1 (15), 147.1 > 132.1 (17), 147.1 > 58.1 (17), 147.1 > 59.1 (17), 147.1 > 42.1 (60); for emoxypine, 138.1 > 138.1 (7), 138.1 > 123.1 (15), 138.1 > 110.1 (20), 138.1 > 95.1 (20).

Results. The possibility of simultaneous identifying meldonium and emoxypine obtained after enzymatic hydrolysis with β -glucuronidase in urine samples of volunteers after oral intake of single dose of Brainmax[®] and consuming a large amount of Emidonol[®]-contaminated milk using the HPLC–MS/MS method with different numbers and variants of SRM transitions was demonstrated. Differences in the excretion profiles of these substances were found after ingestion of large amounts of contaminated milk and a single oral dose of Brainmax[®] 15–18 h later and further. After taking contaminated milk 12 h or more later, emoxypine is detected in concentrations 5 or more times higher than meldonium concentrations and is excreted for a longer period of time. Conversely, after taking a single dose of Brainmax[®], which contains both substances, the content of meldonium in urine samples of volunteers 15–18 h after taking it is several times higher in relation to emoxypine. The constant ratio of estimated concentrations of meldonium and emoxypine in Emidonol[®] was found to be approximately 1 : 2.

Conclusions. Identification of meldonium in the presence of emoxypine in urine under certain conditions can be used to distinguish contamination of food products with a prohibited metabolic modulator from intentional ingestion of real doping.

Keywords

Emidonol®, emoxypine, meldonium, Brainmax®, high-performance liquid chromatography–tandem mass spectrometry

Submitted: 29.04.2025

Revised: 14.05.2025

Accepted: 09.06.2025

For citation

Postnikov P.V., Askretkov A.D., Polosin A.V., Efimova Yu.A., Mochalova E.S. Semiquantitative determination of meldonium and emoxypine in human urine by HPLC–MS/MS after receiving a single therapeutic dose of Brainmax® and milk from cows receiving a preventive course of Emidonol®. *Tonk. Khim. Tekhnol. = Fine Chem. Technol.* 2025;20(4):382–398. <https://doi.org/10.32362/2410-6593-2025-20-4-382-398>

НАУЧНАЯ СТАТЬЯ

Полуколичественное определение мельдония и эмоксипина в моче методом ВЭЖХ–МС/МС после приема однократной терапевтической дозы препарата Брейнмакс® и молока коров, получавших профилактический курс Эмидонола®

П.В. Постников¹✉, А.Д. Аскретков¹, А.В. Полосин¹, Ю.А. Ефимова², Е.С. Мочалова¹

¹ Московский государственный университет им. М.В. Ломоносова, Национальная антидопинговая лаборатория (Институт) (НАДЛ МГУ), Москва 105005 Россия

² МИРЭА – Российский технологический университет (Институт тонких химических технологий им. М.В. Ломоносова), Москва, 119454 Россия

✉ Автор для переписки, e-mail: drpavelpostnikov@gmail.com

Аннотация

Цели. Эмидонол® — лекарственный препарат ветеринарного назначения, применяемый для лечения у крупного рогатого скота патологических состояний, связанных с гипоксией. Продуктом биотрансформации Эмидонола® в организме животных помимо мельдония, входящего в Запрещенный список Всемирного антидопингового агентства, является антиоксидант и антигипоксант эмоксипин, который может выступать в качестве маркера контаминации продуктов питания вышеуказанным получившим широкую известность модулятором метаболизма. Цель исследования заключалась в полуколичественном определении эмоксипина и мельдония и сравнении профилей выведения этих веществ методом высокоэффективной жидкостной хроматографии–тандемной масс-спектрометрии (ВЭЖХ–МС/МС) в образцах мочи добровольцев после однократного перорального приема терапевтической дозы препарата Брейнмакс® и большого количества молока коров, получавших профилактический курс ветпрепаратом Эмидонол®.

Методы. Пробоподготовку образцов мочи для определения мельдония проводили посредством подхода «dilute and shoot», для определения эмоксипина использовали ферментативный гидролиз с β-глюкуронидазой и последующей очисткой методом твердофазной экстракции. Идентификация мельдония и эмоксипина осуществлялась методом ВЭЖХ–МС/МС в условиях электрораспылительной ионизации с регистрацией положительно-заряженных ионов в режиме мониторинга селективных (выбранных) реакций (SRM) по следующим переходам и энергиям соударения: 147.1 > 147.1 (15), 147.1 > 132.1 (17), 147.1 > 58.1 (17), 147.1 > 59.1 (17), 147.1 > 42.1 (60) для мельдония и 138.1 > 138.1 (7), 138.1 > 123.1 (15), 138.1 > 110.1 (20), 138.1 > 95.1 (20) для эмоксипина.

Результаты. Показана возможность одновременной идентификации мельдония, определенного прямым разбавлением, и эмоксипина, полученного после ферментативного гидролиза β-глюкуронидазой, в образцах мочи добровольцев после перорального приема однократной дозы препарата Брейнмакс® и употребления большого количества молока, загрязненного Эмидонолом®, методом ВЭЖХ–МС/МС с использованием различного количества и вариантов SRM-переходов. Установлены различия в профилях выведения данных веществ после приема больших количеств контаминированного молока и однократного перорального приема препарата Брейнмакс® спустя 15–18 ч и позже. После приема контаминированного молока спустя 12 ч и позже эмоксипин определяется в концентрациях в 5 и более раз превышающих концентрации мельдония и выводится более длительное время. При однократном приеме препарата Брейнмакс®, содержащего оба вещества, напротив, содержание мельдония в образцах мочи добровольцев спустя 15–18 ч и позднее после приема в несколько раз выше по отношению к эмоксипину. Также обнаружено, что постоянное соотношение оценочных концентраций мельдония и эмоксипина в чистом препарате Эмидонол® соответствует 1 : 2.

Выводы. Идентификация мельдония в присутствии эмоксипина в моче при определенных условиях может быть использована для отличия контаминации продуктов питания запрещенным модулятором метаболизма от намеренного приема реального допинга.

Ключевые слова

Эмидонол®, эмоксипин, мельдоний, Брейнмакс®, высокоэффективная жидкостная хроматография–тандемная масс-спектрометрия

Поступила: 29.04.2025

Доработана: 14.05.2025

Принята в печать: 09.06.2025

Для цитирования

Постников П.В., Аскретков А.Д., Полосин А.В., Ефимова Ю.А., Мочалова Е.С. Полуколичественное определение мельдония и эмоксипина в моче методом ВЭЖХ–МС/МС после приема однократной терапевтической дозы препарата Брейнмакс® и молока коров, получавших профилактический курс Эмидонола®. *Тонкие химические технологии*. 2025;20(4):382–398. <https://doi.org/10.32362/2410-6593-2025-20-4-382-398>

INTRODUCTION

The antihypoxic, antioxidant, and membrane-protective effects of veterinary drug Emidonol® (3-(2,2,2,2-trimethylhydrazinium) propionate-2-ethyl-6-methyl-3-hydroxy-pyridine disuccinate) are due to its components [1] (Fig. 1). Its use in cattle is authorized by the Federal Service for Veterinary and Phytosanitary Surveillance (Rosselkhozadzor) for various pathologies accompanied by hypoxia in the form of 5 and 10% solutions¹.

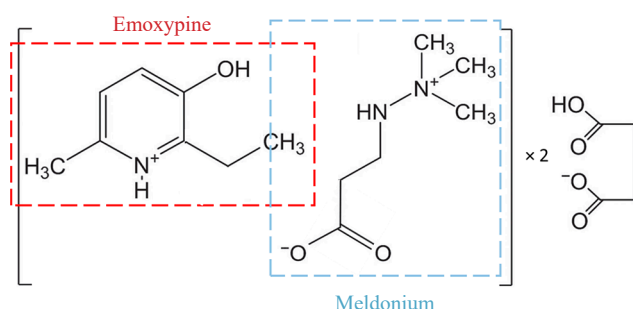


Fig. 1. Structural formula of Emidonol®

In animals, Emidonol® undergoes biotransformation to form trimethylhydrazinium propionate (meldonium) and emoxypine succinate, which is known in Russia as Mexidol®. The former is a metabolic modulator on the World Anti-Doping Agency (WADA) List of Prohibited Substances² [2]. The effect of the latter, which has been recently described by a number of authors as an antioxidant and antihypoxant, can also lead to an increase in performance, and is comparable to the effect of doping

substances [2], but it has not yet been included in the WADA monitoring program³ as a hypoxen [3].

The problem of contamination of foodstuffs with meldonium is extremely relevant for athletes due to the real risk of positive doping tests, given that it has been the most used doping substance for more than 15 years⁴. Earlier studies were published on the determination of the banned metabolic agent both in food [4] and in the urine of volunteers after consumption of milk from cows treated with the veterinary drug Emidonol® [5] or spiked with meldonium [6].

Our study proposes the use of emoxypine as an additional marker of Emidonol® degradation in urine biosamples simultaneously with the identification of meldonium. Of course, the simultaneous use of these two drugs to improve athletic performance is not excluded, given that emoxypine succinate (Mexidol®) is not prohibited and is often used to correct functional status in sports, but such a coincidence may be accidental and occur under conditions other than food contamination. Preparations containing meldonium and emoxypine succinate in one tablet (e.g., Brainmax®), which have recently appeared on the Russian pharmaceutical market, show a slightly different pattern of excretion with urine than contaminated milk consumption.

In this study, we conducted pilot studies comparing the excretion profiles of these two substances following a single oral administration of Brainmax® and ingestion of a large amount of milk from cows receiving a prophylactic course of Emidonol®. The proposed approaches for identifying biotransformation products of veterinary drugs meldonium and emoxypine using

¹ State Register of Medicines for Veterinary Use (list of medicines that have undergone state registration). URL: <https://fsvps.gov.ru/files/gosudarstvennyj-reestr-lekarstvennyh-sredstv-dlja-veterinarnogo-primeneniya-perechen-lekarstvennyh-preparatov-proshedshih-gosudarstvennuju-registraciju/>. Accessed February 17, 2025.

² International Standard Prohibited List 2025. URL: https://www.wada-ama.org/sites/default/files/2024-09/2025list_en_final_clean_12_september_2024.pdf. Accessed March 10, 2025.

³ WADA 2025 Monitoring Program. URL: https://www.wada-ama.org/sites/default/files/2024-09/2025_list_monitoring_program_en_final_clean_11_september_2024.pdf. Accessed December 15, 2024.

⁴ RUSADA: the number of positive samples for meldonium in 2024 has decreased. URL: <https://rsport.ria.ru/20240522/rusada-1947725070.html>. Accessed December 17, 2024.

the method of high-performance liquid chromatography–tandem mass spectrometry (HPLC–MS/MS) in the selective reaction monitoring (SRM) mode can be varied by using a different number of transitions. This approach can potentially be used to differentiate between the real ingestion of a prohibited metabolic modulator and contamination of foodstuffs by it when using a veterinary drug in farm animals.

MATERIALS AND METHODS

Analysis samples and reagents

The study was based on urine samples provided by volunteers ($n = 3$) before and after a single morning intake of three glasses (900 mL) of fresh milk of cows treated with the veterinary drug Emidonol® 10% (AVZ Animal Health, Russia) collected within 60 h. Dosages of Emidonol® were administered to animals for 15 days daily in the morning depending on animal weight according to the drug instructions. Milk samples were collected on the 15th (last) day of the course in plastic sterile bottles of 1 L.

Urine samples of other volunteers ($n = 3$) collected during 14–16 days were also used for experiments before and after a single intake of 1 tablet of the combination comparison drug Brainmax® containing 250 mg of meldonium and 250 mg of emoxypine succinate (Mexidol®), which is available in pharmacy chains without a prescription.

Volunteers ($n = 3$; age 35–52 years; body weight 60–92 kg; gender was not considered) had not previously taken any meldonium or mexidol preparations, nor had they consumed dietary supplements, milk or meat products 1–2 days before the urine specimen collection. Urine samples were collected in sterile 100 mL medical containers, which were labeled with the date and time of collection and stored at +4°C or frozen at –20°C before sample preparation.

The study follows the principles of the Declaration of Helsinki⁵. Written permission was obtained from the volunteers to use their biological material for research purposes.

A solution with a concentration of 1 mg/mL was prepared from deuterated meldonium (meldonium- d_3 , certified standard) (TLC PharmaChem Inc., Canada) used as an internal standard for the determination of meldonium. For preparation of positive urine control samples with meldonium content of 10, 100, and 1000 ng/mL, a stock solution of meldonium dihydrate reference standard (European Pharmacopoeia, Meldonium Dihydrate CRS, batch 1, European Directorate

for the Quality of Medicines and HealthCare, France) having a concentration of 1 mg/mL was used.

A solution with a concentration of 1 mg/mL was prepared from Bupranolol (certified standard, Clearsynth Labs, 500 mg, India) used as an internal standard for the determination of emoxypine. To prepare positive control urine samples and solutions with concentrations of 10, 100, and 1000 ng/mL, a stock solution of the reference standard ethylmethylhydroxypyridine (emoxypine) succinate (MEZ-096, GEO 12209-2023, MCO 2931:2023 produced by the Moscow Endocrine Plant, Russia) having a concentration of 1 mg/mL was used. To estimate the concentrations of substances, calibration graphs were plotted for 3 solutions of standards in urine with the above concentrations.

The following substances were used for the study: methanol for chromatography (purity not less than 99.8%); acetonitrile; acetic acid (high-performance liquid chromatography (HPLC) grade, JT Baker, Netherlands); water (HPLC grade, Thermo Scientific Chemical, USA); sodium azide; ammonium acetate (purity not less than 99.9%, Sigma-Aldrich, USA); potassium carbonate; potassium hydrogen carbonate; potassium dihydrophosphate; sodium phosphate bivalent dihydrate (purity not less than 99%); β -glucuronidase from *E. Coli* K12 (Roche, Germany); compressed argon 5.0 with purity not less than 99.999%. To prepare buffer solutions, deionized water having resistivity of 18.2 mOsm·cm (Millipore, USA) was used.

Auxiliary equipment and materials

Crimper, decapper, 1.5 mL glass vials (Macherey-Nagel GmbH & Co, Düren, Germany); 0.3 mL polypropylene vials (Macherey-Nagel GmbH & Co, Düren, Germany); automatic variable volume pipettes 0.5–10 μ L, 20–200 μ L, 100–1000 μ L, 500–5000 μ L (Eppendorf, Germany) and their tips; liquid temperature thermostat ($-30 \pm 5^\circ\text{C}$), automatic orbital shaker, benchtop centrifuge with horizontal rotor for 16×125 mm tubes, incubator thermostat for glass tubes, Centrifuge 5430 benchtop centrifuge with rotor for 1.5–2 mL (Eppendorf, Germany); polypropylene test tubes 1.5 mL (Eppendorf, Germany); 15 mL and 50 mL Falcon tubes (Greiner Bio-One, Austria); Oasis HLB solid-phase extraction cartridges (60 mg, 3 mL) (Waters, USA); 16×125 mm glass tubes with screw cap; Ohaus Discovery DV215CD analytical scale (5-digit accuracy) (OHAUS CORPORATION, USA); Vortex liquid shaking apparatus.

⁵ World Medical Association. Declaration of Helsinki. URL: <https://asmu.ru/upload/iblock/067/Хельсинкская%20декларация.pdf>. Accessed February 17, 2025.

Sample preparation

For the determination of meldonium, 100 µL of urine samples were collected from volunteers before (blank) and after milk intake, as well as before and after taking 1 tablet of Brainmax®. 100 µL of negative and positive (10, 100, and 1000 ng/mL) control urine samples were also taken into 1.5 mL Eppendorf tubes. 900 µL of diluent was added (to prepare the diluent, 22 µL of 0.1 mg/mL internal standard solution (meldonium-*d*₃) was added to a 100 mL volumetric flask and brought to the mark with methanol). After shaking, this was centrifuged for 10 min at 14000g. Then 800 µL of supernatant was collected into glass vials and covered with lids.

For the determination of emoxypine, 1 mL of blank urine, 1 mL of positive control urine samples with different emoxypine content (10, 100, and 1000 ng/mL) and 1 mL of the analyzed samples were collected into 16 mL tubes with screw cap. 1 mL of hydrolysis buffer mixture was added to each tube (the contents of 2 vials of β-glucuronidase (15 mL) were brought to 1000 mL in a measuring flask with freshly prepared phosphate buffer solution (54 g Na₂HPO₄·2H₂O, 68 g K₂HPO₄, 0.5 g sodium azide was brought to 1000 mL with deionized water, pH 6.2–6.5), stirred and incubated at 55 ± 3°C for 60 ± 10 min. After incubation, 50 µL each of the internal standard (15 ng/mL bupranolol solution in methanol) was added to the tubes and mixed. 1 mL of the contents was then applied to Oasis HLB solid phase extraction cartridges (60 mg, 3 mL) preconditioned with 3 mL of methanol and then 3 mL of purified water. The cartridges were washed with 3 mL of 20% methanol solution in water and the contents eluted into clean tubes with 2 mL of 70% methanol solution in water. 800 µL of the eluate was placed in glass vials and sealed with lids.

For the determination of meldonium for the preparation of mobile phase A, 15 mL was removed from a 2.5 L water bottle and then 2.5 mL of concentrated acetic acid and 12.5 mL of 2 M ammonium acetate solution were added.

The mobile phase B was acetonitrile. For the determination of emoxypine, the mobile phase B consisted of acetonitrile/methanol mixture in the ratio 3 : 1.

The concentration of the determined substances was evaluated by selective SRM transitions: 147.1 > 58.1 for meldonium and 138.1 > 123.1 for emoxypine, respectively.

Parameters of instrumental analysis by HPLC–MS/MS method

For the determination of meldonium and emoxypine in urine samples of volunteers, HPLC–MS/MS analysis was performed using an Ultimate 3000 liquid chromatograph

coupled to a TSQ Vantage model triple quadrupole mass spectrometer (Thermo Fisher Scientific, USA) with an electrospray ionization source with a heated spray gas stream in positive ion detection (ESI+) mode. Acquity UPLC® BEH HILIC 3.0 × 100 mm HPLC column with 1.7 µm particle size and Acquity UPLC® BEH HILIC 2.1 × 5 mm HPLC pre-column with 1.7 µm VanGuard™ particle size (Waters, USA) were used for analysis.

The following parameters were selected for the determination of meldonium: flow rate, 0.3 mL/min; sample injection volume, 10 µL; column temperature 40°C. The gradient elution program is shown in Table 1.

Table 1. Gradient elution program for the determination of meldonium

Time, min	Mobile phase A	Mobile phase B
0.0	5	95
0.5	5	95
4.0	95	5
5.5	95	5
5.51	5	95
9.0	5	95

The parameters for the determination of emoxypine are as follows: flow rate 0.5 mL/min; sample injection volume 10 µL; column temperature 40°C; gradient elution program is given in Table 2.

Table 2. Gradient elution program for the determination of emoxypine

Time, min	Mobile phase A	Mobile phase B
0.0	10	90
0.5	10	90
2.9	80	20
3.5	80	20
3.51	10	90
5.0	10	90

Positive ions were registered in SRM mode: MS run time, 9 min; collision gas pressure, 1.5 mTorr; full width at half maximum (FWHM) Q1 — 1.0, Q3 — 1.0; direct current voltage (DCV), 5 V; capillary temperature, 300°C;

evaporator temperature, 370°C; time of one complete cycle, 0.3 s; capillary voltage (ESI+), 4000 V; sheath gas pressure, 50.0; auxiliary atomizing gas flow, 20.0; ion sweep gas pressure, 0.0.

Evaluation of meldonium and emoxypine in the veterinary drug Emidonol®

In order to evaluate the content of the determined substances in the veterinary preparation Emidonol®, two solutions of the preparation in water (samples were diluted $5 \cdot 10^4$ times) were prepared. Solutions of meldonium and emoxypine in deionized water with concentrations of 10, 100, 250, and 1000 ng/mL were used as comparison solutions. To 100 µL of each of two samples of Emidonol® solution, in one of which meldonium was determined, while the other contained emoxypine, 900 µL of diluent containing meldonium- d_3 and bupranolol, respectively, were added. The assays were performed according to the programs for the determination of mexidol and meldonium described above.

RESULTS AND DISCUSSION

There are practically no data on the pharmacokinetics of Emidonol® in the literature. However, meldonium is known to be a biotransformation product of the veterinary drug in animals [4, 5]. Based on the structure of the drug, emoxypine in the form of succinate (mexidol) represents an additional metabolite. Meldonium, being an analog of gamma-butyrobetaine, contributes to the restoration of equilibrium of the processes of oxygen delivery and consumption in cells under conditions of ischemia, where glycolysis occurs without additional oxygen consumption to affect the key enzyme phosphofructokinase, which contributes to the reduction of mitochondrial damage and oxidative stress under hypoxia. In previously published studies on model experiments, we have shown the possibility of obtaining a positive doping test for meldonium after consumption of milk and meat of cows, which were administered Emidonol® veterinary drug for veterinary indications [4–6].

According to some authors, emoxypine succinate (the second component of Emidonol®) has similar biological effects to meldonium and trimetazidine included in the WADA Prohibited List and therefore should be considered as a candidate for inclusion in the monitoring program [2]. Jędrejko *et al.* state that combining emoxypine (a synthetic pyridoxine analog) with succinate in drugs increases their therapeutic efficacy. The authors claim that combinations of 3-oxypyridine

derivatives with succinic acid salts can improve the performance of athletes due to their metabotropic and antihypoxic effects [2]. Lukyanova *et al.* have noted that hypoxia-induced expression of HIF-1 α transcription factor is regulated by succinate and induced by succinate-containing drugs [7]. Succinate itself acts as a signaling molecule involved in the molecular adaptation of the organism to oxygen deficiency. In normoxia, succinate is rapidly eliminated with the formation of carbon dioxide and water; since its half-life is about 45 min, it is impossible to determine its content in the body.

In a study by Voronina *et al.* [8], it was found that emoxypine succinate (Mexidol®) at single and sub-chronic intraperitoneal administration at doses of 50 and 100 mg/kg significantly increased the physical performance of mice in the swimming test with load. Mildronate®, being the comparison drug in this study, increased the physical performance of animals when administered at a dose of 100 mg/kg. The authors concluded that the effect of mexidol at doses of 50 and 100 mg/kg was comparable to that of Mildronate® at a dose of 100 mg/kg.

According to the data of P.A. Baranov's dissertation work⁶ and experimental studies [9], emoxypine succinate (mexidol) is metabolized with the formation of two products of phase I (2,6-dimethyl-3-oxypyridine and 6-methyl-3-oxypyridine) and three conjugated products of metabolism phase II mainly comprised of glucuronoconjugate and small amounts of phosphate. It is noted that the unchanged substance can be detected in urine in insignificant amounts within 2 days following drug administration. Baranov also noted that $0.39 \pm 0.02\%$ of the unchanged drug, $20.71 \pm 4.18\%$ of the glucurono-conjugated derivative, $30.15 \pm 4.27\%$ of the sulfoconjugated forms, and $15.56 \pm 1.54\%$ of other forms of conjugated products are excreted with urine during the first 24 h after emoxypine succinate administration. Since 20% of emoxypine is excreted in the urine as glucurono-conjugate, its determination in urine samples was performed by enzymatic hydrolysis with β -glucuronidase followed by purification of the hydrolysate by solid-phase extraction, which minimized the matrix effect. Here, the degree of extraction of emoxypine was 97.5%. Determination of emoxypine in urine samples of volunteers without solid-phase extraction and hydrolysis by the “dilute and shoot” method was difficult due to interfering peaks of matrix components complicating identification.

In an earlier study [5], the possibility in principle to determine meldonium by HPLC–MS/MS in the SRM mode using five SRM transitions

⁶ Baranov P.A. Investigation of glucuronoconjugation processes based on pharmacokinetic and biochemical studies: Cand. Sci. Thesis (Biol.). Moscow: 2009. 155 p.

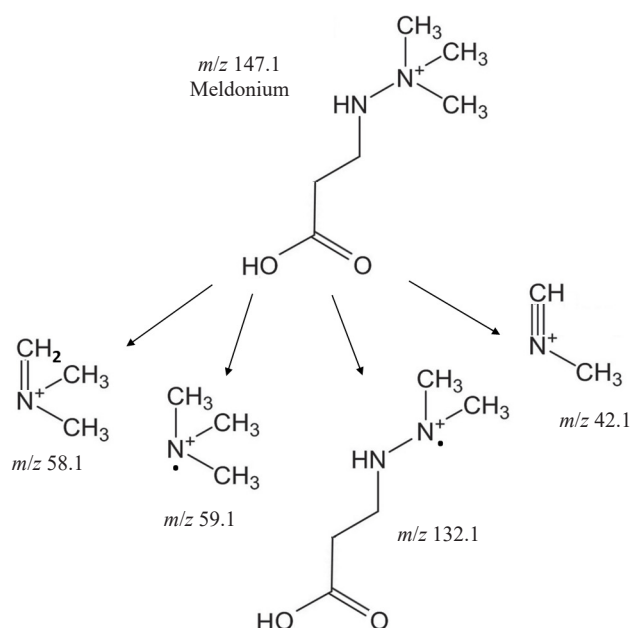


Fig. 2. Proposed fragmentation scheme of meldonium [6]

(147.1 > 147.1 (15), 147.1 > 132.1 (17), 147.1 > 59.1 (17), 147.1 > 58.1 (17), 147.1 > 42.1 (60)) after ingestion of large amounts of milk from cows (900 mL) having received a prophylactic course of the veterinary drug Emidonol® 4–12 h after consumption and 40–42 h later using the two longest-lived SRM transitions (147.1 > 59.1 (17), 147.1 > 58.1 (17)) was demonstrated. The fragmentation scheme of meldonium is shown in Fig. 2.

According to available data, meldonium is practically not metabolized and its significant part is excreted from the body in an unaltered form [10]; for this reason, the “dilute and shoot” approach was used for sample preparation. In this case, the maximum estimated concentrations of meldonium in analyzed urine samples of volunteers (taking into account 10-fold dilution according to the sample preparation method) of up to 400 ng/mL, which is higher than the minimum required performance level of WADA (Minimum Required Performance Level, MRPL⁷, for meldonium—100 ng/mL), are reached after 5–10 h (when using morning milk samples) [5]. After 40–42 h, the concentrations of the metabolic modulator fell to 5 ng/mL (limit of detection) and below, and then its identification becomes difficult (Fig. 3) [5].

In the experiments performed, along with meldonium, emoxypine obtained during the hydrolysis of its glucurono-conjugated form is identified in the

urine samples of all volunteers who consumed milk samples by HPLC–MS/MS using four SRM transitions (138.1 > 138.1 (7), 138.1 > 123.1 (15), 138.1 > 110.1 (20), 138.1 > 95.1 (20)). Emoxypine is identified at 32–34 h from hydrolysis of its glucurono-conjugated form; up to 50–52 h, it is identified using three SRM transitions (138.1 > 138.1 (7), 138.1 > 123.1 (15), 138.1 > 110.1 (20)) (see Appendix 1). Its maximum urinary concentrations in volunteers were 1250, 1400, and 1430 ng/mL (1360 ± 239.6 ng/mL, $p = 0.95$), reached 5–8 h after

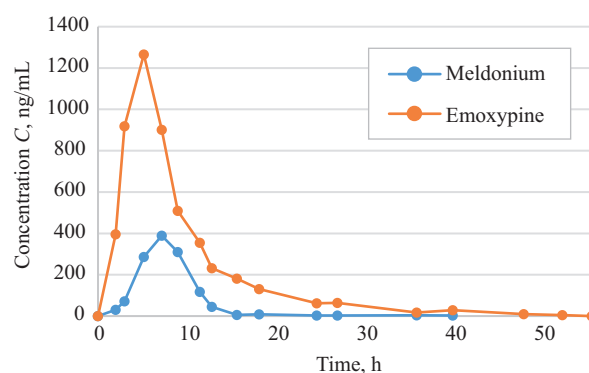


Fig. 3. Graph of meldonium and emoxypine excretion in urine for 54 h after a single consumption of a milk sample (900 mL) (volunteer sample). Estimated emoxypine concentrations are 5 or more times higher than meldonium concentrations 12 h and further after ingestion of contaminated milk

⁷ WADA Technical Document – TD2022MRPL. URL: https://www.wada-ama.org/sites/default/files/2022-01/td2022mrpl_v1.1_eng_0.pdf. Accessed March 10, 2025.

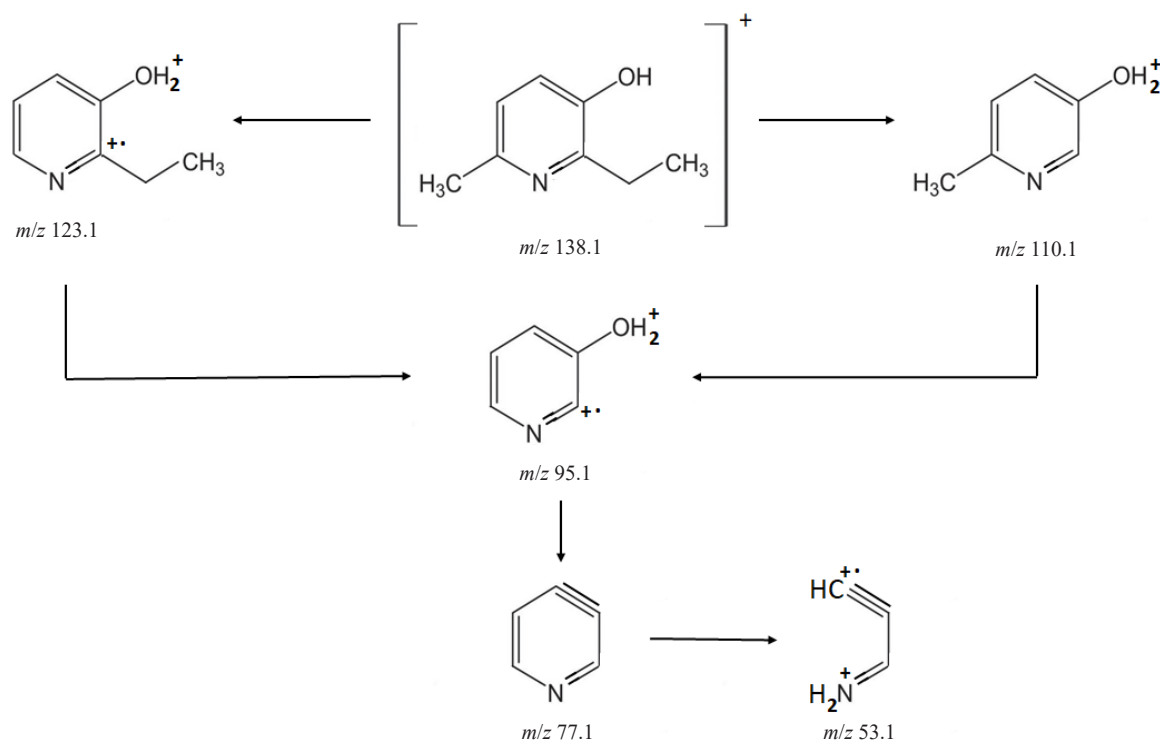


Fig. 4. Proposed fragmentation scheme of the protonated precursor ion of 2-ethyl-6-methyl-3-oxypyridine (emoxypine)⁶

administration, and fell to 5 ng/mL or lower by 52–54 h. The limit of detection of emoxypine was about 5 ng/mL. Figure 4 shows its putative fragmentation pattern.

Although the present study evaluated emoxypine released following enzymatic hydrolysis of its glucurono-conjugated form and unchanged during metabolism, the estimated concentrations in all volunteers are 3–4 times higher at the peak of excretion and 5–10 times higher at 12 h and later as compared with meldonium concentrations. This pattern of excretion is observed when analyzing urine samples from all three volunteers collected following ingestion of large doses of contaminated milk at up to 40–42 h when detection of meldonium becomes problematic due to the presence of extraneous interfering peaks of matrix components. Of course, urinary excretion depends on many factors, such as fluid intake, renal function, differences in glucuronoconjugation of emoxypine among volunteers, etc., and may vary slightly.

A different picture is observed with a single oral administration of the only combined drug Brainmax®, which contains both meldonium and mexidol and is included in the State Register of Medicinal Products of the Russian Federation. We would like to draw attention to the fact that the recommended daily dosage of meldonium is about 250–500 mg/day, while that of mexidol is 250–375 mg/day. The description of the drug states that its antioxidant, anti-ischemic, anxiolytic, nootropic, antihypoxic and membrane-protective effect exceeds the

pharmacological effect of each of the components when used separately. It is also widely used for the treatment of post-coital asthenic syndrome in patients following viral infection, for complex therapy of acute and chronic cerebral circulatory disorders, as well as to improve cognitive functions and increase work capacity.

When analyzing urine samples of volunteers by HPLC–MS/MS in SRM mode, meldonium was reliably detected after a single oral administration of 1 tablet of Brainmax® using all five SRM transitions ($147.1 > 147.1$ (15), $147.1 > 132.1$ (17), $147.1 > 59.1$ (17), $147.1 > 58.1$ (17), $147.1 > 42.1$ (60)) for longer times, after 80–85 h; after 140–150 h using four SRM transitions (except $147.1 > 132.1$ (17)); after 200–220 h using three SRM transitions ($147.1 > 59.1$ (17), $147.1 > 59.1$ (17), $147.1 > 58.1$ (17), $147.1 > 42.1$ (60)) (Appendices 3d, 3e, 3f, respectively); up to 360–380 h using the two longest-lived SRM transitions ($147.1 > 59.1$ (17), $147.1 > 58.1$ (17), data not shown). In this case, the maximum concentrations of meldonium in the urine samples of volunteers of 14070, 15280, and 15890 ng/mL (mean value 15080 ± 926.3 ng/mL) were reached 5–10 h after administration (Fig. 5). These figures take into account dilution according to the sample preparation technique. After 90–92 h, estimated metabolic modulator concentrations fell to 98, 105, and 110 ng/mL, respectively (mean 104.3 ± 15.0 ng/mL is at the MRPL level) (see Fig. 6); after 220 h, the respective concentrations fell to 18, 23,

and 20 ng/mL (20.3 ± 6.3 ng/mL). After 15–16 days (more than 360–380 h), the identification of meldonium from the above two SRM transitions became difficult (around 5 ng/mL and below) due to interfering peaks of matrix components; nevertheless, its trace amounts were still present in urine (data not shown).

Emoxyphine after Brainmax® administration was significantly determined by HPLC–MS/MS using four SRM transitions ($138.1 > 138.1$ (7), $138.1 > 123.1$ (15), $138.1 > 110.1$ (20), $138.1 > 95.1$ (20)) over 50–55 h and using three SRM transitions ($138.1 > 138.1$ (7), $138.1 > 123.1$ (15), $138.1 > 110.1$ (20)) after 80–85 h (see Appendix 2). Its maximum urinary concentrations, which reached 59, 67, and 71 µg/mL (65.7 ± 15.2 µg/mL) 4–9 h after administration, were approximately 3–4 times higher than meldonium concentrations. However, 15–18 h later, concentrations fell to 690, 805, and 760 ng/mL (751.7 ± 144.0 ng/mL)

and were then significantly lower than meldonium concentrations throughout the elimination time. After 90 h or more, emoxyphine concentrations were below the established detection limit of 5 ng/mL; thereafter, the drug no longer detectable.

In a study of the veterinary drug Emidonol®, the ratio of estimated concentrations of meldonium to mexidol was found to be about 1 : 2, i.e., there are two molecules of emoxyphine per molecule of the prohibited metabolic modulator (see Appendix 4). In general, while the maximum concentrations of emoxyphine in both cases (milk consumption/single tablet administration) exceed meldonium concentrations after approximately the same time 4–10 h and up to 42 h after milk consumption, meldonium concentrations significantly exceed emoxyphine concentrations 15–18 h after Brainmax® administration to reveal the opposite pattern. At the same time, as noted above, the study evaluated the content of

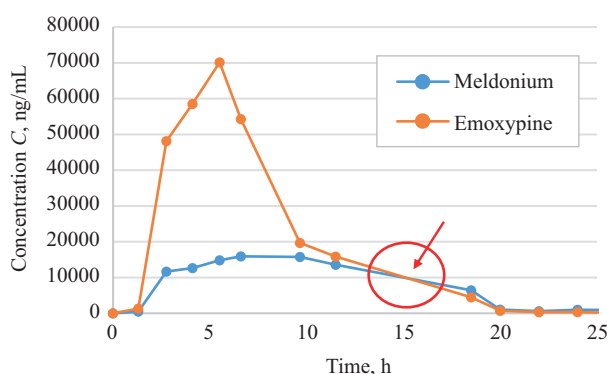


Fig. 5. Graph of meldonium and emoxyphine excretion in urine during the first 25 h after oral administration of 1 tablet of Brainmax® (volunteer sample). Estimated emoxyphine concentrations during the first 15 h exceed meldonium concentrations; however, the opposite scenario is observed after 15–18 h (see Fig. 6)

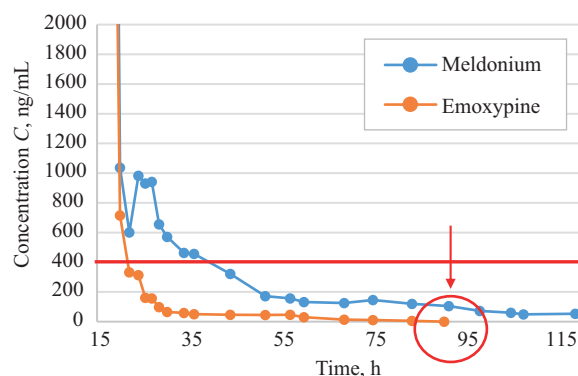


Fig. 6. Graph of meldonium and emoxyphine excretion with urine during the following 15–120 h following oral administration of 1 tablet of Brainmax® (volunteer sample). After 18–20 h, the estimated concentrations of meldonium significantly exceed the concentrations of emoxyphine. The red line highlights the maximum estimated concentration of meldonium in urine obtained after consumption of contaminated milk, while the arrow shows the impossibility of simultaneous determination of meldonium and emoxyphine by the developed method after 90 h or more

emoxyphine in urine samples released after enzymatic hydrolysis of its glucurono-conjugated form.

Similar results can be obtained after separate administration of Mildronate® and Mexidol®; however, emoxyphine is evidently excreted faster, and the detection of higher concentrations of meldonium on the background of its presence in smaller amounts may indicate the same administration pattern as in the case of Brainmax®.

CONCLUSIONS

As a result of the undertaken pilot studies, it has been shown that the excretion profiles of meldonium and emoxyphine are different when contaminated milk is consumed and 1 tablet of Brainmax® is taken orally. The possibility of identification of these substances in urine samples of volunteers by HPLC–MS/MS using different number and variants of SRM transitions was demonstrated.

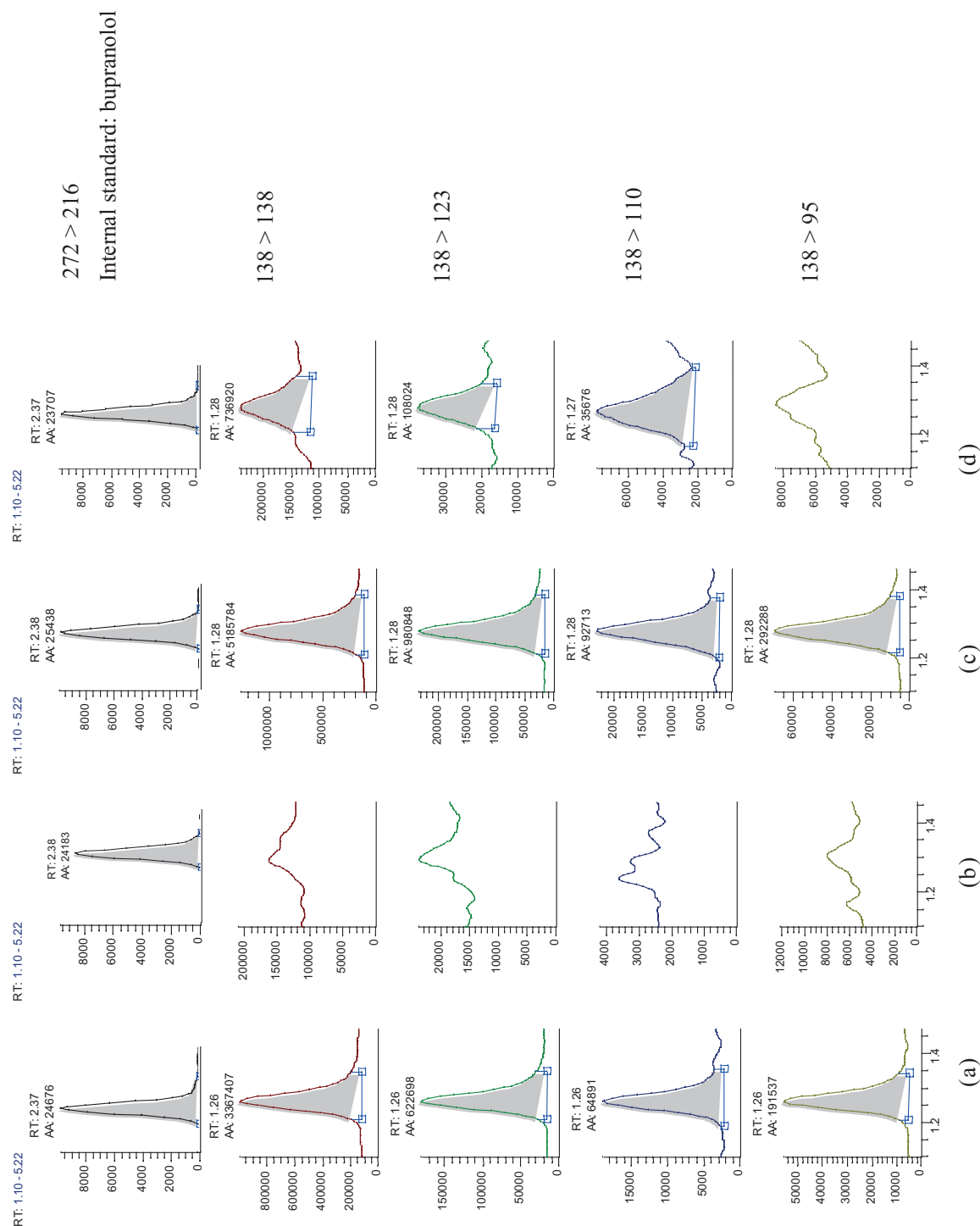
In case of simultaneous detection of meldonium and emoxyphine in a urine sample, attention should be paid to the ratio of their estimated concentrations. It appears that, in order to definitively resolve the problem of trace

amounts of meldonium in urine, the two substances should be quantified: the content of emoxyphine should be taken into account along with the different excretion patterns following consumption of contaminated milk and deliberate ingestion of illicit drugs. The veterinary drug Emidonol® has also been found to contain 2 times more emoxyphine than meldonium, which may also be useful for identification purposes.

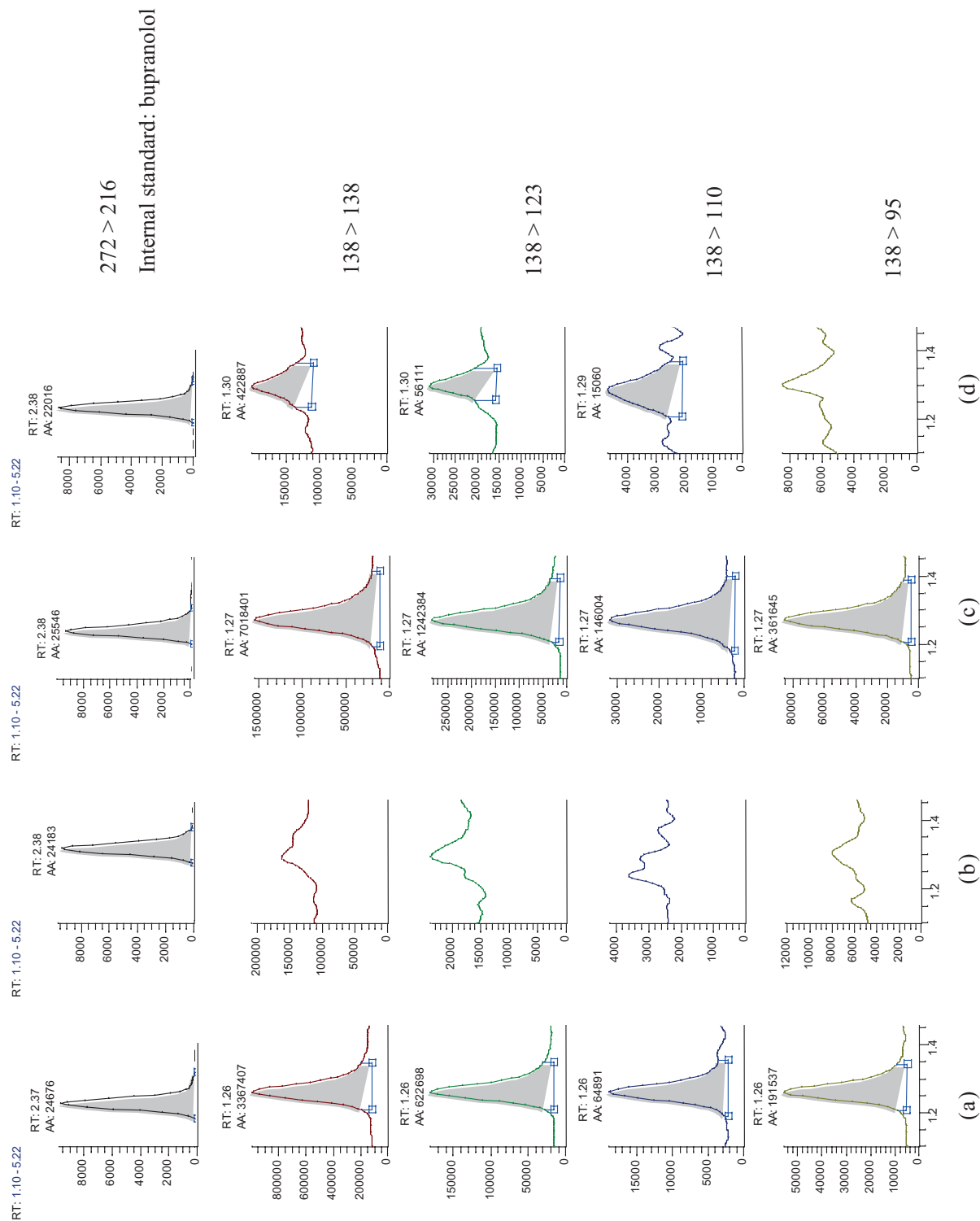
When its concentration exceeds several times in relation to meldonium, emoxyphine can act as an additional marker of food contamination since also representing a biodegradation product of the veterinary drug Emidonol®. At the same time, even when large amounts of contaminated milk (900 mL) are consumed, meldonium concentrations do not exceed 320–400 ng/mL (within a few hours after consumption). Conversely, when taking 1 tablet of Brainmax®, meldonium is detected up to 80–85 h by all five SRM transitions, while emoxyphine is almost undetectable. In our opinion, this approach can be used for differentiating between actual doping with products containing meldonium and the contamination of foodstuffs with meldonium due to the use of the veterinary drug Emidonol® in farm animals.

APPENDICES

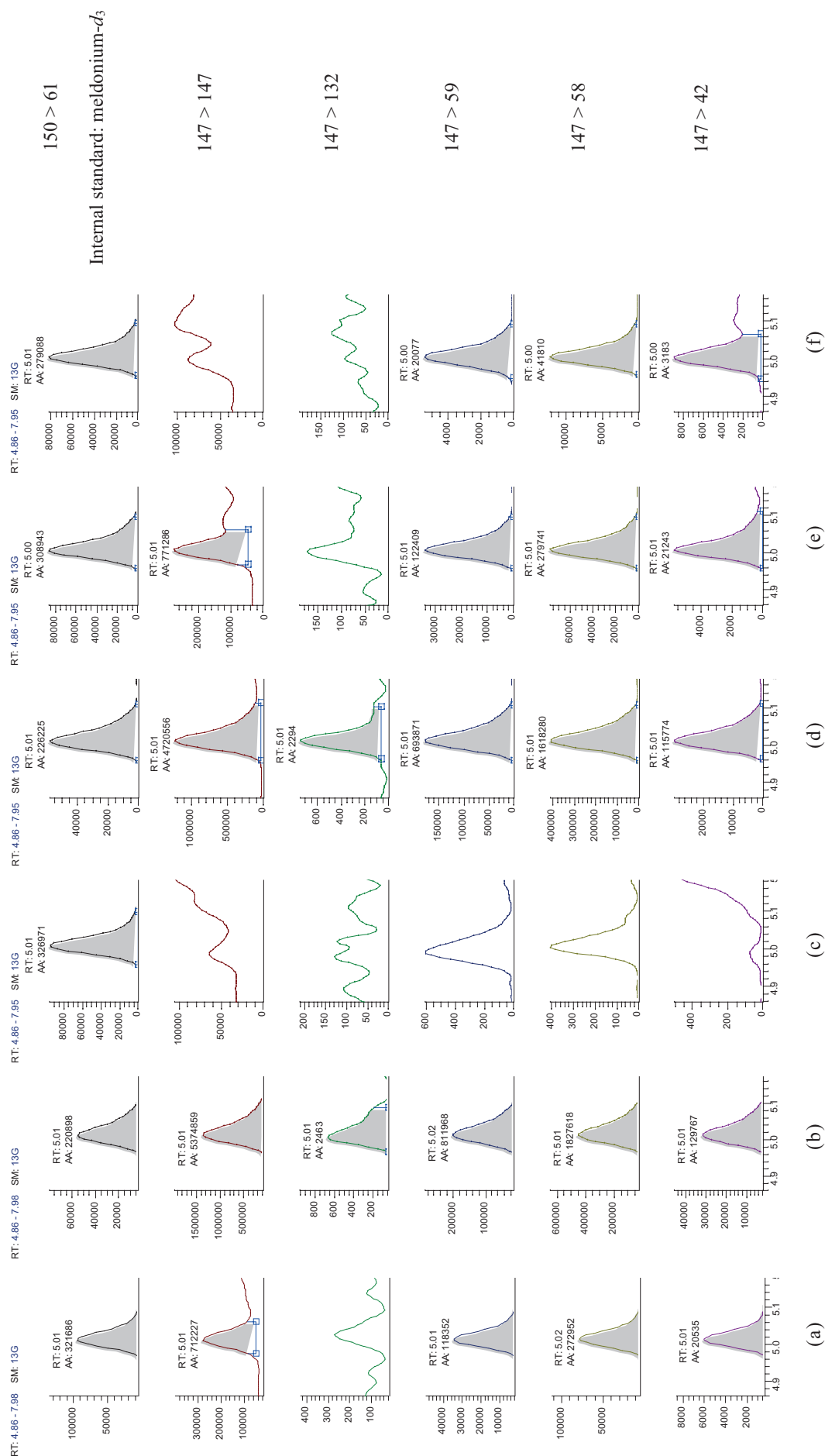
Appendix 1. Determination of emoxypine in a volunteer urine sample after consuming 900 mL of contaminated milk. (a) Positive control of urine containing 100 ng/mL of emoxypine; (b) negative control of urine; (c) volunteer urine sample in 18 h after drinking milk; (d) urine sample in 36 h after drinking milk



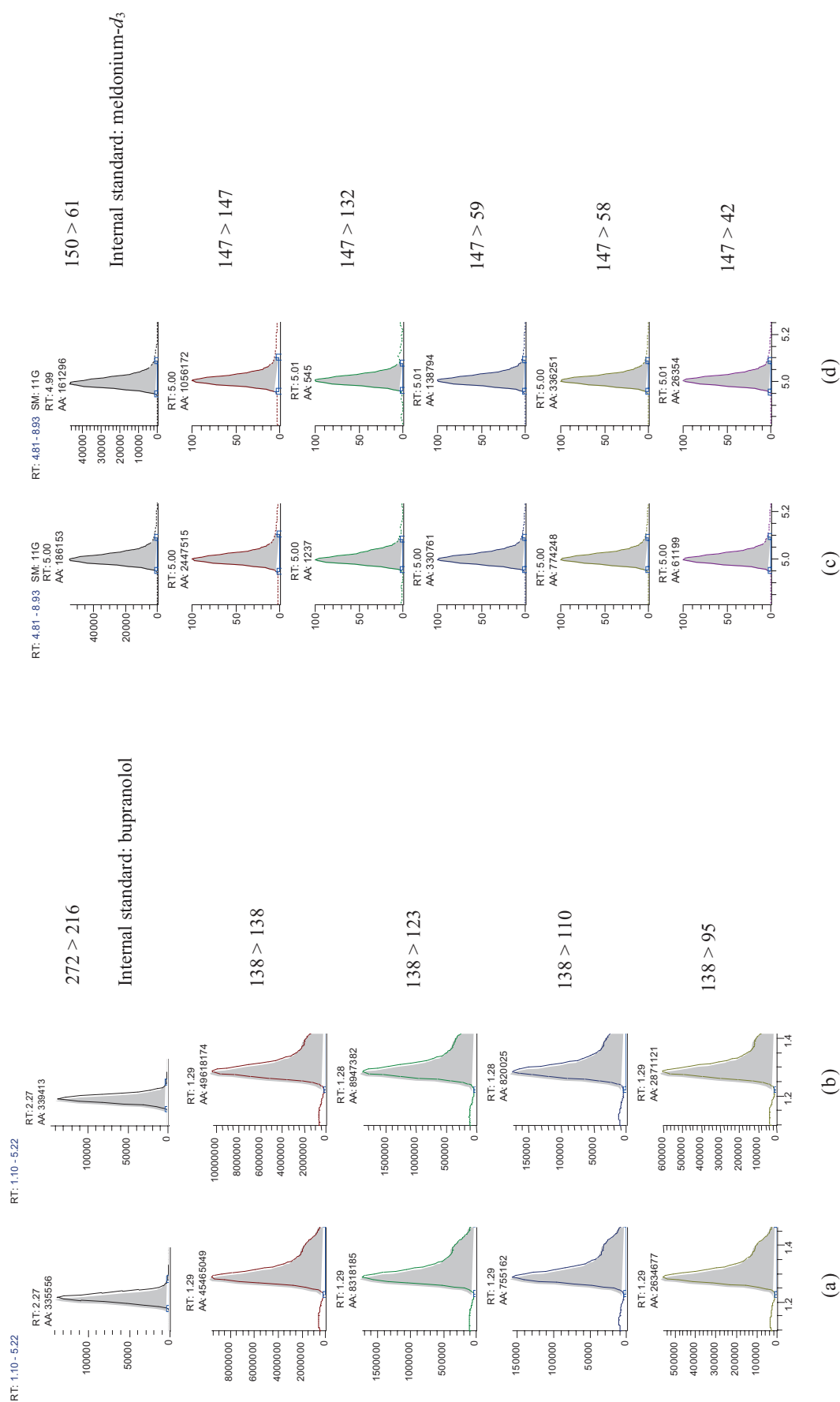
Appendix 2. Determination of emoxypine in a volunteer urine sample after oral administration of 1 tablet of Brainmax®. (a) Positive control of urine containing 100 ng/mL of emoxypine; (b) negative control of urine; (c) volunteer urine sample in 26 h after taking the drug; (d) urine sample in 80 h after taking the drug



Appendix 3. Determination of meldonium in a urine sample of a volunteer after oral administration of 1 tablet of the drug Brainmax®. (a) Positive control of urine containing 100 ng/mL of meldonium; (b) positive control of urine containing 1000 ng/mL of meldonium; (c) negative control of urine; (d) volunteer urine sample in 24 h after taking the drug; (e) urine sample in 90–92 h after taking the drug; (f) urine sample in 200 h after taking the drug



Appendix 4. Determination of meldonium and emoxypine in the Emidonol® veterinary drug. (a) Positive control containing 1000 ng/mL of emoxypine (in water); (b) sample of the Emidonol® veterinary drug—solution in water (dilution by 50000 times); (c) positive control containing 1000 ng/mL of meldonium (in water); (d) sample of the Emidonol® veterinary drug—solution in water (dilution by 50000 times)



Acknowledgments

The authors thank Natalia Vladimirovna Mesonzhnik, Senior Research Engineer of the Resource Center for Analytical Methods of the Sirius University of Science and Technology, Cand. Sci. in Biology, for her valuable commentary and recommendations on the design of the research work material.

Authors' contributions

P.V. Postnikov—writing the text of the article, formulation of aims and objectives, development of a plan for conducting experiments,

conducting experimental research, discussion of experiments and results, editing the manuscript, editing the final version of the article, and preparing materials for publication.

A.D. Askretkov—conducting experimental research, discussion of experiments and results.

A.V. Polosin—conducting experimental research.

Yu.A. Efimova—editing the final version of the article and preparing materials for publication.

E.S. Mochalova—preparing materials for publication.

The authors declare no conflict of interest.

REFERENCES

1. Vasiliev A.A., Galatdinova I.A., Zhigalova Yu.A. Ichthyotoxicological properties of Emidonol® 20%. *Vestnik APK Stavropol'ya = Agricultural Bulletin of Stavropol Region*. 2015;1:13–15 (in Russ.).
2. Jędrejko K., Catlin O., Stewart T., Muszyńska B. Mexidol, Cytoflavin, and succinic acid derivatives as antihypoxic, anti-ischemic metabolic modulators, and ergogenic aids in athletes and consideration of their potential as performance enhancing drugs. *Drug Test. Anal.* 2024;16(12):1436–1467. <https://doi.org/10.1002/dta.3655>
3. Postnikov P.V., Polosin A.V., Savelieva N.B., Kurbatkin S.A., Efimova Yu.A., Mochalova E.S. Identification of hypoxene metabolites in urine samples using gas chromatography–tandem mass spectrometry for anti-doping control. *Fine Chem. Technol.* 2024;19(5):393–407. <https://doi.org/10.32362/2410-6593-2024-19-5-393-407>
4. Temerdashev A., Azaryan A., Dmitrieva E. Meldonium determination in milk and meat through UHPLC–HRMS. *Heliyon*. 2020;6(8):e04771. <https://doi.org/10.1016/j.heliyon.2020.e04771>
5. Postnikov P.V., Polosin A.V., Mochalova E.S., Ordzhonikidze Z.G., Nikityuk D.B., Tutelyan V.A. Identification of meldonium in the urine of volunteers using high-performance liquid chromatography–tandem mass spectrometry after consumption of milk of cows treated with a preventive course of the veterinary drug Emidonol®. *Voprosy pitaniya = Problems of Nutrition. Vopr. Pitan.* 2024;93(5):94–103 (in Russ.). <https://doi.org/10.33029/0042-8833-2024-93-5-94-103>
6. Guddat S., Görgens C., Sobolevsky T., Thevis M. Meldonium residues in milk: A possible scenario for inadvertent doping in sports? *Drug Test. Anal.* 2021;13(11–12):1906–1910. <https://doi.org/10.1002/dta.3145>
7. Lukyanova L.D., Kirova Yu.I., Germanova E.L. The Role of Succinate in Regulation of Immediate HIF-1 α Expression in Hypoxia. *Bull. Exp. Biol. Med.* 2018;164(3):298–303. <https://doi.org/10.1007/s10517-018-3976-2>
[Original Russian Text: Lukyanova L.D., Kirova Yu.I., Germanova E.L. The Role of Succinate in Regulation of Immediate HIF-1 α Expression in Hypoxia. *Byulleten' Eksperimental'noi Biologii i Meditsiny*. 2017;164(9):273–279 (in Russ.).]

СПИСОК ЛИТЕРАТУРЫ

1. Васильев А.А., Галатдинова И.А., Жигалова Ю.А. Ихтиотоксикологические свойства Эмидонола® 20%. *Вестник АПК Ставрополя*. 2015;(спецвыпуск 1):13–15.
2. Jędrejko K., Catlin O., Stewart T., Muszyńska B. Mexidol, Cytoflavin, and succinic acid derivatives as antihypoxic, anti-ischemic metabolic modulators, and ergogenic aids in athletes and consideration of their potential as performance enhancing drugs. *Drug Test. Anal.* 2024;16(12):1436–1467. <https://doi.org/10.1002/dta.3655>
3. Постников П.В., Полосин А.В., Савельева Н.Б., Курбаткин С.А., Ефимова Ю.А., Мочалова Е.С. Идентификация метаболитов гипоксена в образцах мочи методом газовой хроматографии – тандемной масс-спектрометрии с целью антидопингового контроля. *Тонк. хим. технологии*. 2024;19(5):393–407. <https://doi.org/10.32362/2410-6593-2024-19-5-393-407>
4. Temerdashev A., Azaryan A., Dmitrieva E. Meldonium determination in milk and meat through UHPLC–HRMS. *Heliyon*. 2020;6(8):e04771. <https://doi.org/10.1016/j.heliyon.2020.e04771>
5. Постников П.В., Полосин А.В., Мочалова Е.С., Орджоникидзе З.Г., Никитюк Д.Б., Тутельян В.А. Выделение мельдония в моче добровольцев методом высокоэффективной жидкостной хроматографии в сочетании с тандемной масс-спектрометрией после употребления молока коров, прошедших профилактический курс применения ветеринарного препарата Эмидонол®. *Вопросы питания*. 2024;93(5):94–103. <https://doi.org/10.33029/0042-8833-2024-93-5-94-103>
6. Guddat S., Görgens C., Sobolevsky T., Thevis M. Meldonium residues in milk: A possible scenario for inadvertent doping in sports? *Drug Test. Anal.* 2021;13(11–12):1906–1910. <https://doi.org/10.1002/dta.3145>
7. Лукьянова Л.Д., Кирова Ю.И., Германова Э.Л. Роль сукцината в регуляции срочной экспрессии HIF-1 α при гипоксии. *Бюллетень экспериментальной биологии и медицины*. 2017;164(9):273–279.
8. Воронина Т.А., Капица И.Г., Иванова Е.А. Сравнительное исследование влияния мексидола и милдроната на физическую работоспособность в эксперименте. *Журнал неврологии и психиатрии им. С.С. Корсакова*. 2017;117(4):71–74. <https://doi.org/10.17116/jnevro20171174171-74>

8. Voronina T.A., Kapitsa I.G., Ivanova E.A. A comparative study of the effects of mexidolum and mildronatum on the physical performance of experimental animals. *Zhurnal nevrologii i psikiatrii im. S.S. Korsakova = S.S. Korsakov J. Neurology Psychiatry*. 2017;117(4):71–74 (in Russ.). <https://doi.org/10.17116/jnevro20171174171-74>
9. Sariev A.K., Kravtsova O.Yu., Zherdev V.P., Berdimuratova G.D., Abdrakhmanov M.Zh., Seredenin S.B. Kinetics of excretion of mexidol and its glucuronide-conjugated metabolite in volunteers of Kazakh and Russian populations. *Klinicheskaya Farmakokinetika = Clinical Pharmacokinetics*. 2005;1(2):23–28 (in Russ.).
10. Rabin O., Uiba V., Miroshnikova Yu., Zabelin M., Samoylov A., Karkischenko V., Semyonov S., Astrelina T., Razinkin S. Meldonium long-term excretion period and pharmacokinetics in blood and urine of healthy athlete volunteers. *Drug Test. Anal.* 2019;11(4):554–566. <https://doi.org/10.1002/dta.2521>
9. Сариев А.К., Кравцова О.Ю., Жердев В.П., Бердимуратова Г.Д., Абдрахманов М.Ж., Середенин С.Б. Кинетика экскреции мексидола и его глюкуроноконъюгированного метаболита у добровольцев популяций казахов и русских. *Клиническая Фармакокинетика*. 2005;1(2): 23–28.
10. Rabin O., Uiba V., Miroshnikova Yu., Zabelin M., Samoylov A., Karkischenko V., Semyonov S., Astrelina T., Razinkin S. Meldonium long-term excretion period and pharmacokinetics in blood and urine of healthy athlete volunteers. *Drug Test. Anal.* 2019;11(4):554–566. <https://doi.org/10.1002/dta.2521>

About the Authors

Pavel V. Postnikov, Cand. Sci. (Chem.), Head of the Doping Control Department, National Anti-Doping Laboratory (Institute), Lomonosov Moscow State University (10-1, Elizavetinskii per., Moscow, 105005, Russia). E-mail: drpavelpostnikov@gmail.com. Scopus Author ID 57021610900, RSCI SPIN-code 7251-9937, <https://orcid.org/0000-0003-3424-0582>

Alexander D. Askretkov, Cand. Sci. (Pharm.), Senior Specialist, Doping Control Department, National Anti-Doping Laboratory (Institute), Lomonosov Moscow State University (10-1, Elizavetinskii per., Moscow, 105005, Russia). E-mail: askretkov@dopingtest.ru. Scopus Author ID 57196465758, <https://orcid.org/0000-0003-0110-8323>

Andrey V. Polosin, Chief Specialist, Doping Control Department, National Anti-Doping Laboratory (Institute), Lomonosov Moscow State University (10-1, Elizavetinskii per., Moscow, 105005, Russia). E-mail: polosin@dopingtest.ru. <https://orcid.org/0000-0002-0009-7362>

Yuliya A. Efimova, Cand. Sci. (Chem.), Assistant Professor, I.P. Alimarin Department of Analytical Chemistry, M.V. Lomonosov Institute of Fine Chemical Technologies, MIREA – Russian Technological University (78, Vernadskogo pr., Moscow, 119454, Russia). E-mail: efimova_yulia@bk.ru. Scopus Author ID 25228417800, <https://orcid.org/0000-0002-3582-0012>

Elena S. Mochalova, Acting Director, National Anti-Doping Laboratory (Institute), Lomonosov Moscow State University (10-1, Elizavetinskii per., Moscow, 105005, Russia). E-mail: mochalova@dopingtest.ru. Scopus Author ID 56416432400

Об авторах

Постников Павел Викторович, к.х.н., начальник отдела допингового контроля, Национальная антидопинговая лаборатория (Институт), Московский государственный университет им. М.В. Ломоносова (Россия, 105005, Москва, Елизаветинский пер., д. 10, стр. 1). E-mail: drpavelpostnikov@gmail.com. Scopus Author ID 57021610900, SPIN-код РИНЦ 7251-9937, <https://orcid.org/0000-0003-3424-0582>

Аскретков Александр Дмитриевич, к.фарм.н., старший специалист, отдел допингового контроля, Национальная антидопинговая лаборатория (Институт), Московский государственный университет им. М.В. Ломоносова (Россия, 105005, Москва, Елизаветинский пер., д. 10, стр. 1). E-mail: askretkov@dopingtest.ru. Scopus Author ID 57196465758, <https://orcid.org/0000-0003-0110-8323>

Полосин Андрей Вячеславович, главный специалист, отдел допингового контроля, Национальная антидопинговая лаборатория (Институт), Московский государственный университет им. М.В. Ломоносова (105005, Россия, Москва, Елизаветинский пер., д. 10, стр. 1). E-mail: polosin@dopingtest.ru. <https://orcid.org/0000-0002-0009-7362>

Ефимова Юлия Александровна, к.х.н., доцент, кафедра аналитической химии им. И.П. Алимарина, Институт тонких химических технологий им. М.В. Ломоносова, ФГБОУ ВО «МИРЭА – Российский технологический университет» (119454, Россия, Москва, пр-т Вернадского, д. 78). E-mail: efimova_yulia@bk.ru. Scopus Author ID 25228417800, <https://orcid.org/0000-0002-3582-0012>

Мочалова Елена Сергеевна, исполняющая обязанности директора Национальной антидопинговой лаборатории (Института), Московский государственный университет им. М.В. Ломоносова (105005, Россия, Москва, Елизаветинский пер., д. 10, стр. 1). E-mail: mochalova@dopingtest.ru. Scopus Author ID 56416432400

Translated from Russian into English by H. Moshkov

Edited for English language and spelling by Thomas A. Beavitt

